FOI-R--0256--SE
November 2001
ISSN 1650-1942
Technical report

Johan Magnusson, Mattias Unosson, Anders Carlberg

High Performance Concrete “HPC”
Field Experiments and Production

Weapons and Protection
SE-147 25 Tumba

SWEDISH DEFENCE RESEARCH AGENCY
Weapons and Protection
SE-147 25 Tumba

FOI-R--0256—SE
November 2001
ISSN 1650-1942
Technical report

Johan Magnusson, Mattias Unosson, Anders Carlberg

High Performance Concrete “HPC”
Field Experiments and Production

Issuing organization	Report number, ISRN	Report type
FOI – Swedish Defence Research Agency Weapons and Protection SE-147 25 Tumba	FOI-R--0256--SE	Technical report
	Research area code 5. Combat	
	Month year November 2001	**Project no.** E2210
	Customers code 5. Contracted Research	
	Sub area code 53 Protection and Fortification Techniques	

Author/s (editor/s)	Project manager
Johan Magnusson Mattias Unosson Anders Carlberg	Anders Carlberg
	Approved by Michael Jacob
	Scientifically and technically responsible

Report title

High Performance Concrete "HPC"-Field Experiments and Production

Abstract (not more than 200 words)

This investigation involves production and penetration tests of high performance concrete (HPC). A total of 62 penetration tests were performed seperated into six test series. The compressive strength of the targets varied between 30 MPa and 220 MPa. At one occasion concrete with a strength exceeding 250 MPa was produced. In the penetration tests, three different projectiles with a diameter of 43 mm, 75 mm and 152 mm were used.

The results from the production tests show that concrete with strengths up to and including 150 MPa enabled large scale production. Experience from these tests in field conditions show the difficulties in large scale production of concrete with a compressive strength exceeding 180 MPa due to its high viscosity.

The penetration tests clearly show that an increase in concrete strength enhances the penetration resistance of concrete structures. However, the tests indicate that concrete strengths exceeding 120 – 160 MPa result in relatively moderate enhancements of the protective level. Reinforcement also increases the penetration resistance of concrete. The volume fraction, however, needs to be around 6 % in order to obtain a reduction of 25 % in penetration depth. The effects of different impact velocities were also studied. Relatively large penetration enhancements were observed with an increasing projectile velocity.The tests showed that the results may be influenced by the target dimensions. In order to avoid boundary effects the target diameter may need to be around 15 to 20 times the penetrator diameter.

Keywords

High performance concrete (HPC), production, reinforcement, penetration tests, impact velocity, boundary effects

Further bibliographic information	Language English
ISSN 1650-1942	**Pages** 166 p.
	Price acc. to pricelist **Security classification**

Utgivare
Totalförsvarets Forskningsinstitut – FOI
Vapen och skydd
147 25 Tumba

Rapportnummer, ISRN
FOI-R--0256--SE

Klassificering
Teknisk rapport

Forskningsområde
5. Bekämpning

Månad, år
November 2001

Projektnummer
E2210

Verksamhetsgren
5. Uppdragsfinansierad verksamhet

Delområde
53 Skydd och anläggningsteknik

Författare/redaktör
Johan Magnusson
Mattias Unosson
Anders Carlberg

Projektledare
Anders Carlberg

Godkänd av
Michael Jacob

Tekniskt och/eller vetenskapligt ansvarig

Rapportens titel (i översättning)
Högpresterande betong ”HPC”-Fältförsök och produktion

Sammanfattning (högst 200 ord)

Föreliggande rapport behandlar produktion och skjutförsök på högpresterande betong (HPC). Sammanlagt 62 försök var genomförda indelade i sex försöksserier. Målens tryckhållfasthet varierade mellan 30 MPa och 220 MPa. Vid ett tillfälle tillverkades en betong överstigande en hållfasthet på 250 MPa. Vid skjutförsöken användes tre olika projektiltyper vilka hade en diameter av 43 mm, 75 mm samt 152 mm.

Resultaten från provgjutningarna visar att betong med hållfastheter t o m 150 MPa tillåter storskalig produktion. Erfarenheterna från dessa gjutningar pekar på svårigheterna med fältmässig produktion av betonghållfastheter överstigande 180 MPa p g a dess höga viskositet.

Skjutförsöken visar tydligt att en ökning av betonghållfastheten resulterar i ett ökat penetrationsmotstånd av betongkonstruktioner. Försöken visar emellertid att betonghållfastheter på mellan 120 MPa och 160 MPa endast ger en relativt måttlig ökning av skyddsförmågan. Armering ökar också betongkonstruktioners skyddsförmåga. Experimenten visar emellertid att armringsmängden bör ligga omkring 6 volymprocent för att erhålla en reducering av penetrationsdjupet på 25 %. Effekten av olika anslagshastigheter studerades dessutom. Relativt stora ökningar av penetrationsförmågan observerades vid ökande projektilhastighet. Vidare visade försöken att de erhållna resultaten kan påverkas av valet av måldimensioner. För att minimera inverkan av randeffekter bör måldiametern vara 15 – 20 gånger så stor som projektildiametern.

Nyckelord
Högpresterande betong (HPC), produktion, armering, skjutförsök, penetration, anslagshastighet, randeffekter

Övriga bibliografiska uppgifter

Språk Svenska

ISSN 1650-1942

Antal sidor: 166 s.

Distribution enligt missiv

Pris: Enligt prislista

Sekretess

PREFACE

The present report consists of several penetration tests carried out during the years 1996 – 1999. All experiments were performed at Aborrtjärn shooting range at the Bofors Test Centre in Karlskoga. The objectives were to study the ability to produce high performance concrete and also its protective level against projectiles.

During the last decade, high performance fibre reinforced concretes with compressive strengths exceeding 200 MPa have been developed. To evaluate if such materials may provide protection against modern penetrators, Swedish and Norwegian defence organisations have formed a joint project named “High Performance Concrete”. This project is divided into five subprojects, namely: “Threat” (SP1), “Material and Structural Design” (SP2), ”Analysis and Numerical Simulation” (SP3), “Field Experiments and Production” (SP4) and “Standards and Guidelines” (SP5). This investigation was carried out within SP4 and funded by the Swedish Armed Forces Headquarters.

Stockholm, November 2001

The Authors

LIST OF CONTENTS

1 INTRODUCTION

1.1 Background

The development of precision guided penetrating weapons provides a significant threat to existing military concrete facilities. Therefore, other protection concepts and materials need to be considered in order to increase the protective level of these structures. One possible solution is to use concrete of very high strength in protective barriers. Nowadays, a number of different high performance concrete (HPC) material concepts exist as the result of many years of worldwide research. Here, HPC is referred to concrete with a compressive strength exceeding 80 MPa. These concepts are, however, often based on exotic constituents (i.e. binders and aggregates) and the mix design may not be commonly available due to patent. Consequently, the material costs of these concepts may be 10 – 20 times the costs of conventional concrete. Also, the HPC material concepts are in many cases developed for small scale purposes. For this reason, the needs to test different types of HPC in large scale production and with conventional production methods were recognised. It is also important to be able to use commonly available materials in the mix design. It may be possible to reduce the production costs by using conventional production methods and commonly available materials.

1.2 Objectives of the investigation

One objective of this investigation was to study the ability of HPC to be used as shelters against weapons effects. The work focused upon performing penetration tests on concrete targets of different strengths. Naturally, it was of interest to investigate the protective level of HPC in relation to that of conventional concrete. Furthermore, it was of interest to study the ability of mixing and producing different types of HPC in order to investigate the ability to construct protective structures of this material. In order to obtain useful results of all these issues, the following parameters were studied:

- the ability of producing HPC, both with the use of conventional concrete producers and in field conditions
- the effects of concrete strength, reinforcement, projectile velocity and projectile diameter on the penetration resistance
- the effects of target size (i.e. boundary effects)

2 PRODUCTION OF HIGH PERFORMANCE CONCRETE

2.1 General aspects on high performance concrete

Research on HPC is carried out all over the world. It is possible to produce concrete that exceeds a compressive strength of 200 MPa. Development of modern superplasticizers enables a reduction of the water binder ratio at the same workability with the result of an increasing strength. The reason for this is the ability of the superplasticizer to separate clumps of cement particles. As the particles separate, confined water is released and is available for further chemical reactions with the cement, see /4/ and /6/. Introducing puzzolan additives such as silica fume can increase the strength of the concrete even further. The average particle size of silica fume is only about 1 % the size of cement particles. Thus, introducing silica particles results in a filler effect that gives the cement paste a more compact structure with a smaller amount of pores. The silica particles also react with the calcium hydroxide that is released during the chemical reaction between the cement and the water.

Energy is consumed in the process of crack initiation and propagation in concrete. It is well known that microcracks are initiated at relatively low stress levels prior to fracture of concrete. As the stress is increased these microcracks propagate and link up into larger cracks, which eventually forms the fracture zone. The fracture zone of HPC is narrower in comparison to normal strength concrete (NSC). As a result, the ability of HPC to distribute the stress over larger areas is reduced, which in turn increases the stress concentration. A fracture zone in the interface of the aggregates and the cement paste (i.e. the transition zone) characterises the fracture of NSC. Coarser aggregates arrest crack growth, which produces meandering and branching of cracks. The fracture of HPC, however, is mainly characterised by fracture through the aggregates and the cement paste. The fracture surface of HPC is for that reason relatively plane in comparison to that of NSC. Additional energy is consumed for every change in direction of the fracture surface. The fracture energy (G_F) of HPC is therefore proportionally smaller in relation to that of NSC. G_F is defined as the total energy consumed per unit area of the fracture surface in a fracture zone during failure. However, G_F is not an adequate measure of the fracture toughness of a material. A material can prove to have large fracture energy but still exhibit a brittle behaviour. A more adequate parameter to describe the behaviour of materials is the so-called characteristic length, l_{ch}. This parameter can be calculated according to Eq. (1):

$$l_{ch} = \frac{E \cdot G_F}{f_t^2} \tag{1}$$

where

l_{ch} = characteristic length

E = Young's modulus

G_F = fracture energy

f_t = concrete tensile strength

Generally, the fracture energy increases with concrete strength. However, this does not lead to higher toughness because the concrete tensile strength also increases. The increase of tensile strength is larger in relation to the increase of both the fracture energy and the elastic modulus. Thus, the value of the characteristic length decreases with increasing concrete strength. This can be interpreted as an increasing brittleness. For HPC, l_{ch} can decrease to ⅓ of the l_{ch} for NSC /4/. The ductility of HPC, however, can be improved considerably by introducing steel fibres to the matrix. Note that if the parameters G_F, E and f_t are determined under quasi-static loading, then comparisons between structural members at different loading rates by using l_{ch} may lead to incorrect conclusions.

In NSC, the cement paste is the weakest link of the composite material while the aggregates are normally stronger. Cracks are initiated in the transition zones and propagate through the matrix. In HPC, however, both the cement paste and the interface are stronger in relation to conventional concrete. Thus, the aggregate strength has a larger influence on the concrete strength. The maximum aggregate size of HPC needs to be limited. There are two reasons for this. Firstly, larger aggregates result in weaker interface between aggregate and cement paste due to the separation of water that usually occurs beneath coarse aggregates. Secondly, reduced aggregate size leads to the probability of a slight strength increase of the aggregates. This is due to statistics stating that there is a higher probability of a larger number of weakness zones existing in specimens of larger volumes, see further /3/. In addition, reduced aggregate size makes it more difficult for cracks to propagate in the cement paste, due to the reduced mean space between the aggregates at a constant aggregate content /4/. Furthermore, surprisingly small variations in aggregate content and grading result in large variations in workability of the fresh concrete. The natural moisture content of the aggregates is also of great importance regarding the workability, because a relatively large portion of the total water added originates from the aggregates. The amount of sand in the concrete mix also plays an important role because the sand content largely determines the necessary amount of water, thus, that way indirectly determining the possible concrete strength. Another characteristic of HPC is the relatively rapid strength development the first days after casting.

2.2 Concrete types used in the tests and production

At the time when FOA's research on HPC started at the end of 1994, contacts with Luleå University of Technology were established. There, a cementitious binder denoted EMC (Energetically Modified Cement) had been developed. This material is produced by high frequency compaction of cement, silica fumes and other additives. EMC has a number of enhanced characteristics compared to conventional cement, e.g. increased workability, higher strength at early age, a more compact structure of the binder and also an increased adhesion. EMC can be used with conventional production methods. EMC was tested at FOA by casting slabs of different thickness. These slabs were then tested as ballistic protection against small calibre ammunition, i.e. 7.62 mm and 12.7 mm. Slabs of Reactive Powder Concrete were in connection to these experiments also tested. These slabs were cast at the Swedish Cement and Concrete Research Institute (CBI). Reactive Powder Concrete consists of Portland cement, sand of very fine quarts grains only measuring 150 – 400 μm and additives. An extremely low amount of water is used with a water binder ratio of 0.09 – 0.13. The slabs were hardened in a heating oven and the compressive strength reached about 200 MPa. Extreme strengths of 800 MPa can be obtained if the hardening takes place under heat and pressure. No further discussions regarding EMC and Reactive Powder Concrete are made in this investigation because these materials were not included in the tests series with larger penetrators.

Several types of concrete were tested in the penetration tests at Bofors Test Centre. In some cases, rebars or steel fibres of different quantities and sizes were added, and in some cases, the target consisted of plain concrete. The different concrete types are presented with mix proportions and comments in the following sections. In some cases, the mix design was not available from the company that developed them. The presentations of the concrete types are listed on a progressive nominal concrete strength, which is also in parenthesis.

2.2.1 NSC (30 MPa)

Targets of NSC (normal strength concrete) were used in all test series as reference with concrete targets of higher strengths. There are many varieties in mix proportions available to produce this kind of concrete. For this reason only one example is presented here, see Table 2.1. Figure 2.1 shows casting of NSC at FOA, Märsta.

Table 2.1 Mix proportions of NSC.

Materials	kg/m^3
Portland cement, *c*	448
Aggregate 0 – 8 mm	920
Aggregate 8 – 16 mm	681
Water, *w*	296
w/c = 0.66	
Total:	2345

Figure 2.1 Casting of NSC in July 1999 (Märsta, FOA).

2.2.2 Abetong and Fredrikstad concrete (90 MPa)

These types of concrete were produced by Abetong Precon (Sweden) and in Fredrikstad (Norway), respectively. They were of similar concrete strengths and were only used in a limited number of tests. The mix proportions were not available.

2.2.3 Optiroc concrete (90 MPa)

The concrete used was a bridge deck concrete developed by Optiroc which can be delivered ready mixed without water. It is normally used for frost resistant bridge decks but also for roads and wharves. Usually this type of concrete also contains steel fibres but it can also be delivered without any reinforcement. Optiroc concrete has mix proportions according to Table 2.2.

Production of Optiroc concrete is carried out as follows. After adding water, the concrete is mixed for about five minutes. When moulds with large depths are poured, compacting needs to be done for each 300 mm layer by the use of rod vibrators. After completed casting, the free concrete surfaces need to be protected from evaporation as soon as possible. The strength development of the concrete ceases at temperatures below + 5 ºC. The workability of this concrete type was good. Optiroc concrete is pumpable.

Table 2.2 Mix proportions of Optiroc concrete.

Materials	kg/m^3
Sulphate resistant Portland cement, *c*	440
Porphyric granite 0 – 20 mm	not available
Steel fibres (Dramix 0.5 × 30 mm with end hooks)	55
Water, *w*	145
w/c = 0.33	
Total:	~ 2450

2.2.4 Abetong concrete (150 MPa)

Abetong Precon delivered concrete of this strength. The mix proportions are not available but the concrete consisted of sulphate resistant standard Portland cement with a low alkali content (Anläggningscement in Swedish), silica fume, superplasticizer and artificial aggregate consisting of slag in the 0 – 8 mm fraction. After casting, the free concrete surfaces needs to be protected from evaporation as soon as possible. Abetong concrete is pumpable.

The workability of this type of concrete is viscous but still flowable. Some targets of test series 1999 were cast in June on a warm and sunny day with temperatures of about + 25 °C. The evaporation from the surface of the concrete increased in the relatively warm weather and small cracks appeared on the surface due to plastic shrinkage. The appearance of shrinkage cracks were prevented by pouring a thin layer of water over the surface and then covering it with plastic sheets as soon as possible after casting. Figures 2.2 – 2.3 show casting of Abetong concrete at FOA, Märsta.

Figure 2.2 Casting of Abetong concrete in June 1999 at FOA, Märsta.

Figure 2.3 Casting of Abetong concrete in July 1999 at FOA, Märsta.

2.2.5 Trondheim concrete (150 MPa)

This type of concrete was developed in Norway, see /7/. The aim was to develop a high strength concrete with a compressive strength of about 150 MPa and based on commonly available materials. It was also important to obtain a workability of the fresh concrete, which would be suitable for traditional construction practice. The aggregates used consisted entirely of washed, crushed mylonite from the south-western region of Norway. This rock type is characterised by its high strength, high modulus of elasticity and high fracture toughness. Furthermore, it is well known that steel fibres reduce the workability of the fresh concrete

significantly. The fibre length was therefore limited to 12.5 mm. Table 2.3 presents the mix design.

The workability of the fresh Trondheim concrete may be described as very viscous but still flowable /7/. The concrete is probably pumpable but this has not been verified by testing. The workability retention of the concrete is 60 – 90 minutes at +20 ºC provided that the concrete is stored in a revolving automixer. At the time of casting concrete targets, the mixing time was increased from 45 seconds to 180 seconds to allow for manual feeding of the fibres and also to ensure full effect of the superplasticizer. When casting of targets with relatively large depths was performed, compaction was done for each 400-mm layer by the use of rod vibrators. The free concrete surface was levelled out about 75 minutes after completed batching. The concrete workability was at this point of time reduced significantly but not critically. The free concrete surfaces need to be protected from evaporation as soon as possible after completed casting. Figure 2.4 shows the casting of Trondheim concrete.

Table 2.3 Mix proportions of Trondheim concrete /7/.

Materials	kg/m^3
Norcem Anlegg cement, *c*	572.8
Silica fume, *s*	114.6
Mylonite 0 – 2 mm, crushed sand	545.2
Mylonite 2 – 5 mm	229.5
Mylonite 5 – 8 mm	482.5
Mylonite 8 – 11 mm	310.3
Steel fibres (length = 12.5 mm)	73.9 (volume fraction ~1 %)
Water, *w*	158.1
Water absorbed by aggregates	6.3
Superplasticizer (Mighty 150)	34.4
w/(c+s) = 0.23	
Total:	2521

Figure 2.4 Casting of Trondheim concrete in September 1998 in Trondheim, Norway.

2.2.6 Densit concrete (200 MPa)

Densit concrete is delivered by the Danish company Densit A/S. Densit A/S uses a technique they call DSP, which stands for Densified System with extremely fine Particles. Extremely fine particles combined with a careful grading of the aggregates, a superplasticizer and small amounts of water result in a dense concrete with high strength. The binder used is denoted Inducast 6000 GT and consists of Portland cement, finely ground bauxite in the fraction 0 – 3 mm and a superplasticizer of type Mighty as a powder. The mix proportions according to Densit A/S are shown in Table 2.4.

Production of Densit concrete is similar to that of conventional concrete. However, the mixing time is prolonged along with some other changes. Firstly, the constituents without any steel fibres are mixed dry. After about one minute, water is added and then the concrete is mixed for another ten minutes. The steel fibres are then added and then mixed for about five minutes. At this time, the fresh concrete is very viscous but as casting begins with simultaneous compaction by the use of rod vibrators, the viscosity decreases. In the case of large amounts of reinforcement, the compaction may be transmitted through the reinforcement to the concrete. Due to the high cohesion of the concrete, no noticeable separation occurs during this process. Similar to other types of HPC, the free concrete surface needs to be sealed to prevent plastic shrinkage.

Table 2.4 Mix proportions of Densit concrete according to Densit A/S.

Materials	kg/m^3
Inducast 6000 GT	1500
Bauxite 5 – 8 mm	1050
Steel fibres 0.4 × 12.5 mm	156 (volume fraction 2 %)
Water	150
Total:	2856

In order to investigate the ability of full-scale production of Densit concrete, castings in field conditions were performed at Vaxholm in November 1997. Three targets were cast in moulds made of corrugated steel cylinders with a diameter of 1600 mm and depths of 500 mm, 1000 mm and 1500 mm, respectively. The volume fraction of steel fibres in the concrete was 2 %. The amount of fresh concrete in the pan mixers needed to be reduced due to the high viscosity of the concrete. One mixer had to be replaced during casting after the electric motor broke down. Rod vibrators were used continuously during casting for each 300-mm layer. One of the rod vibrators also broke down at one point due to the viscous concrete. The experiences from these tests show the difficulties in field production of large volumes with this type of concrete. Figure 2.5 shows the field production tests at Vaxholm.

Figure 2.5 Casting of Densit concrete at Vaxholm in November 1997.

2.2.7 Densit special concrete (200 MPa)

The mix design of Densit special concrete differs from the ordinary Densit concrete as presented in Table 2.5. The authors do not know the constituents of Inducast 6000 special. For production techniques see Densit concrete above. Densit special concrete is characterised by an increased workability compared to that of Densit concrete.

Table 2.5 Mix proportions of Densit special concrete according to Densit A/S.

Materials	kg/m^3
Inducast 6000 special	1340
Bauxite 2 – 4 mm	580
Bauxite 5 – 8 mm	580
Steel fibres 0.4 × 12.5 mm	156 (volume fraction 2 %)
Water	175
Total:	2831

2.2.8 CRC (200 MPa)

CRC stands for Compact Reinforced Composite and was developed by Aalborg Portland in Denmark. CRC is, basically, Densit concrete with heavy reinforcement. The reinforcement volume fraction is 5 – 15 % but can in some cases reach 25 %. The maximum aggregate size is limited to 8 mm in order to ensure that the fresh concrete can flow readily around the reinforcement, see Table 2.6. In the case of reinforcement volume fractions of 25 %, the spacing of the rebars is only about 50 mm, which only gives a free space of 25 mm with a rebar diameter of 25 mm. Also, note that the length of the steel fibres is limited to 12.5 mm to ensure satisfying workability. Production of CRC in field conditions cannot be accomplished because advanced vibrator equipment is necessary. For instance, compaction of panels of fresh CRC needs to be made by the use of vibrating tables. In this investigation, all targets of this concrete were cast at Densit A/S. For production techniques see Densit concrete above in section 2.2.6. Figures 2.6 – 2.7 show casting of CRC elements at Densit A/S in Denmark.

Table 2.6 Mix proportions of CRC according to Densit A/S.

Materials	kg/m^3
Inducast 6000 GT	1486
Bauxite 5 – 8 mm	1024
Steel fibres 0.4 × 12.5 mm	156 (volume fraction 2 %)
Water	143
Total:	2960

Figure 2.6 Casting of CRC concrete at Densit A/S in February 1997.

Figure 2.7 Casting of CRC concrete at Densit A/S in February 1997.

2.2.9 Ballistocrete (~ 250 MPa)

This type of concrete was delivered by IBD - Deisenroth Engineering in Karlsruhe, Germany. Ballistocrete contains steel micro fibres and is mainly intended for ballistic protection. Very high strengths were obtained but it was only used in a limited number of tests. The aggregate used was of very high strength. The mix design of this concrete type is unknown to the authors.

2.3 Concrete mechanical properties

2.3.1 Mechanical properties of concrete types used in the penetration tests

The mechanical properties of the different types of concrete used in all test series are presented in Tables 2.7 – 2.13 below. In most cases, only compressive strengths and densities have been determined. Unfortunately, some compressive strengths were not determined in test series 1996:2 and 1997. In most test series more than one casting with the same concrete type was performed. Variations in concrete strength were observed after these castings, which are denoted with numerals (e.g. Densit 1 and Densit 2 in Table 2.8). The concrete strength was in some test series determined on specimens of different sizes and shapes. In these cases, there are more than one value of the compressive strength presented for one concrete type, see Tables 2.10 – 2.12. In Table 2.12, the modulus of elasticity E_o was determined according to CEB-FIP model code for concrete structures and E_c was determined according to ISO 6784. E_o is obtained at the first loading and E_c is obtained after at least three unloading-reloading cycles. Fracture mechanics tests were performed on concrete of different strengths in two separate investigations, see /1/ and /2/. The fracture energies were determined by means of

three point bend tests on notched beams and both static and dynamic loading tests were performed.

Table 2.7 Mechanical properties of concrete in test series 1996 (mean value).

Test series	Concrete type	f_{cc} (MPa)	Reinforcement volume fraction	Comments
1996:1	NSC	~ 30	-	Cast in April 1996 at FOA, Märsta
	Densit	~ 180	0.9 % and 1.8 % steel fibres	Cast in April 1996 at Densit A/S
	CRC	~ 220	2 % steel fibres ϕ 25 rebars 25 %	Cast in April 1996 at Densit A/S
1996:2	NSC	36	-	Cast in October 1996 at FOA, Märsta. Max aggregate size 18 mm
	Densit	180	0.9 % and 1.7 % steel fibres	Cast in November 1996 at Densit A/S
	CRC	220	4 % steel fibres ϕ 25 rebars 25 %	Cast in November 1996 at Densit A/S c/c rebars 50 mm
	Ballistocrete	>250	Unknown amount of steel fibres	Cast in October 1996 by IBD Max aggregate size 64 mm

Table 2.8 Mechanical properties of concrete in test series 1997 (mean value).

Concrete type	f_{cc} (MPa)	Reinforcement volume fraction	Comments
NSC	38	-	Cast in September – October 1997 at FOA, Märsta
Densit 1	~ 200	2 % steel fibres	Cast in October 1996 at Densit A/S
Densit 2	180	2 % steel fibres	Cast in November 1997 in Vaxholm

Table 2.9 Mechanical properties of concrete in test series 1998:1 (mean value ± standard deviation).

Concrete type	f_{cc} (MPa)	ρ (kg/m^3)	Reinforcement volume fraction	Comments
NSC 1	41 ± 1[1]	2280[1]	-	Cast in February 1998 by FOA, Märsta
NSC 2	34	-	ϕ25 rebars 7 %	Cast in March 1998 by Densit A/S
Abetong (K90)	83	-	1.5 % steel fibres	Cast in March 1998 by Abetong
Optiroc	108 ± 1[2]	2500[2]	1 % steel fibres	Cast in March 1998 by FOA, Märsta
Fredrikstad	90	-	-	Cast in March 1998 at Fredrikstad, Norway
CRC	200	-	ϕ25 rebars 7 % 1.5 % steel fibres	Cast in March 1998 by Densit A/S
Densit	203 ± 11[3]	-	-	Cast in March 1998 by Densit A/S
Densit Special	199 [4]	-	1.5 % steel fibres	Cast in March 1998 by Densit A/S
Ballistocrete	>250	-	Unknown amount of fibres	Cast in October 1996 by IBD

1 = determined on three 150 mm cubes
2 = determined on three 100 mm cubes
3 = determined on three ϕ100 × 200 mm cylinders
4 = determined on two ϕ100 × 200 mm cylinders

Table 2.10 Mechanical properties of concrete in test series 1998:2 (mean value ± standard deviation).

Concrete type	f_{cc} (MPa)	ρ (kg/m^3)	Reinforcement volume fraction	Comments
NSC 1	36[1]	-	-	Cast in September 1998 by FOA, Märsta
NSC 2	41 ± 1[1] 24[3] (two cylinders)	2280[1]	-	Cast in February 1998 by FOA, Märsta
NSC 3	38 23 ± 2[3] (four cylinders)	-	-	Cast in September 1997 by FOA, Märsta
Abetong (K90)	83 72[3] (one cylinder)	-	1.5 % steel fibres	Cast in March 1998 by Abetong
Optiroc	108 ± 1[2] 75[3] (two cylinders)	2500[2]	1 % steel fibres	Cast in March 1998 by FOA, Märsta
Fredrikstad	90	-	-	Cast in March 1998 at Fredrikstad, Norway
Abetong (K150)	134	-	-	Cast in September 1998 by Abetong
Trondheim 1[4]	141	-	1 % steel fibres	Cast in September 1998 at Trondheim
Trondheim 2[4]	141	-	ϕ 32 rebars 6.5 % 1 % steel fibres	Cast in September 1998 at Trondheim
Densit 1	183 ± 2[3] (three cylinders)	-	2 % steel fibres	Cast in November 1997 at Vaxholm
Densit 2	~ 200	-	2 % steel fibres	Cast in October 1996 by Densit A/S

1 = determined on three 150 mm cubes
2 = determined on three 100 mm cubes
3 = determined on ϕ 92 × 199 mm cylinders (drilled cores)
4 = see Table 2.11 for mechanical properties

Table 2.11 Mechanical properties of Trondheim concrete in test series 1998:2 (mean value ± standard deviation) /7/.

Concrete type	f_{cc} (MPa)	E (GPa)
Trondheim	141 ± 2[1] 130 ± 2[2]	50 ± 1[2]

1 = determined on nine 100 mm cubes
2 = determined three ϕ 150 × 300 mm cylinders

Table 2.12 Mechanical properties of concrete in test series 1999 (mean value ± standard deviation).

Concrete type	ρ (kg/m^3)	f_{cc} (MPa)	f_{spl} (MPa)	Young's modulus E_o (GPa)	Young's modulus E_c (GPa)	G_F (N/m)	Reinforcement volume fraction
NSC *B*	2300	38.6 ± 2.5	3.6 ± 0.0	-	-	-	-
Optiroc *C*	2420	103 ± 2 92 ± 2[2]	6.5 ± 0.2 5.9 ± 0.6[2]	44.0 ± 0.5	44.5 ± 0.9	-	-
Trondheim *D*	-	120	-	-	-	-	1 % steel fibres
Abetong 1[4] *B*	2750	149 ± 7 182 ± 3[3] 163[1,2]	8.0[1]	56.5[1]	59.0[1]	159[1]	-
Abetong 2[4] *A*	2770	153 ± 4 170 ± 3[3] 144[1,2]	9.1[1]	57.4[1]	58.8[1]	162[1]	-
Abetong 3[4] *C*	2830	158 ± 4 176[1,2]	9.6[1]	65.4[1]	67.0[1]	-	-

ρ = density determined on three 150 mm cubes

f_{cc} = compressive strength of concrete determined on three 150 mm cubes

f_{spl} = splitting tensile strength of concrete determined on three 150 mm cubes

E_o = determined on ϕ 100 × 200 cylinders

E_c = determined on ϕ 100 × 200 cylinders

G_F = fracture energy determined on one notched beam

A = cast in June 1999 by FOA, Märsta

B = cast in July 1999 by FOA, Märsta

C = cast in August 1999 by FOA, Märsta

D = cast in August 1999 at Trondheim, Norway

1 = determined on one specimen

2 = determined on ϕ 100 × 200 cylinders

3 = determined on three 100 mm cubes

4 = three different days of casting the targets

The concrete tensile strength of Abetong concrete (150 MPa) was determined by performing uniaxial tensile tests on six cylindrical cores with a diameter of 72 mm. Steel plates were

glued to each end of the specimens. This glue line failed in half the tests, thus, only three tests are presented in Table 2.12. The relationship between the splitting tensile strength and the uniaxial tensile strength has been studied in earlier investigations /4/. According to the CEB-FIP model code the relationship can be expressed as Eq (2) and according to Haghpassand the uniaxial strength can be calculated according to Eq (3). Clearly, the results of both equations are reasonably close to the tensile test results of this concrete strength, see Table 2.13.

$$f_t = 0.9 \cdot f_{spl} \tag{2}$$

$$f_t = 0.78 \cdot f_{spl} + 0.49 \tag{3}$$

Table 2.13 Abetong concrete tested in March 1999 (mean value ± standard deviation).

f_{cc}[1] (MPa)	f_{spl}[1] (MPa)	f_t[2] (MPa)	ρ[1] (kg/m^3)	$f_t^{eq(2)}$ (MPa)	$f_t^{eq(3)}$ (MPa)
167 ± 3.5	7.2 ± 0.4	6.28 ± 0.40	2750	6.5	6.1

f_{spl} = splitting tensile strength of concrete

f_t = uniaxial tensile strength tests

$f_t^{eq(2)}$ = concrete tensile strength according to eq (2)

$f_t^{eq(3)}$ = concrete tensile strength according to eq (3)

1 = determined on six 150-mm cubes.

2 = determined on three ϕ 72-mm cylinder cores.

2.3.2 Compressive strength development

The compressive strength development was also studied for most concrete types used in the different test series, see Figures 2.8 – 2.16. As shown in these figures, all concrete types exhibit a significant strength development during the first days after casting. Especially, the Abetong concrete and the Densit concrete proved to have a compressive strength of about 80 MPa and 100 MPa, respectively, 24 hours after casting. This is shown in Figures 2.10 and 2.14. This characteristic of HPC may be of practical use, i.e. repairs of damaged structures such as runways at airfields. Most curves level off about 40 to 60 days after casting in this investigation, but NSC and Densit concrete show an upward trend beyond this point of time. The more rapid strength development of Densit concrete with steel fibres is shown in Figures 2.15 and 2.16. This increase is probably only caused by small differences in the mixing of the concrete. Furthermore, the strength development curves are based on tests on 150-mm cubes, except for Densit concrete where the curves are based on 100-mm cubes. For comparison, compressive tests determined on cylinders are also presented in Figures 2.9 – 2.15.

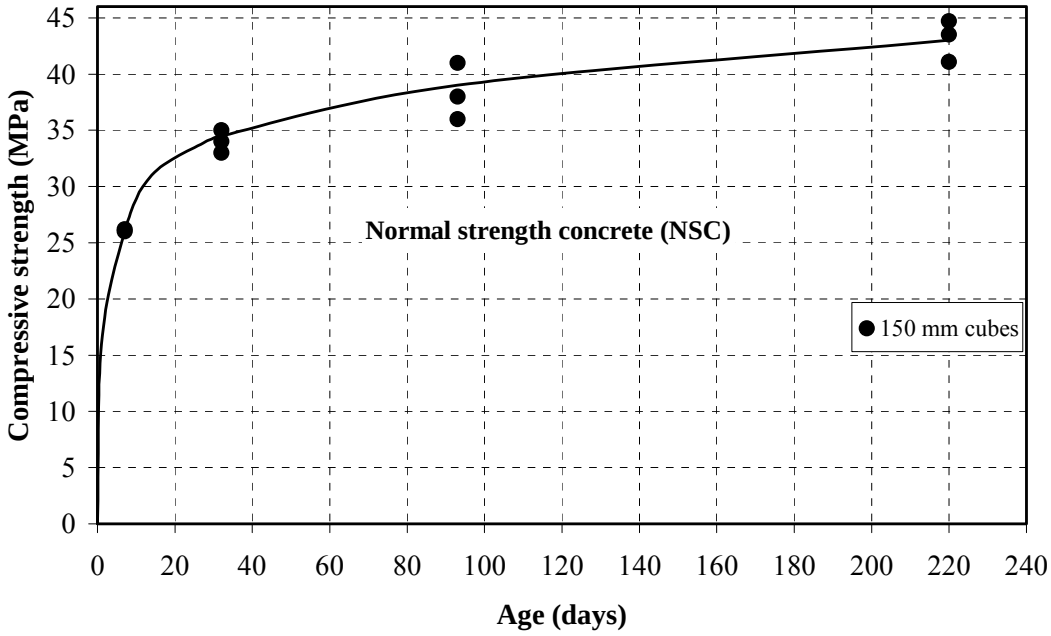

Figure 2.8 Compressive strength development of NSC.

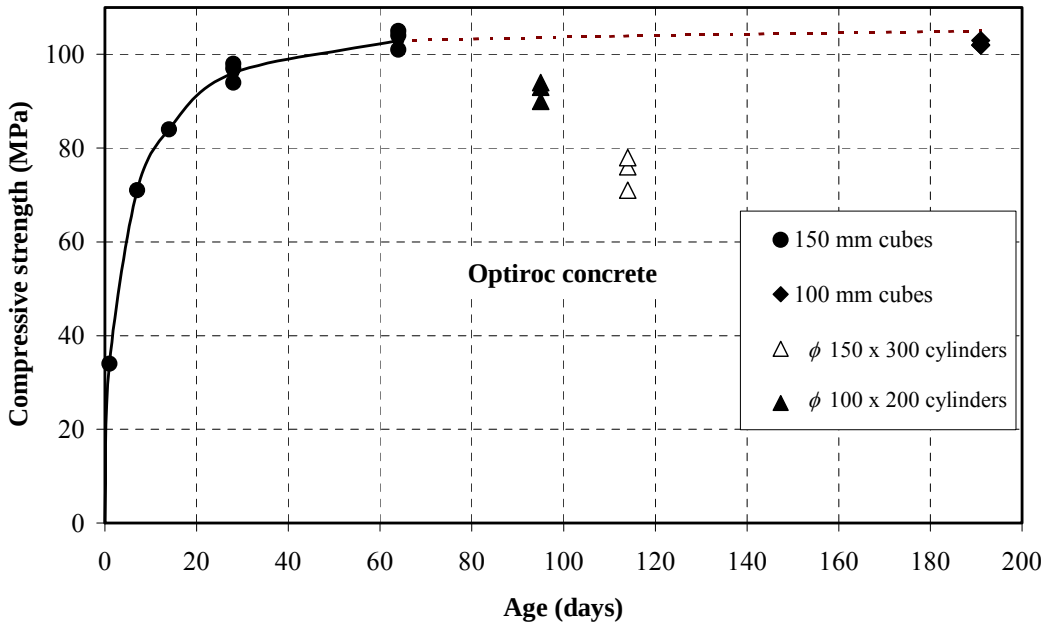

Figure 2.9 Compressive strength development of Optiroc concrete.

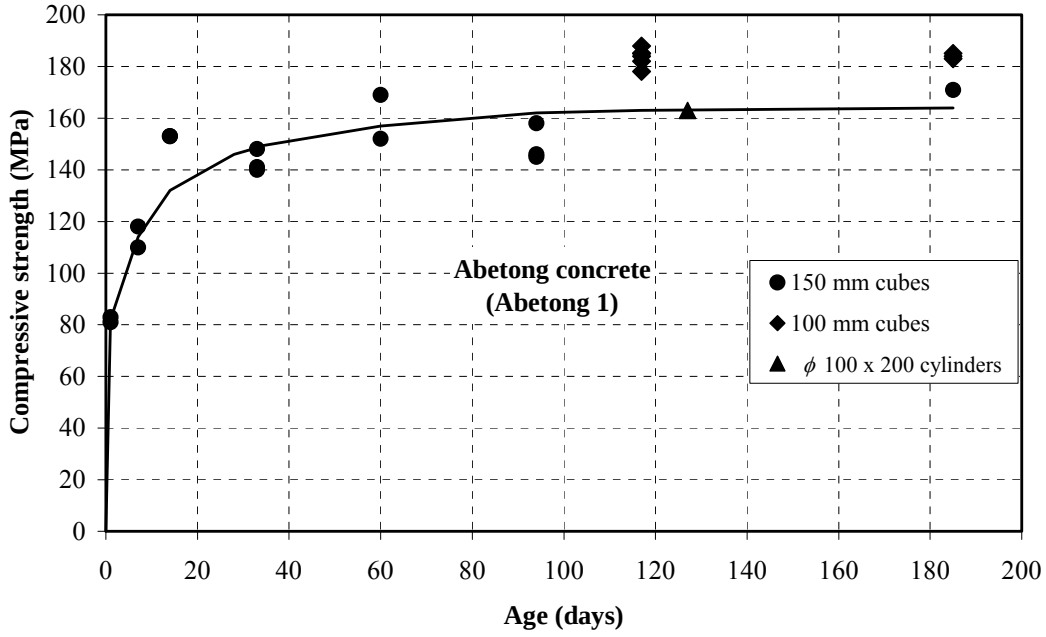

Figure 2.10 Compressive strength development of Abetong concrete (1st casting).

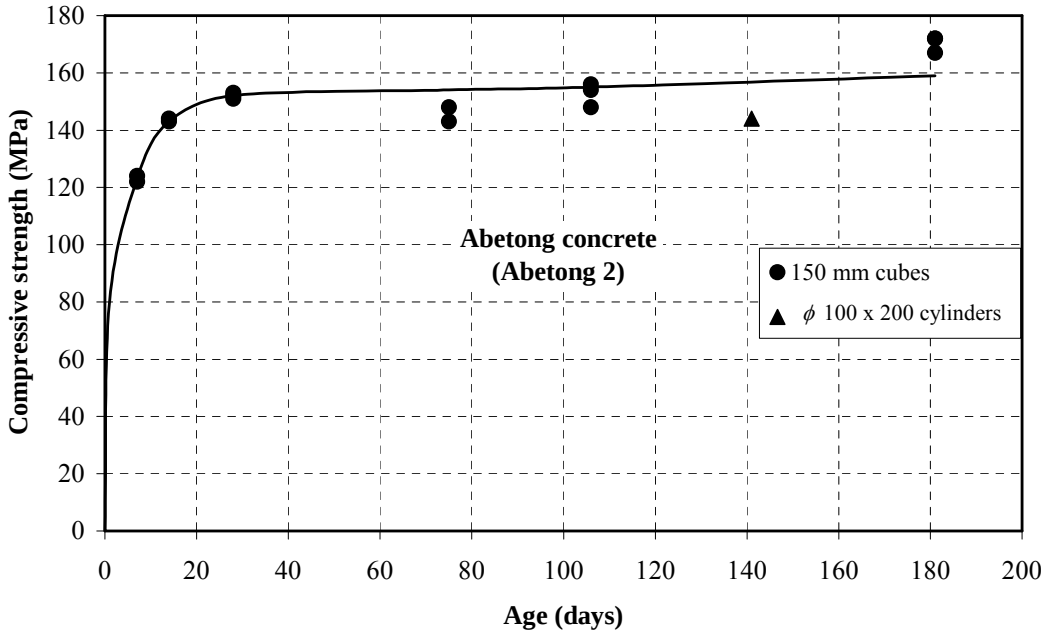

Figure 2.11 Compressive strength development of Abetong concrete (2nd casting).

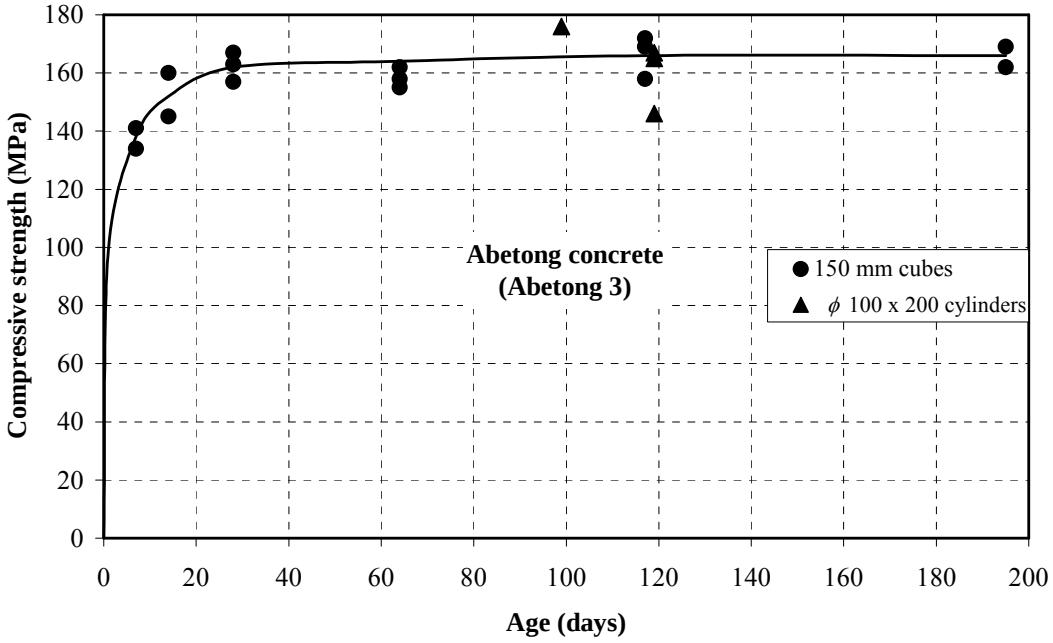

Figure 2.12 Compressive strength development of Abetong concrete (3rd casting).

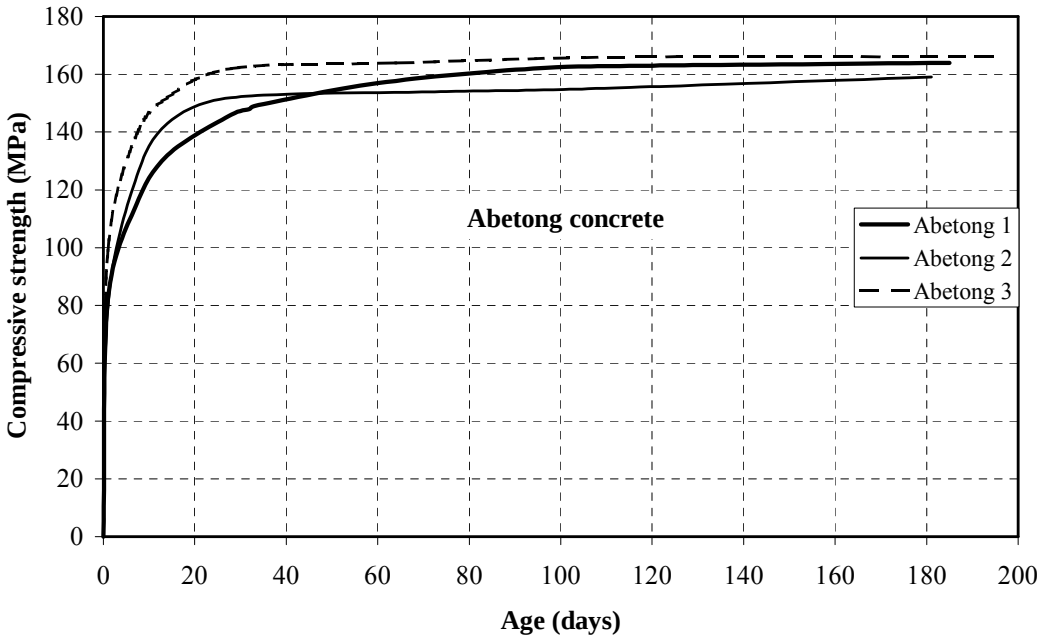

Figure 2.13 Compressive strength development of Abetong concrete (all three castings).

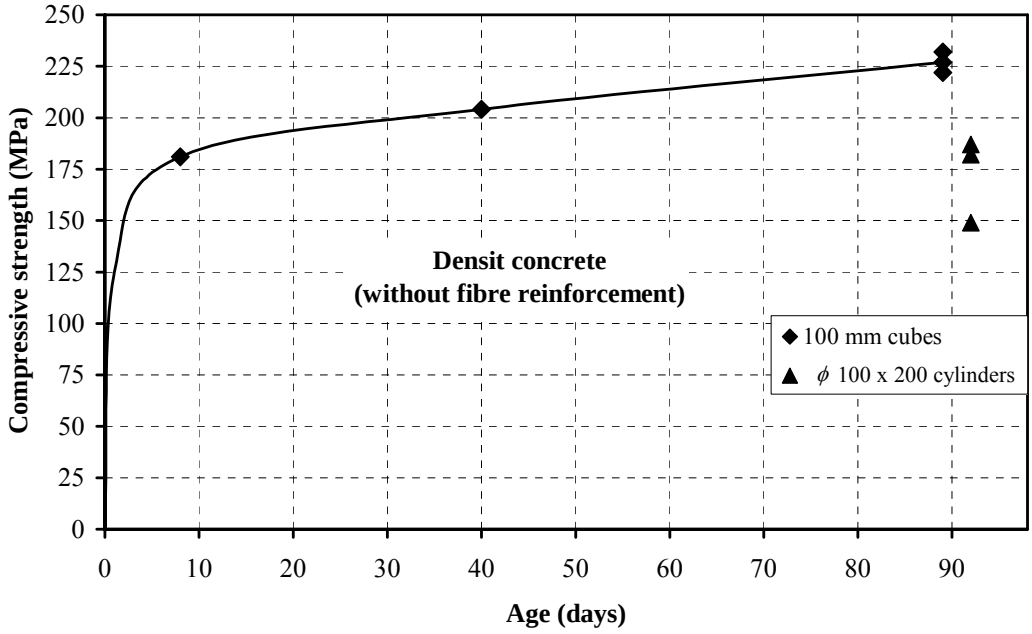

Figure 2.14 Compressive strength development of Densit concrete (without steel fibre reinforcement).

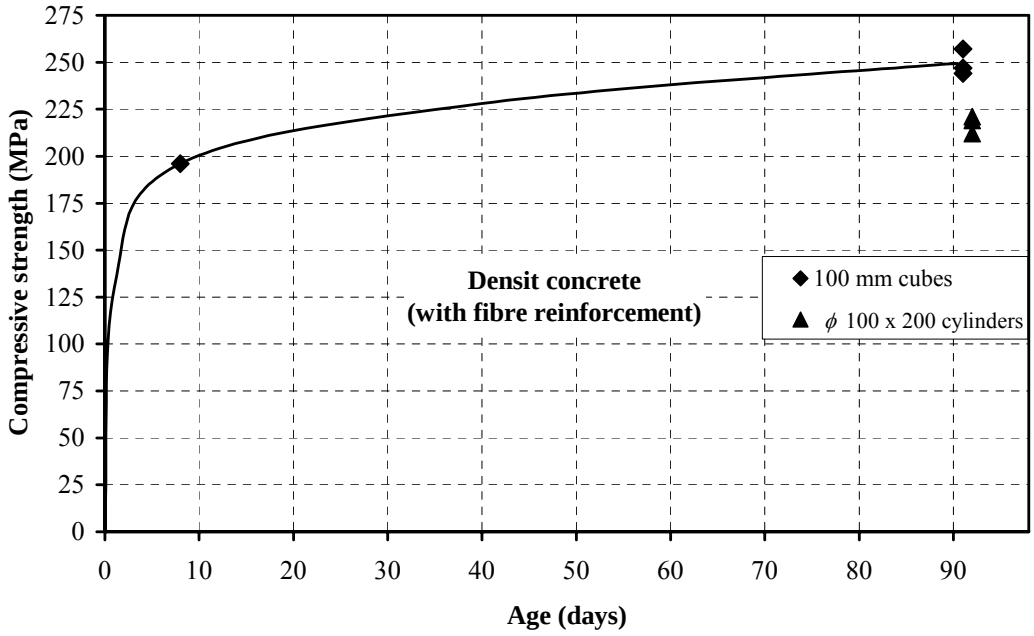

Figure 2.15 Compressive strength development of Densit concrete (with steel fibre reinforcement).

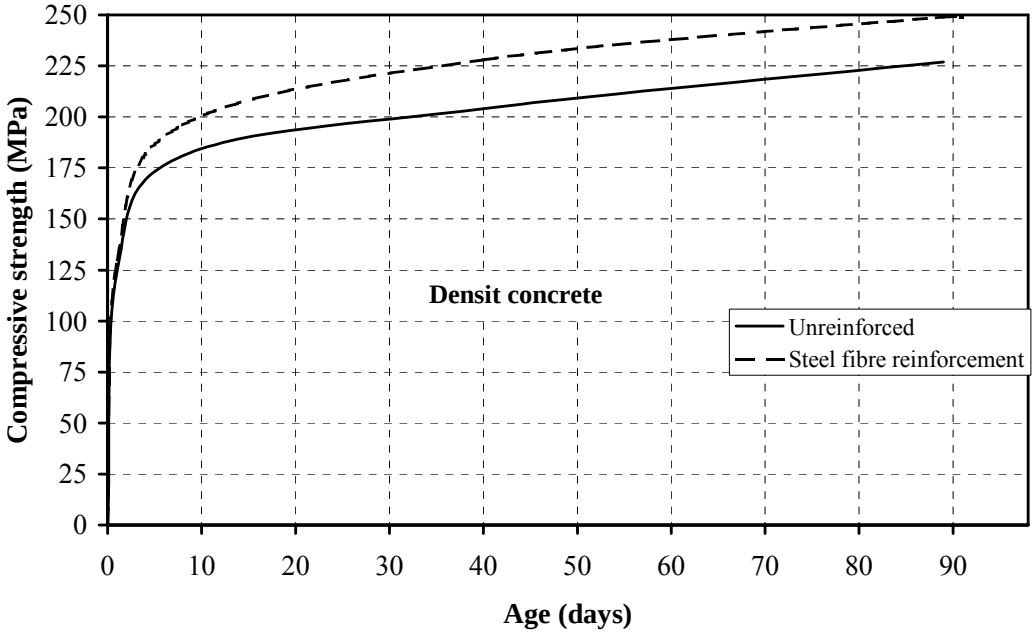

Figure 2.16 Compressive strength development of Densit concrete. Comparison between steel fibre reinforced and unreinforced concrete.

2.3.3 Material characterisation of Optiroc concrete

Triaxial tests were performed at FFI in Norway in October – November 1999 by the use of a GREAC cell method (Gauged REActive Confinement), see /8/. In this type of compression test, the cylindrical concrete samples are confined in a steel cylinder. Measurements are performed on the axial force, on the axial strain and also on the hoop strain on the outside of the steel cylinder. The state of stress and strain in the concrete specimen can then be calculated during the whole loading process by the use of a mathematical model, which describes the behaviour of the steel cylinder. From these data the deviatoric and hydrostatic response can then be calculated. The results of one GREAC test give the whole yield curve along the compressive meridian. The concrete tested was of type Optiroc from test series 1999. Two cylinders of different steel strengths and different cylinder wall thickness were used. The results are presented in the following:

Table 2.14 Specimen of "Optimised normal" concrete tested in GREAC cell by FFI.

Test no	Steel cylinder				Weight of specimen (gram)	Initial length (mm)	Initial density (g/cm^3)	Date of testing
	O.D (mm)	I.D (mm)	Length (mm)	Material				
X	122	76.4	150	Hardened Orvar Supreme	1624	148.1	2.39	November 9, 1999
IX	101.6	76.2	150	High strength steel NS 13411-05	1624	148.7	2.39	October 15, 1999

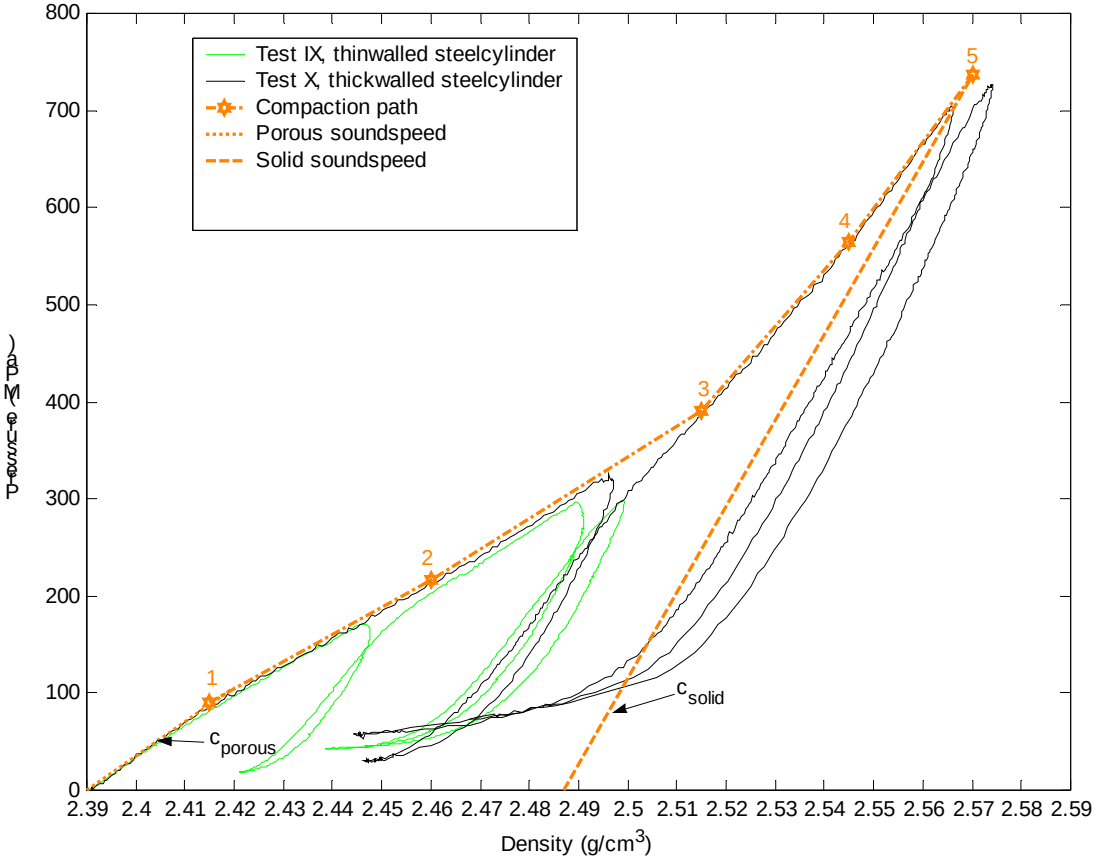

Figure 2.17 Equation of state curve from tests IX and X.

Table 2.15 Equation of state data from test IX and X.

Porous sound velocity		**Solid sound velocity**
$c_p = \sqrt{\frac{dp}{d\rho}} = \sqrt{\frac{105 \cdot 10^6 \, {}^{N}/_{m^2}}{2420 - 2390 \, {}^{Kg}/_{m^3}}} = 1871$ m/s		$c_s = \sqrt{\frac{dp}{d\rho}} = \sqrt{\frac{737 \cdot 10^6 \, {}^{N}/_{m^2}}{2570 - 2487 \, {}^{Kg}/_{m^3}}} = 2980$ m/s
5 point piecewise linear compaction path		
	Density (g/cm^3)	Pressure (MPa)
1	2.415	90
2	2.460	216
3	2.515	390
4	2.545	565
5	2.570	737

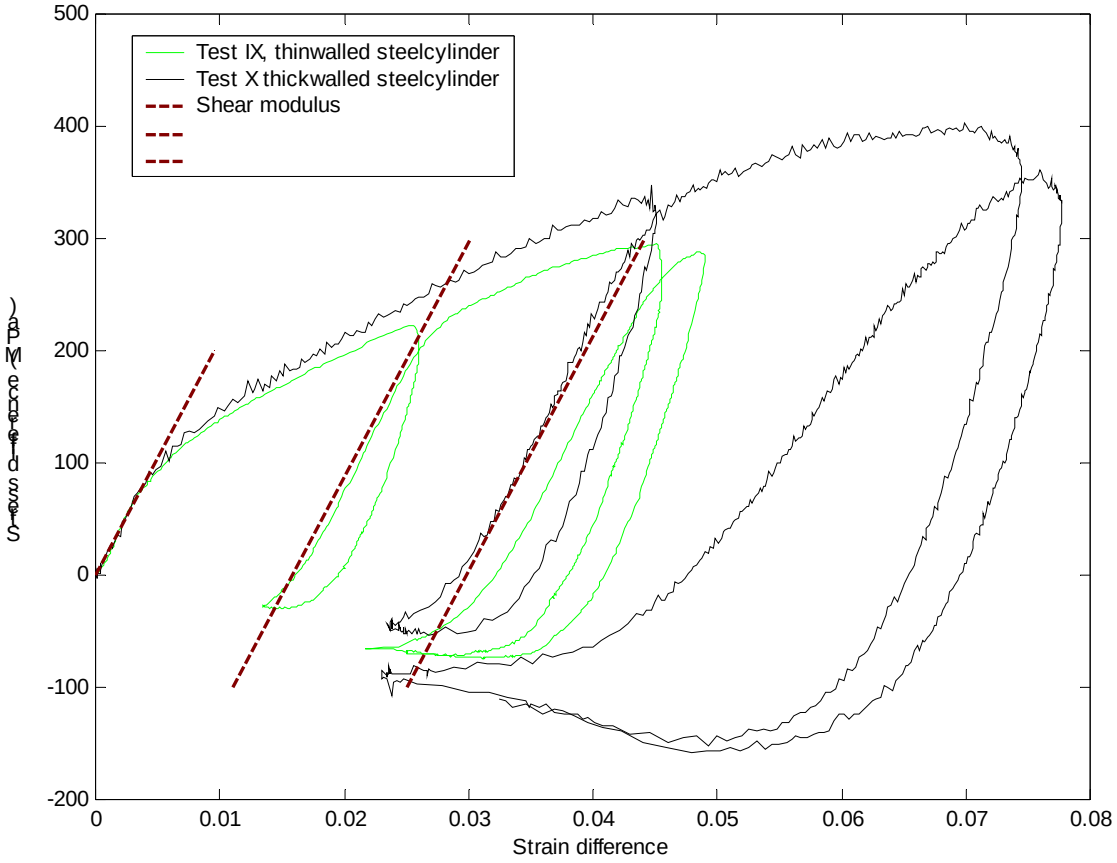

Figure 2.18 Shear curve from tests IX and X.

Table 2.16 Shear data.

Shear modulus
$G = \frac{1}{2}\frac{ds}{de} = 10417$ MPa

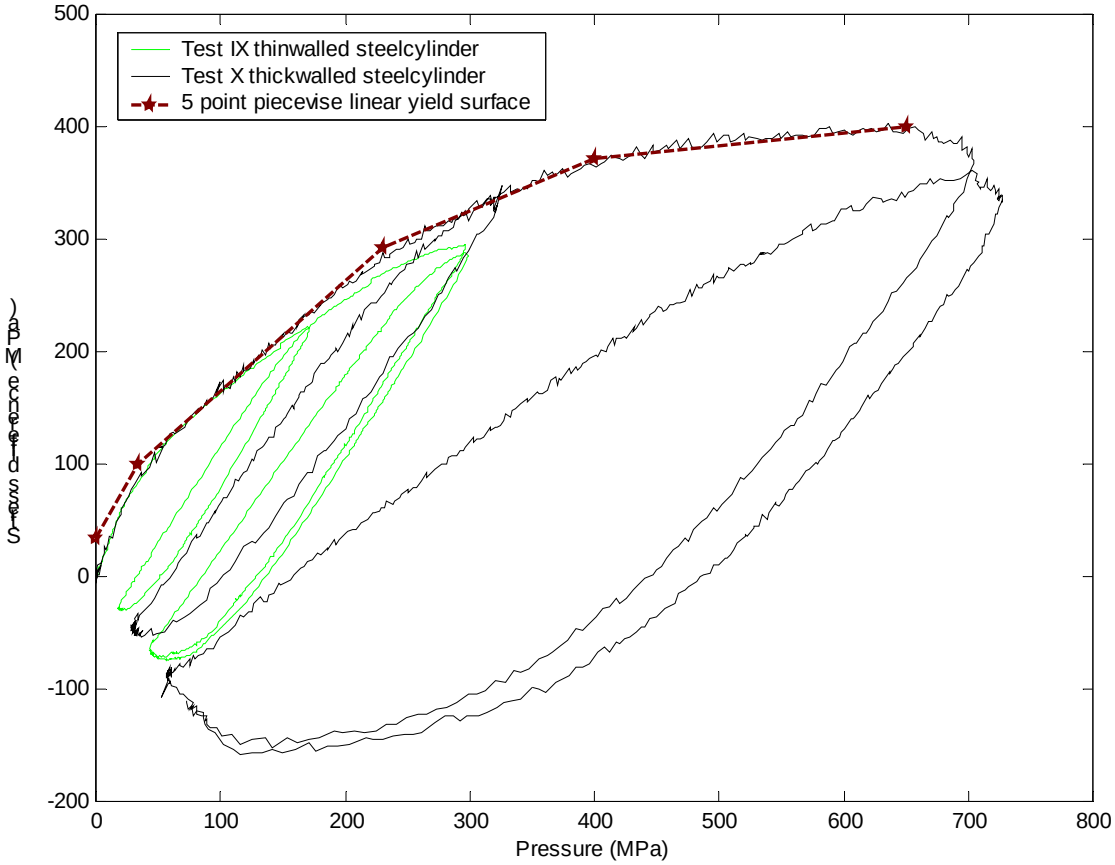

Figure 2.19 Yield curve from tests IX and X.

Table 2.17 Yield data from tests IX and X.

5 point piecewise linear yield surface			
	Pressure (MPa)	Stress difference (MPa)	Hardening slope
1	0	34	
2	33	100	2.00
3	230	292	0.97
4	400	371	0.46
5	650	400	0.12

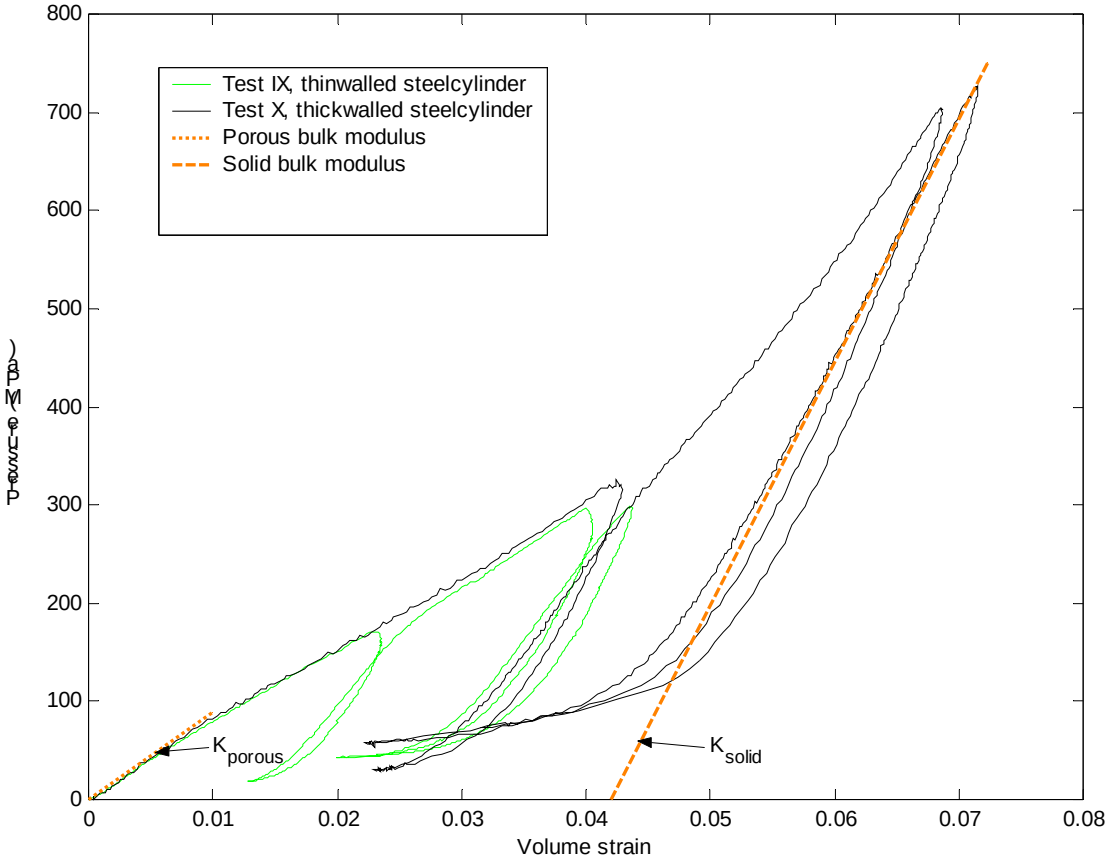

Figure 2.20 Pressure versus volume strain from tests IX and X.

Table 2.18 Volume strain data from tests IX and X.

Porous bulk modulus	**Solid bulk modulus**
8800 MPa	$K_p = \frac{p}{\varepsilon_V} = \frac{750}{0{,}072 - 0{,}042} = 25000$ MPa

2.4 Reinforcement

The effects of reinforcement on the penetration resistance were also studied in this investigation. Targets were cast with volume fractions of conventional reinforcement varying between 1.55 – 25 %. Thus, these targets were extremely reinforced. Figures 2.21 and 2.22 show targets with reinforcement volume fractions of 6 % and 6.5 %, respectively. The heavy reinforcement of CRC concrete is shown in Figure 2.23. One target in test series 1999 was reinforced with some lengths of Swedish rails profile BV 50. The cross section of these rails have a height of 155 mm and a base of 132 mm. The rail bits were welded together in two layers as shown in Figure 2.24 and positioned at the bottom of the cylindrical mould. Figure B56 in Appendix B shows the location of the rails in the target. Figure 2.25, finally, shows the target in test series 1999, which was partly filled with boulders measuring 200 – 400 mm across and with an amount of about 25 % by volume. The layer of boulders was about 400 mm in thickness. Figure B54 in Appendix B shows the location of the boulders. The boulders consisted of granite (about 80 % by volume), gneiss (about 10 % by volume) and diabase (about 10 % by volume). Some of the boulders rose to the concrete surface during casting due to the high density of the concrete.

Figure 2.21 Target 8 of test series 1999. The reinforcement consisted of rebars (ϕ 25 mm) and with a volume fraction of 6 %.

Figure 2.22 Target 7 of test series 1998:2. The reinforcement consisted of rebars (ϕ 32 mm) with a volume fraction of 6.5 %.

Figure 2.23 Reinforcement of CRC concrete. Volume fraction of 25 %.

Figure 2.24 Target 20 in test series 1999. The rails are welded together.

Figure 2.25 Target 19 of test series 1999. Rock boulders measuring 200 – 400 mm across.

3 SPECIMENS AND TEST SET-UPS

A total of six separate test series were performed comprising 62 penetration tests. All of these tests were conducted at the Aborrtjärn shooting range at the Bofors Test Centre in Karlskoga. The cylindrical targets were cast in corrugated steel tubes with a wall thickness of 2 mm. The back stop was a concrete structure covered with steel armour. More details are found in Appendix B regarding specimens and test set-up.

3.1 Test series 1996:1

The first test series was performed on June 18, 1996. The shooting range was approximately 100 m and a Doppler radar positioned near the gun muzzle was used to track the velocity history of the projectile until impact. A plan and elevation view of the test set-up is shown in Figure 3.1. A more detailed description of the set-up of each test is given in Appendix B. Four square shaped concrete slabs assembled by tension bolts were tested in this test series, see Table 3.1. In the second column where the target dimensions are listed, the parentheses denote that the actual target consisted of a number of concrete slabs held together in some way. Thus, '□ 200 × (5 × 20)' in Table 3.1 denotes a square target with each side measuring 200 cm and that the target consisted of five separate slabs, each slab with a thickness of 20 cm.

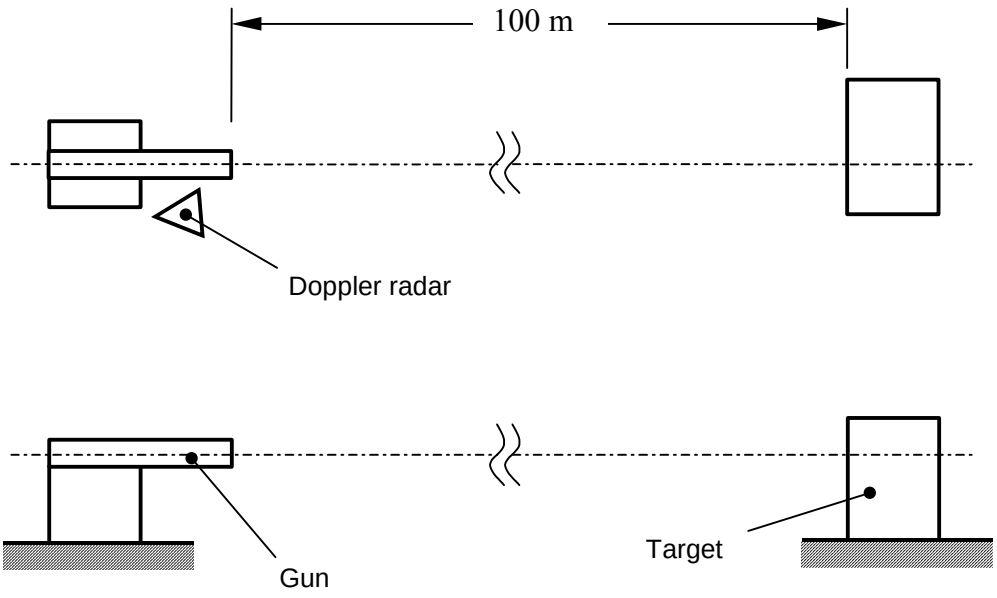

Figure 3.1 Plan and elevation view of the test set-up for test series 1996:1.

Table 3.1 Target specifications for test series 1996:1.

Target no	Target dimensions (diameter × length) (cm)	Nominal f_{cc} (MPa)	Real f_{cc} (MPa)	Reinforcement volume fraction	Calibre of projectile (mm)	Remarks
1	□ 200 × (5 × 20)	200	~ 180	2.7 % steel fibres	43	-
2	□200 × (10 × 20)	30	~ 30	-	43	-
3	□200 × (10 × 20)	200	~ 180	2.7 % steel fibres	43	The 5 panels of target 1 was used in this test
4	□ 64 × (6 × 20)	200	~ 220	ϕ25 mm rebars 25 % and 2 % steel fibres	43	-

The weapon loading applied to the targets was achieved by:

- 105 mm-calibre gun from the Swedish tank model strv 103 on a mount, see Figure 3.2.
- 57 mm-calibre armour-piercing sabot discarding projectile with a 43 mm-calibre penetrator at a nominal impact velocity of 1400 m/s, see Figure 3.3 and Appendix A.

Figure 3.2 The 105-mm calibre gun and Doppler radar used for test series 1996:1.

Figure 3.3 The 57-mm-calibre armour-piercing sabot discarding projectile with a 43 mm-calibre penetrator used in test series 1996:1.

3.2 Test series 1996:2

The second test series was performed on December 5, 1996. The shooting range was approximately 100 m. A Doppler radar placed near the gun muzzle was used to track the velocity history of the projectile until impact. A high-speed camera gave a side view of the target and captured the residual velocity of the projectile. A white board was used as background for the high-speed camera to enhance the contour of the impacting projectile. A plan and elevation view of the test set-up is shown in Figure 3.4. Four square concrete slabs assembled by tension bolts were tested in this test series. The targets were cast with four different types of concrete and reinforcement, see Table 3.2.

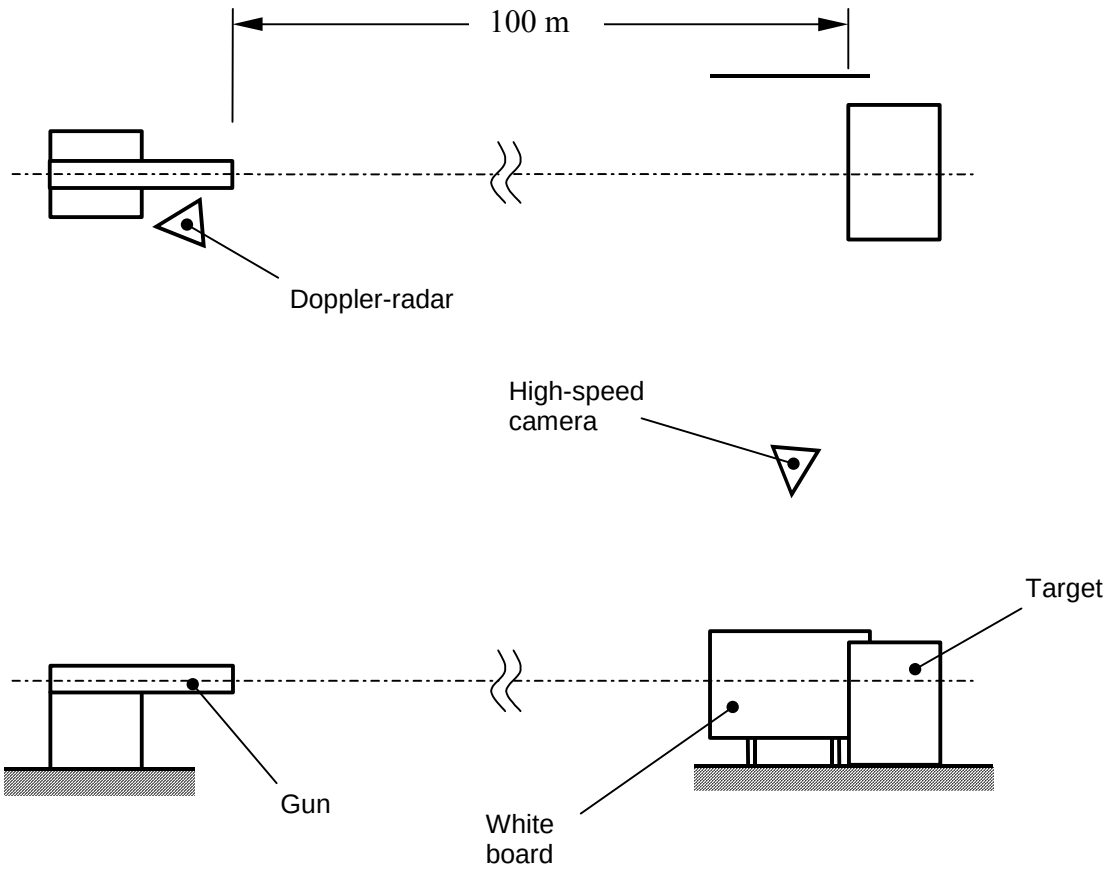

Figure 3.4 Plan and elevation view of the test set-up for test series 1996:2.

Table 3.2 Target specifications for test series 1996:2.

Target no	Target dimensions (diameter × length) (cm)	Nominal f_{cc} (MPa)	Real f_{cc} (MPa)	Reinforcement volume fraction	Calibre of projectile (mm)	Remarks
1	□ 150 × (4 × 20)	200	>250	steel fibres	152	No back stop
2	□ 150 × (5 × 20)	30	36	-	152	No back stop
3	□ 150 × (5 × 20)	200	180	ϕ 25 mm rebars 25 % and 4 % steel fibres	152	No back stop
4	□ 150 × (5 × 20)	200	220	2.6 % steel fibres	152	No back stop

The weapon loading applied to the targets was achieved by

- 152-mm-calibre gun mount, see Figure 3.5.
- 152-mm-calibre semi-armour-piercing grenade at a nominal impact velocity of 480 m/s, see Figure 3.5, 3.6 and Appendix A.

(a)

(b)

Figure 3.5: (a) The 152-mm calibre gun used in test series 1996:2.
(b) 152-mm semi-armour-piercing grenade used in test series 1996:2.

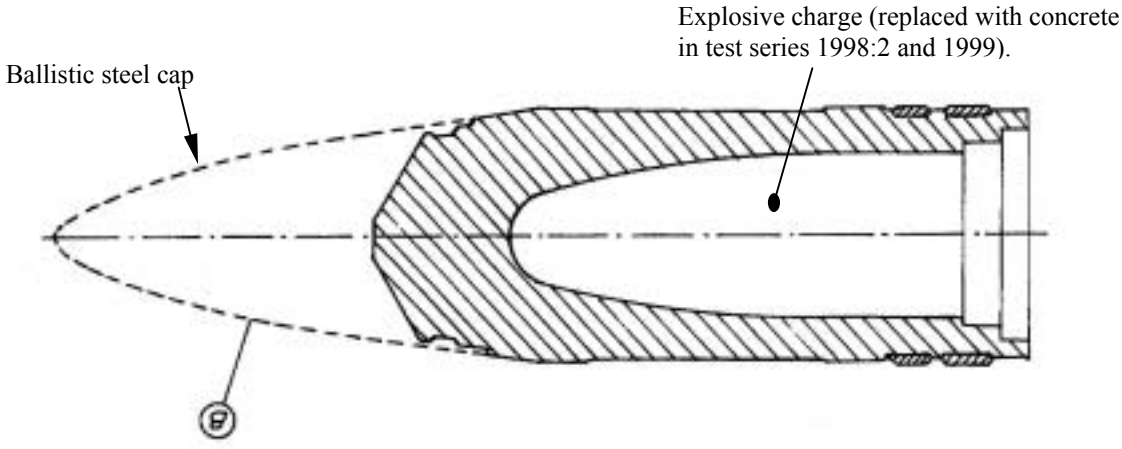

Figure 3.6 Cross section of a 152 mm semi-armour-piercing grenade.

3.3 Test series 1997

This test series was performed on November 25, 1997. The shooting range was approximately 100 m and a Doppler radar placed near the gun muzzle was used to track the velocity history for the projectile until impact. Three high-speed cameras captured the penetration process and the residual velocity of the projectile. A white board was used as background for the high-speed cameras to enhance the contour of the impacting projectile. A plan and elevation view of the test set-up is shown in Figure 3.7. Six cylindrical targets and one square target were tested in this test series, see Table 3.3.

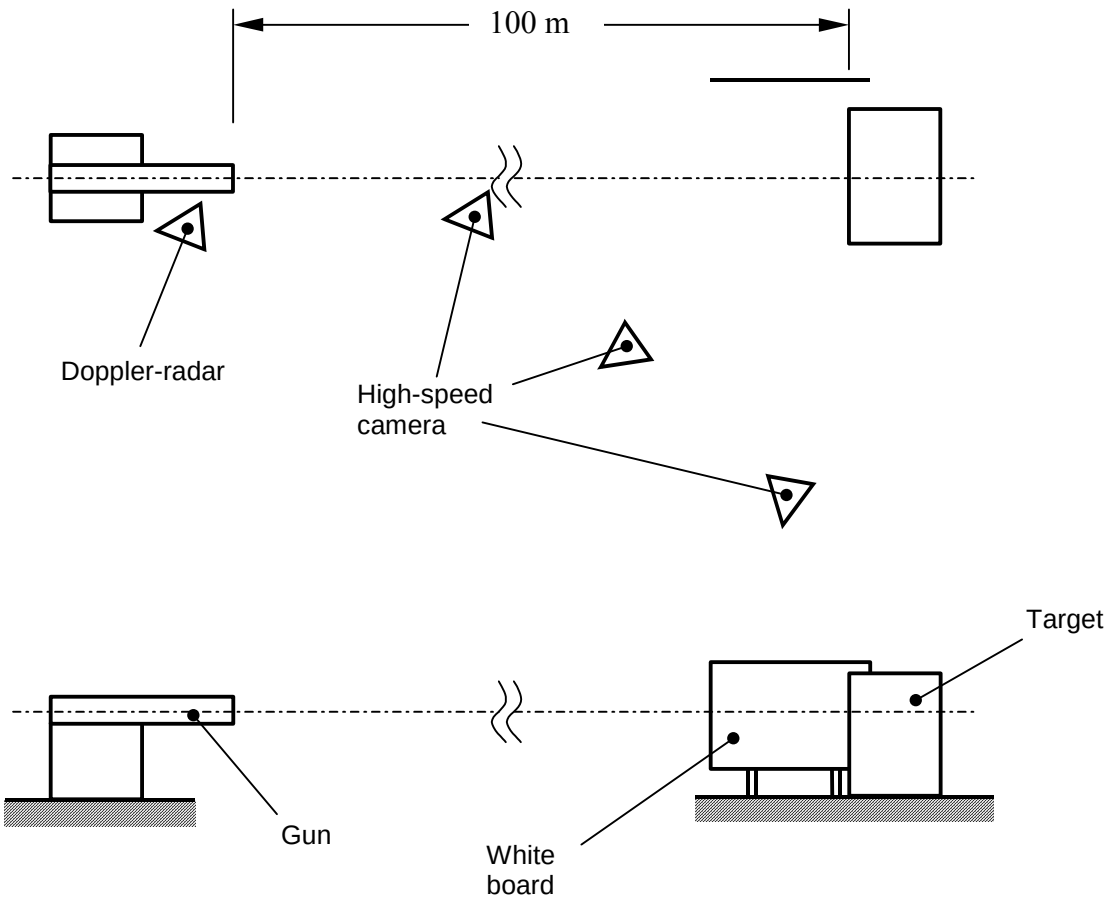

Figure 3.7 Plan and elevation view of the test set-up for test series 1997.

Table 3.3 Target specifications for test series 1997.

Target no	Target dimensions (diameter × length) (cm)	Nominal f_{cc} (MPa)	Real f_{cc} (MPa)	Reinforcement volume fraction	Calibre of projectile (mm)	Remarks
1	ϕ 160 × (10 × 20)	30	38	-	75	Back stop
2	□ 150 × (5 × 20)	200	~ 200	2 % steel fibres	75	Back stop
3	ϕ 160 × 200	30	38	-	75	Back stop
4	ϕ 160 × 200	30	38	-	75	-
5	ϕ 160 × 100	200	180	2 % steel fibres	75	Back stop
6	ϕ 160 × 100	200	180	2 % steel fibres	75	Back stop. Target no 5 used (turned backwards)
7	ϕ 160 × 50	200	180	2 % steel fibres	75	Back stop

The weapon loading applied to the targets was achieved by:

- 75-mm-calibre gun mount, see Figure 3.8.
- 75-mm-calibre armour-piercing projectile at a nominal impact velocity of 480 m/s, see Figure 3.8 and Appendix A.

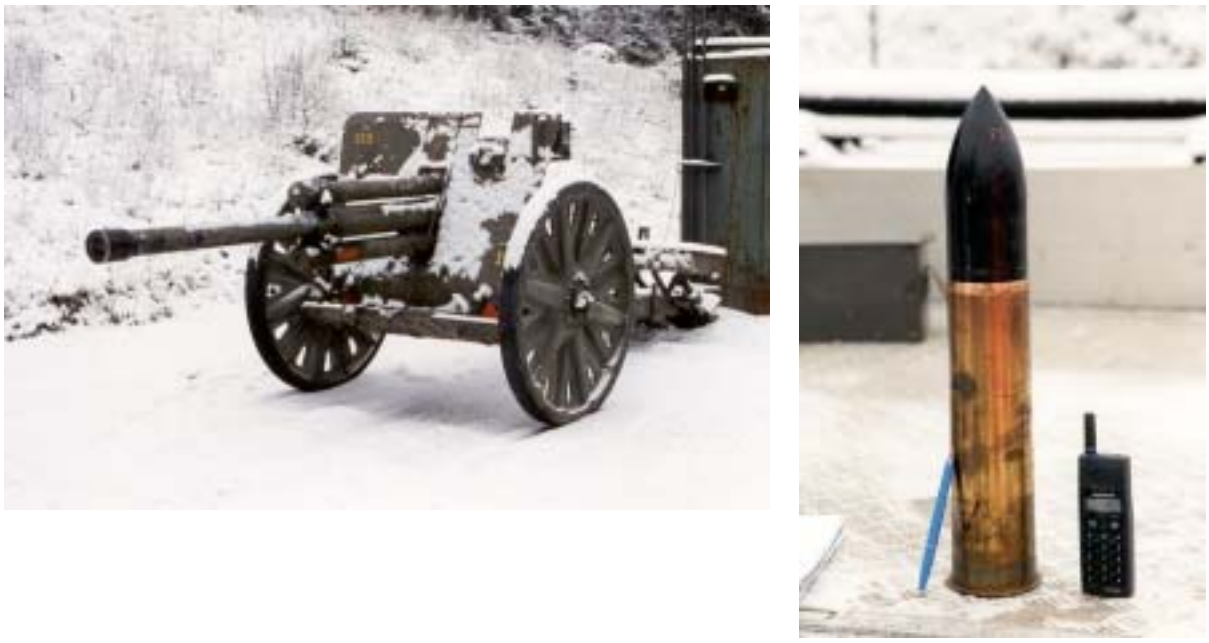

Figure 3.8 The 75-mm-calibre gun and the 75-mm-calibre armour-piercing projectile and case used in test series 1997.

3.4 Test series 1998:1

This test series was performed on April 21, 1998. The shooting range was approximately 100 m and a Doppler radar placed near the gun muzzle was used to track the velocity history of the projectile until impact. Two high-speed cameras captured the penetration process. A plan and elevation view of the test set-up is shown in Figure 3.9. Seven cylindrical targets and two square targets were tested in this test series, see Table 3.4.

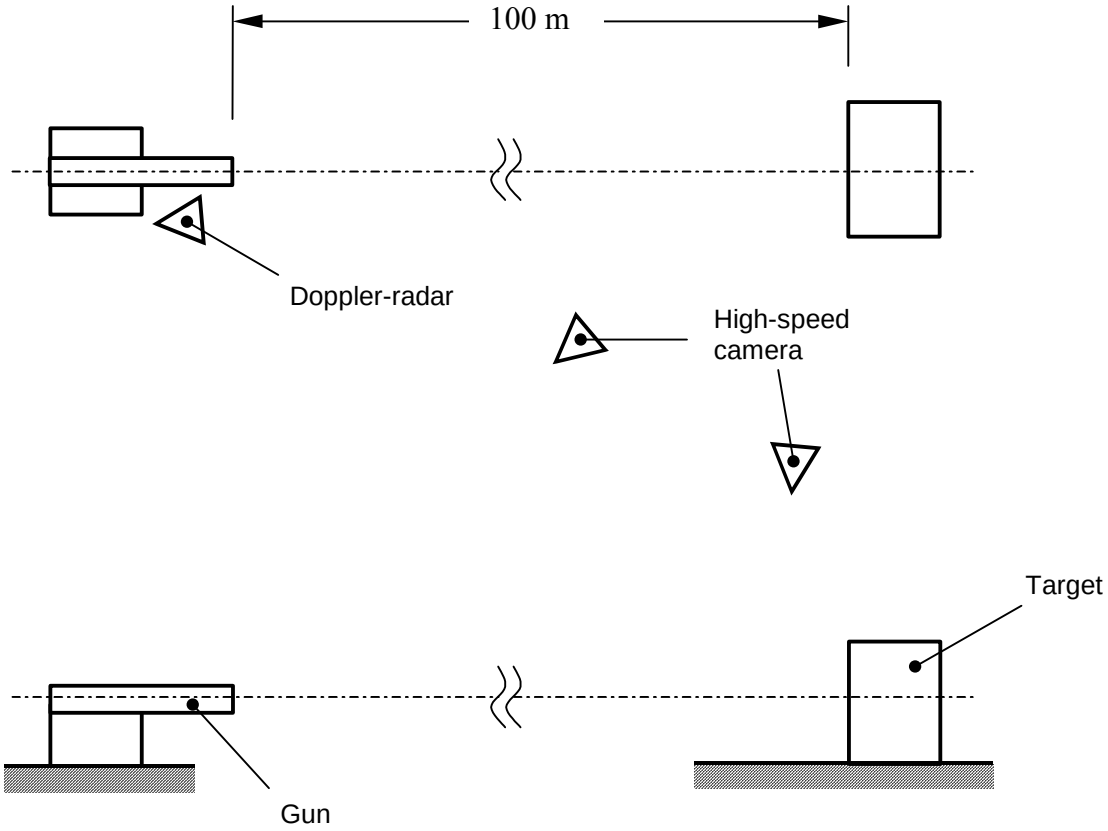

Figure 3.9 Plan and elevation view of the test set-up for test series 1998:1

Table 3.4 Target specifications for test series 1998:1.

Target no	Target dimensions (diameter × length) (cm)	Nominal f_{cc} (MPa)	Real f_{cc} (MPa)	Reinforcement volume fraction	Calibre of projectile (mm)	Remarks
1	ϕ 160 × 300	30	41	-	152	Back stop
2	ϕ 220 × (5×20)	200	> 250	steel fibres	152	Back stop
3	□ 150 × 100	200	200	ϕ 25 mm rebars 7 % and 1.5 % steel fibres	152	Back stop
4	□ 150×(2×100)	30	34	ϕ 25 mm rebars 7 %	152	Back stop
5	ϕ 160 × 120	200	203	-	152	Back stop
6	ϕ 160 × 100	200	199	1.5 % steel fibres	152	Back stop
7	ϕ 160 × 150	90	90	-	152	Back stop
9*	ϕ 160 × 150	90	108	1 % steel fibres	152	Back stop
10	ϕ 160 × 150	90	83	1.5 % steel fibres	152	Back stop

* = target no 8 was not tested

The weapon loading applied to the targets was achieved by

- 152-mm-calibre gun, see Figure 3.5.
- 152-mm-calibre semi-armour-piercing grenade at a nominal impact velocity of 480 m/s, see Figure 3.5 and Appendix A.

3.5 Test series 1998:2

This test series was performed on October 26 – 27, 1998. The shooting range was approximately 100 m and a Doppler radar placed near the gun muzzle was used to track the velocity history of the projectile until impact. A high-speed camera gave a side view of the target and captured the residual velocity of the projectile. A plan and elevation view of the test set-up is shown in Figure 3.10. Eleven cylindrical targets and two square targets were tested in this test series, see Table 3.5.

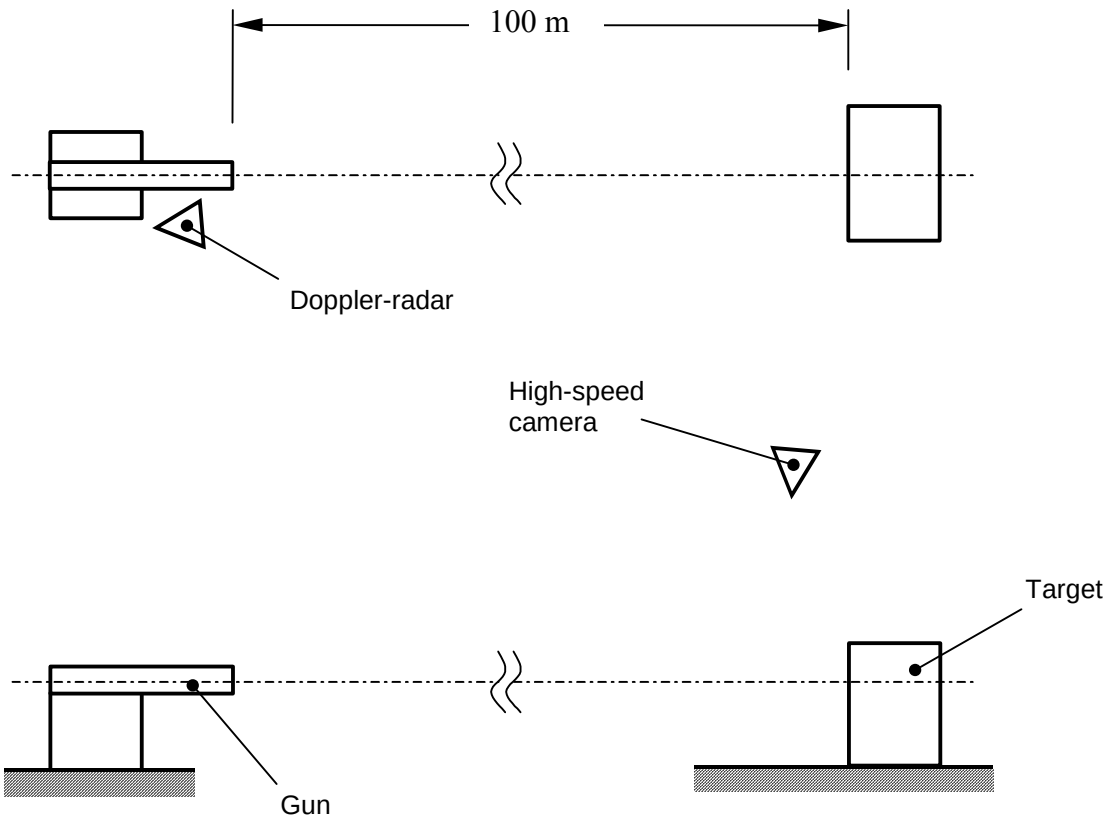

Figure 3.10 Plan and elevation view of test set-up for test series 1998:2

Table 3.5 Target specifications for test series 1998:2.

Target no	Target dimensions (diameter × length) (cm)	Nominal f_{cc} (MPa)	Real f_{cc} (MPa)	Reinforcement volume fraction	Calibre of projectile (mm)	Remarks
1	ϕ 160 × 300	30	36	-	152	Back stop
2	ϕ 160 × 150	90	~ 90	-	152	Back stop
3	ϕ 160 × 150	150	141	1 % steel fibres	152	Back stop
4	ϕ 160 × 150	200	183	2 % steel fibres	152	Back stop
5	ϕ 160 × 300	30	41	-	152	Back stop. Target no 1 from test series 1998:1
6	ϕ 160 × 120	150	141	1 % steel fibres	152	Back stop
7	□ 150 × 120	150	141	ϕ 32 mm rebars 6.5 % and 1 % steel fibres	152	Back stop
8	ϕ 160 × 200	30	38	-	75	Back stop. Target no 3 from test series 1997
9	ϕ 160 × 150	90	108	1 % steel fibres	75	Back stop. Target no 9 from test series 1998:1
10	ϕ 160 × 120	150	141	1 % steel fibres	75	Back stop
11	□ 150 × (4 × 20)	200	~ 200	2 % steel fibres	75	Back stop
12	ϕ 160 × 150	90	83	1.5% steel fibres	75	Back stop
13	ϕ 160 × 150	150	134	-	152	Back stop

The weapon loading applied to targets 1 – 7 and 13 was achieved by:

- 152-mm-calibre gun, see Figure 3.5.
- 152-mm-calibre semi-armour-piercing grenade at nominal impact velocities of 480 m/s and 580 m/s, see Figure 3.5 and Appendix A. The explosive charge was removed and replaced by concrete.

The weapon loading applied to targets 8 – 12 was achieved by:

- 75-mm-calibre gun, see Figure 3.2.
- 75-mm-calibre armour-piercing projectile at a nominal impact velocity of 580 m/s and 660 m/s, see Figure 3.8 and Appendix A. The explosive charge was removed and replaced by concrete.

3.6 Test series 1999

This test series was performed on October 5 – 7, 1999. The shooting range was approximately 100 m and a Doppler radar placed near the gun muzzle was used to track the velocity history of the projectile until impact. High-speed cameras gave a side view of the target and captured the residual velocity of the projectile. A plan and elevation view of the test set-up is shown in Figure 3.11. Twenty-five cylindrical targets were tested specified in Table 3.6. Rock boulders measuring 200 – 400 mm across were added to target 19. Target 20 was reinforced with Swedish steel-rail profile BV 50. A more detailed description of the rock boulders and the rails is given above in section 2.4.

The 43-mm penetrator was used in this test series in order to perform a dimensional analysis on empirical equations by FFI in Norway. A large number of these equations exist for penetration prediction into concrete.

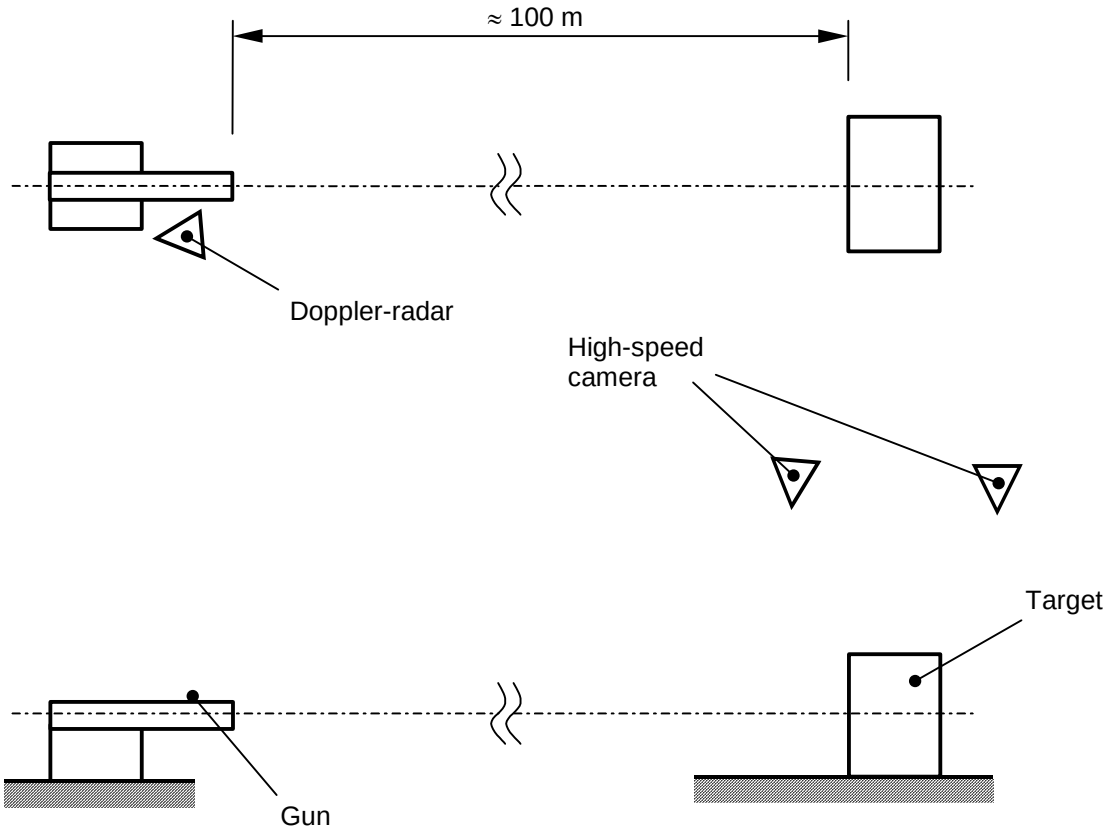

Figure 3.11 Plan and elevation view of test set-up for test series 1999.

Table 3.6 Target specifications for test series 1999.

Target no	Target dimensions (diameter × length) (cm)	Nominal f_{cc} (MPa)	Real f_{cc} (MPa)	Reinforcement volume fraction	Calibre of projectile (mm)	Remarks
1	ϕ 140 × 80	150	153	-	75	Back stop
2	ϕ 140 × 80	150	153	-	75	Back stop
3	ϕ 140 × 80	150	153	-	75	Back stop
4	ϕ 140 × 40	150	153	-	75	Back stop
5	ϕ 140 × 40	150	153	-	75	Back stop
6	ϕ 140 × 40	150	153	-	75	Back stop
7	ϕ 140 × 40	150	153	ϕ 25 mm rebars 6 %	75	Back stop
8	ϕ 140 × 40	150	153	ϕ 25 mm rebars 6 %	75	Back stop
9	ϕ 140 × 40	150	153	ϕ 25 mm rebars 6 %	75	No back stop

Target no	Target dimensions (diameter × length) (cm)	Nominal f_{cc} (MPa)	Real f_{cc} (MPa)	Reinforcement volume fraction	Calibre of projectile (mm)	Remarks
10	ϕ 140 × 300	30	39	-	43	Back stop
11	ϕ 140 × 250	150	149	-	43	Back stop
12	ϕ 140 × 200	150	158	-	43	Back stop
13	ϕ 160 × 200	30	39	-	152	Back stop
14	ϕ 240 × 200	30	39	-	152	Back stop
15	ϕ 100 × 120	150	153	-	152	Back stop
16	ϕ 160 × 120	150	153	-	152	Back stop
17	ϕ 240 × 120	150	149	-	152	Back stop
18	ϕ 300 × 120	150	149	-	152	Back stop
19	ϕ 160 × 150	150	149	rock boulders	152	Back stop
20	ϕ 160 × 150	150	149	rails	152	Back stop
21	ϕ 160 × 120	140	120	1 % steel fibres	152	Back stop
22	ϕ 160 × 120	140	120	ϕ 25 mm rebars 1.55 % and 1% steel fibres	152	Back stop
23	ϕ 240 × 75	90	103	-	152*	Back stop
24	ϕ 240 × 75	90	103	-	152**	Back stop
25	ϕ 240 × 75	90	103	-	152**	Back stop

* = new projectile nose

** = new projectile nose and accelerometer instrumentation

The weapon loading applied to targets 1 – 9 was achieved by:

- 75-mm-calibre gun, see Figure 3.8.
- 75-mm-calibre armour-piercing projectile at a nominal impact velocity of 620 m/s, see Figure 3.8 and Appendix A.

The weapon loading applied to targets 10 – 12 was achieved by:

- 105-mm-calibre gun from the Swedish tank model strv103 on a mount, see Figure 3.2.
- 57-mm-calibre armour-piercing sabot discarding projectile with a 43-mm calibre penetrator at a nominal impact velocity of 1400 m/s. Target 12 was tested with this projectile at a nominal impact velocity of 1000 m/s, see Figure 3.3 and Appendix A.

The weapon loading applied to targets 13 – 22 was achieved by:

- 152-mm-calibre gun mount, see Figure 3.5.
- 152-mm-calibre semi-armour-piercing grenade at nominal impact velocities of 470 m/s for targets 13 – 18 and 21 – 22, and nominal impact velocities of 580 m/s for targets 19 – 20, see Figure 3.5 and Appendix A. The explosive charge was removed and replaced by concrete.

The weapon loading applied to targets 23 – 25 was achieved by:

- 152-mm calibre gun mount, see Figure 3.5.
- modified 152-mm-calibre semi-armour-piercing grenade at nominal impact velocities of 460 m/s, see Figure 3.12.

The three last tests in this test series were performed as a governmental collaboration between FOA, FFI (Norway), DERA (UK) and TNO (the Netherlands). The purpose of this collaboration was to obtain data for numerical simulations. FOA was responsible for target manufacturing, the tests on the firing range and uniaxial static material tests. FFI designed the modified penetrators and manufactured them, see further /8/. Triaxial static material tests were also performed at FFI as described earlier in section 2.3.3. The projectile instrumentation was performed by DERA and the target instrumentation with carbon resistor pressure probes were provided by TNO.

For two targets (i.e. targets 24 – 25), the modified projectiles were equipped with an instrument package that registered the acceleration history in one direction. A separate capsule was developed as housing for the instruments consisting of an accelerometer, a data recorder and a battery, see further /5/. The capsule was installed in the nose section of the modified penetrator by DERA in the UK, see Figures 3.12 and 3.13. The data recorder and the battery were ‘floating’ in glass beads while the accelerometer was fixed to the capsule. Target 23 was tested with the same modified penetrator but without instrumentation. This was performed in order to ensure that no cables would be disrupted due to the spinning of the penetrator.

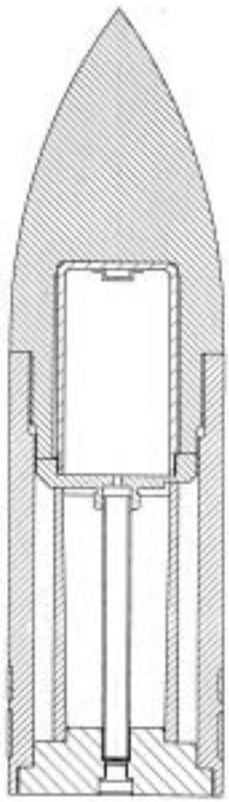

Figure 3.12 Modified 152-mm-calibre semi-armour-piercing grenade with a new nose section used for targets 23 – 25 in test series 1999, see /8/. A separate capsule containing instruments for acceleration measurements was positioned in the nose section.

Figure 3.13 Disassembled modified 152 mm-calibre projectile used in test-series 1999.

The pressure in the concrete was measured in targets 24 – 25 by the use of carbon resistor pressure probes, one probe in each target. These probes were provided by TNO and enables measurements of the mean pressure. A carbon resistor is embedded in epoxy and then connected to a bridge amplifier, see Figure 3.14. Two 9-Volt batteries provide the electricity for the bridge amplifier. A 300-mm deep hole with a diameter of 8 mm was drilled on the back surface of each target and on its central axis. The probe was then positioned in the hole in such a way that the end with the carbon resistor ended up 300 mm from the back surface into the target. A two-component resin was finally poured into the hole with the pressure probe and then allowed to cure for 5 days at room temperature. For triggering of the measurement system, a trigger board was positioned on the front surface of each target. An oscilloscope of type LeCroy was used to record the registrations and sampling rates of 250 MS/s and 100 MS/s were chosen for targets 24 and 25, respectively. Figure 3.15 illustrates the principal instrumentation of the measurement system.

Figure 3.14 Carbon resistor pressure probe provided by TNO.

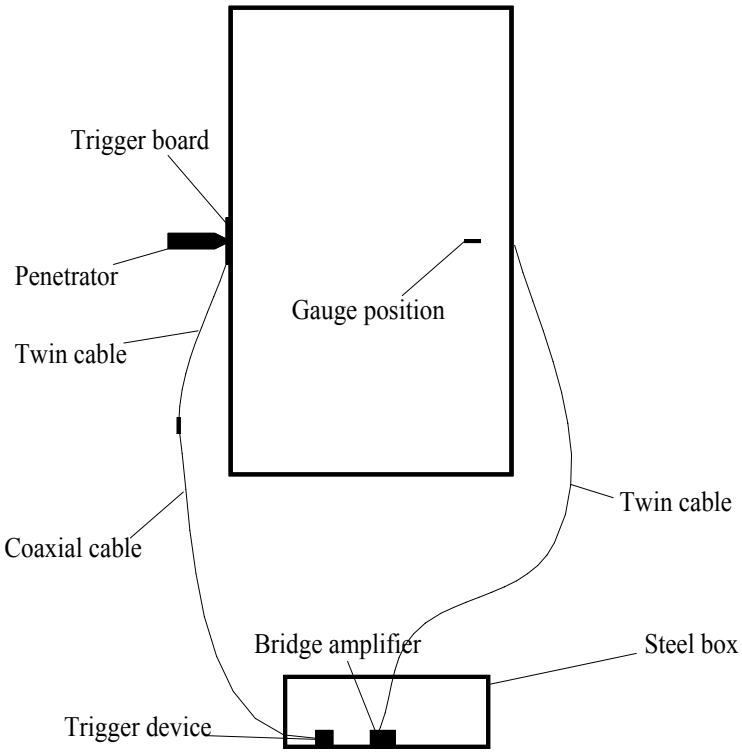

Figure 3.15 Instrumentation of targets 24 and 25.

4 TEST RESULTS

The test results from all tests are presented below and in a number of Appendices. Target specific comments are given in Appendix C for each test series and Appendix D presents post test target configurations. Doppler radar data are found in Appendix E, and pressure gauge registrations and projectile acceleration registrations are found in Appendices F and G, respectively.

The results of all test series conducted at Bofors during the years 1996 – 1999 are presented in Tables 4.1 – 4.3 where targets are listed with respect to concrete strength. The concrete strengths specified in these tables refer to tests of different specimen geometries. Conversions of the results were not performed because the formulas available are not valid for HPC. Also, each of these tables presents the result of one type of penetrator. In the second column where the target dimensions are listed, the parentheses denote that the actual target consisted of a number of concrete slabs held together in some way. Thus, '□ 200 × (10 × 20)' in Table 4.1 denotes a square target with each side measuring 200 cm and that the target consisted of ten separate slabs, each slab with a thickness of 20 cm. Evaluations and discussions of the results from the penetration tests are given in the following.

Table 4.1 Results of tests with a 43-mm penetrator. Targets listed with respect to compressive strength.

Test series - target no	Target dimensions (diameter× length) (cm)	f_{cc} (MPa)	Concrete type	Reinforcement volume fraction	Penetration depth (m)	Impact velocity (m/s)	Residual velocity (m/s)	Entrance crater (diameter/ depth) (m)	Exit crater (diameter/ canal) (m)
1996:1-2	□ 200 × (10 × 20)	~ 30	NSC	-	perforation	1394	-	-	-
1999-10*	ϕ 140 × 300	39	NSC	-	2.62	1364	-	1.30/0.30	-
1999-11*	ϕ 140 × 250	149	Abetong 1	-	1.35	1387	-	1.10/0.40	-
1999-12*	ϕ 140 × 200	158	Abetong 3	-	0.76	985	-	0.80/0.50	-
1996:1-1	□ 200 × (5 × 20)	~ 180	Densit	2.7 % steel fibres	perforation	1380	-	-	-
1996:1-3	□ 200 × (10 × 20)	~ 180	Densit	2.7 % steel fibres	1.25	1394	-	-	-
1996:1-4	□ 64 × (6 × 20)	~ 220	CRC	ϕ 25 mm rebars 25 % and 2 % steel fibres	0.52	1391	-	-	-

f_{cc} = concrete compressive strength

* = back stop

Table 4.2 Results of tests with a 75-mm penetrator. Targets listed with respect to compressive strength.

Test series - target no	Target dimensions (diameter×length) (cm)	f_{cc} (MPa)	Concrete type	Reinforcement volume fraction	Penetration depth (m)	Impact velocity (m/s)	Residual velocity (m/s)	Entrance crater (diameter/ depth) (m)	Exit crater (diameter/ canal) (m)
1997-1*	ϕ 160 × (10 × 20)	38	NSC	-	0.68	484	-	0.65/-	-
1997-3*	ϕ 160 × 200	38	NSC	-	0.66	483	-	0.75/-	-
1997-4	ϕ 160 × 200	38	NSC	-	0.66	482	-	0.75/-	-
1998:2-8*	ϕ 160 × 200	38	NSC 3	-	0.99	647	-	-	-
1998:2-12*	ϕ 160 × 150	83	Abetong	1.5 % steel fibres	0.41	571	-	-	-
1998:2-9*	ϕ 160 × 150	108	Optiroc	1 % steel fibres	0.56	653	-	-	-
1998:2-10*	ϕ 160 × 120	141	Trondheim 1	1 % steel fibres	0.44	647	-	-	-
1999-4*	ϕ 140 × 40	153	Abetong 2	-	perforation	615	276	0.85/0.15	0.90/ϕ0.30
1999-5*	ϕ 140 × 40	153	Abetong 2	-	perforation	618	303	0.85/0.20	0.90/ϕ0.27
1999-6*	ϕ 140 × 40	153	Abetong 2	-	perforation	612	293	0.80/0.20	0.80/ϕ0.25
1999-1*	ϕ 140 × 80	153	Abetong 2	-	0.45	620	-	0.90/0.30	-
1999-2*	ϕ 140 × 80	153	Abetong 2	-	0.54	612	-	0.90/0.26	-
1999-3*	ϕ 140 × 80	153	Abetong 2	-	0.51	619	-	0.85/0.21	-

Table 4.2 continued

Test series - target no	Target dimensions (diameter×length) (cm)	f_{cc} (MPa)	Concrete type	Reinforcement volume fraction	Penetration depth (m)	Impact velocity (m/s)	Residual velocity (m/s)	Entrance crater (diameter/ depth) (m)	Exit crater (diameter/ canal) (m)
1999-7*	ϕ 140 × 40	153	Abetong 2	ϕ 25 mm rebars 6 %	perforation	617	-	0.85/0.06	0.65/-
1999-8*	ϕ 140 × 40	153	Abetong 2	ϕ 25 mm rebars 6 %	perforation	616	-	0.75/0.06	0.65/-
1999-9	ϕ 140 × 40	153	Abetong 2	ϕ 25 mm rebars 6 %	perforation	619	260	0.75/0.08	0.85/-
1997-5*	ϕ 160 × 100	180	Densit 2	2 % steel fibres	0.25	485	-	0.60/-	-
1997-6*	ϕ 160 × 100	180	Densit 2	2 % steel fibres	0.24	489	-	0.60/-	-
1997-7*	ϕ 160 × 50	180	Densit 2	2 % steel fibres	0.24	485	-	0.50/-	-
1997-2*	□ 150 × (5 × 20)	~ 200	Densit 1	2 % steel fibres	0.20	480	-	0.50/-	-
1998:2-11*	□ 150 × (4 × 20)	~ 200	Densit 2	2 % steel fibres	0.44	650	-	-	-

f_{cc} = concrete compressive strength

* = back stop

Table 4.3 Results of tests with a 152-mm penetrator. Targets listed with respect to compressive strength.

Test series - target no	Target dimensions (diameter× length) (cm)	f_{cc} (MPa)	Concrete type	Reinforcement volume fraction	Penetration depth (m)	Impact velocity (m/s)	Residual velocity (m/s)	Entrance crater (diameter/ depth) (m)	Exit crater (diameter/ canal) (m)
1998:1-4*	□ 150 × (2 × 100)	34	NSC 2	ϕ 25 mm rebars 7 %	0.67	481	-	-	-
1996:2-2	□ 150 × (5 × 20)	36	NSC	-	perforation	478	160	-	-
1998:2-1*	ϕ 160 × 300	36	NSC 1	-	1.70	576	-	-	-
1999-13*	ϕ 160 × 200	39	NSC	-	1.09	466	-	1.00/0.58	-
1999-14*	ϕ 240 × 200	39	NSC	-	1.01	468	-	1.40/0.50	-
1998:1-1*	ϕ 160 × 300	41	NSC 1	-	1.03	468	-	-	-
1998:2-5*	ϕ 160 × 300	41	NSC 2	-	1.02	481	-	-	-
1998:1-10*	ϕ 160 × 150	83	Abetong	1.5 % steel fibres	0.56	488	-	-	-
1998:1-7*	ϕ 160 × 150	90	Fredrikstad	-	0.63	479	-	-	-
1998:2-2*	ϕ 160 × 150	90	Fredrikstad	-	0.98	583	-	-	-
1999-23*[1]	ϕ 240 × 75	103	Optiroc	-	perforation	460	183	-	-
1999-24*[2]	ϕ 240 × 75	103	Optiroc	-	perforation	455	204	-	-
1999-25*[2]	ϕ 240 × 75	103	Optiroc	-	perforation	459	181	-	-

Table 4.3 continued

Test series - target no	Target dimensions (diameter× length) (cm)	f_{cc} (MPa)	Concrete type	Reinforcement volume fraction	Penetration depth (m)	Impact velocity (m/s)	Residual velocity (m/s)	Entrance crater (diameter/ depth) (m)	Exit crater (diameter/ canal) (m)
1998:1-9*	ϕ 160 × 150	108	Optiroc	1 % steel fibres	0.59	486	-	-	-
1999-21*	ϕ 160 × 120	120	Trondheim	1 % steel fibres	0.57	464	-	-/0.35	-
1999-22*	ϕ 160 × 120	120	Trondheim	ϕ 25 mm rebars 1.55 % and 1 % steel fibres	0.50	467	-	0.80/0.20	-
1998:2-13*	ϕ 160 × 150	134	Abetong	-	0.83	581	-	-	-
1998:2-3*	ϕ 160 × 150	141	Trondheim 1	1 % steel fibres	0.81	584	-	-	-
1998:2-6*	ϕ 160 × 120	141	Trondheim 1	1 % steel fibres	0.60	480	-	-	-
1998:2-7*	□ 150 × 120	141	Trondheim 2	ϕ 32 mm rebars 6.5 % and 1 % steel fibres	0.42	480	-	-	-
1999-17*	ϕ 240 × 120	149	Abetong 1	-	0.38	468	-	1.50/0.34	-
1999-18*	ϕ 300 × 120	149	Abetong 1	-	0.44	465	-	1.70/0.40	-
1999-15*	ϕ 100 × 120	153	Abetong 2	-	0.75	466	-	-/0.60	-
1999-16*	ϕ 160 × 120	153	Abetong 2	-	0.66	467	-	1.40/0.47	-
1999-19*	ϕ 160 × 150	158	Abetong 3	Rock boulders	0.79	576	-	-	-

Table 4.3 continued

Test series - target no	Target dimensions (diameter× length) (cm)	f_{cc} (MPa)	Concrete type	Reinforcement volume fraction	Penetration depth (m)	Impact velocity (m/s)	Residual velocity (m/s)	Entrance crater (diameter/ depth) (m)	Exit crater (diameter/ canal) (m)
1999-20*	ϕ 160 × 150	158	Abetong 3	Rails	0.44	573	-	-	-
1996:2-4	□ 150 × (5 × 20)	180	Densit	2.6 % steel fibres	0.60	473	-	-	-
1998:2-4*	ϕ 160 × 150	183	Densit 1	2 % steel fibres	0.53	580	-	-	-
1998:1-6*	ϕ 160 × 100	199	Densit Special	1.5 % steel fibres	0.45	480	-	-	-
1998:1-3*	□ 150 × 100	200	CRC	ϕ 25 mm rebars 7 % and 1.5 % steel fibres	0.30	480	-	-	-
1998:1-5*	ϕ 160 × 120	203	Densit	-	0.45	480	-	-	-
1996:2-3	□ 150 × (5 × 20)	220	CRC	ϕ 25 mm rebars 25% and 4 % steel fibres	0.35	478	-		
1996:2-1	□ 150 × (4 × 20)	>250	Ballistocrete	Steel fibres	Perforation	476	-		
1998:1-2*	ϕ 220 × (5 × 20)	>250	Ballistocrete	Steel fibres	0.46	481	-	-	-

f_{cc} = concrete compressive strength

1 = new nose modified by FFI

2 = new nose modified by FFI and accelerometers

* = back stop

A lot of damage was done to some targets in the penetration tests. Relatively large craters were observed both on the front side of the targets and on the back side (i.e. in the tests where perforation occurred). There were also a lot of concrete parts on the ground in front of the targets after each test. Figure 4.1 shows a sequence of a test with a 152-mm penetrator impacting a target of conventional concrete in test series 1998:1.

Figure 4.1 A 152-mm projectile impacting a target of conventional concrete (target 1 in test series 1998:1).

It was observed that some concrete types tend to give more resistance against penetration than others. In Table 4.3 the results surprisingly show that similar penetration depths were obtained for targets 7, 9 and 10 in test series 1998:1, target 6 in test series 1998:2 and targets 16 and 21 in test series 1999. The compressive strength in these targets ranged from 83 MPa to 153 MPa whereas the penetration depth varied between 0.56 m and 0.66 m. The different types of aggregate used in the different concrete types may have an influence on the results. Also, the penetrators in test series 1998:1 contained explosives without a detonator. Unfortunately, the explosives started to combust during the penetration process, which resulted in the penetrator fracturing into several pieces, see Figure C29 in Appendix C. This event may also have influenced the results. No further conclusions could be drawn due to the limited number of tests.

The results from all tests clearly show that the penetration depth can be reduced considerably by increasing the concrete strength, see Figures 4.2 – 4.7. The relative penetration depth in these figures refers to the penetration depth of targets of conventional concrete. As these figures show, the curves level off at higher concrete strengths. Thus, an increase of concrete strength does not result in a corresponding reduction in penetration depth at these strength levels. Furthermore, concrete strengths of 120 – 160 MPa give a 50 % reduction in penetration compared to that of conventional concrete. This refers to unreinforced concrete.

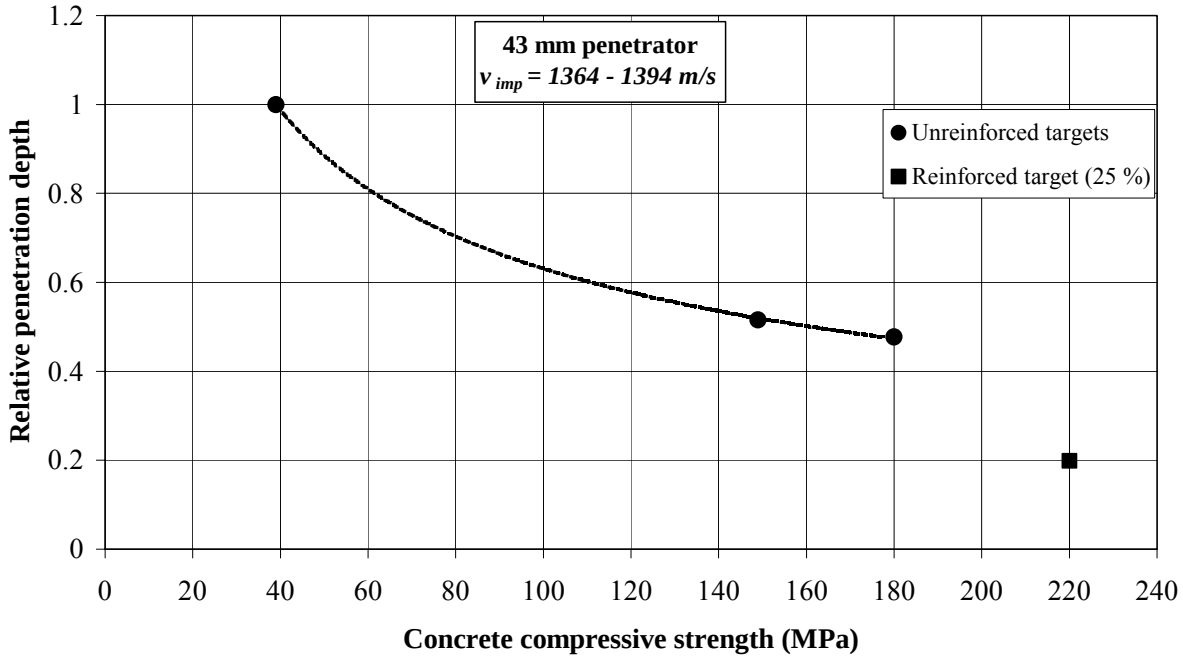

Figure 4.2 Penetration depth with respect to that of NSC versus concrete compressive strength. Tests with a 43-mm penetrator at impact velocities 1364 – 1394 m/s.

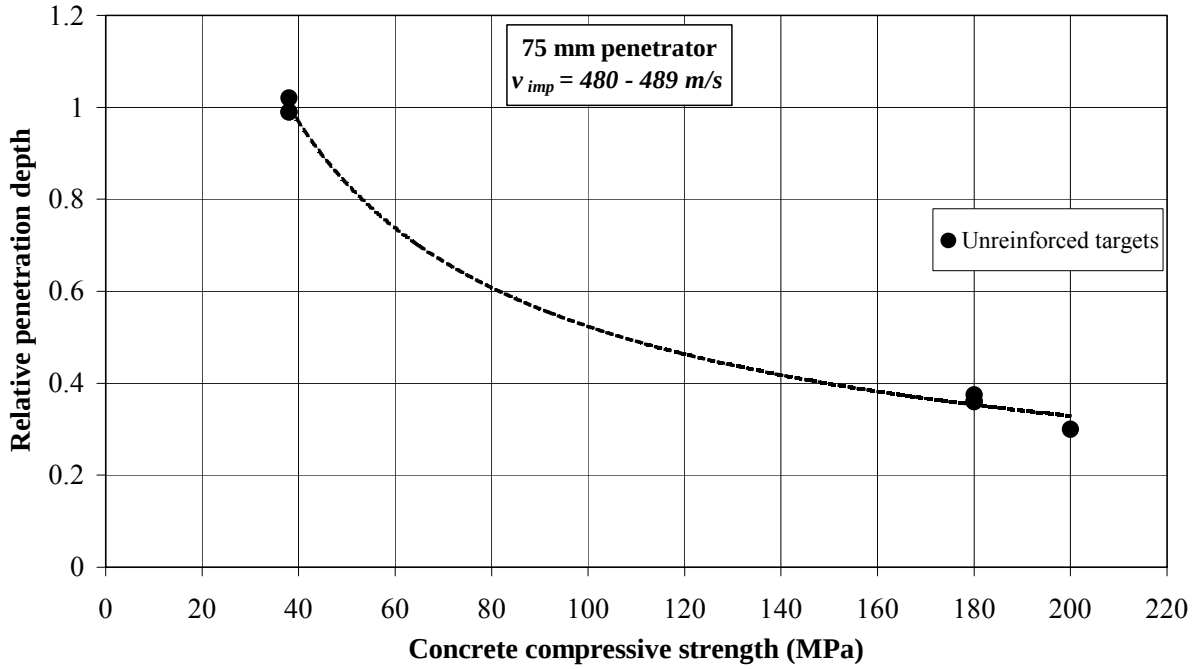

Figure 4.3 Penetration depth with respect to that of NSC versus concrete compressive strength. Tests with a 75-mm penetrator at impact velocities 480 – 489 m/s.

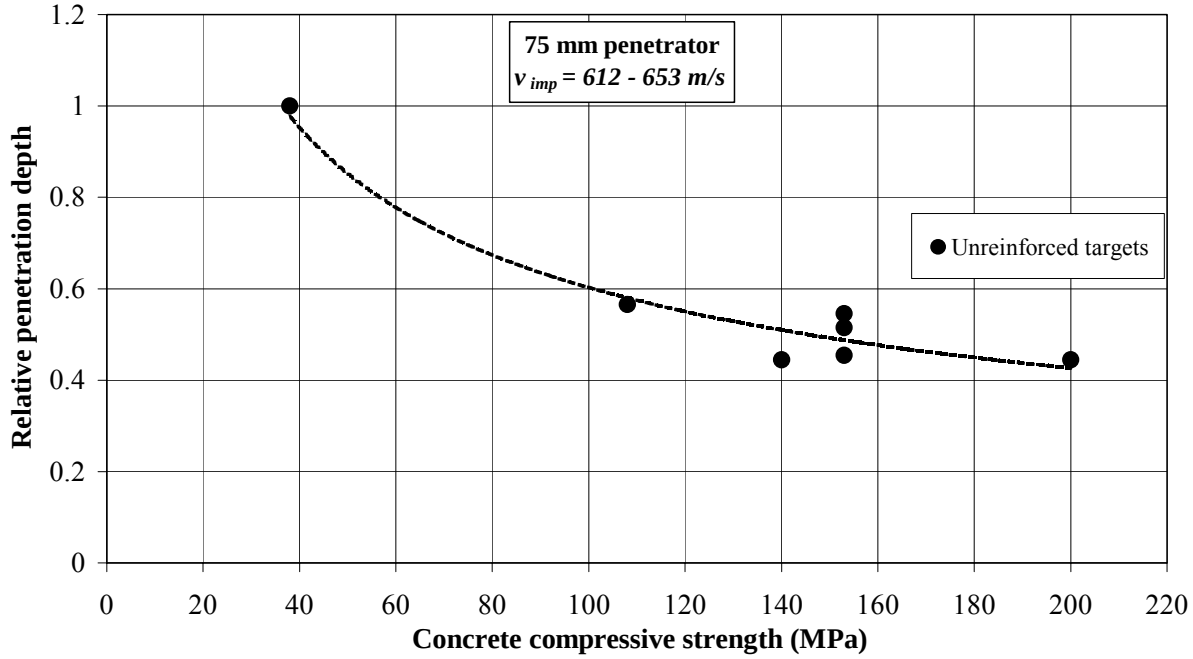

Figure 4.4 Penetration depth with respect to that of NSC versus concrete compressive strength. Tests with a 75-mm penetrator at impact velocities 612 – 653 m/s.

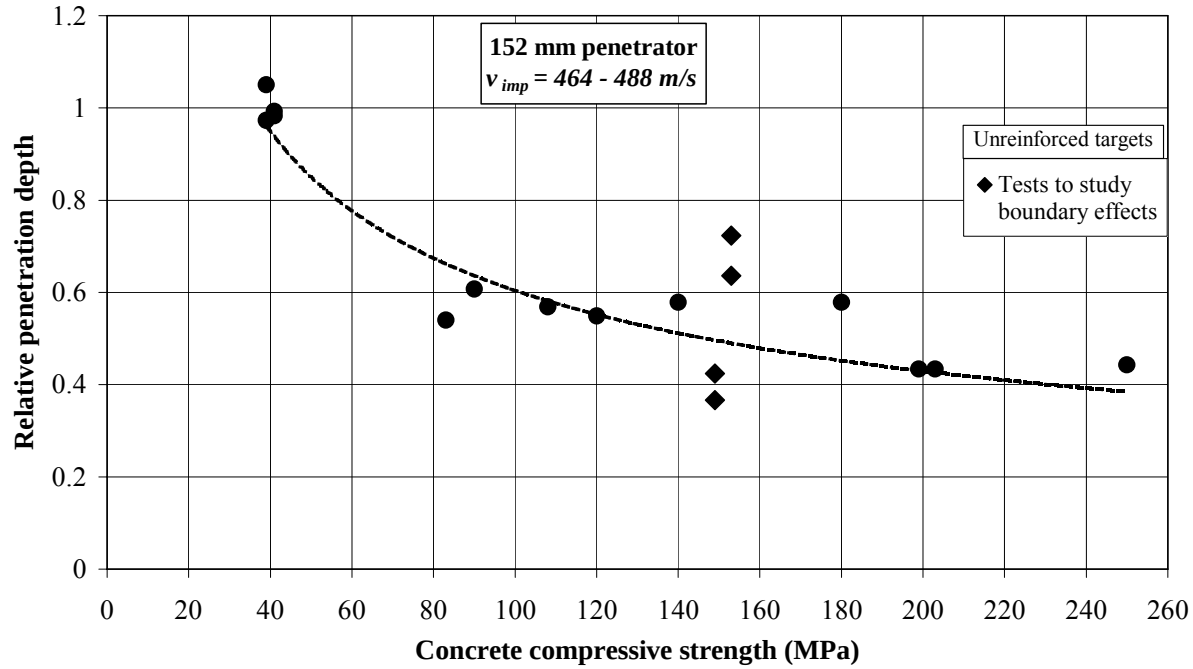

Figure 4.5 Penetration depth with respect to that of NSC versus concrete compressive strength. Tests with a 152-mm penetrator at impact velocities 464 – 488 m/s.

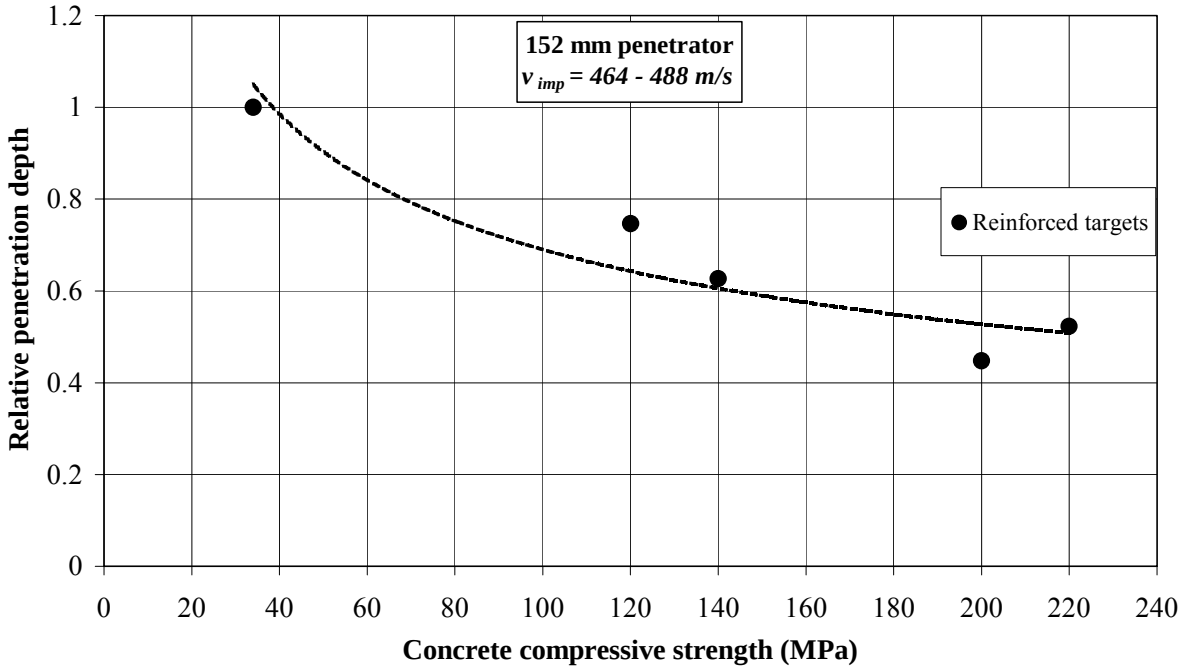

Figure 4.6 Penetration depth with respect to that of NSC (reinforced targets) versus concrete compressive strength. Tests with a 152-mm penetrator at impact velocities 464 – 488 m/s.

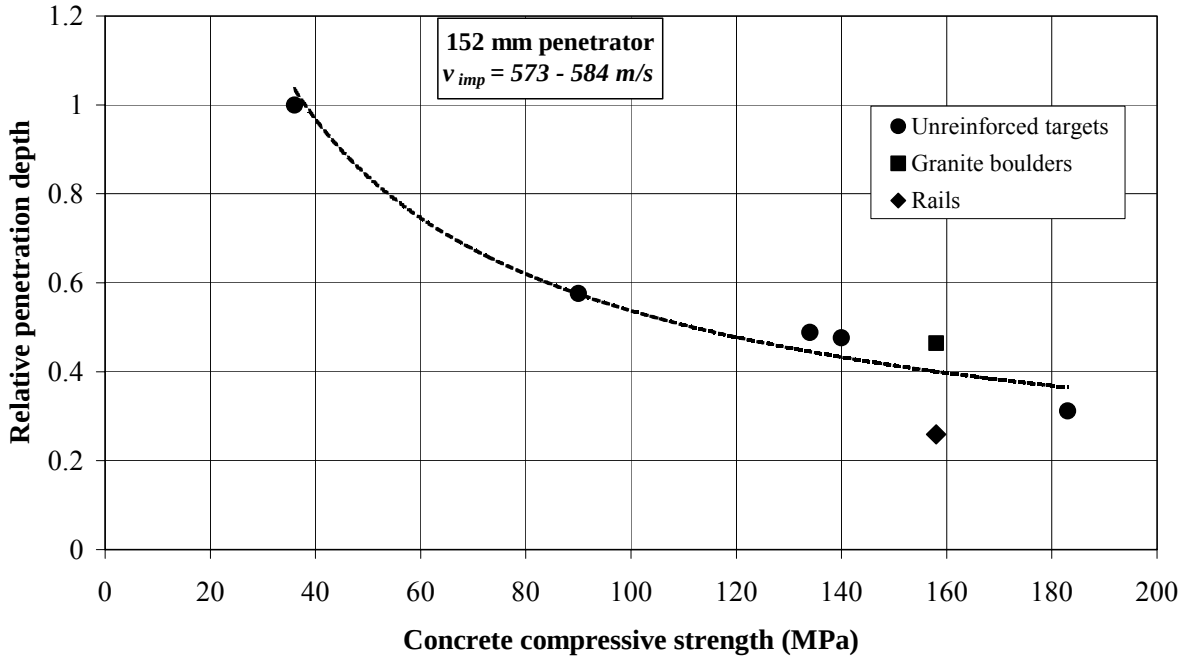

Figure 4.7 Penetration depth with respect to that of NSC versus concrete compressive strength. Tests with a 152-mm penetrator at impact velocities 573 – 584 m/s.

The results show that the amount of reinforcement has effects on the penetration resistance of concrete targets, see Figures 4.8 and 4.9. A penetration reduction of about 25 % was observed for reinforced targets compared to those that were unreinforced. Observe that these results are obtained with extreme amounts of reinforcement. The reinforcement volume fraction in these tests varied between 6.5 % and 25 %. A reinforcement amount of 1.55 % by volume resulted in a penetration reduction of about 10 % in comparison to unreinforced targets. Also, the amount of damage done to the concrete was reduced in reinforced targets. Hence, a significant reduction of the entrance crater depth was observed. The entrance crater diameter was also slightly reduced, as was the exit crater diameter in tests where perforation occurred. Thus, the reinforcement contributed in holding the concrete together in the targets. Furthermore, the inclusion of steel fibres did not appear to have any effects on the penetration depth. However, the diameter of the entrance crater was reduced due to the increase in ductility.

In test series 1999, granite boulders were added in one target (target 19) and rails were added in another target (target 20). The effects of the rock boulders appear to be relatively small, see Figure 4.7. After the test with rails, bits of rails were found on the ground in front of the target. The penetration depth was indeed reduced about 30 % with respect to unreinforced concrete, but no further conclusions could be drawn due to the limited number of tests.

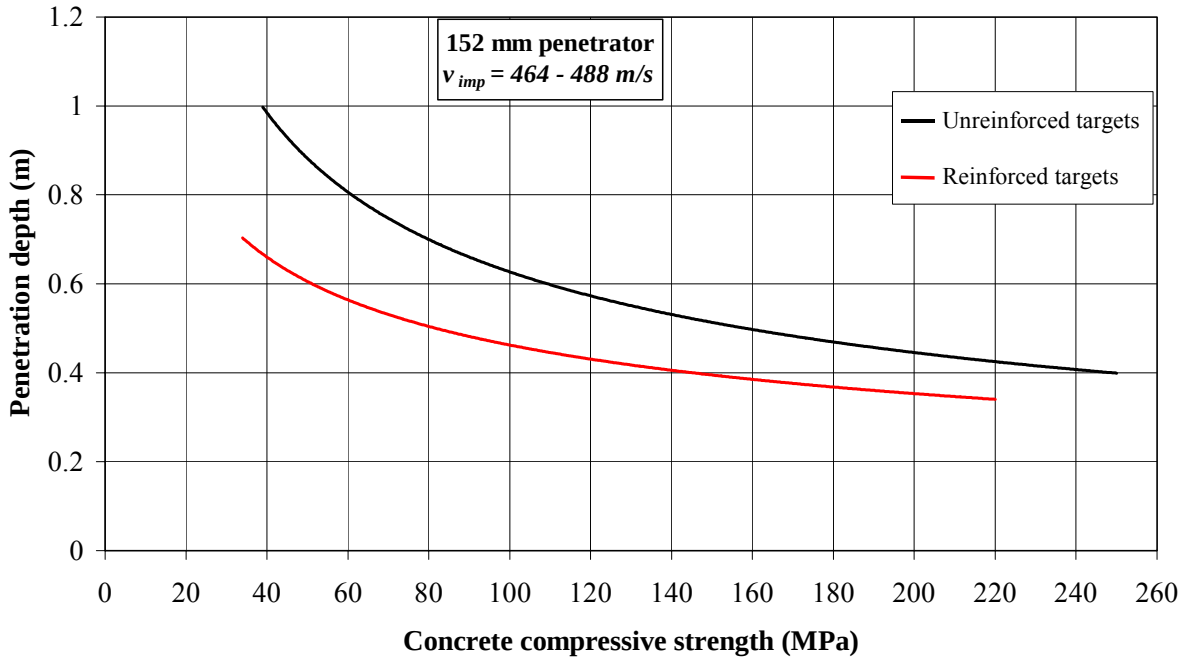

Figure 4.8 Penetration depth versus concrete compressive strength of tests with a 152-mm penetrator and impact velocities 464 – 488 m/s.

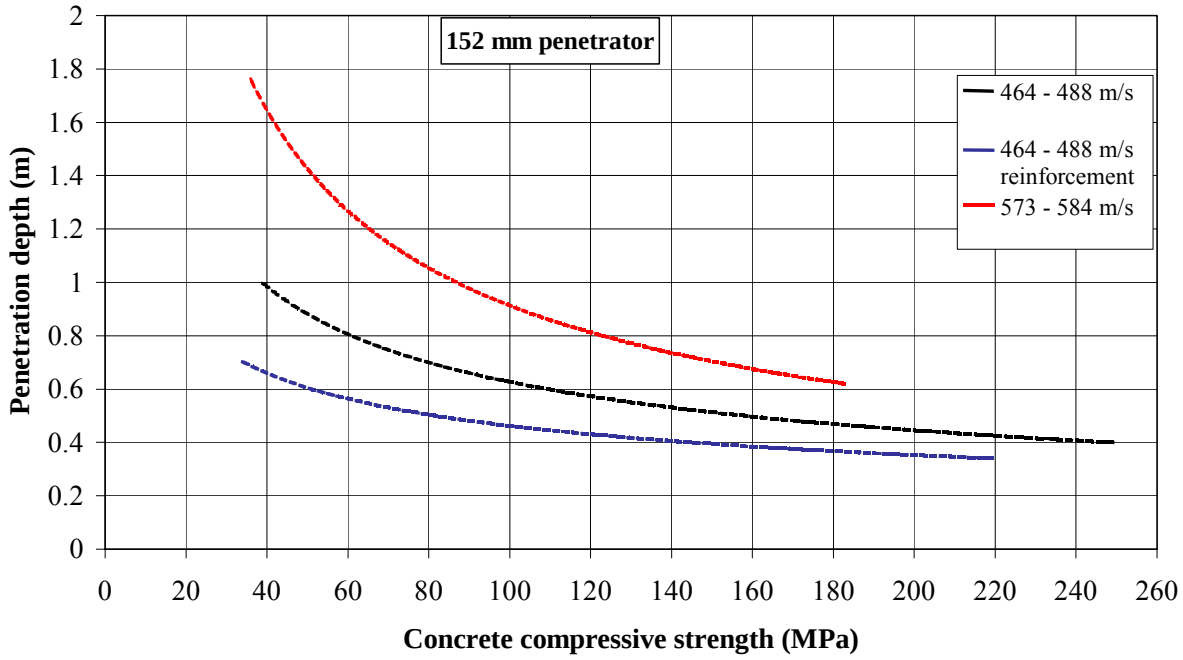

Figure 4.9 Penetration depth versus concrete compressive strength of all tests with a 152-mm penetrator.

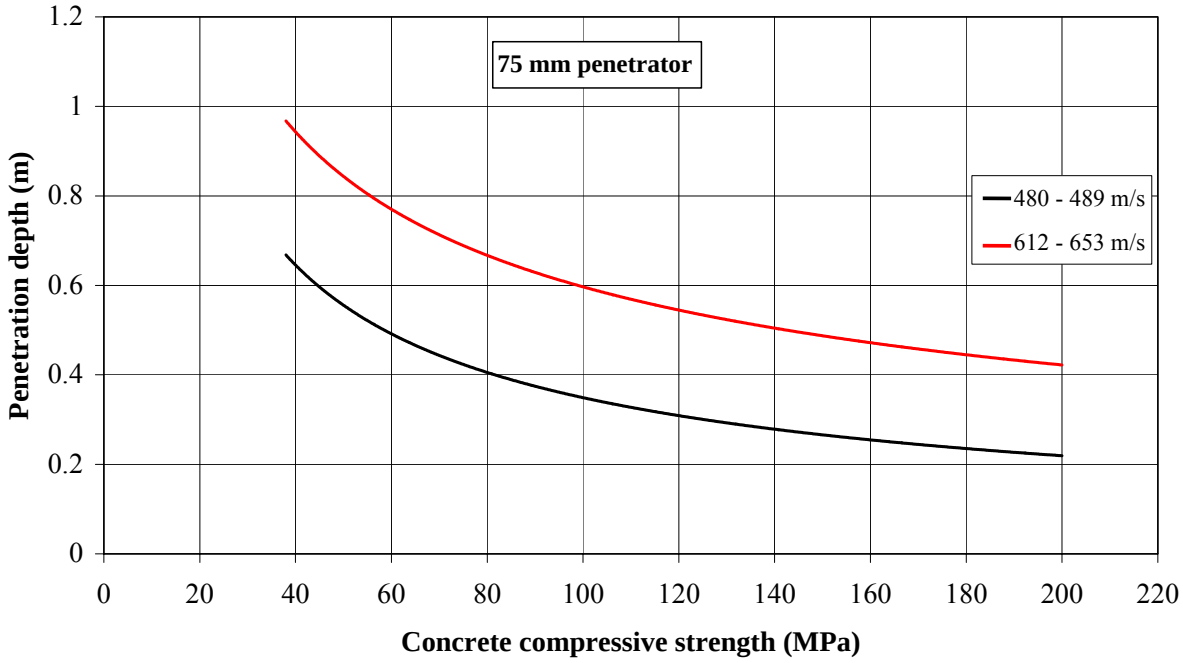

Figure 4.10 Penetration depth versus concrete compressive strength of tests with a 75-mm penetrator.

As expected, the impact velocity (v_{imp}) of the penetrator has a relatively large effect on the penetration depth, see Figures 4.9 and 4.10. By increasing v_{imp} of the 75-mm penetrator by a factor of 1.3 the corresponding penetration depth was increased by a factor of about 1.5 and 2.0 for NSC and HPC (with a compressive strength of about 200 MPa), respectively. Furthermore, increasing v_{imp} by a factor of about 1.2 of the 152-mm penetrator resulted in an increase in penetration depth of about 1.6 for NSC and about 1.3 for HPC (with a compressive strength of about 180 MPa) respectively. Figure 4.11 shows a summary of all penetration curves from the tests.

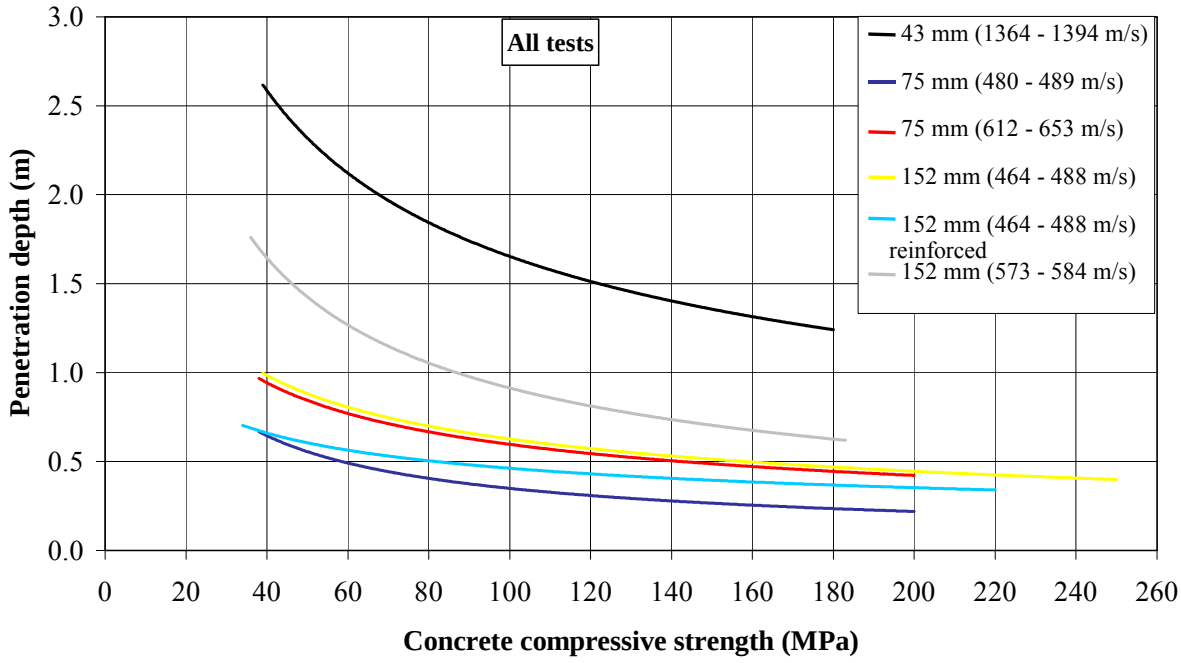

Figure 4.11 Penetration depth versus concrete compressive strength. Tests with all penetrators.

Boundary effects were also investigated in a limited number of tests with a 152-mm penetrator, see Figure 4.12. Clearly, boundary effects were present in the tests with the two smallest targets for a concrete strength of about 150 MPa. The amount of damage done to some of the targets also indicates that boundary effects were present. The mould of the cylindrical targets, which consisted of a corrugated steel cylinder ruptured in a number of tests, e.g. see Figures D83 – D85 in Appendix D. Also, the scattering in Figure 4.5 is most likely due to the presence of boundary effects. The results indicate that the diameter of the concrete target (D) may need to be about twenty times the diameter of the penetrator (d) in order to avoid boundary effects. However, more tests would be necessary in order to determine more accurately the target size with respect to penetrator diameter. A different relationship may also occur when other penetrators are used. Autodyn simulations and calculations by using a modified Forrestal's formula have been performed to study the boundary effects in concrete targets by FFI, Norway, /9/. The authors of that report suggest that a target size satisfying $D/d = 15$ is in most cases reasonably safe in order to avoid boundary effects.

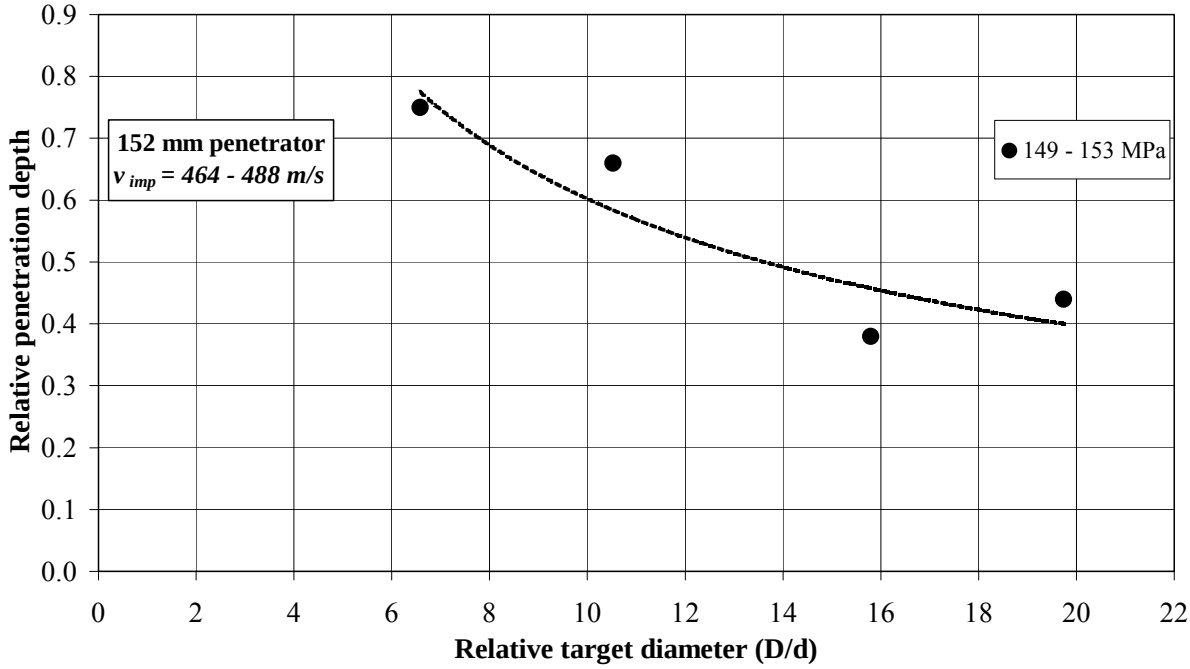

Figure 4.12 Penetration depth versus relative target diameter (i.e. target diameter (D)/projectile diameter (d)). Tests with a 152-mm penetrator.

In the first test with an instrumented penetrator in test series 1999, the instrument pack was unfortunately lost due to the break up of the projectile after target perforation. The accelerometer trace at the test with target 25, however, was successfully obtained and transferred to a computer disc. The deceleration curve is presented in Figure G1 and the calculated velocity history obtained from the deceleration curve is shown in Figure G2, see Appendix G. For further information about analysis of the accelerometer data, see /5/. Numerical simulations with Autodyn were also performed with the use of the material tests, doppler radar measurements and accelerometer data. These results were then presented at an international conference, see /8/.

The registrations from the carbon resistor pressure gauges in test series 1999 are shown in Appendix F. These registrations were filtered digitally by MATLAB with a cut-off frequency of 50 MHz and 20 MHz for tests 24 and 25, respectively. The first spike in each registration is the trigger signal, i.e. at about 0.25 ms and 0.15 ms in the two consecutive tests. Thus, this is the point of time when the penetrator impacts the target. The peak pressure in test 24 was about 120 MPa. The registration in test 25 did not obtain a peak pressure, probably due to rupture of the gauge cable as the penetrator approached the position of the gauge. Furthermore, there are uncertainties about what caused the small drop in pressure prior to the relatively long pressure build-up in both registrations.

5 CONCLUSIONS AND FUTURE WORK

5.1 Conclusions

This investigation involves penetration tests of both normal strength concrete (NSC) and different types of high performance concrete (HPC) targets. The dimensions of the targets varied and some targets were reinforced with rebars and steel fibres. The effects of concrete strength, reinforcement, projectile velocity, projectile diameter and target size (i.e. boundary effects) were studied. Different types of HPC were also tested with respect to the ability to perform production in field conditions. The following conclusions can be drawn from this investigation:

- The experience from the production tests indicates that a concrete compressive strength of about 150 MPa is the maximum strength suitable for field conditions.

- A rapid strength development was observed for HPC with respect to that of conventional concrete.

- The penetration depth can be reduced considerably by increasing the concrete strength. However, concrete strengths exceeding around 150 MPa, does not result in a corresponding reduction in penetration depth.

- A large amount of reinforcement has positive effects on the penetration resistance of concrete. A reduction in penetration of about 25 % was obtained for targets with reinforcement volume fractions of between 6.5 % and 25 % compared to that of unreinforced concrete. Volume fractions of 1.55 % reduced the penetration about 10 % in relation to plain concrete.

- The inclusion of steel fibres did not have any effects on the penetration depth in this investigation. However, the size of the entrance crater was reduced in the tests where fibres were used due to the increase in ductility.

- The impact velocity of the penetrator has a relatively large effect on the penetration depth. The penetration depth increased by a factor of between 1.5 and 2.0 as the impact velocity of a 75-mm penetrator was increased by a factor of 1.3.

- Boundary effects are important to consider and they were clearly present in some of these tests. The results indicate that the target diameter may need to be in the neighbourhood of 15 to 20 times the penetrator diameter in order to avoid boundary effects.

The collaboration between FOA, FFI, DERA and TNO has concluded in the following:

- A modified 152 mm-calibre penetrator has been developed which can be equipped with an instrument pack.

- A special capsule was developed serving as housing for acceleration measurements. The capsule was positioned in the nose section of the modified penetrator.

- Data has been obtained during the penetration process from pressure probes in two concrete targets and from an accelerometer positioned inside the projectile.

5.2 Future work

This investigation has focused upon penetrators with relatively low aspect ratios (i.e. the ratio between length and diameter), which all reach around 3. It would be of great interest to study the penetration capabilities of projectiles with larger aspect ratios. The shape of the projectile nose may also have an influence on the penetration capabilities, thus, a more slender nose is interesting to investigate.

Large volume fractions of reinforcement reduced the penetration depth in this investigation. It is interesting to study how to reinforce concrete in order to prevent the relatively large craters that develop on both sides of the targets. If the size of the craters were minimised, then it would be of utmost interest to study the penetration process.

Further development of concrete with a compressive strength of about 150 MPa may be interesting to investigate. These tests indicate that this concrete strength gives a relatively high protective level against the type of penetrators studied. Also, production of concrete of higher strength with the use of conventional methods and in field conditions is difficult. In a developing process it is important that the mix design is based on commonly available materials and that conventional production methods can be used.

A shaped charge is another weapon that may provide a threat against protective structures. Thus, there is also a need to study the penetration resistance of concrete against this type of weapon.

Another field of interest for HPC may be safety barriers used against burglary.

REFERENCES

/1/ Balazs P., Hallgren M., *Balkar av höghållfast betong belastade med impulslast. Brottmekanisk provning av RILEM-balkar*, *(High Strength Concrete Beams Subjected to Impulse Load)*, FOA Report R--96-00252-6.0--SE, Stockholm, May 1996 (in Swedish with English summary).

/2/ Balazs, P., Hallgren, M., *Brottmekanisk provning av Ballistocrete-, Densit- och Finpartikelbetongbalkar med impulslast och statisk last, (Fracture Mechanics Tests on Beams of Ballistocrete, Densit and Reactive Powder Concrete, with Impulse Load and Static Load)*, FOA Report R--97-00640-311--SE, Stockholm, December 1997 (in Swedish with English summary).

/3/ Betonghandbok, *Material*, AB Svensk Byggtjänst och Cementa AB, 1994 (in Swedish).

/4/ Betonghandbok, *Högpresterande betong – Material och utförande*, AB Svensk Byggtjänst, Stockholm, 2000.

/5/ Honey, N.J., *Instrumented Spinning Projectile Trial Report*, DERA/WSS/WS1/TR990691/1.0, UK, January 2000.

/6/ Malier, Y., *High Performance Concrete: From material to structure*, E&FN Spon, 1992.

/7/ Smeplass, S., *High Strength Concrete for use in Military Structures - Concrete Mix Development*, The Norwegian University of Science and Technology, Trondheim, Norway, August 1999 (in Norwegian).

/8/ Svinsås, E., O'Carroll, C., Wentzel, C.M., Carlberg, A., *Benchmark Trial Designed to Provide Validation Data for Modelling*, Proceedings of the 10th International Symposium on Interaction of the Effects of Munitions with Structures, San Diego, May 7 – 11, 2001.

/9/ Teland, J. A., Sjøl, H., *Boundary Effects in Penetration into Concrete*, FFI Report 2000/05414, Kjeller, Norway, November 2000.

Related URL:s

Norwegian Defence Research Establishment ..... www.ffi.no

Norwegian Defence Construction Service ..... www.mil.no/fbt

Swedish Defence Research Agency ..... www.foi.se

Swedish Armed Forces Headquarters ..... www.hkv.mil.se

Defence Evaluation and Research Agency ..... www.dera.gov.uk

Saab Bofors Test Center..... www.saab.se/testcenter

Imperial College of Science, Technology and Medicine .....www.ic.ac.uk

Abetong Precon ..... www.abetongprecon.se

Densit a/s ..... www.densit.dk
Optiroc AB ..... www.optiroc.se

APPENDICES

A. Ammunition
B. Pre test target configurations
C. Test results
D. Post test target configurations
E. Doppler radar registrations
F. Pressure gauge registrations
G. Projectile acceleration registrations

A AMMUNITION

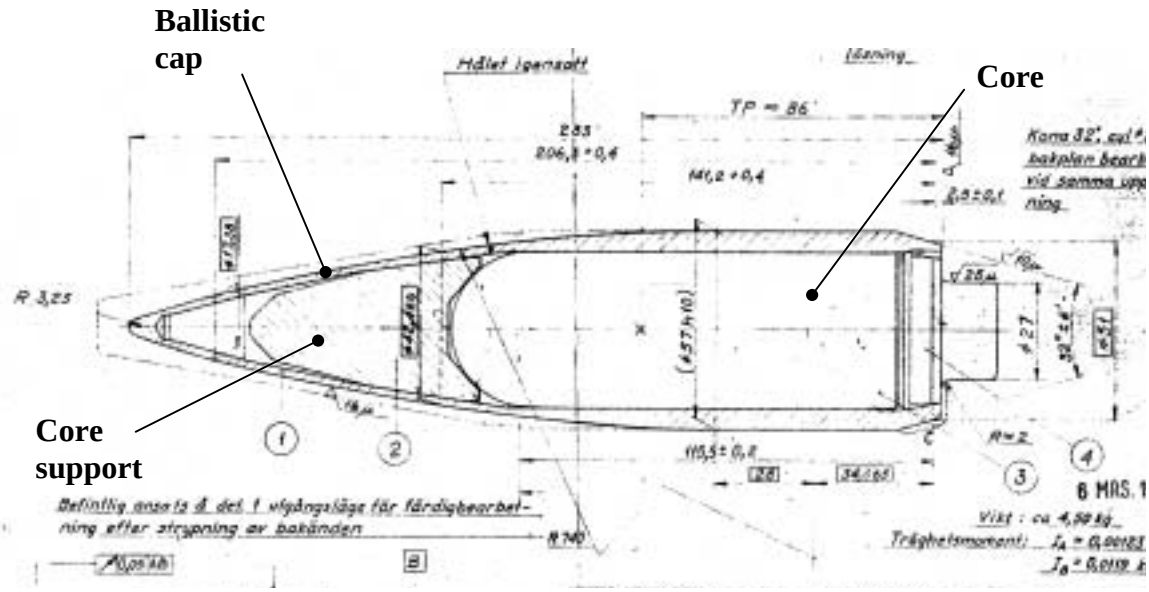

Figure A.1 Cross section of a 57 mm-calibre sabot-discarding projectile.

Table A.1 Specifications for a 57 mm-calibre sabot-discarding projectile.

Swedish Defence Materiel Administration (FMV) designation	M4105-906710 105/61 57SLPPRJ62
Type	Armour-piercing sabot discarding projectile
Projectile mass	4.5 kg
Projectile diameter	57 mm
Projectile length	233 mm
Core mass	2.56 kg
Core diameter	43 mm
Core length	129 mm
Core material	Tungsten carbide
Core support mass	0.89 kg
Core support diameter	42 mm
Core support length	66 mm
Core support material	Tungsten heavy alloy

Table A.2 Specifications for a 152-mm projectile.

The Swedish Defence Materiel Administration (FMV) designation	M4152-004205/06 152HPGR36FBAR
Type	Semi-armour-piercing grenade
Penetrator mass (including explosive charge)	44.76 kg
Penetrator diameter	152 mm
Penetrator length	435 mm
Explosive charge	2.7 kg

Table A.3 Specifications for a 75-mm projectile.

The Swedish Defence Materiel Administration (FMV) designation	M4075-126610 75/00 PV SLPPRJ40B
Type	Armour-piercing projectile
Projectile mass	6.28 kg
Projectile diameter	75 mm
Projectile length	225 mm
Projectile material	Tempered steel

Table A.4 Specifications for the modified 152-mm-calibre projectile (test series 1999).

Mass	46.328 kg
Nose factor (R/D)	2.5
Main material	Steel 34CrNiMoG Yield strength 886 MPa Hardness: 270-330 HB
Instrument package	Accelerometer, battery, recorder and impact G-switch installed in a separate capsule. All parts except accelerometer mounted semi-floating (permitting some rotation) in a bead filling. Volatile memory, i.e. the battery has to be unharmed and connected until the capsule has been demounted and data transferred to a PC (within 24 hours).

B PRE TEST TARGET CONFIGURATIONS

Note that target numbers and firing numbers appearing on photos are not the same for many of the targets and that all measurements are in millimetres.

Many of the targets were cast in the same type of thin-walled corrugated steel cylinder with inner radius R_i ranging from 1600 to 3000 mm. The geometry characteristics of the cylinder geometry are given in Figure B.1.

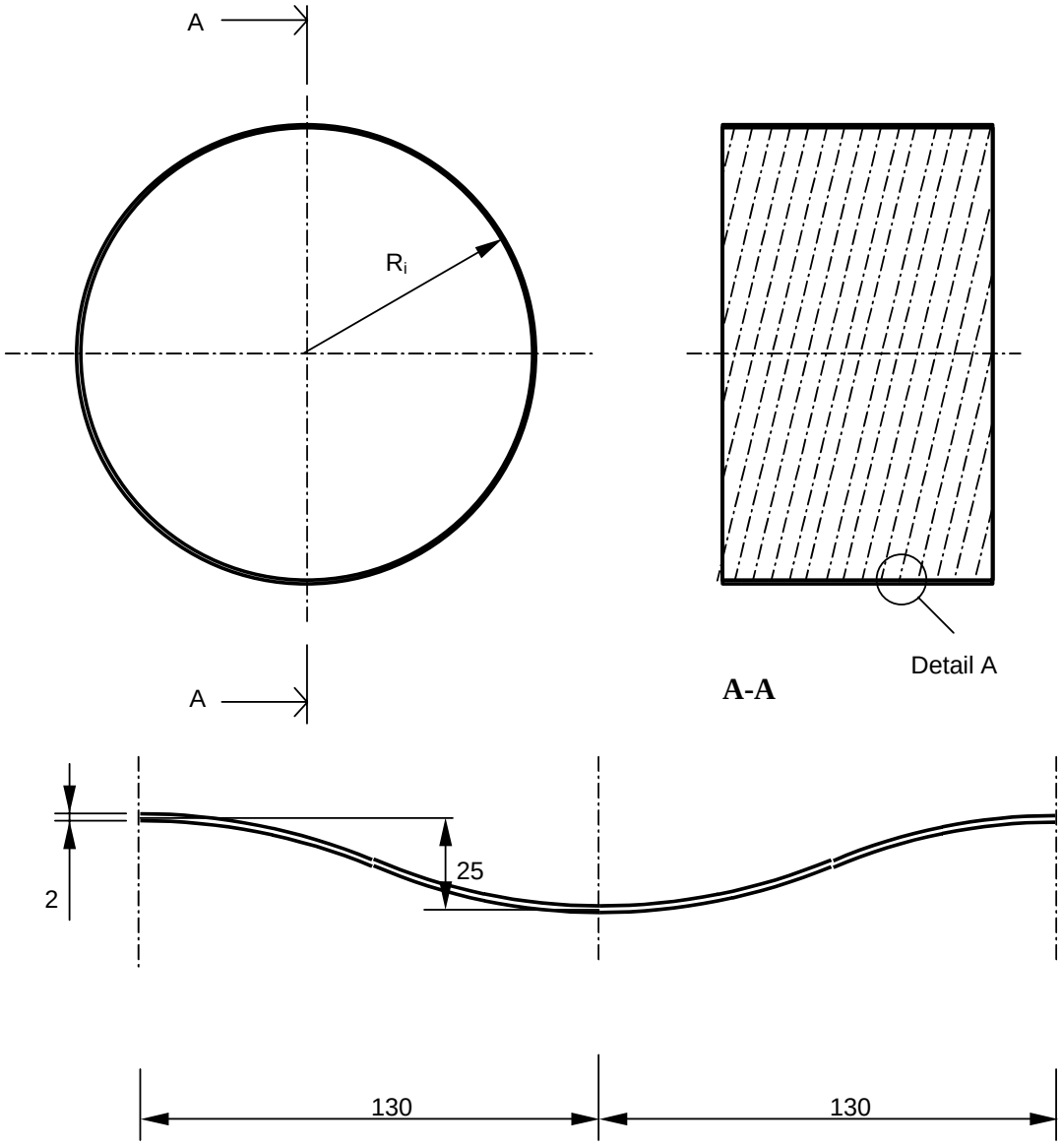

Figure B.1. Thin-walled corrugated steel cylinder used to cast the targets.

Test series 1996:1

Target 1

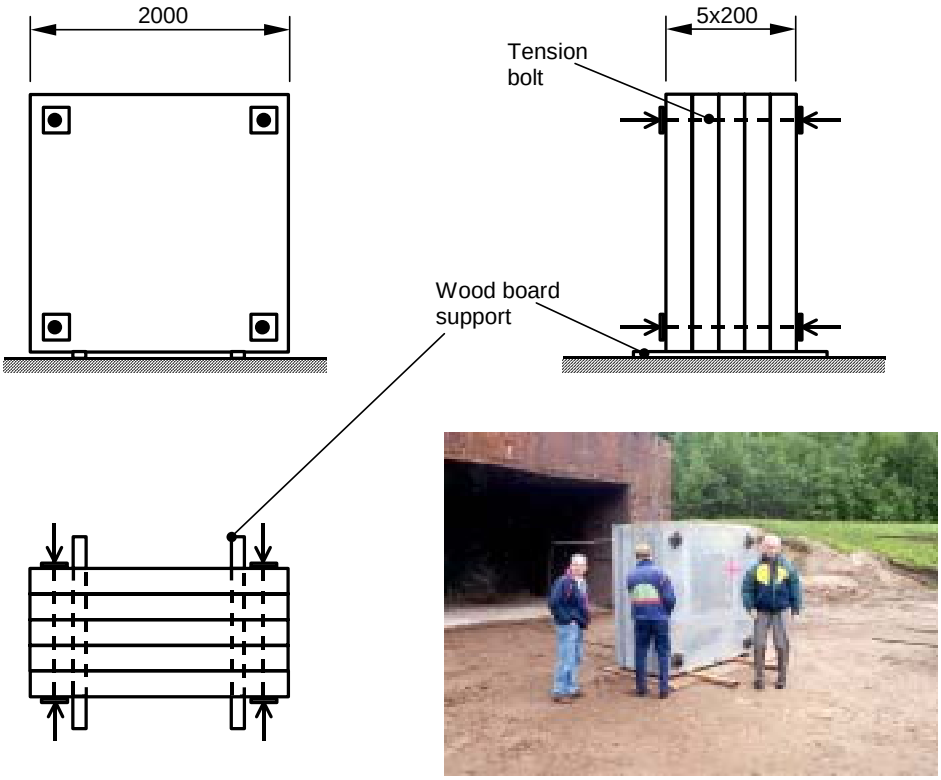

Figure B.2. Geometry for target 1 in test-series 1996:1.

Target 2

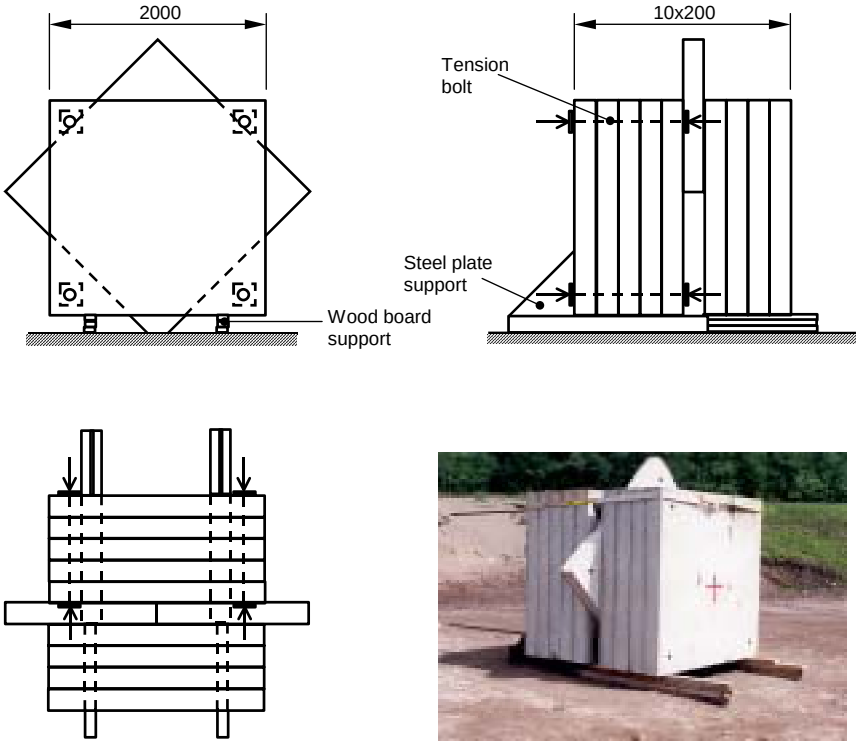

Figure B.3. Geometry for target 2 in test-series 1996:1.

Target 3

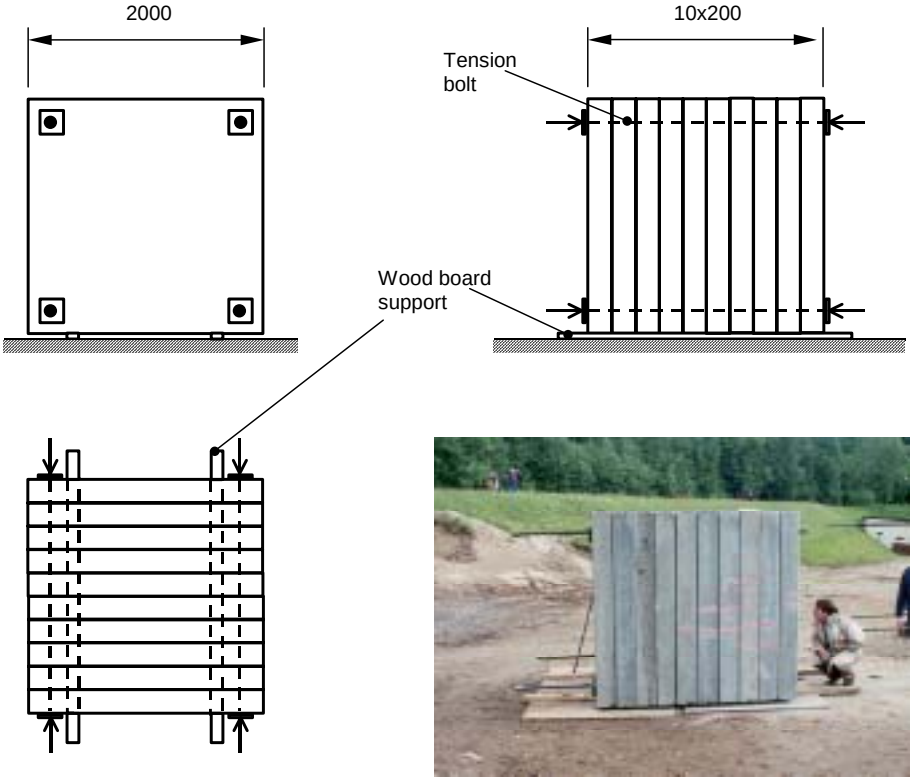

Figure B.4. Geometry for target 3 in test-series 1996:1.

Target 4

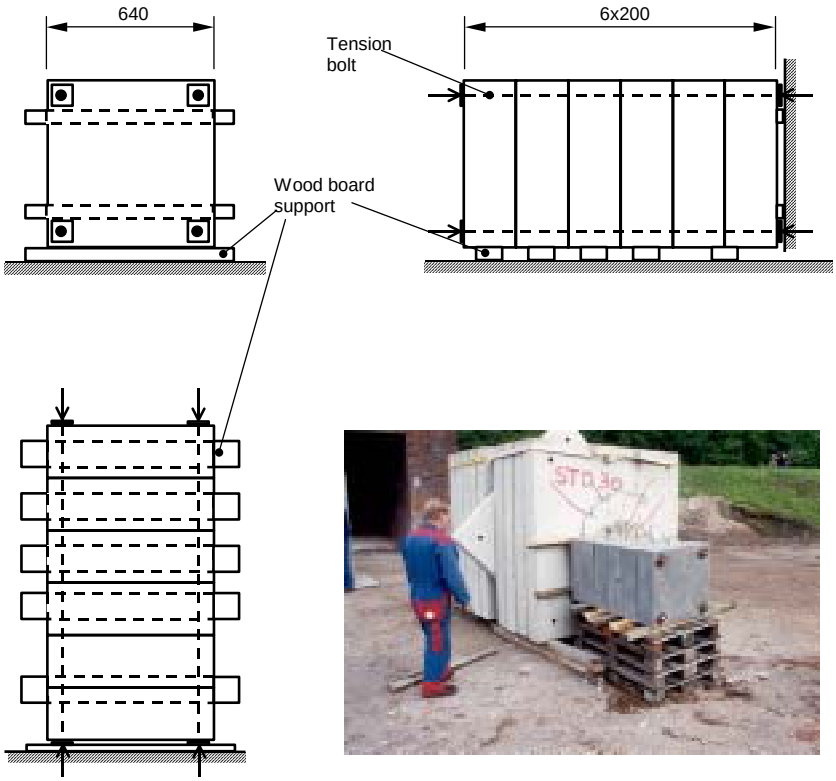

Figure B.5. Geometry for target 4 in test-series 1996:1.

Test series 1996:2

Target 1

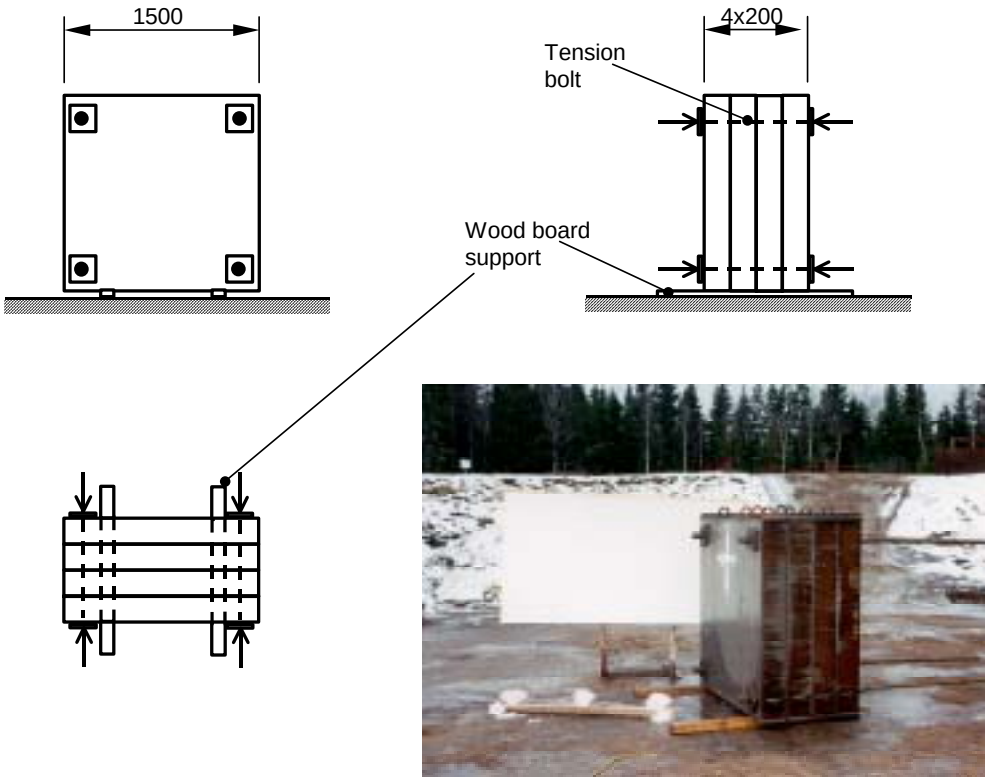

Figure B.6. Geometry for target 1 in test-series 1996:2.

Target 2

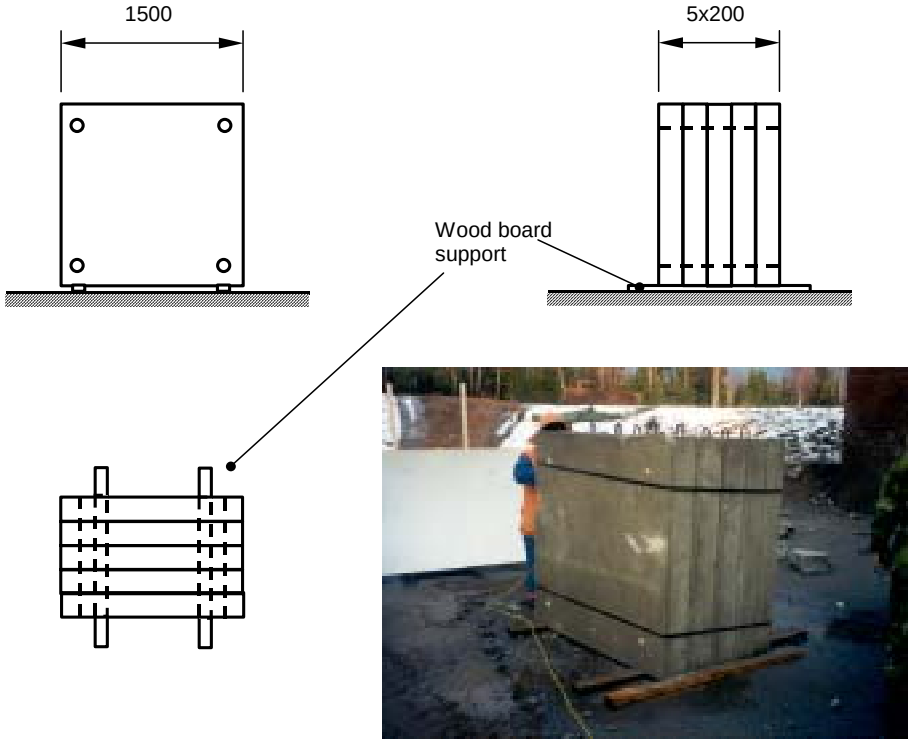

Figure B.7. Geometry for target 2 in test-series 1996:2.

Target 3

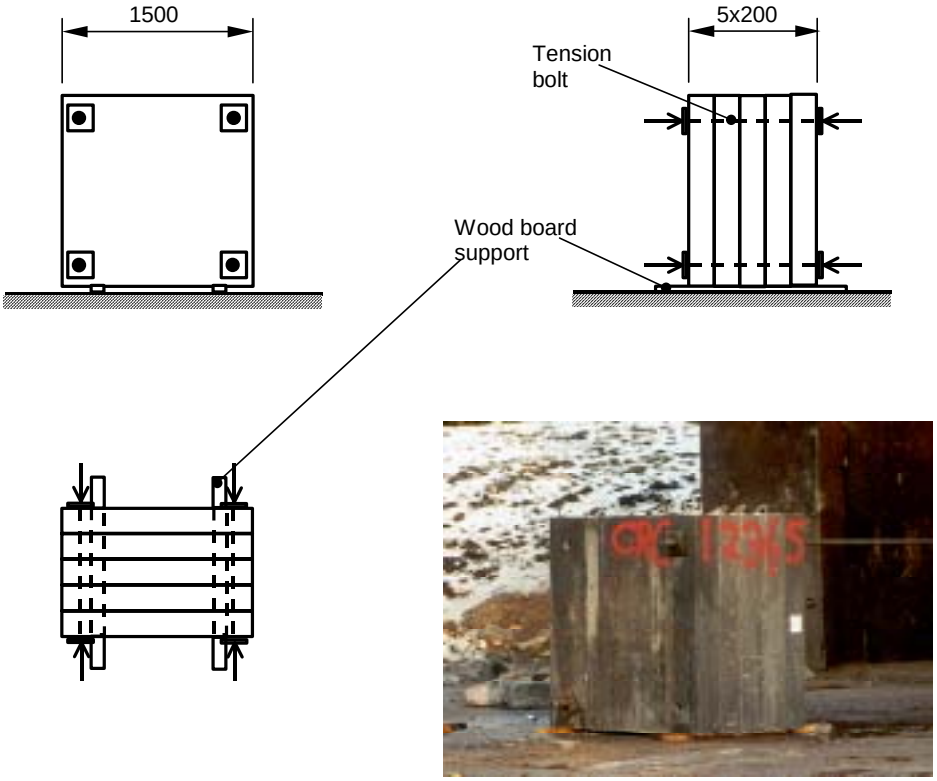

Figure B.8. Geometry for target 3 in test-series 1996:2. Two additional tension bolts were mounted after the photo was taken.

Target 4

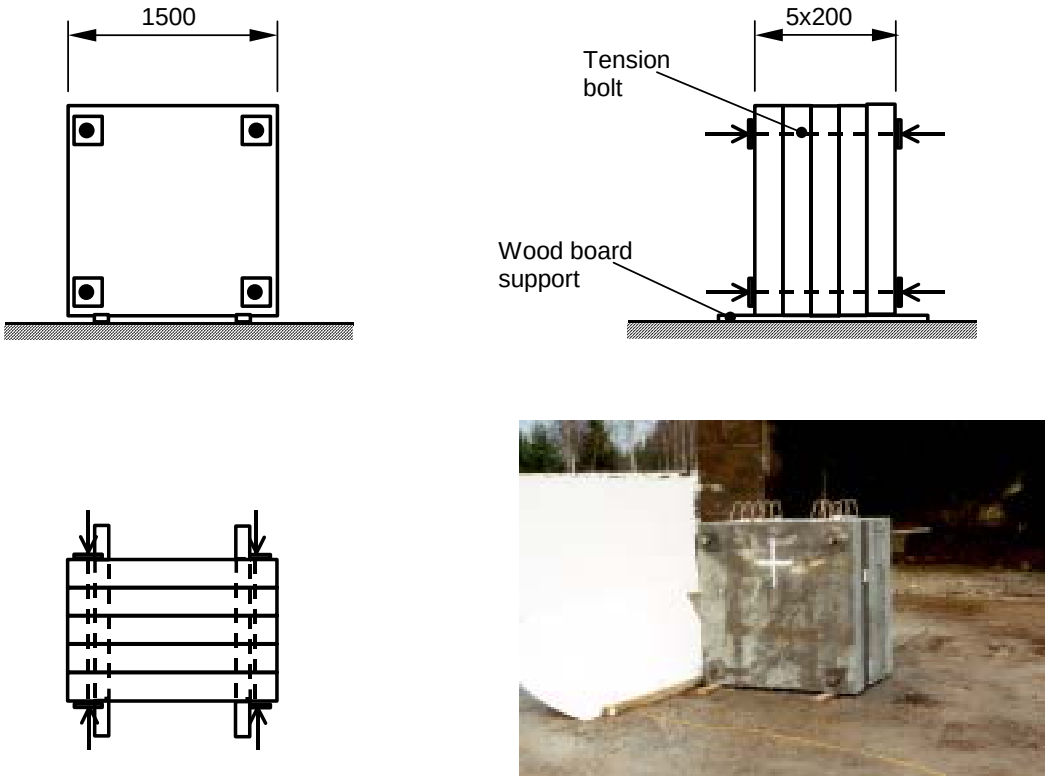

Figure B.9. Geometry for target 4 in test-series 1996:2.

Test series 1997

Target 1

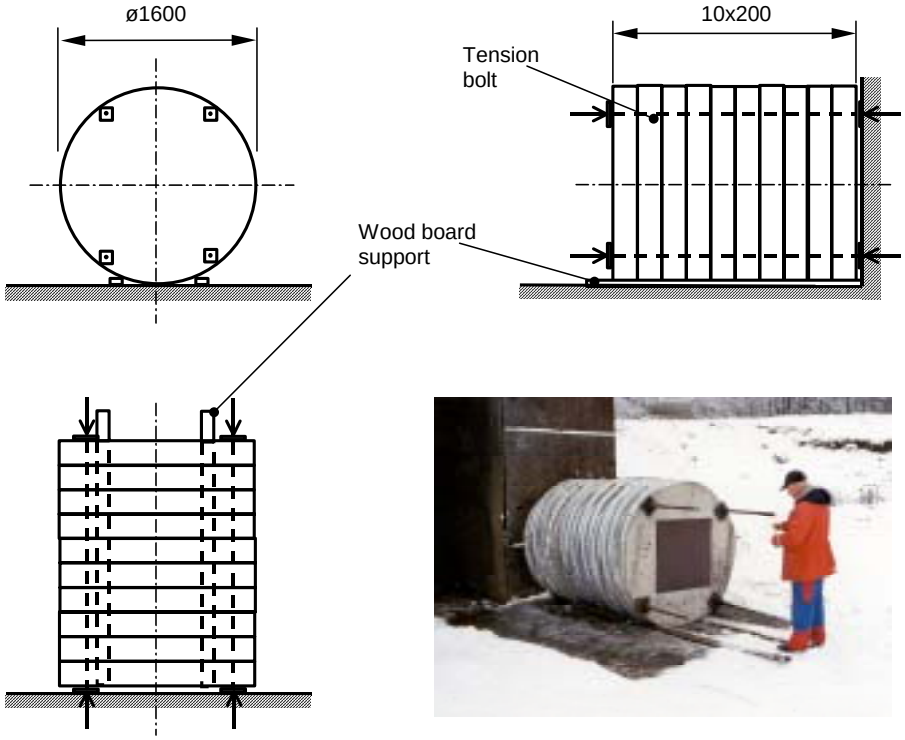

Figure B.10. Geometry for target 1 in test-series 1997.

Target 2

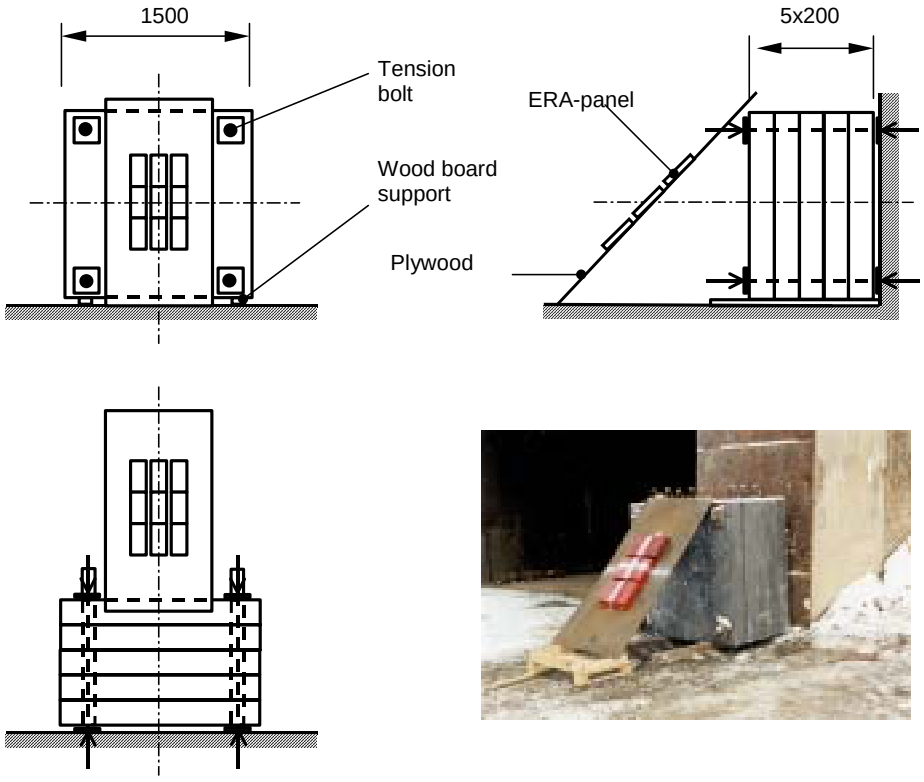

Figure B.11. Geometry for target 2 in test-series 1997.

Target 3

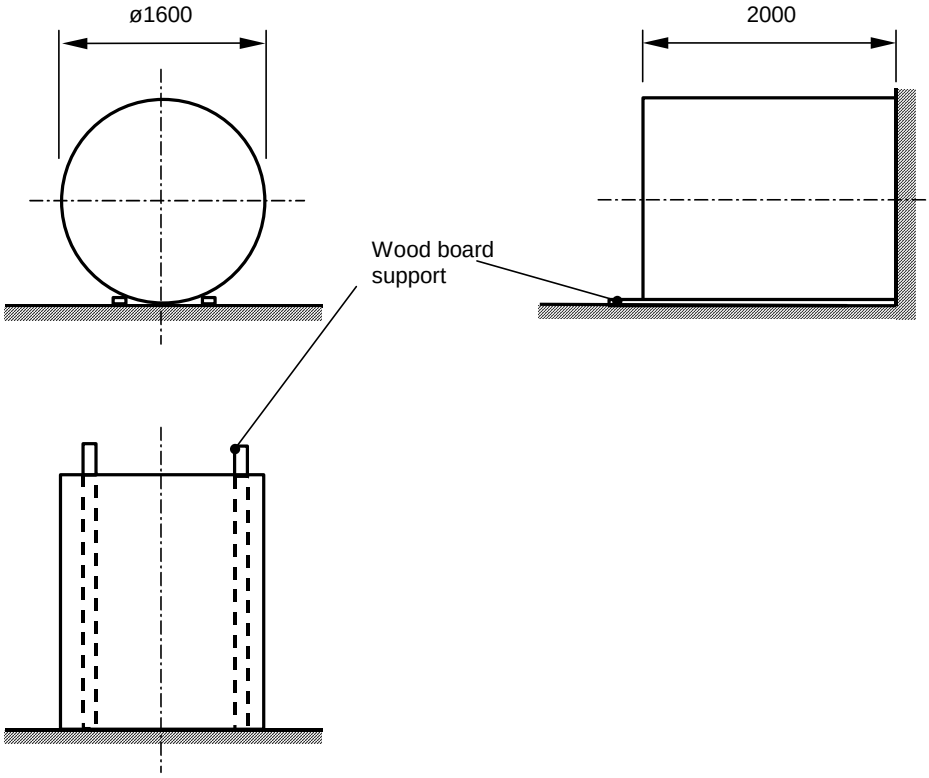

Figure B.12. Geometry for target 3 in test-series 1997.

Target 4

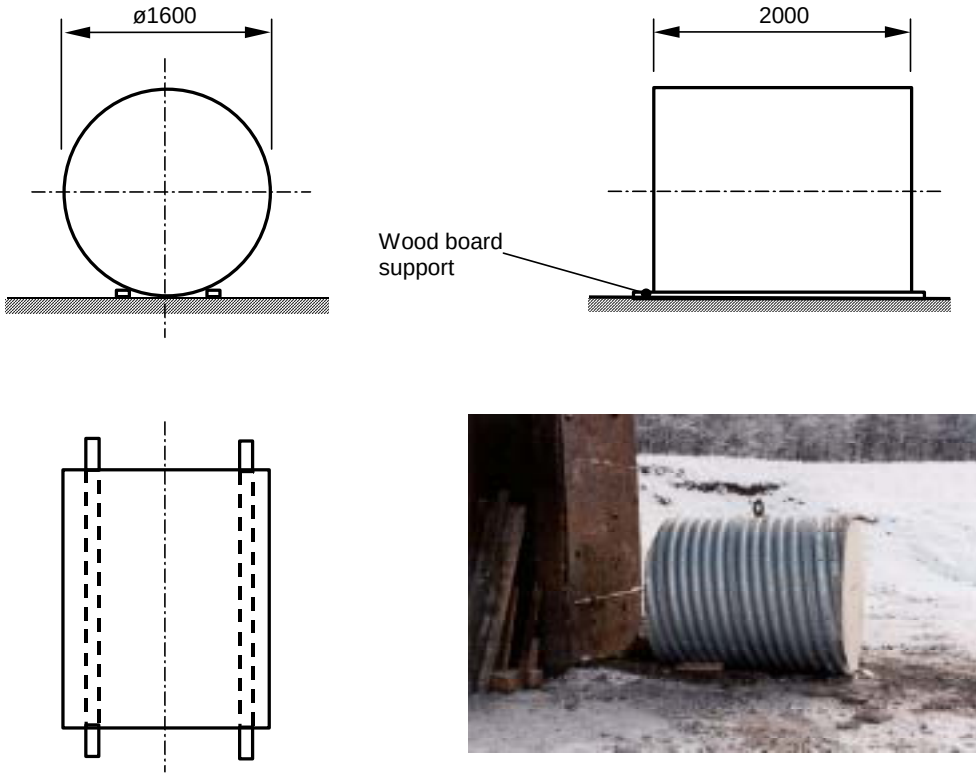

Figure B.13. Geometry for target 4 in test-series 1997.

Target 5

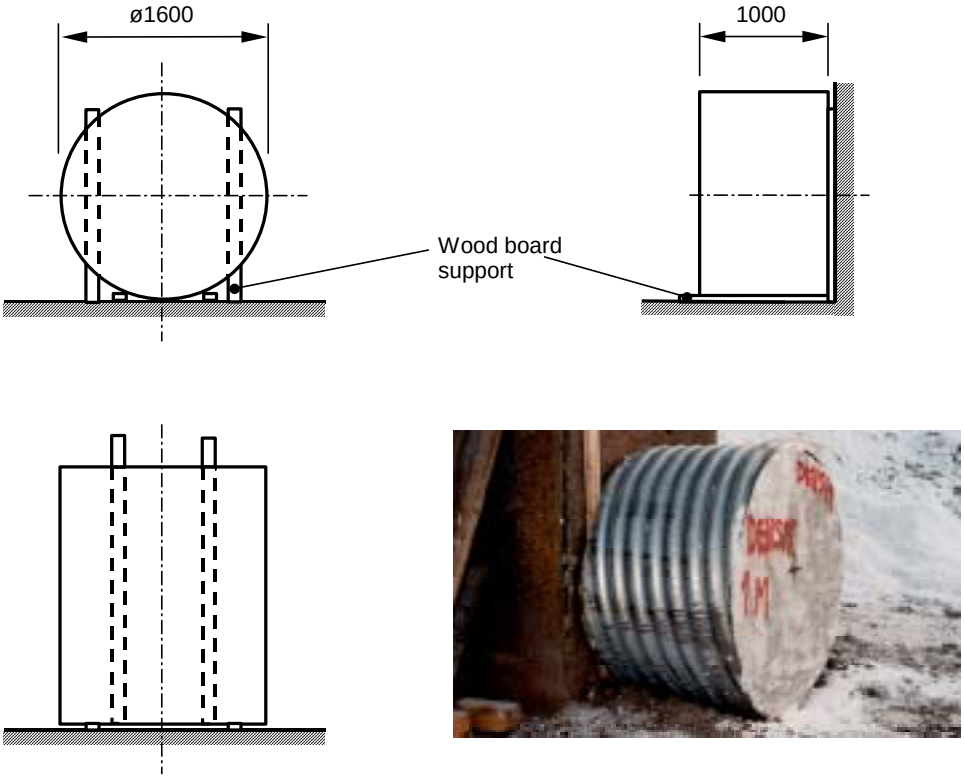

Figure B.14. Geometry for target 5 in test-series 1997.

Target 6

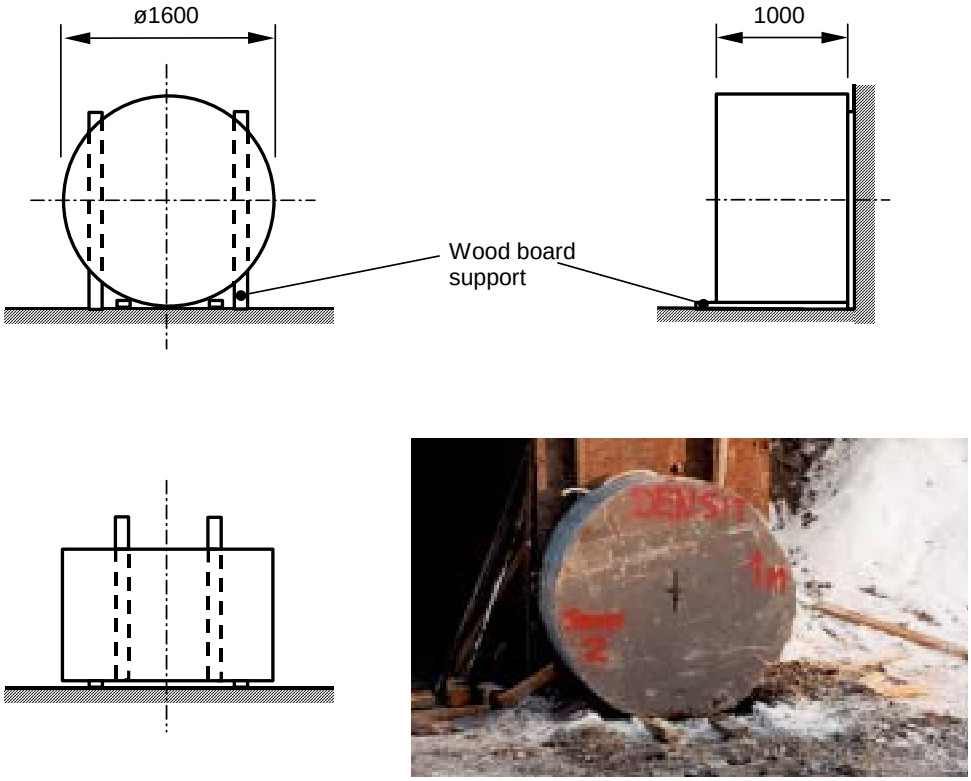

Figure B.15. Geometry for target 6 in test-series 1997.

Target 7

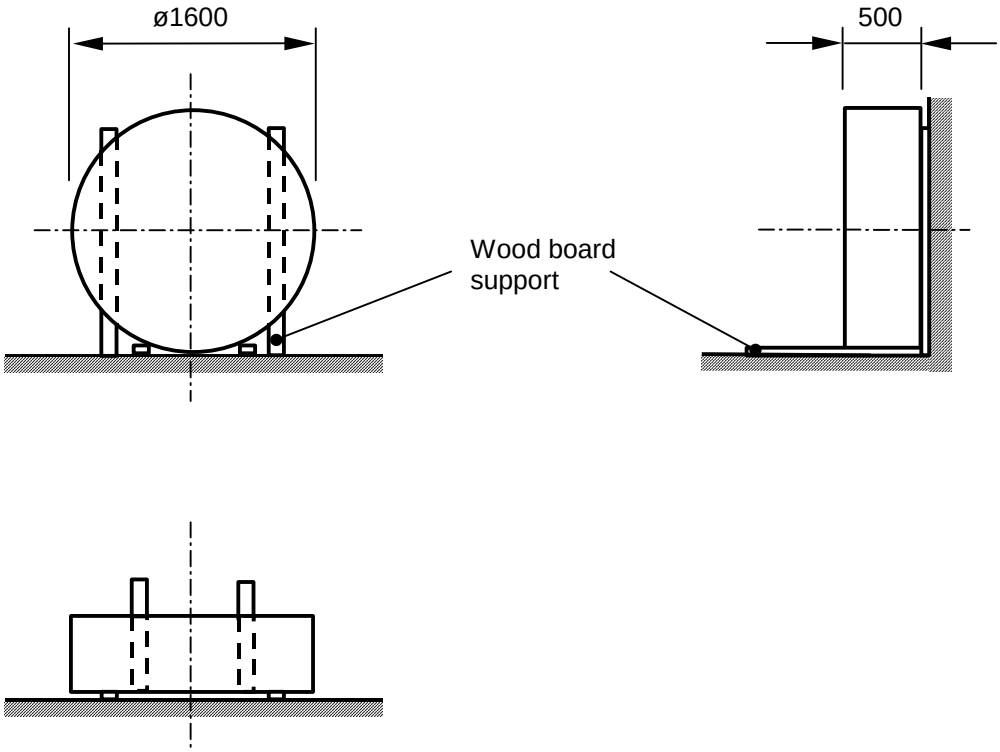

Figure B.16. Geometry for target 7 in test-series 1997.

Test series 1998:1

Target 1

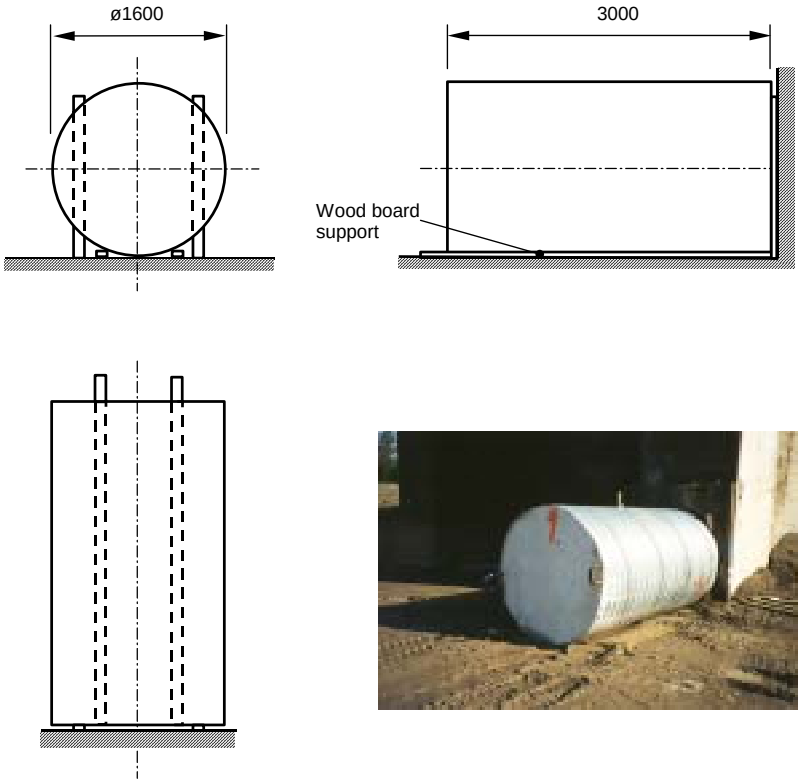

Figure B.17. Geometry for target 1 in test-series 1998:1.

Target 2

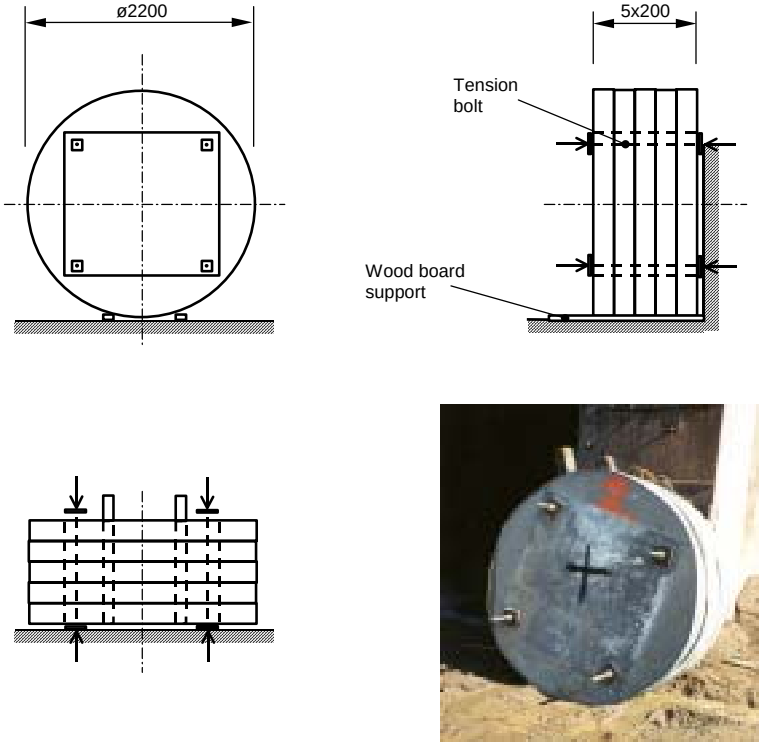

Figure B.18. Geometry for target 2 in test-series 1998:1.

Target 3

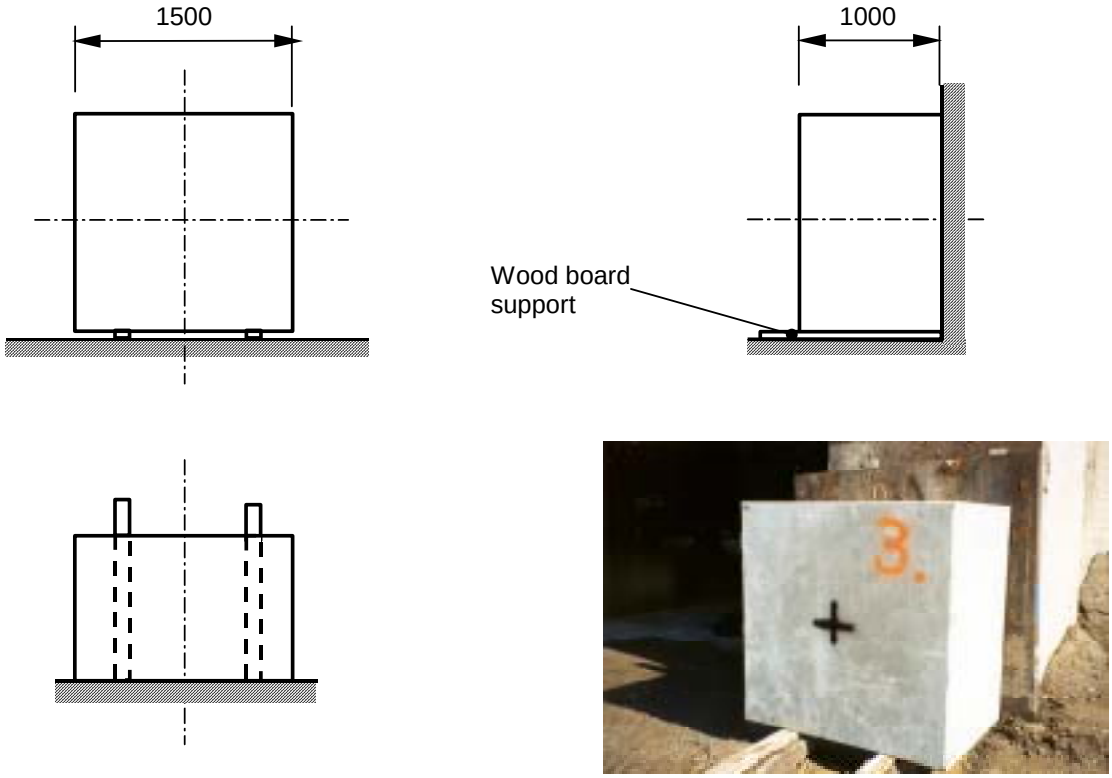

Figure B.19. Geometry for target 3 in test-series 1998:1.

Target 4

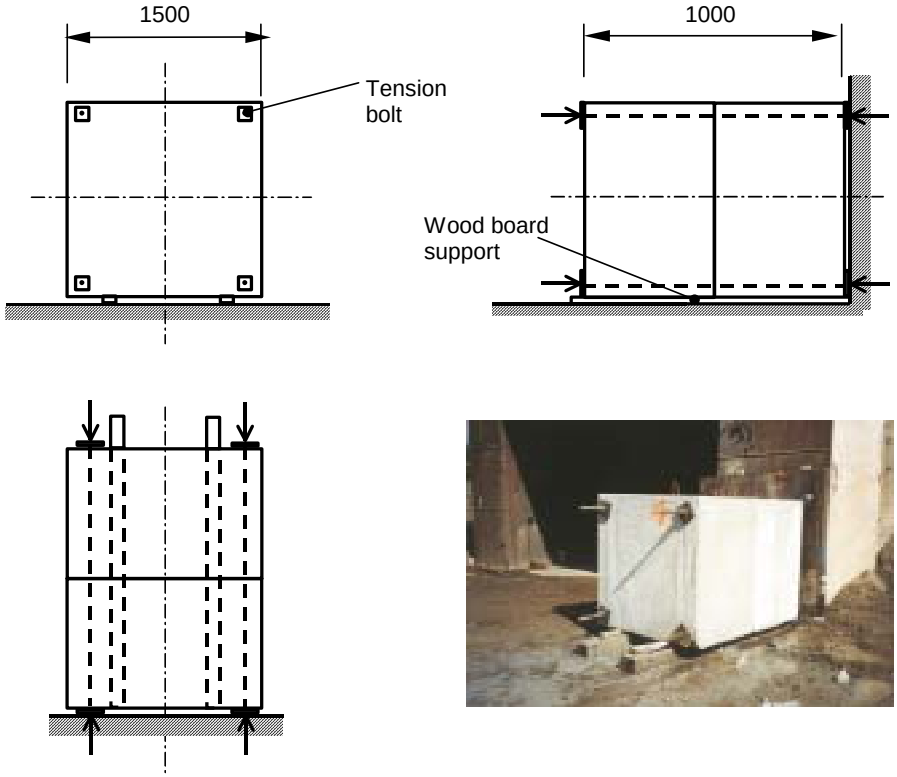

Figure B.20. Geometry for target 4 in test-series 1998:1.

Target 5

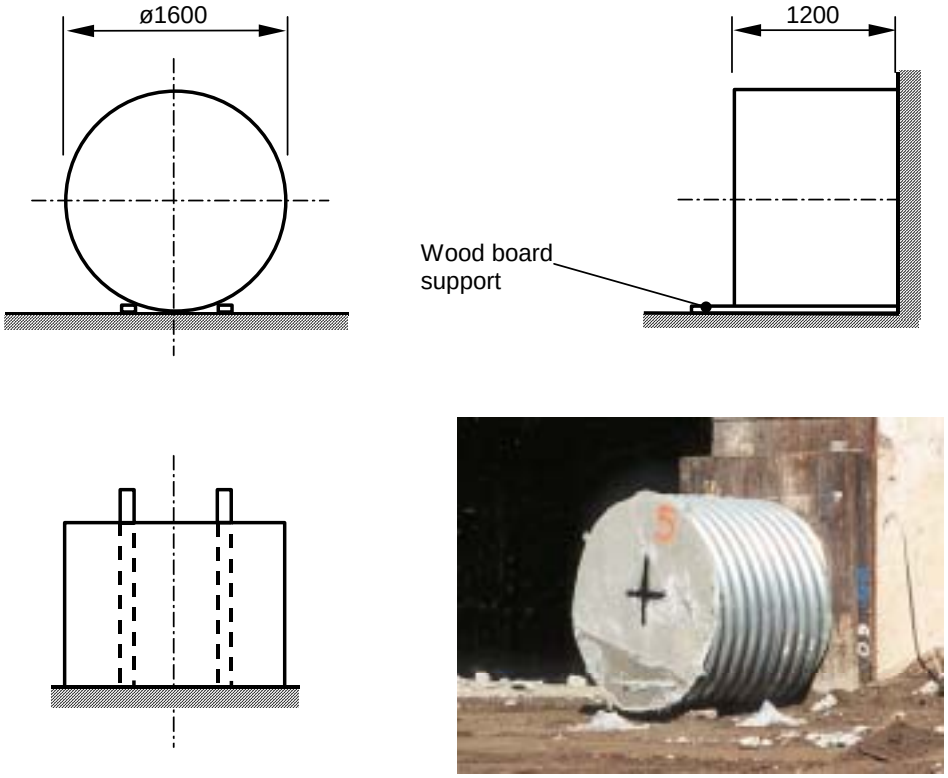

Figure B.21. Geometry for target 5 in test-series 1998:1.

Target 6

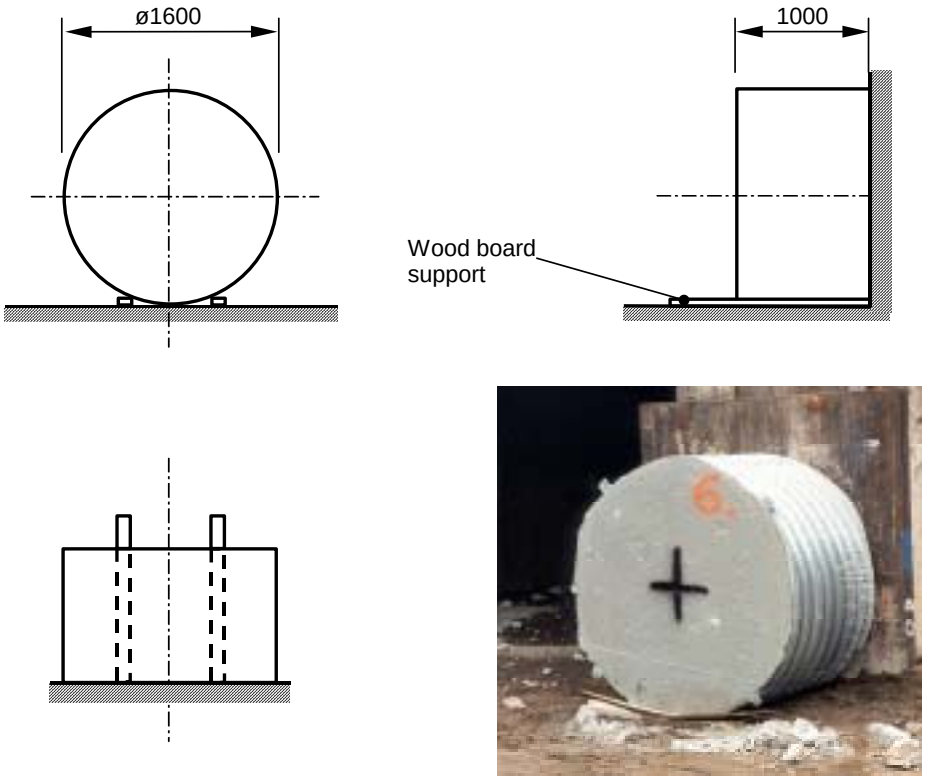

Figure B.22. Geometry for target 6 in test-series 1998:1.

Target 7

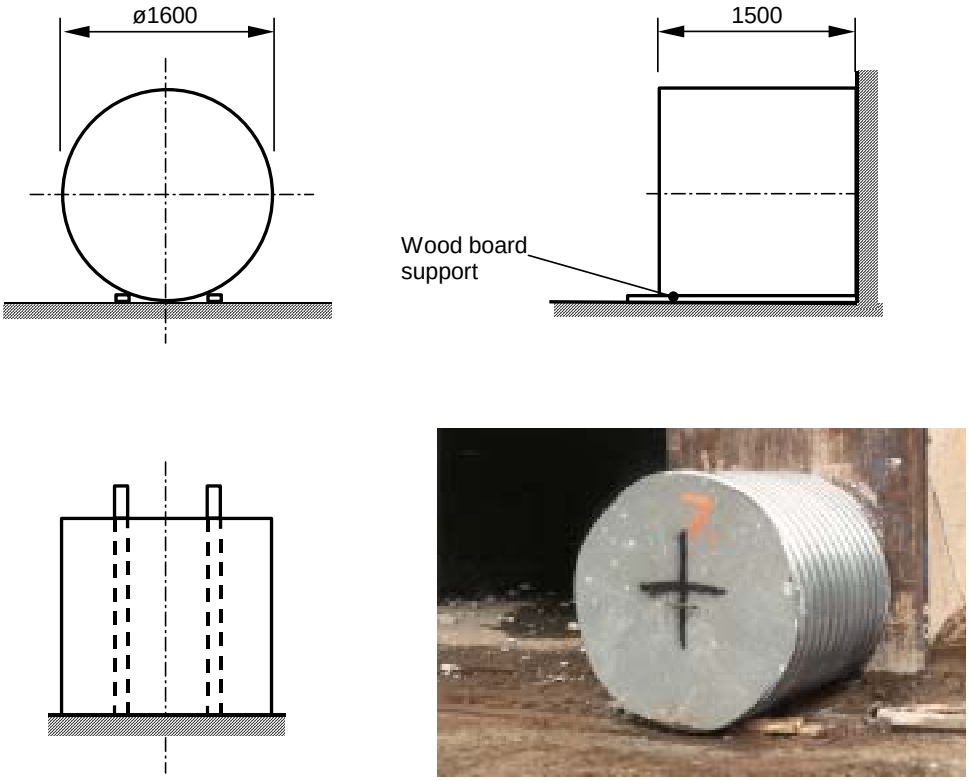

Figure B.23. Geometry for target 7 in test-series 1998:1.

Target 8

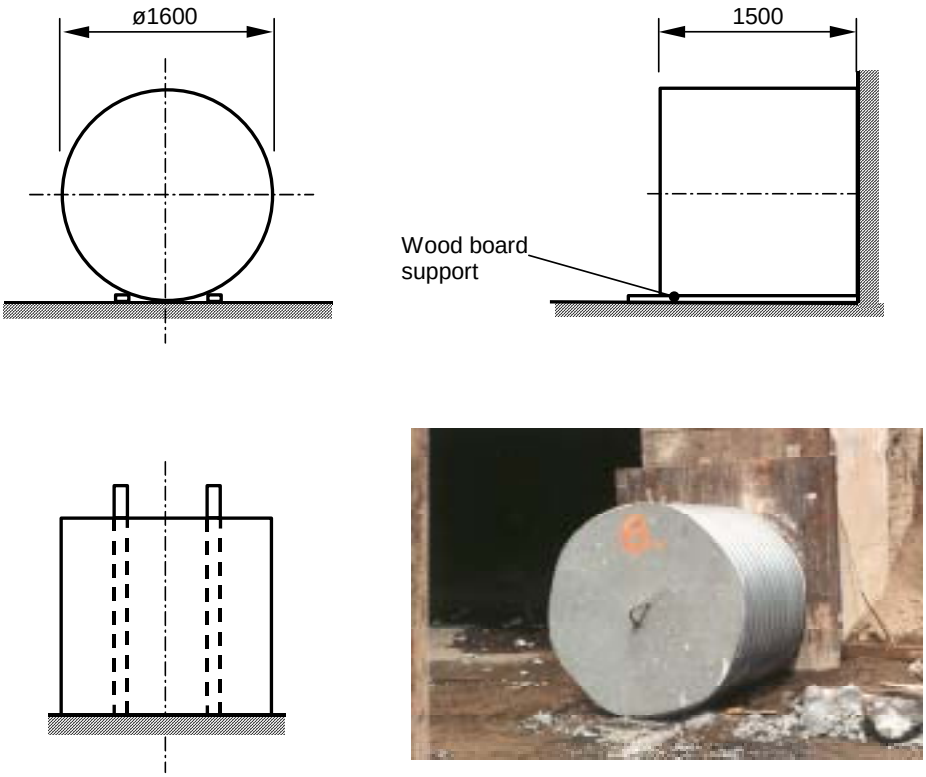

Figure B.24. Geometry for target 8 in test-series 1998:1.

Target 9

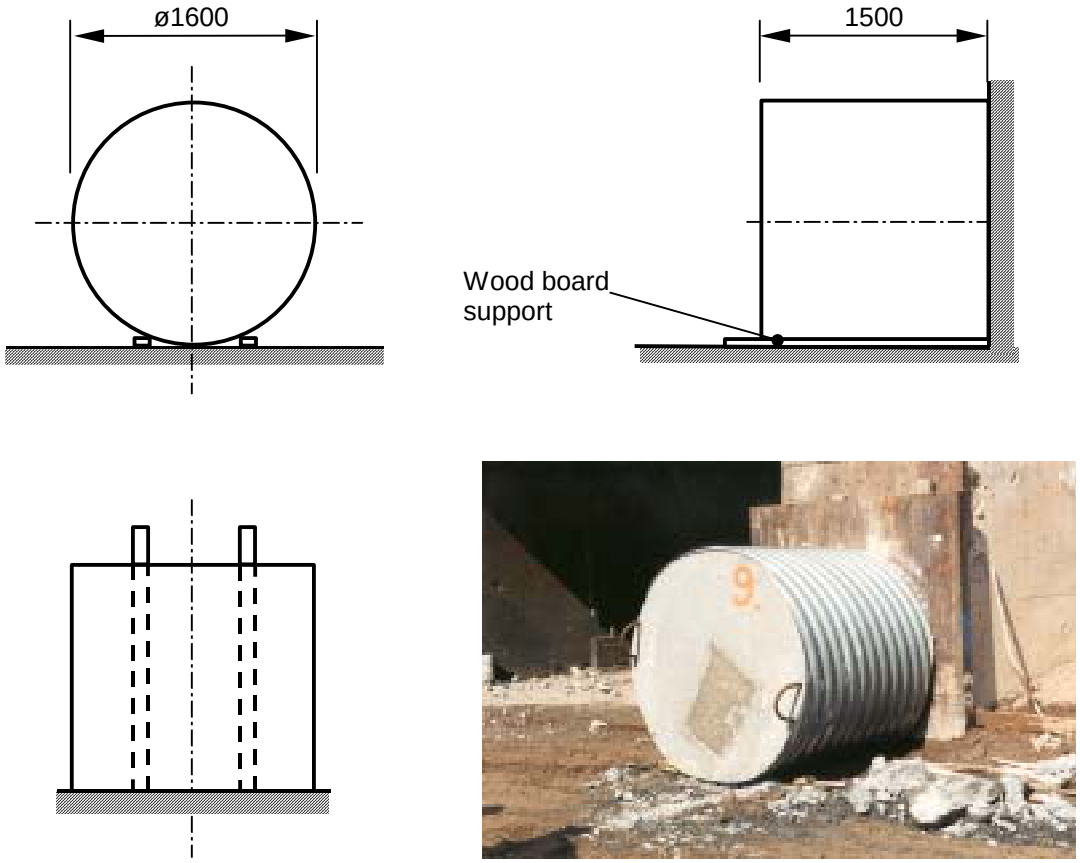

Figure B.25. Geometry for target 9 in test-series 1998:1.

Test series 1998:2

Target 1

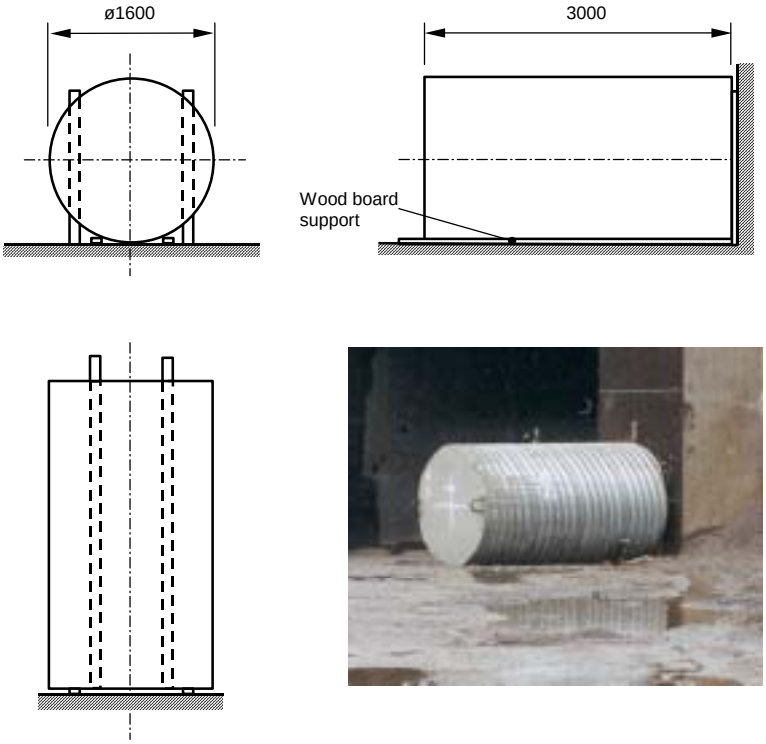

Figure B.26. Geometry for target 1 in test-series 1998:2.

Target 2

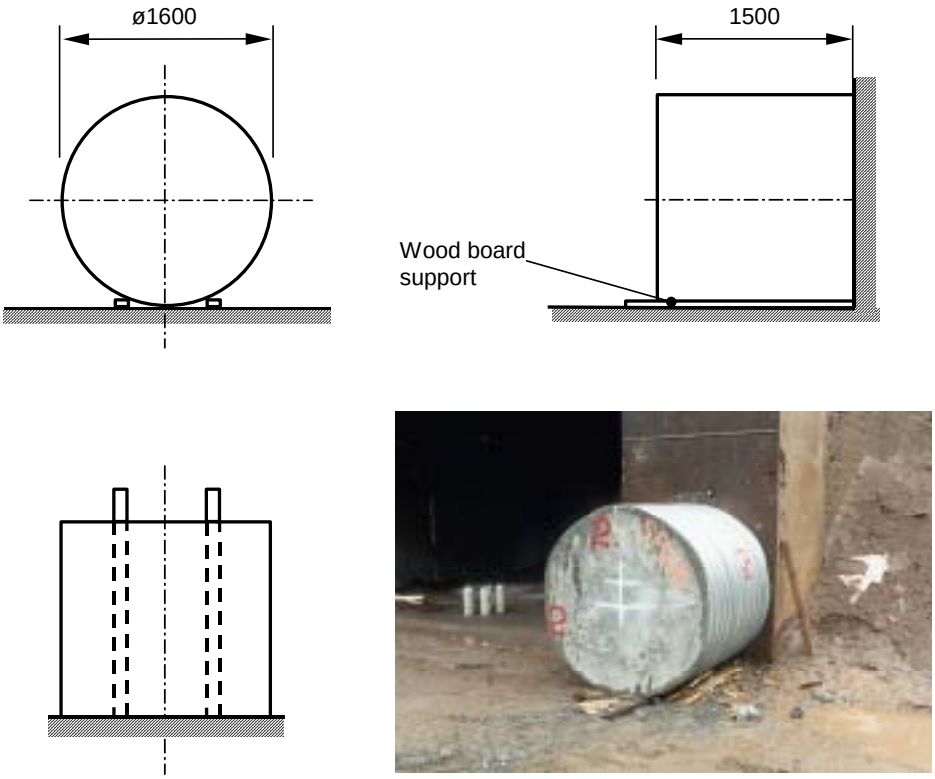

Figure B.27. Geometry for target 2 in test-series 1998:2.

Target 3

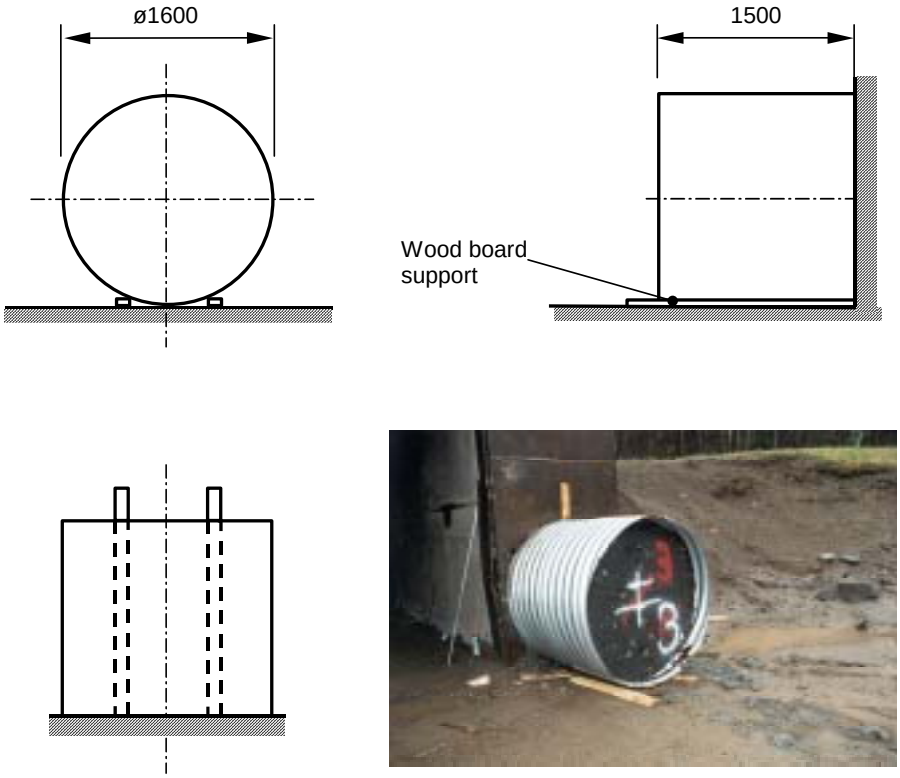

Figure B.28. Geometry for target 3 in test-series 1998:2.

Target 4

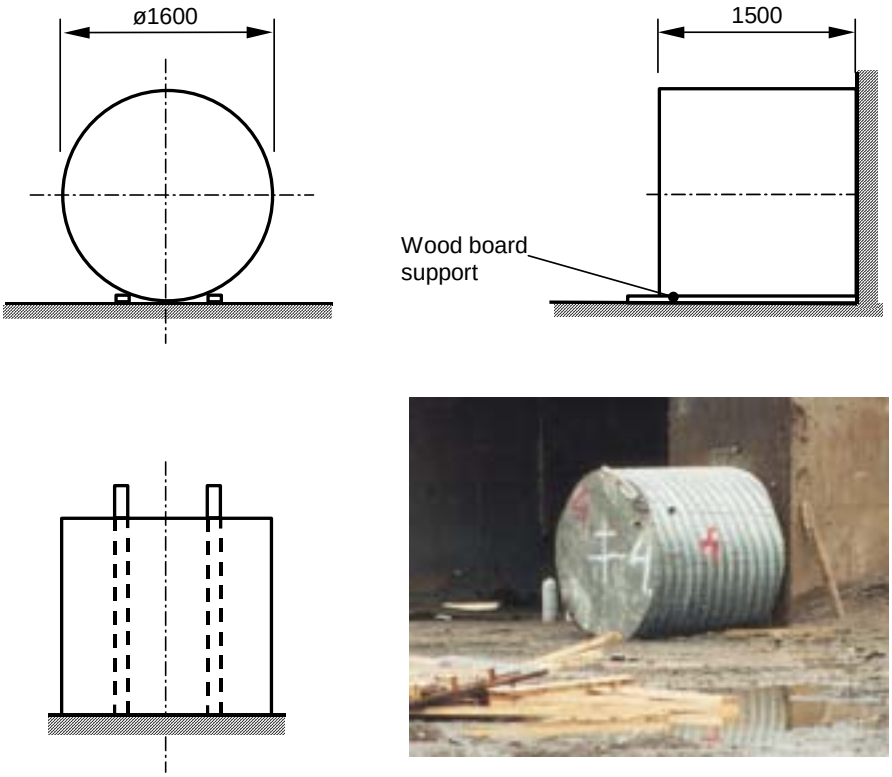

Figure B.29. Geometry for target 4 in test-series 1998:2.

Target 5

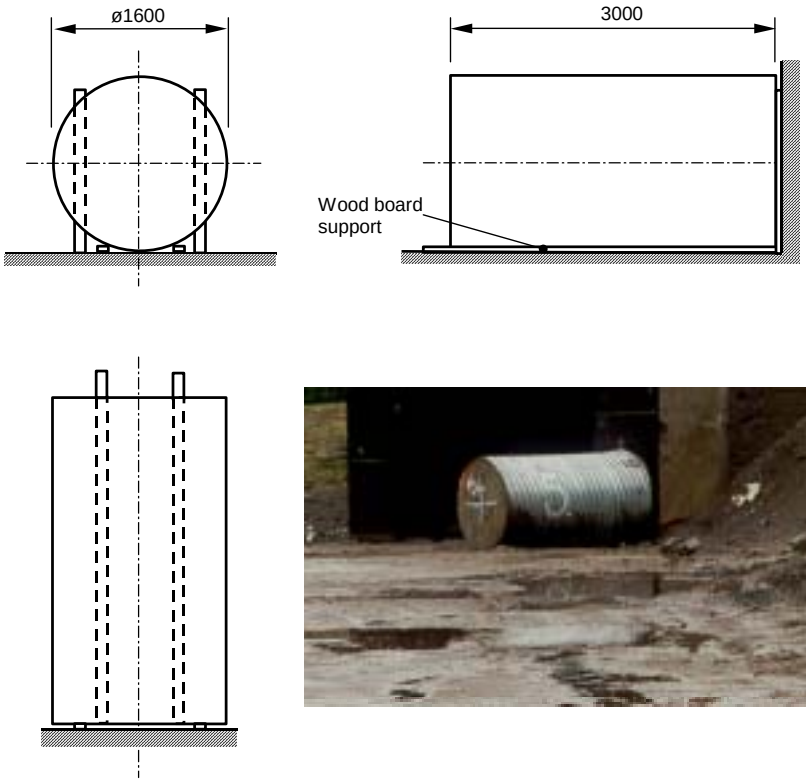

Figure B.30. Geometry for target 5 in test-series 1998:2.

Target 6

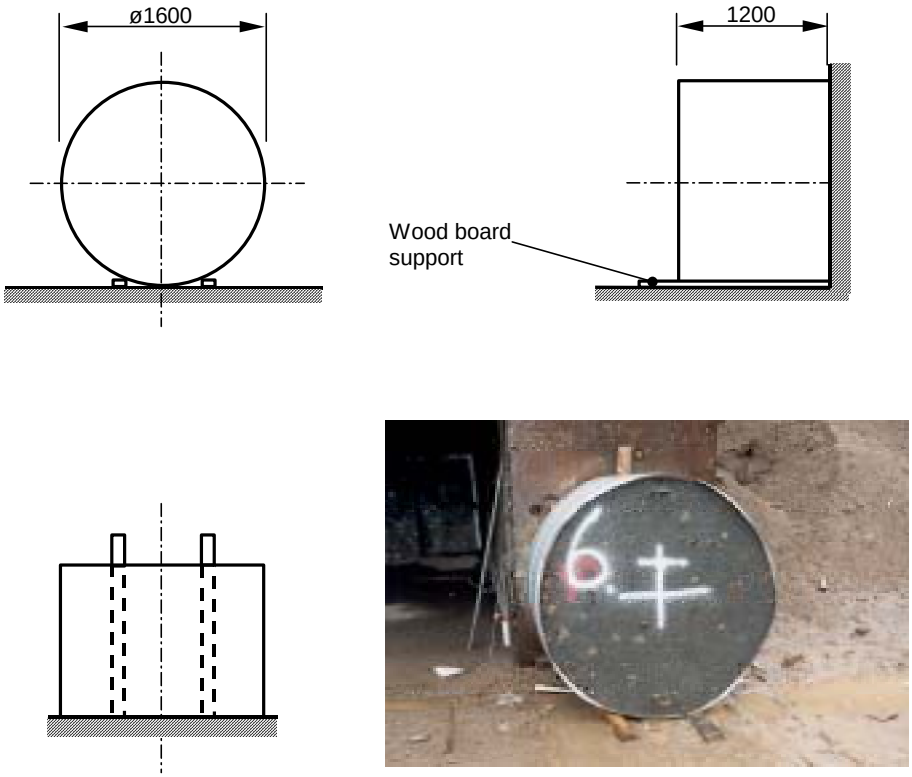

Figure B.31. Geometry for target 6 in test-series 1998:2.

Target 7

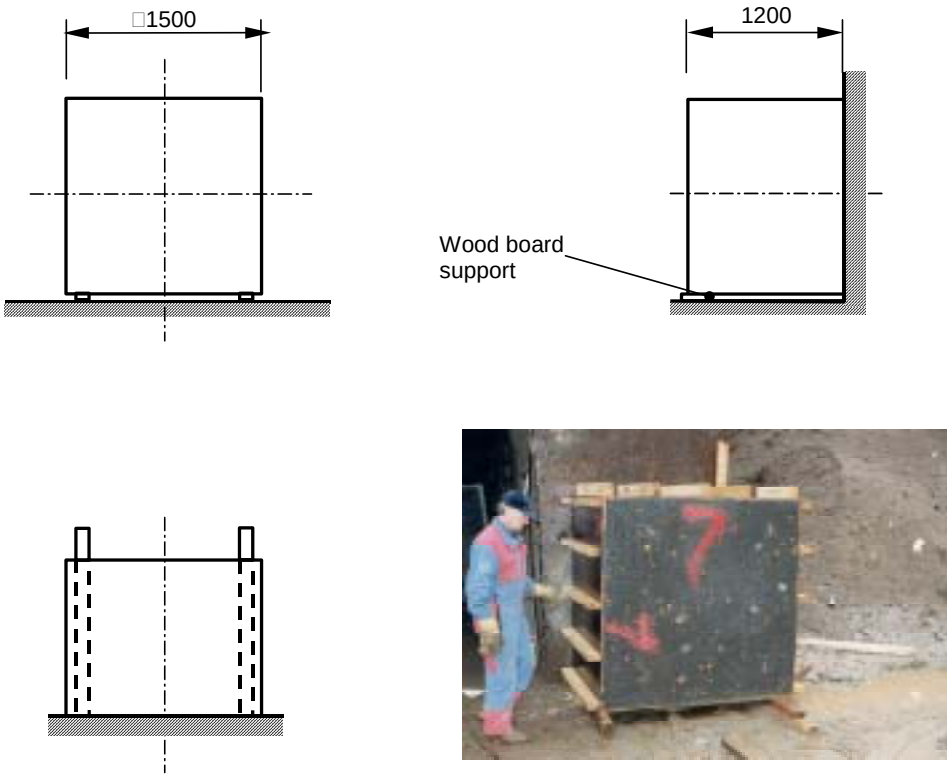

Figure B.32. Geometry for target 7 in test-series 1998:2.

Target 8

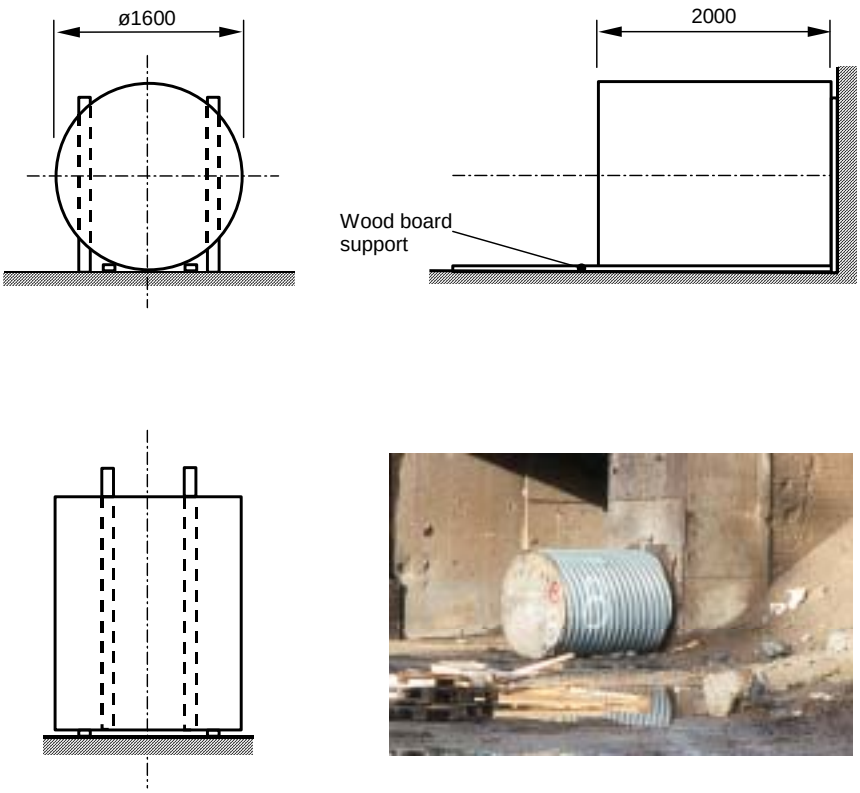

Figure B.33. Geometry for target 8 in test-series 1998:2.

Target 9

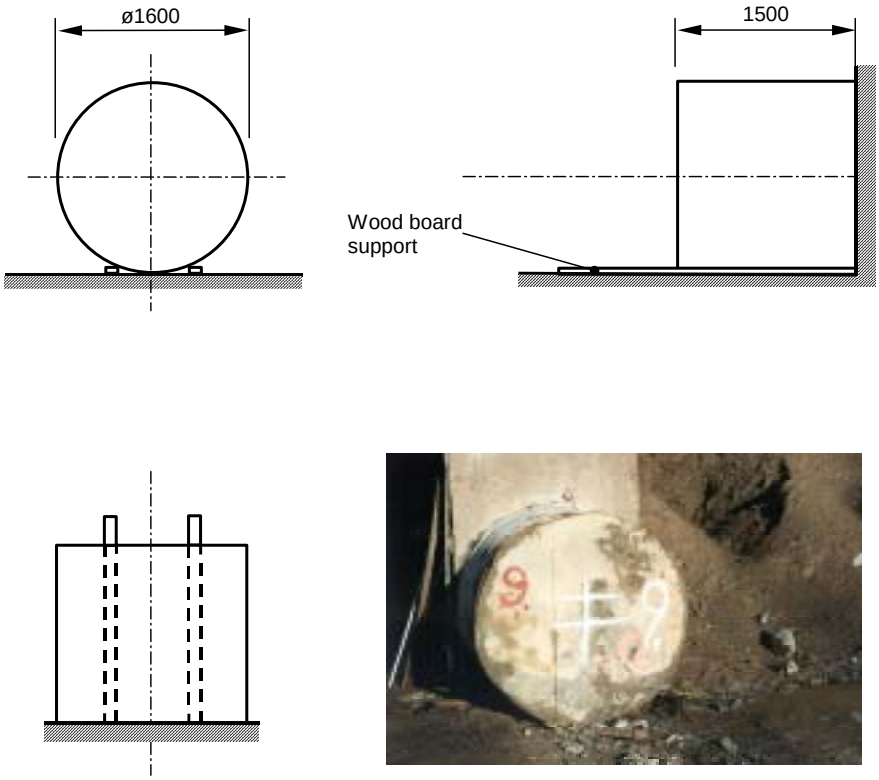

Figure B.34. Geometry for target 9 in test-series 1998:2.

Target 10

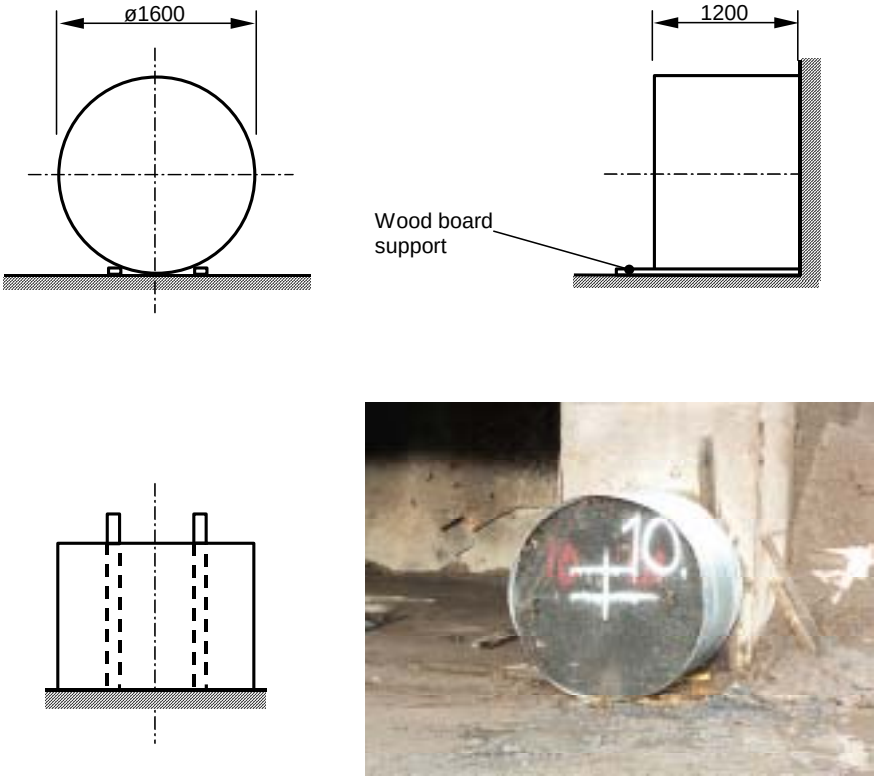

Figure B.35. Geometry for target 10 in test-series 1998:2.

Target 11

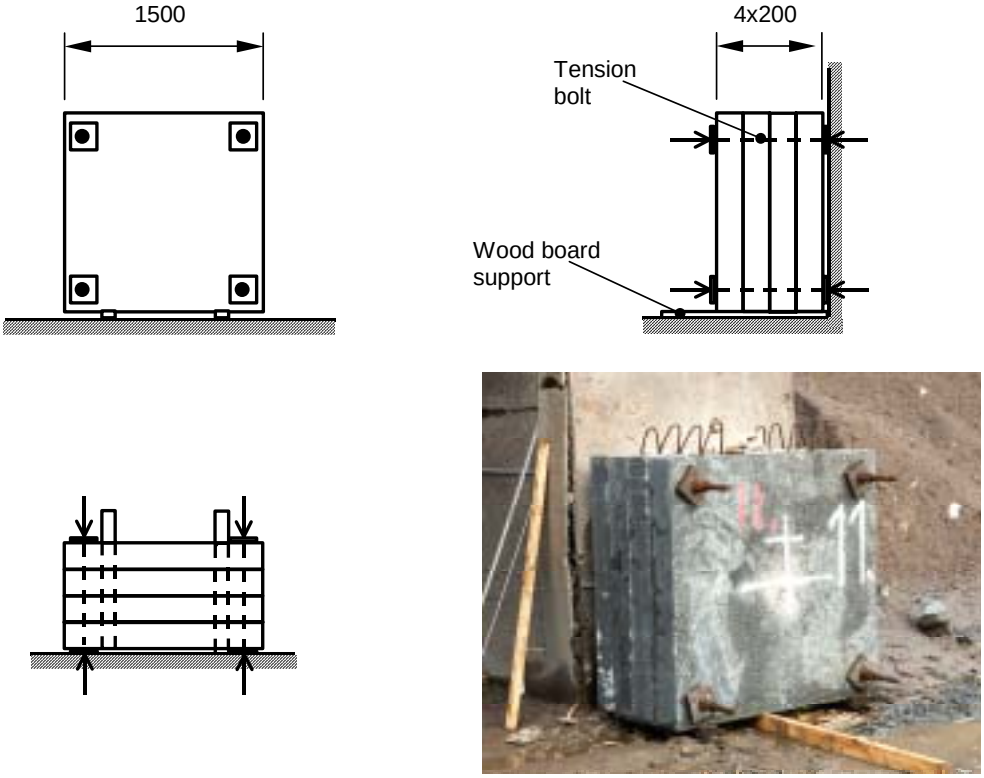

Figure B.36. Geometry for target 11 in test-series 1998:2.

Target 12

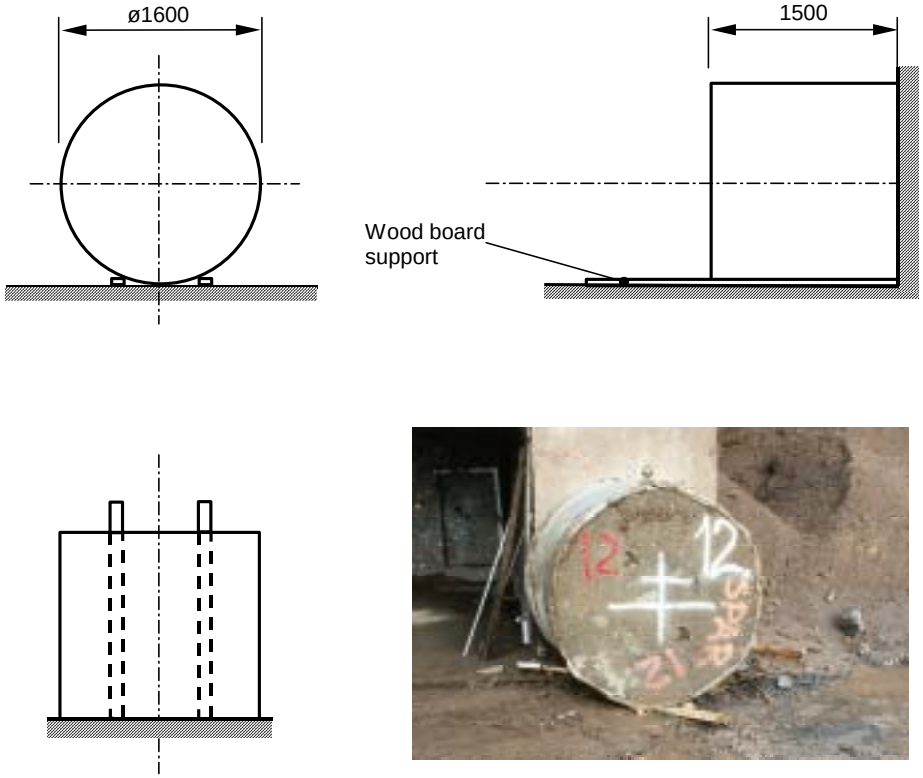

Figure B.37. Geometry for target 12 in test-series 1998:2.

Target 13

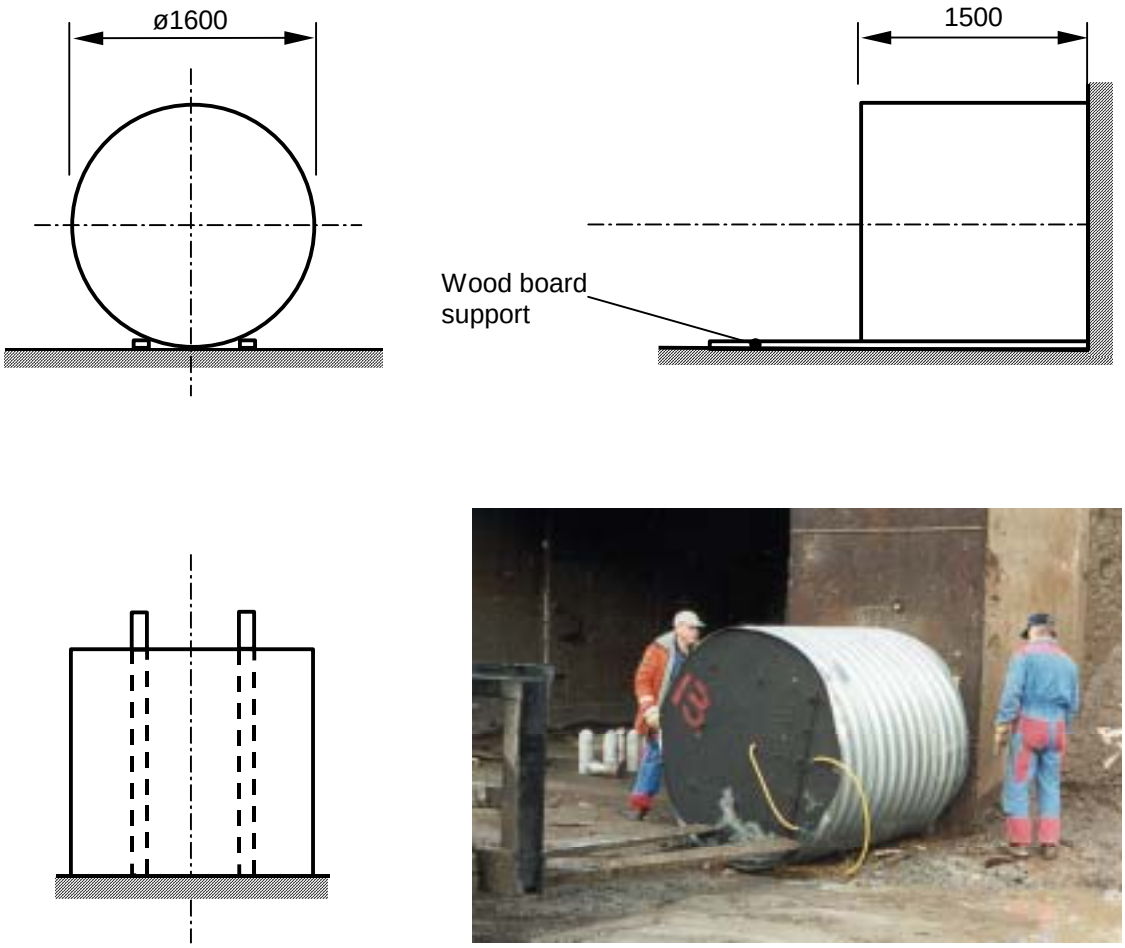

Figure B.38. Geometry for target 13 in test-series 1998:2.

Test series 1999

Target 1-3

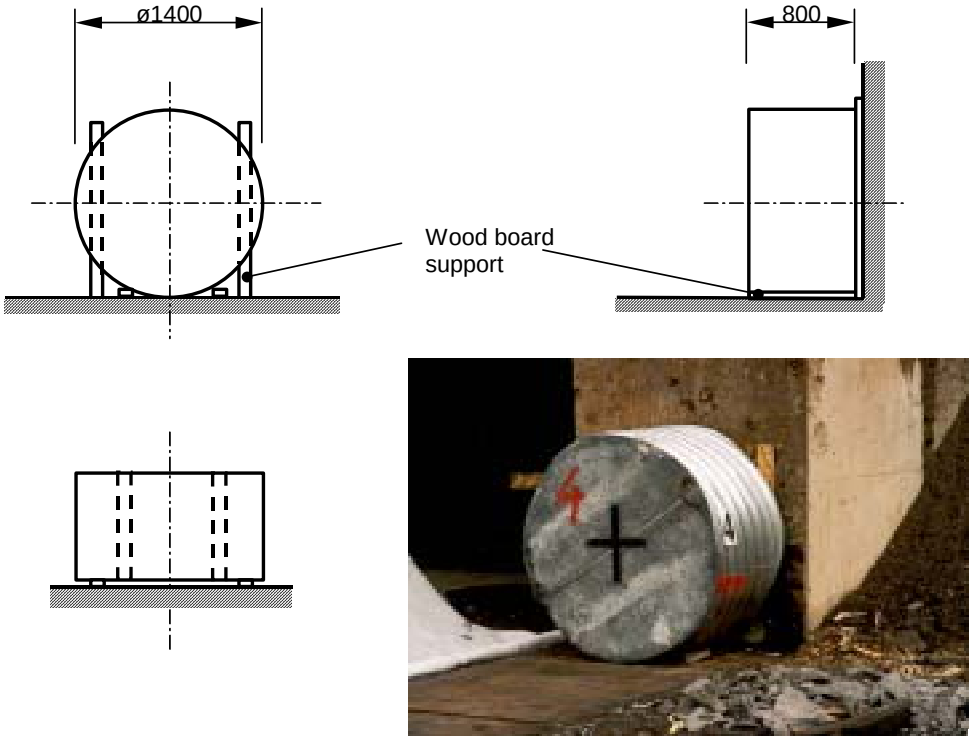

Figure B.39. Geometry for targets 1-3 in test-series 1999 and photo of target 1.

Target 4-6

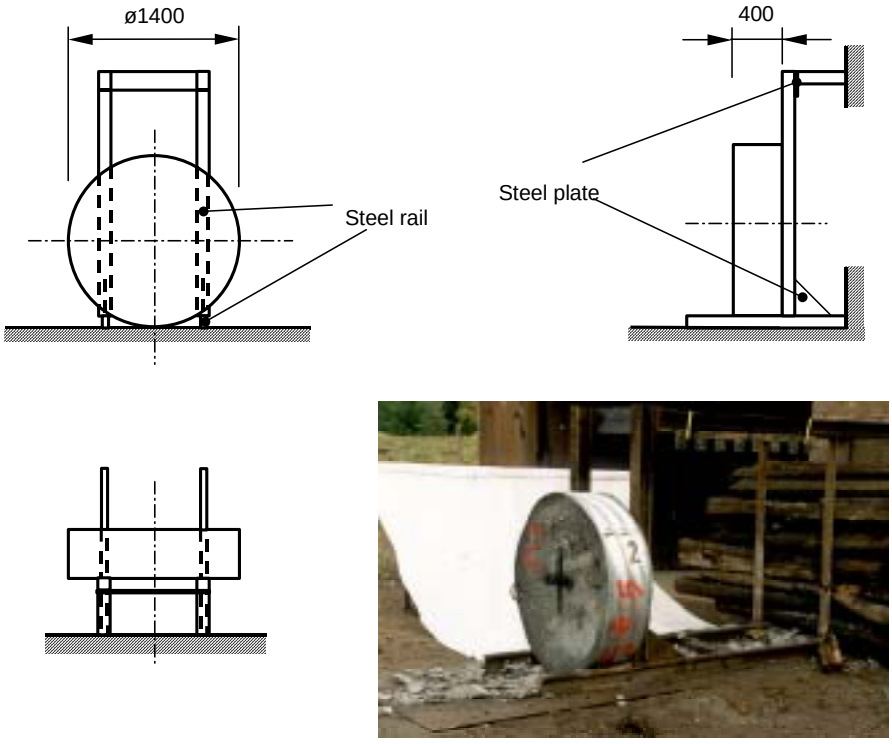

Figure B.40. Geometry for targets 4-6 and photo of target 5 in test-series 1999.

Target 7-8

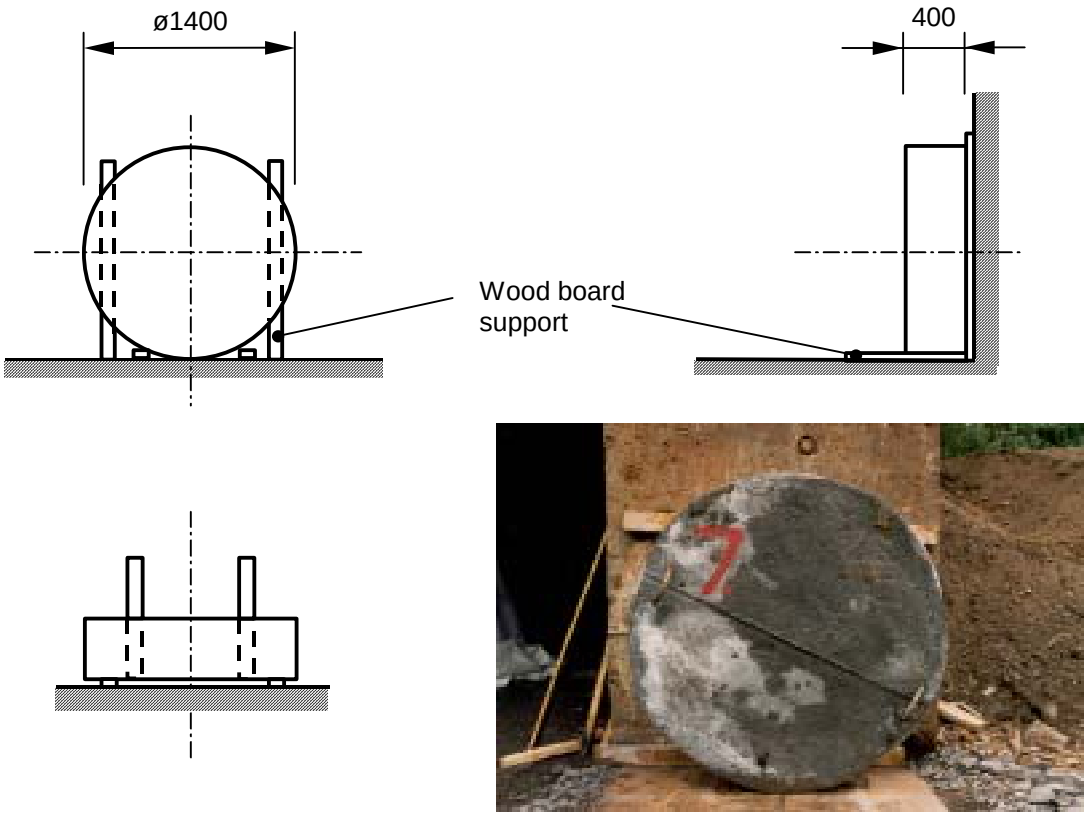

Figure B.41. Geometry for targets 7-8 in test-series 1999.

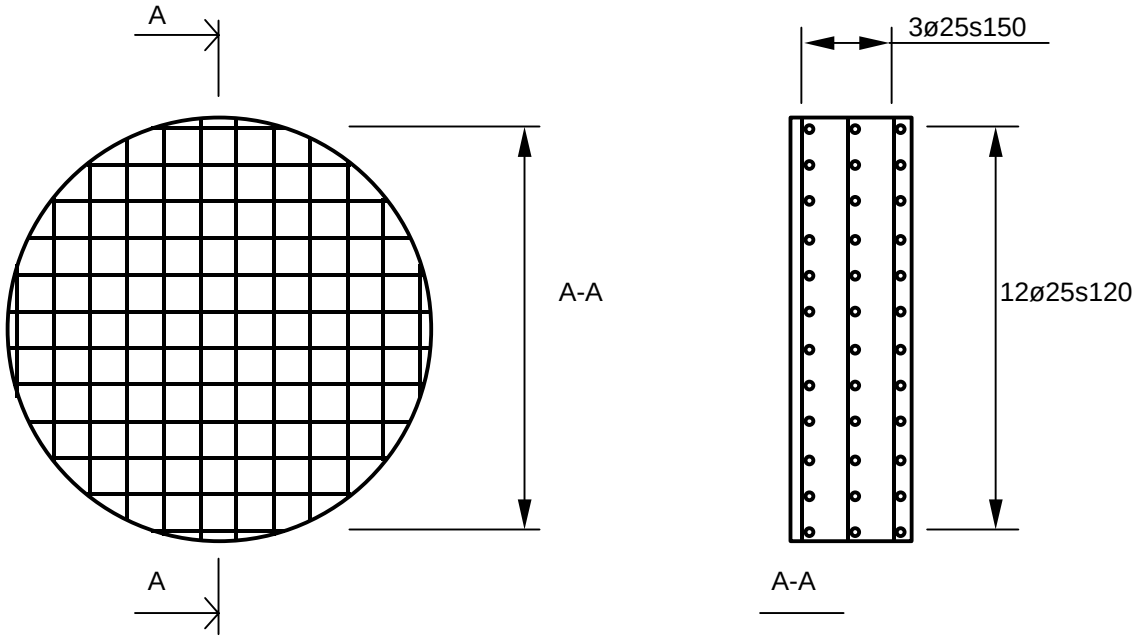

Figure B.42. Reinforcement in targets 7-9 in test-series 1999.

Target 9

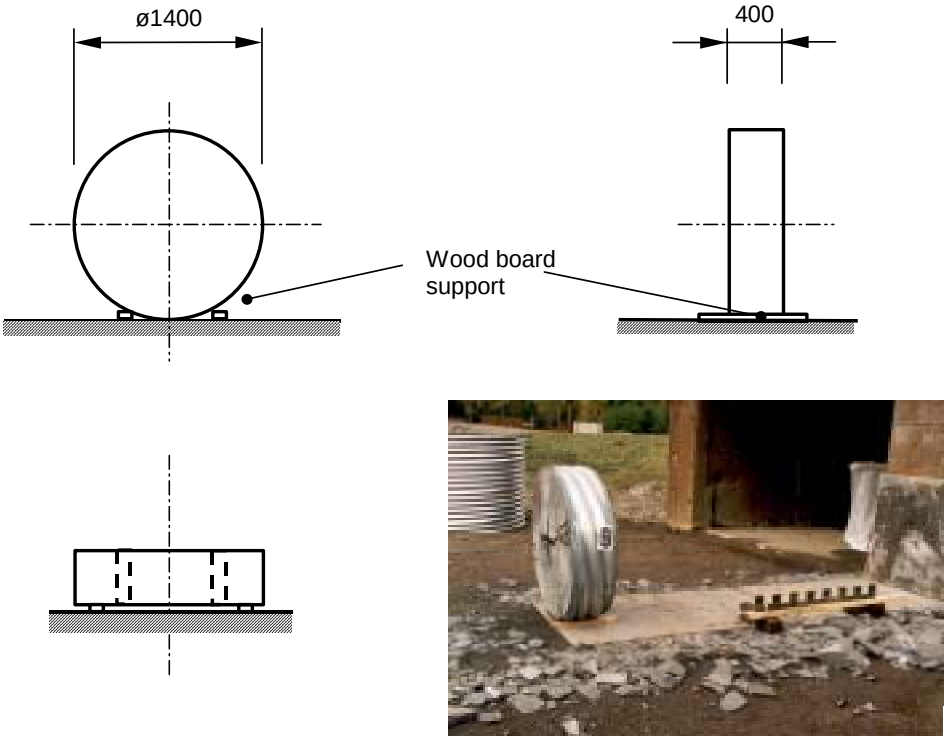

Figure B.43. Geometry for target 9 in test-series 1999.

Target 10

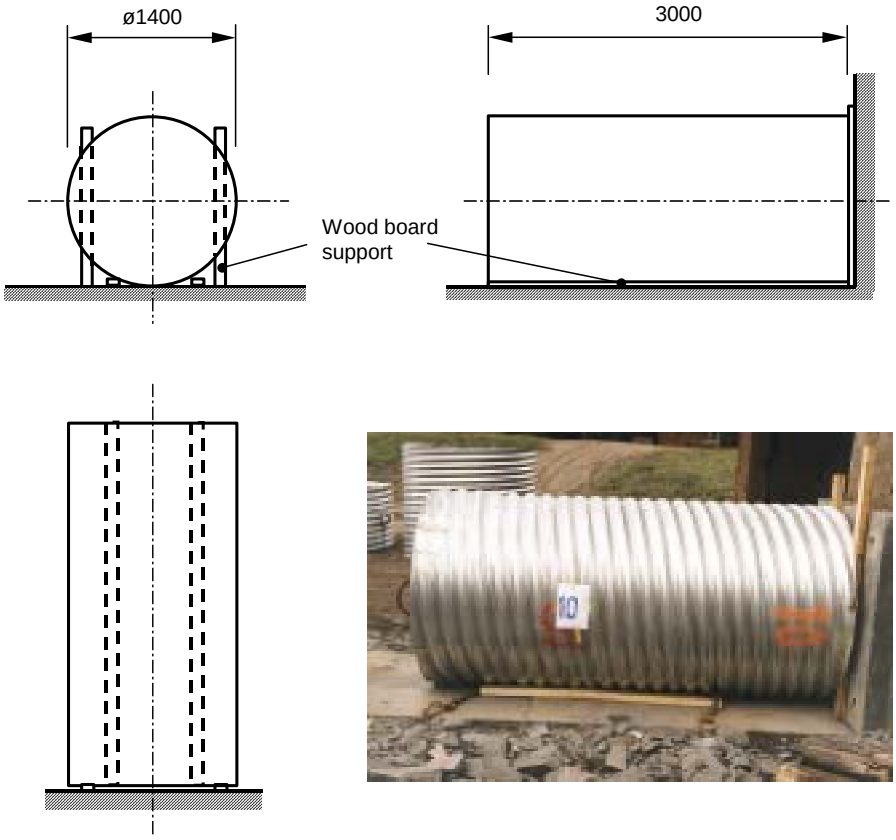

Figure B.44. Geometry for target 10 in test-series 1999.

Target 11

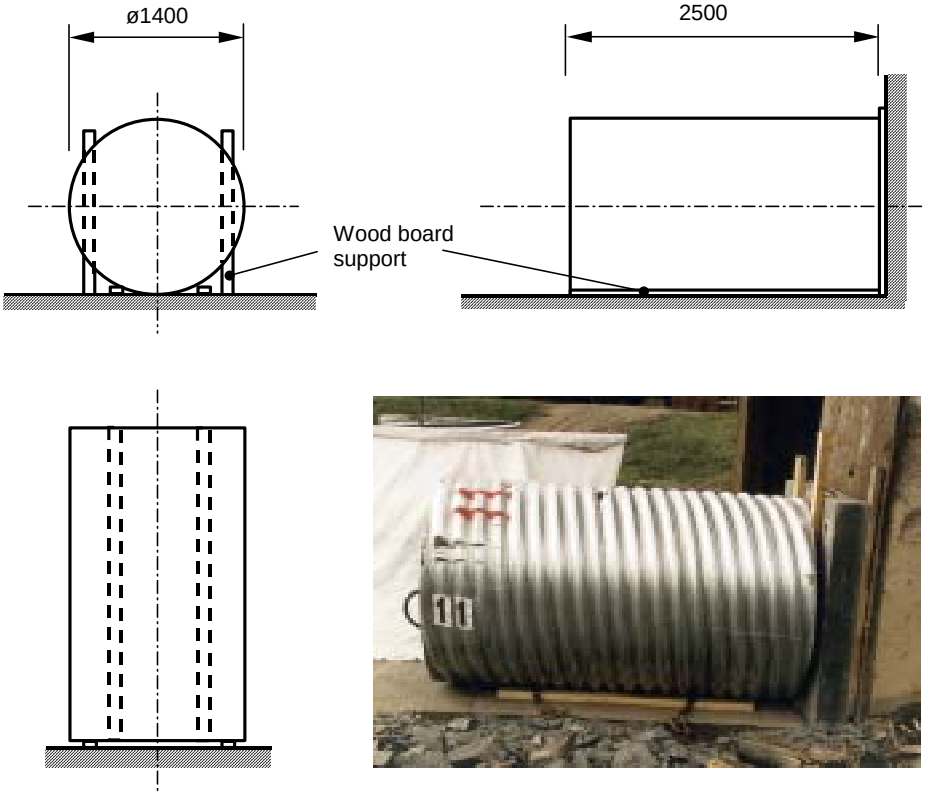

Figure B.45. Geometry for target 11 in test-series 1999.

Target 12

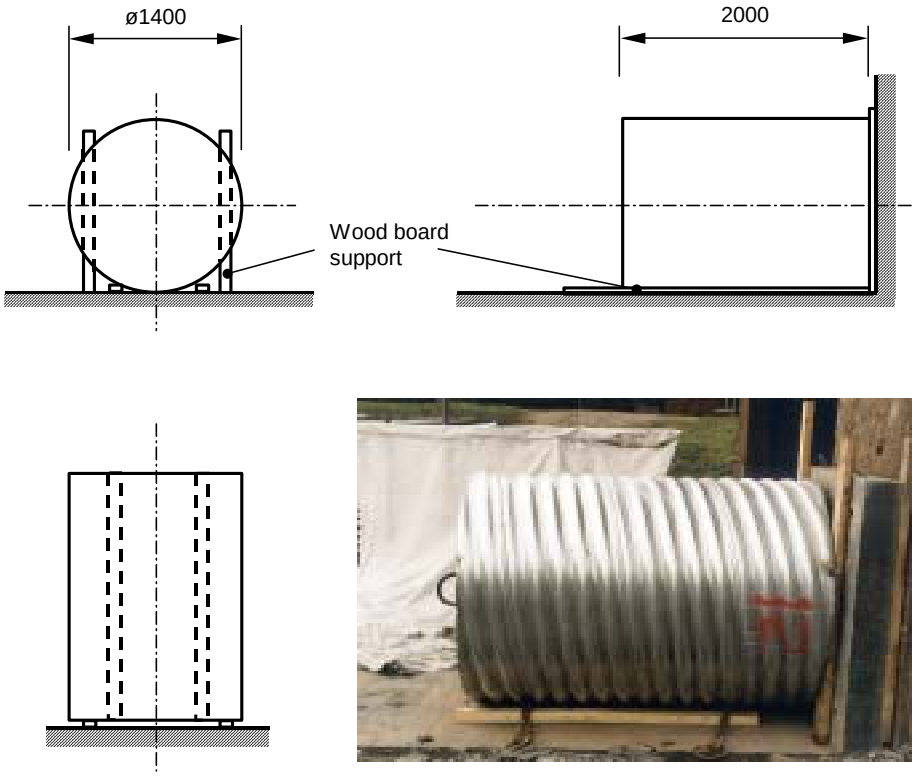

Figure B.46. Geometry for target 12 in test-series 1999.

Target 13

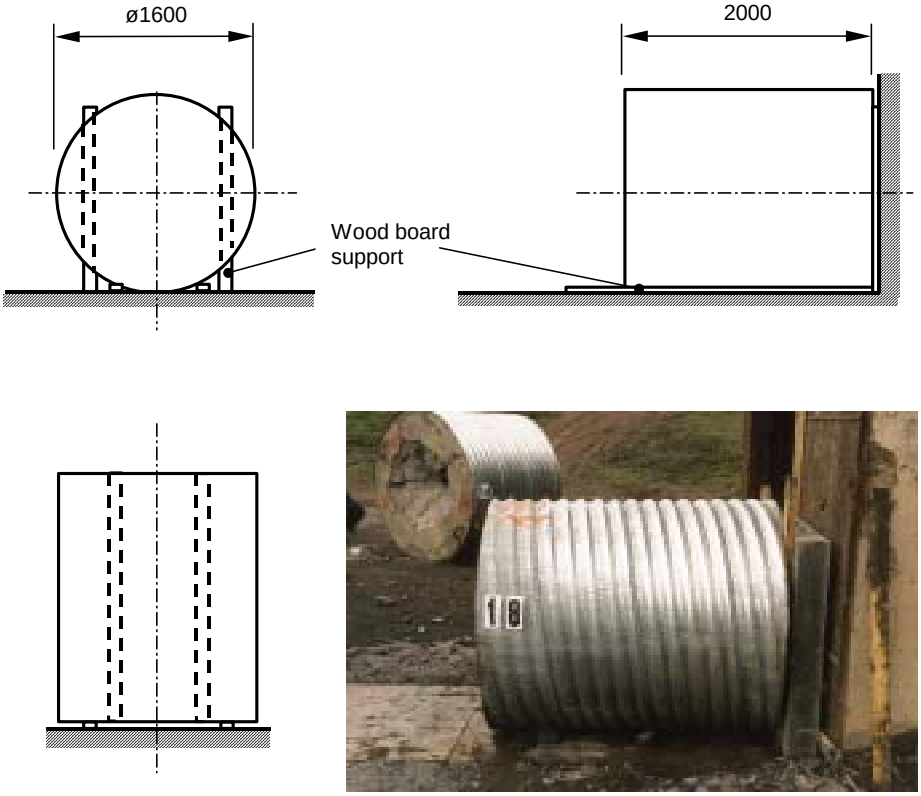

Figure B.47. Geometry for target 13 in test-series 1999.

Target 14

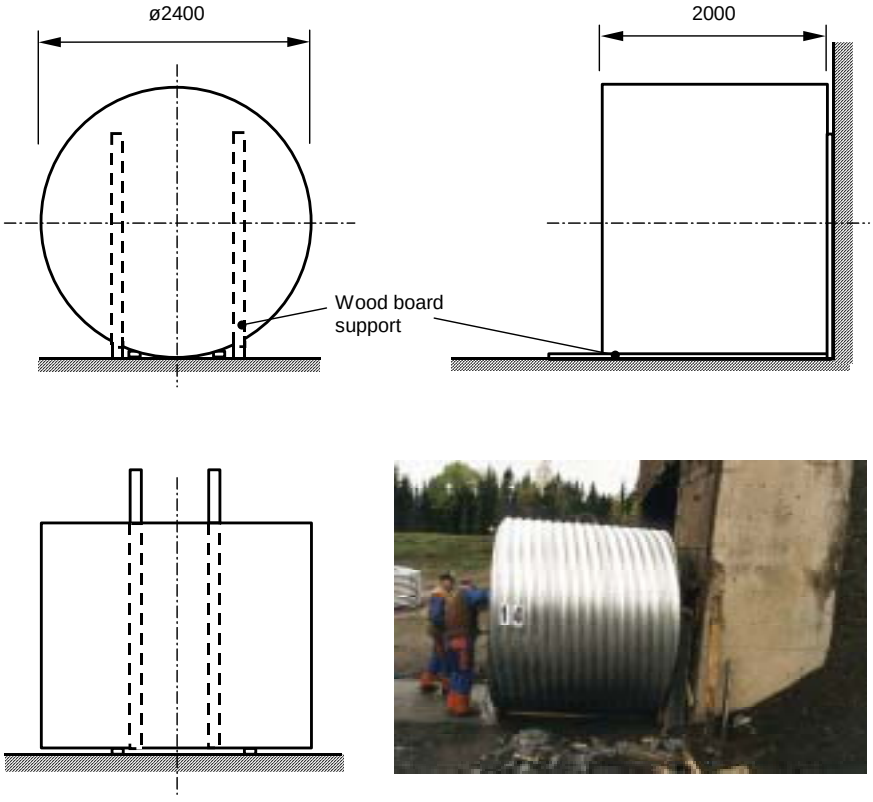

Figure B.48. Geometry for target 14 in test-series 1999.

Target 15

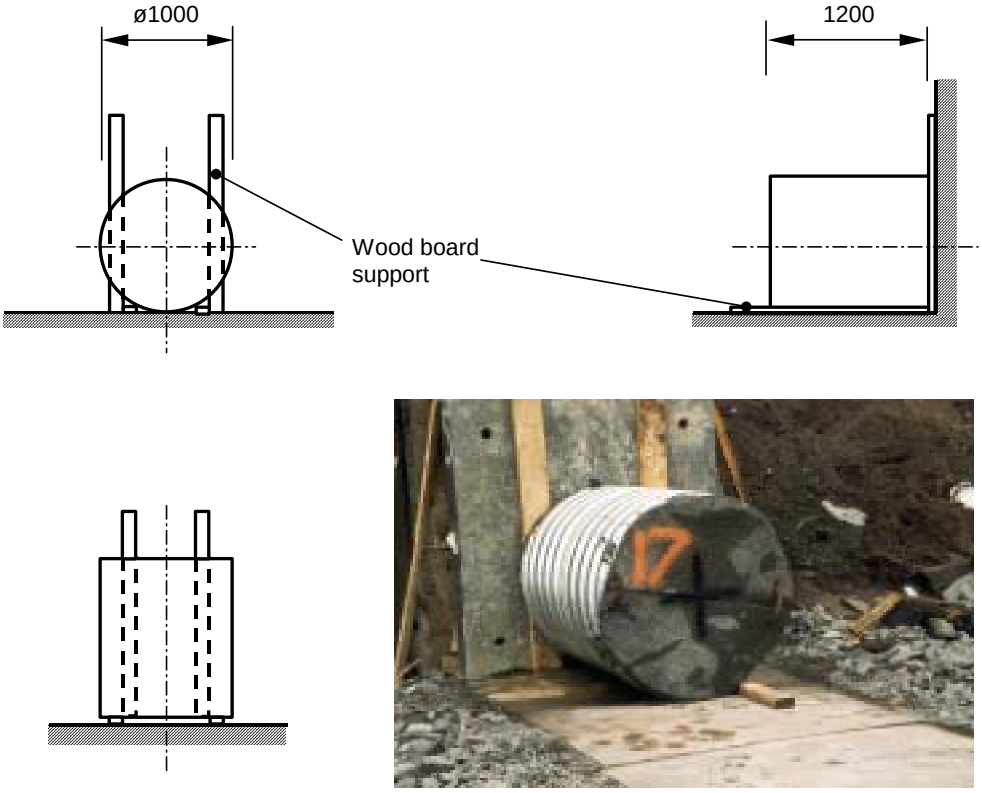

Figure B.49. Geometry for target 15 in test-series 1999.

Target 16

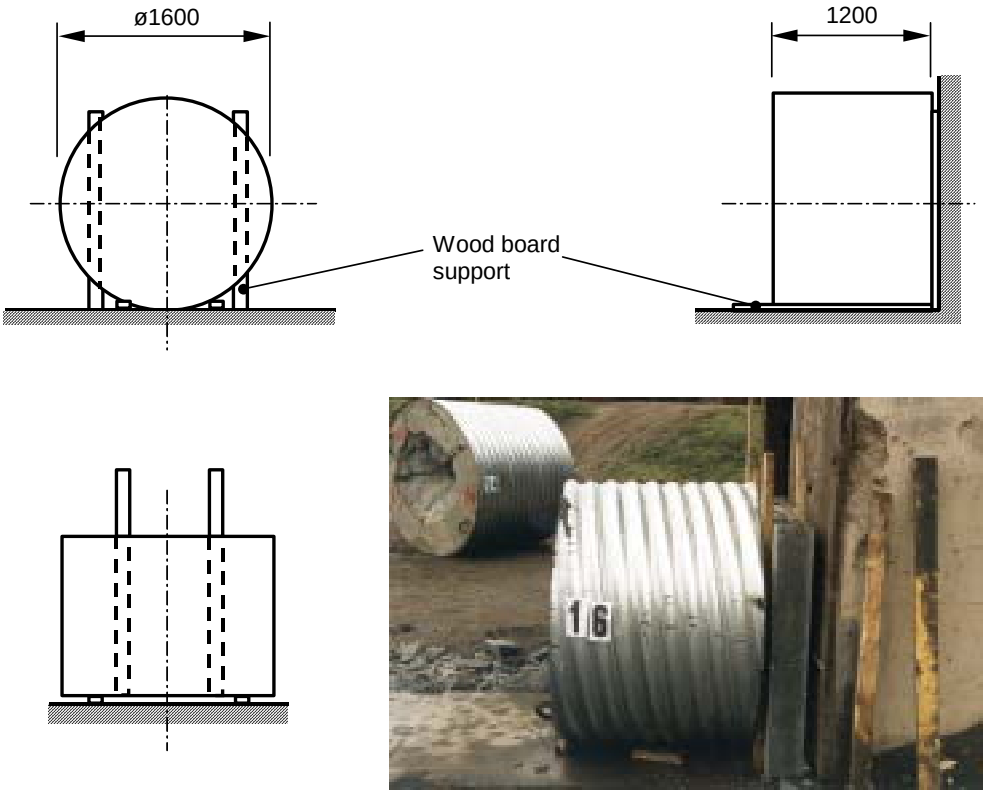

Figure B.50. Geometry for target 16 in test-series 1999.

Target 17

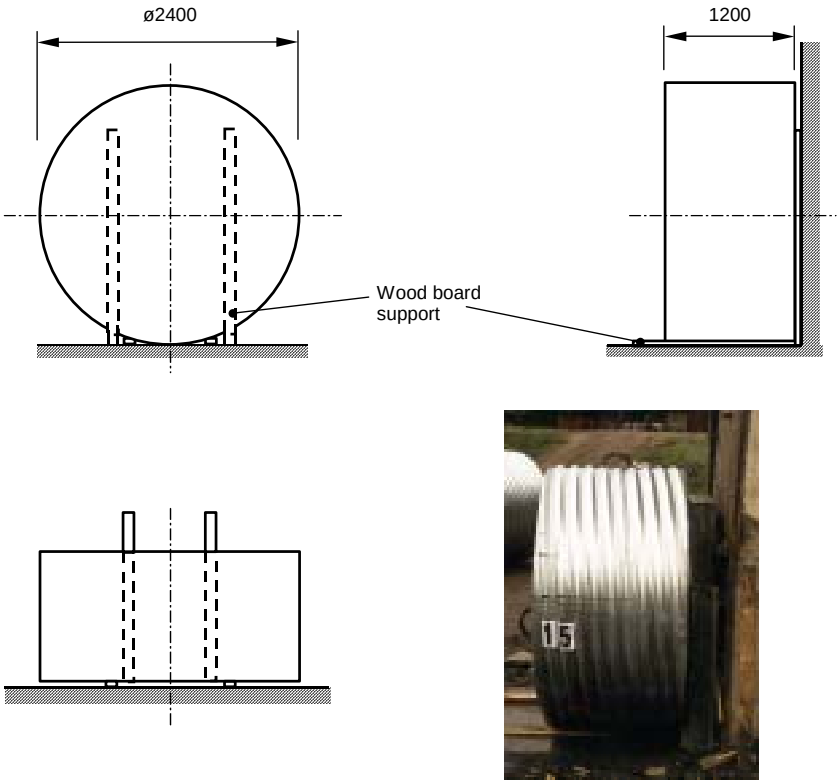

Figure B.51. Geometry for target 17 in test-series 1999.

Target 18

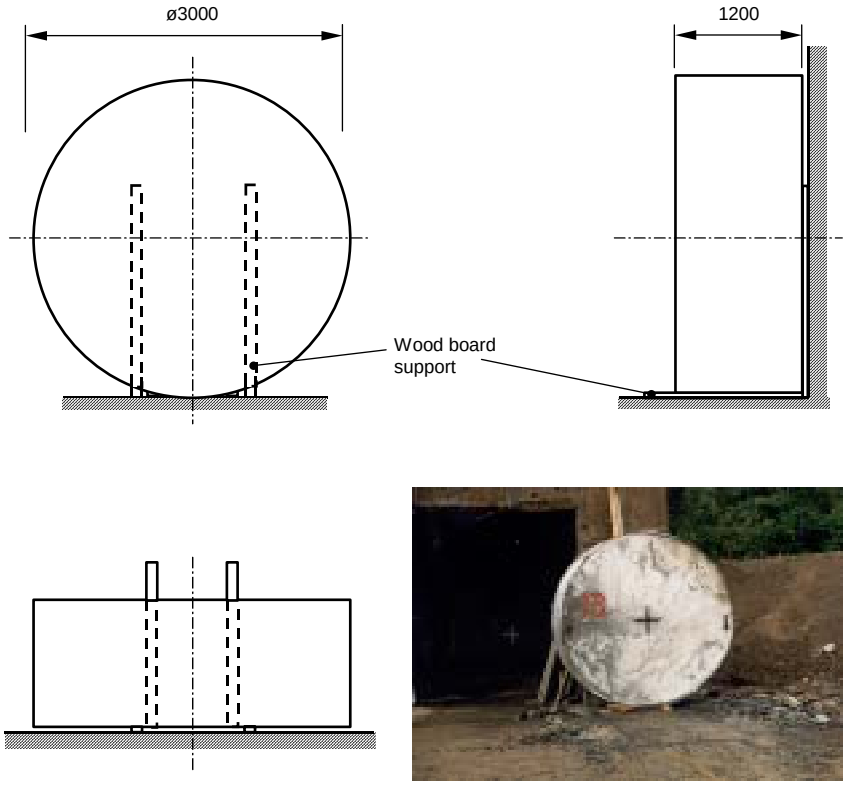

Figure B.52. Geometry for target 18 in test-series 1999.

Target 19

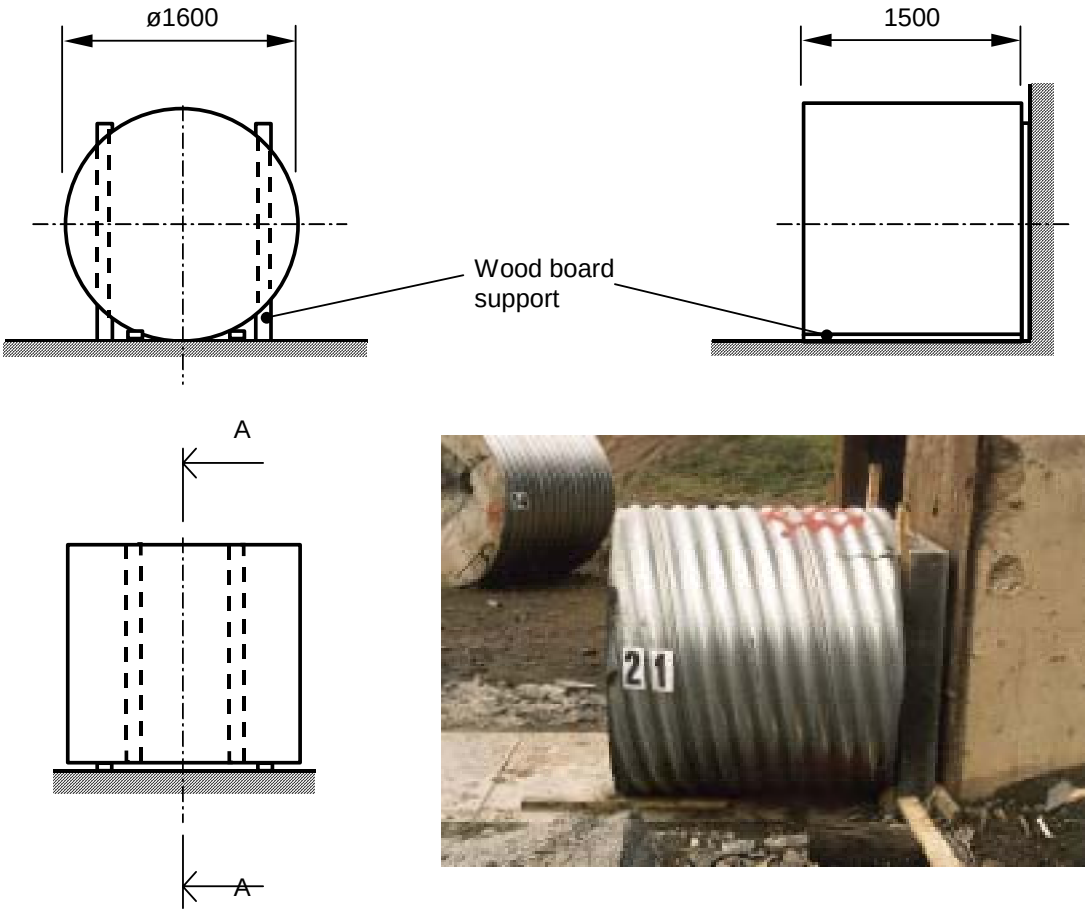

Figure B.53. Geometry for target 19 in test-series 1999.

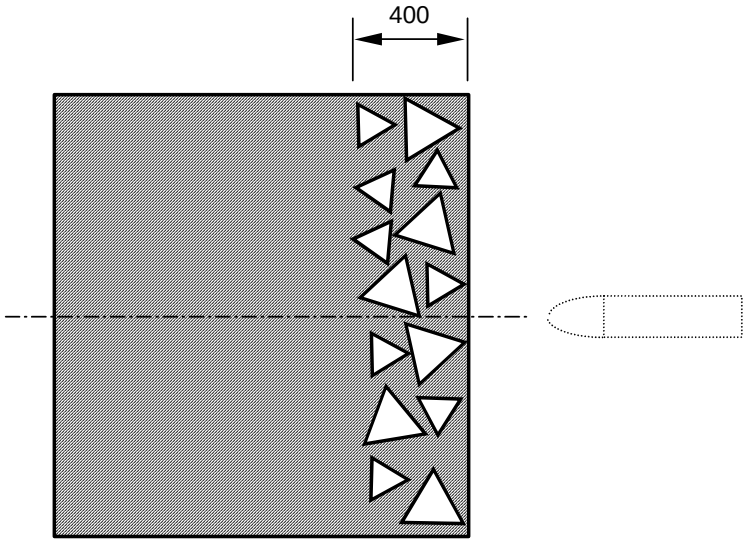

A-A scale 1:25

Figure B.54. Cross-section of target 19 in test-series 1999.

Target 20

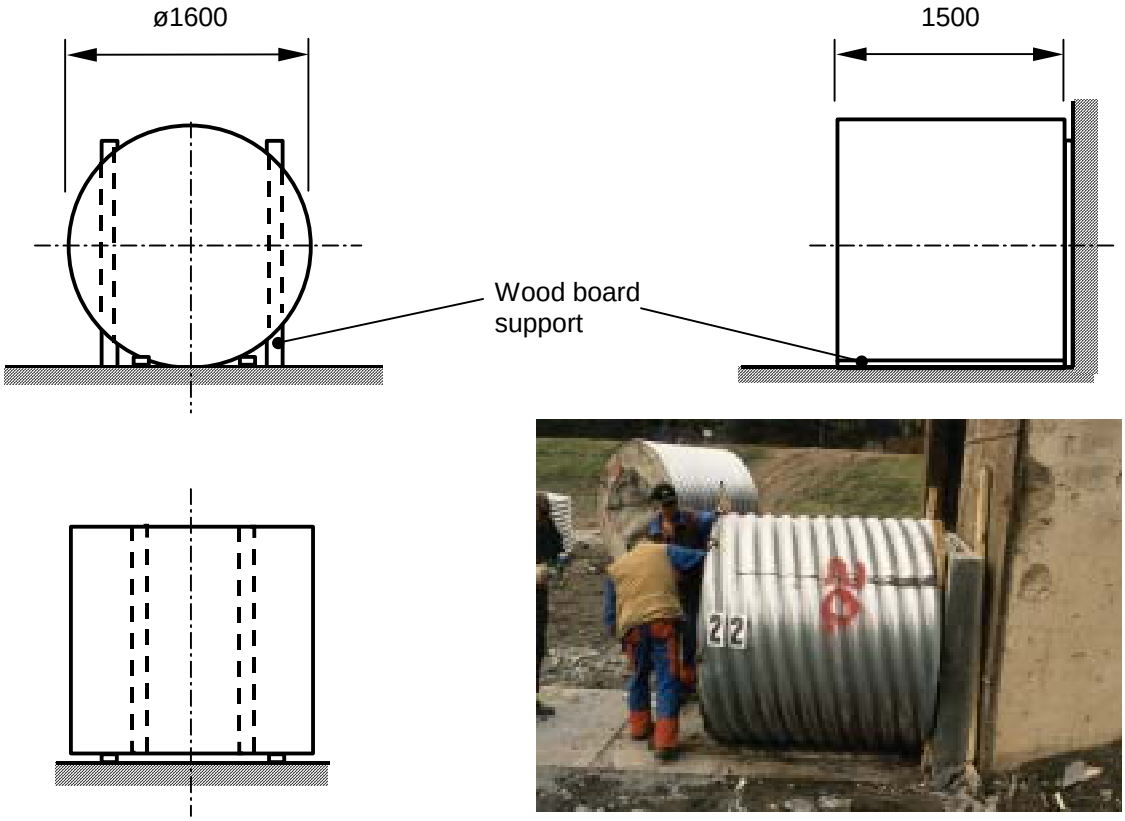

Figure B.55. Geometry for target 20 in test-series 1999.

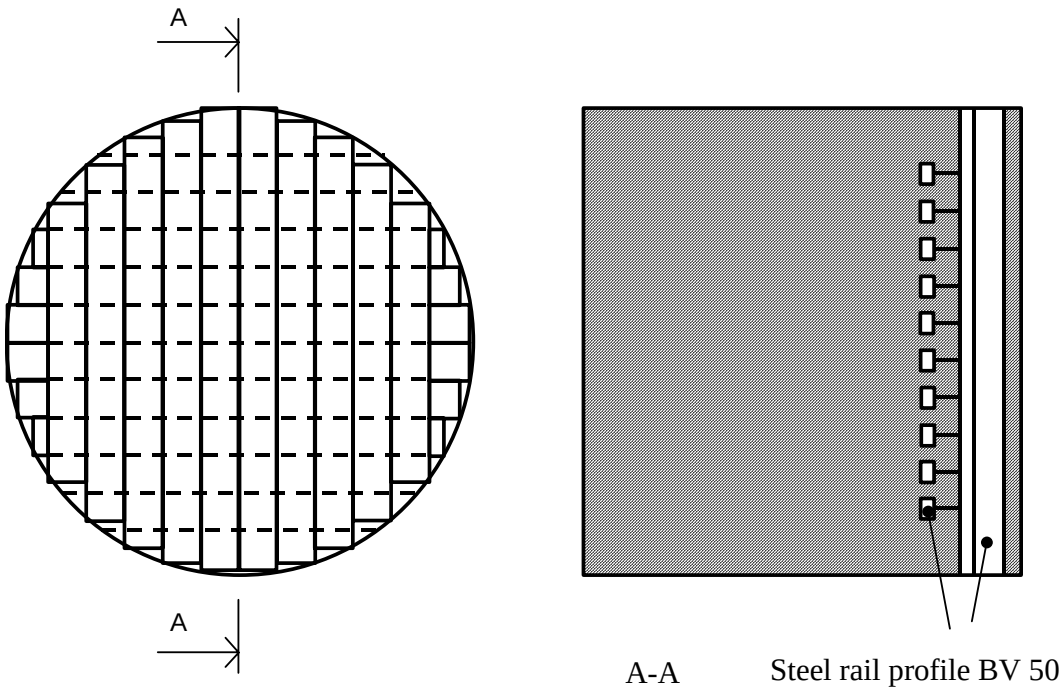

Figure B.56. Reinforcement for target 20 in test-series 1999.

Target 21

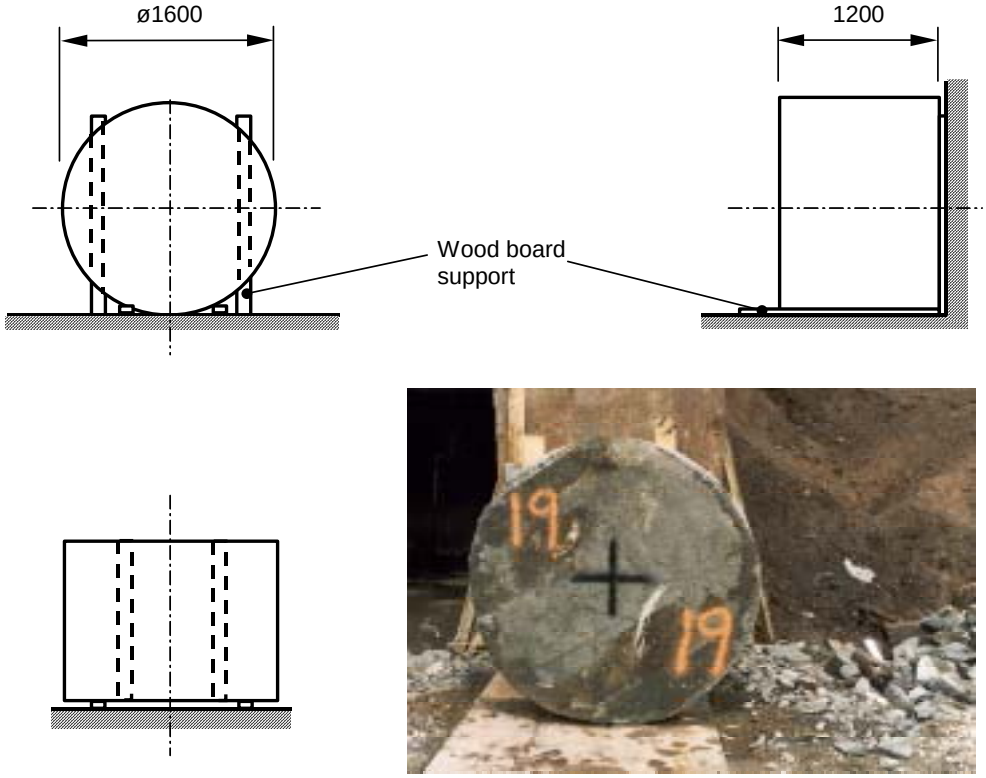

Figure B.57. Geometry for target 21 in test-series 1999.

Target 22

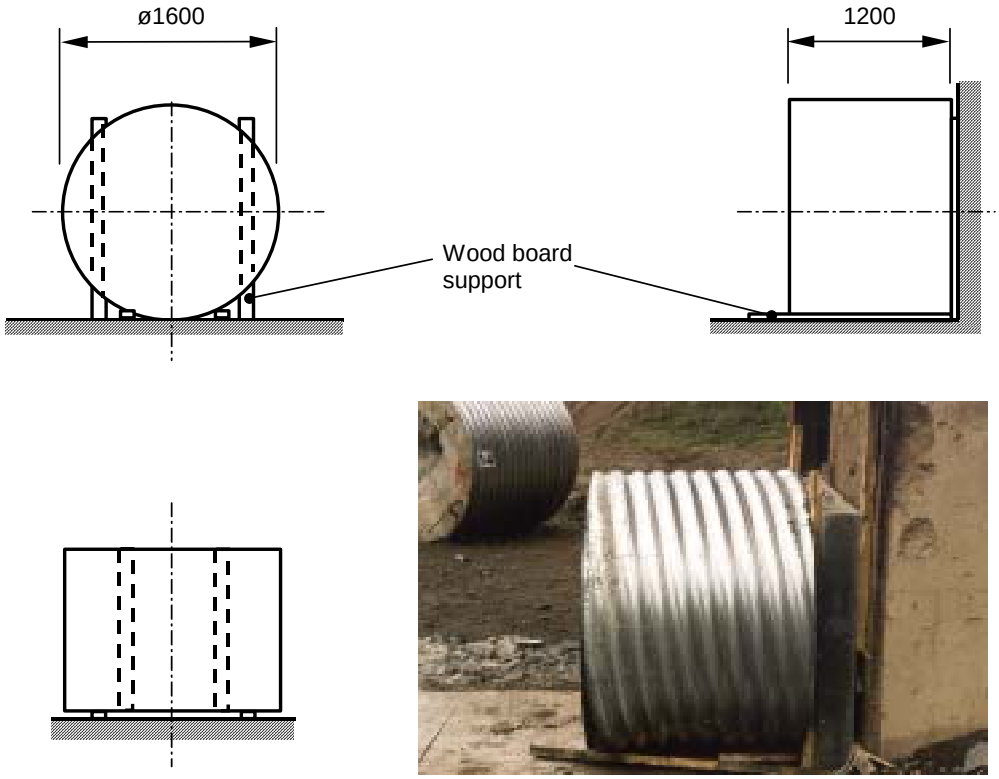

Figure B.58. Geometry for target 22 in test-series 1999.

Target 23-25

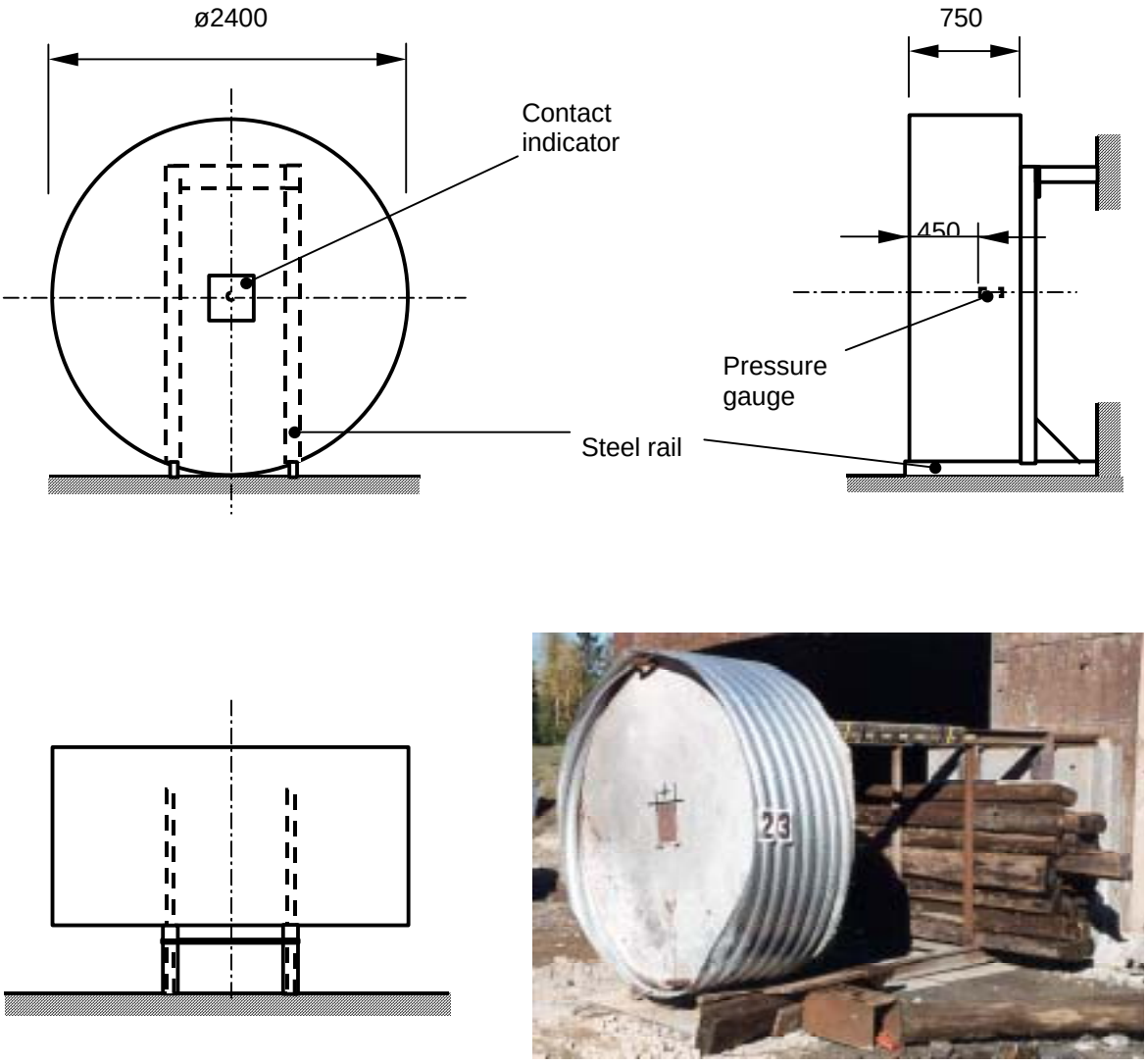

Figure B.59. Geometry for targets 23-25 in test-series 1999.

C TEST RESULTS

Target specific comments are given here and a compilation table for each test series. Appendix C presents post-test target configurations, Appendix D Doppler-radar data, Appendix E pressure gauge registrations and Appendix F projectile acceleration registrations.

Test series 1996:1

The following results were observed after the tests:

Target 1: The projectile perforated the target. When the target was disassembled, it was found that the hole in the first target plate deviated from the projectiles angle of impact, i.e. the projectile changed direction (downwards) when penetrating the first target plate. The projectile continued 25 m until it impacted the backstop which the projectile penetrated approximately 50 mm.

Target 2: The projectile perforated the target. The projectile continued 25 m until it impacted the backstop which the projectile penetrated approximately 30 mm. A part of the sabot was found in the hole.

Target 3: Two shots were fired at this target. One of the projectiles penetrated the target 1.25 m and came to rest in target plates 6 and 7. The projectile was broken into two parts, the rear part was found in target plate 6 and the front part, i.e. the nose, was stuck in target plate 7. A part of the sabot was found in the hole.

Target 4: The projectile penetrated the target 0.52 m and came to rest in target plate 3.

Test series 1996:2

The following results were observed after the tests:

Target 1: The projectile perforated the target with a negligible residual velocity and the target was destroyed. Radial movement of the concrete was not prevented due to failure of the steel frame around the target.

Target 2: The projectile perforated and turned the target over. Each slab was held together by the reinforcement.

Target 3: The projectile penetrated the target 0.35 m. Little damage was made to the target. Cracks were found at the top faces of target plates 1 and 2. Some cracks were found at the back face of target plate 2 due to a 30-mm displacement in the direction of the projectile. The back face of target plate 3 was displaced approximately 10 mm. Target plates 4 and 5 showed no damage at an ocular inspection.

Target 4: The projectile penetrated the target 0.60 m and turned the target over. Large damage was made to target plates 1 and 2. The projectile was stuck in target plate 4 and pushed target plates 4 and 5 without penetrating them. This caused some cracks and punching of target plates 4 and 5. The concrete slabs were held together by the reinforcement. The holes in target plates 1 and 2 were approximately 400 mm in diameter.

Test series 1997

The following results were observed after the tests:

Target 1: The projectile perforated the three first slabs and penetrated the fourth board with 30 mm.

Target 2: The projectile perforated the first slab and stopped a few millimetres into the second slab.

Target 3: Penetration depth 0.66 m.

Target 4: Penetration depth 0.66 m.

Target 5: The projectile was found 16 m away from the target.

Target 6: The projectile was found 40 m away from the target.

Target 7: The projectile was found 16 m away from the target.

Test series 1998:1

The following results were observed after the tests:

Target 1: The projectile penetrated the target 1.03 m. No cracks were observed at the back face. The projectile was split into six large pieces.

Target 2: The projectile penetrated the target 0.46 m. Cracks were observed at the back face of the target. The projectile was found intact apart from a blunted nose.

Target 3: The projectile penetrated the target 0.30 m. No cracks were observed at the back face of the target. The projectile was split into many small pieces.

Target 4: The projectile penetrated the target 0.67 m. Cracks were found at the back face of target plate 1 but target plate 2 was intact.

Target 5: The projectile penetrated the target 0.45 m. Cracks were found at the back face of the target. The projectile was split into pieces.

Target 6: The projectile penetrated the target 0.45 m. Cracks were found at the back face of the target. The projectile was split into pieces.

Target 7: The projectile penetrated the target 0.63 m. Cracks were found at the back face of the target. The projectile was split into pieces.

Target 8: Target 8 was not tested.

Target 9: The projectile penetrated the target 0.59 m. No cracks were found at the back face of the target. The projectile was split into pieces.

Target 10: The projectile penetrated the target 0.56 m. No cracks were found at the back face of the target. The projectile was split into pieces.

Test series 1998:2

No comments are given of these tests.

Test series 1999

The following results were observed after the tests:

Target 1: The projectile was found 4 m in front of the target.

Target 2: The projectile was found stuck in the target.

Target 3: The projectile was found stuck in the target.

Target 4: The projectile perforated the target.

Target 5: The projectile perforated the target.

Target 6: The projectile perforated the target.

Target 7: The projectile impacted the steel armour backstop after perforating the target.

Target 8: The projectile perforated the target and penetrated the backstop concrete slab approximately 90 mm.

Target 9: The projectile perforated the target.

Target 10: Cracks were found on the target back face.

Target 11: No cracks were found on the target back face.

Target 12: -

Target 13: -

Target 14: Cracks were found on the target back face.

Target 15: -

Target 16: -

Target 17: -

Target 18: Cracks were found on the target back face.

Target 19: -

Target 20: -

Target 21: -

Target 22: The projectile was found stuck in the target. Pieces of the rails were found around the target.

Target 23: The projectile perforated the target.

Target 24: The projectile was found split into pieces but the projectile instrument package was lost.

Target 25: The projectile with the instrument package was found and registrations were successfully transferred to a computer disc.

D POST TEST TARGET CONFIGURATIONS

Test series 1996:1

Target 1

Figure D.1. Post test configuration for target 1 in test-series 1996:1. Front face.

Figure D.2. Post test configuration for target 1 in test-series 1996:1. Back face.

Target 2

Figure D.3. Post test configuration for target 2 in test-series 1996:1. Front face.

Figure D.4. Post test configuration for target 2 in test-series 1996:1. Back face.

Target 3

Figure D.5. Post test configuration for target 3 in test-series 1996:1. Front face shot 1.

Figure D.6. Post test configuration for target 3 in test-series 1996:1. Back face of target plate 4.

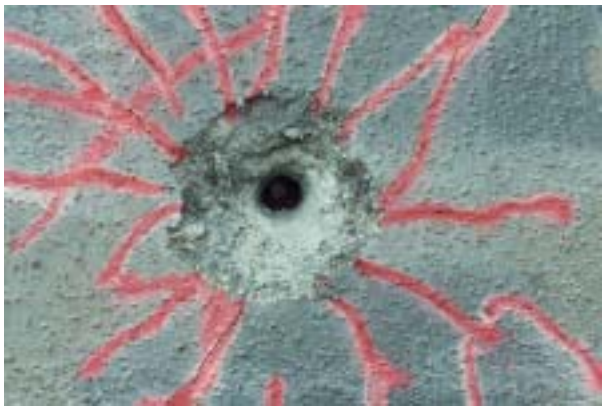

Figure D.7. Post test configuration for target 3 in test-series 1996:1. Front face shot 2.

Figure D.8. Post test configuration for target 3 in test-series 1996:1. Back face of target plate 6.

Target 4

Figure D.9. Post test configuration for target 4 in test-series 1996:1. Top.front face.

Test series 1996:2

Target 1

Figure D.10. Post test configuration for target 1 in test-series 1996:2. Front face.

Figure D.11. Post test configuration for target 1 in test-series 1996:2. Projectile.

Target 2

Figure D.12. Post test configuration for target 2 in test-series 1996:2. Back face.

Figure D.13. Post test configuration for target 2 in test-series 1996:2. Projectile.

Target 3

Figure D.14. Post test configuration for target 3 in test-series 1996:2. Front face.

Figure D.15. Post test configuration for target 3 in test-series 1996:2. Top face oriented with front face to the left.

Target 4

Figure D.16. Post test configuration for target 4 in test-series 1996:2. Front face. The target has been turned over by the projectile.

Figure D.17. Post test configuration for target 4 in test-series 1996:2. Back face after raising the target to a elevated position.

Figure D.18. Post test configuration for target 4 in test-series 1996:2. Front view of projectile inside target.

Test series 1997

Target 1

Figure D.19. Post test configuration for target 1 in test-series 1997. Front face.

Figure D.20. Post test configuration for target 1 in test-series 1997. Projectile stuck in target plate 4.

Target 2

Figure D.21. Post test configuration for target 2 in test-series 1997. Front face.

Figure D.22. Post test configuration for target 2 in test-series 1997. Front face of ERA-panel.

Target 3 and target 4

Figure D.23. Post test configuration for target 3 in test-series 1997. Front face.

Figure D.24. Post test configuration for target 4 in test-series 1997. Front face.

Target 5 and target 6

Figure D.25. Post test configuration for target 5 in test-series 1997. Front face.

Figure D.26. Post test configuration for target 6 in test-series 1997. Front face.

Target 7

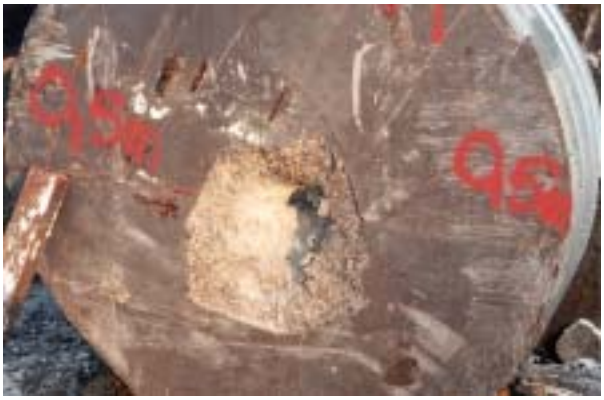

Figure D.27. Post test configuration for target 7 in test-series 1997. Front face.

Test series 1998:1

Target 1

Figure D.28. Post test configuration for target 1 in test-series 1998:1. Front face.

Figure D.29. Post test configuration for target 1 in test-series 1998:1. Projectile.

Target 2

Figure D.30. Post test configuration for target 2 in test-series 1998:1. Front face.

Figure D.31. Post test configuration for target 2 in test-series 1998:1. Back face.

Target 3 and target 4

Figure D.32. Post test configuration for target 3 in test-series 1998:1. Front face.

Figure D.33. Post test configuration for target 4 in test-series 1998:1. Front face.

Target 5

Figure D.34. Post test configuration for target 5 in test-series 1998:1. Front face.

Figure D.35. Post test configuration for target 5 in test-series 1998:1. Back face.

Target 6

Figure D.36. Post test configuration for target 6 in test-series 1998:1. Front face.

Figure D.37. Post test configuration for target 6 in test-series 1998:1. Back face.

Target 7

Figure D.38. Post test configuration for target 7 in test-series 1998:1. Front face.

Target 9

Figure D.39. Post test configuration for target 9 in test-series 1998:1. Front face.

Figure D.40. Post test configuration for target 9 in test-series 1998:1. Back face.

Target 10

Figure D.41. Post test configuration for target 11 in test-series 1998:1. Front face.

Test series 1998:2

Target 1 and target 2

Figure D.42. Post test configuration for target 1 in test-series 1998:2. Front face.

Figure D.43. Post test configuration for target 2 in test-series 1998:2. Front face.

Target 3 and target 4

Figure D.44. Post test configuration for target 3 in test-series 1998:2. Front face.

Figure D.45. Post test configuration for target 4 in test-series 1998:2. Front face.

Target 5 and target 6

Figure D.46. Post test configuration for target 5 in test-series 1998:2. Front face.

Figure D.47. Post test configuration for target 6 in test-series 1998:2. Front face.

Target 7 and target 8

Figure D.48. Post test configuration for target 7 in test-series 1998:2. Front face.

Figure D.49. Post test configuration for target 8 in test-series 1998:2. Front face.

Target 9 and target 10

Figure D.50. Post test configuration for target 9 in test-series 1998:2. Front face.

Figure D.51. Post test configuration for target 10 in test-series 1998:2. Front face.

Target 11 and target 12

Figure D.52. Post test configuration for target 11 in test-series 1998:2. Front face.

Figure D.53. Post test configuration for target 12 in test-series 1998:2. Front face.

Target 13

Figure D.54. Post test configuration for target 13 in test-series 1998:2. Front face.

Test series 1999

Target 1

Figure D.55. Post test configuration for target 1 in test-series 1999. Front face.

Figure D.56. Post test configuration for target 1 in test-series 1999. Back face.

Target 2

Figure D.57. Post test configuration for target 2 in test-series 1999. Front face.

Figure D.58. Post test configuration for target 2 in test-series 1999. Back face.

Target 3

Figure D.59. Post test configuration for target 3 in test-series 1999. Front face.

Figure D.60. Post test configuration for target 3 in test-series 1999. Back face.

Target 4

Figure D.61. Post test configuration for target 4 in test-series 1999. Front face.

Figure D.62. Post test configuration for target 4 in test-series 1999. Back face.

Target 5

Figure D.63. Post test configuration for target 5 in test-series 1999. Front face.

Figure D.64. Post test configuration for target 5 in test-series 1999. Back face.

Target 6

Figure D.65. Post test configuration for target 6 in test-series 1999. Front face.

Figure D.66. Post test configuration for target 6 in test-series 1999. Back face.

Target 7

Figure D.67. Post test configuration for target 7 in test-series 1999. Front face.

Figure D.68. Post test configuration for target 7 in test-series 1999. Projectile.

Target 8

Figure D.69. Post test configuration for target 8 in test-series 1999. Front face.

Figure D.70. Post test configuration for target 8 in test-series 1999. Front face detail.

Target 9

Figure D.71. Post test configuration for target 9 in test-series 1999. Front face.

Figure D.72. Post test configuration for target 9 in test-series 1999. Front face detail.

Target 10

Figure D.73. Post test configuration for target 10 in test-series 1999. Front face.

Figure D.74. Post test configuration for target 10 in test-series 1999. Back face.

Target 11

Figure D.75. Post test configuration for target 11 in test-series 1999. Front face.

Figure D.76. Post test configuration for target 11 in test-series 1999. Back face.

Target 12

Figure D.77. Post test configuration for target 12 in test-series 1999. Front face.

Figure D.78. Post test configuration for target 12 in test-series 1999. Back face.

Target 13

Figure D.79. Post test configuration for target 13 in test-series 1999. Front face.

Figure D.80. Post test configuration for target 13 in test-series 1999. Back face.

Target 14

Figure D.81. Post test configuration for target 14 in test-series 1999. Front face.

Figure D.82. Post test configuration for target 14 in test-series 1999. Back face.

Target 15

Figure D.83. Post test configuration for target 15 in test-series 1999. Front face.

Figure D.84. Post test configuration for target 15 in test-series 1999. Back face.

Target 16

Figure D.85. Post test configuration for target 16 in test-series 1999. Front face.

Target 17

Figure D.86. Post test configuration for target 17 in test-series 1999. Front face.

Figure D.87. Post test configuration for target 17 in test-series 1999. Back face.

Target 18

Figure D.88. Post test configuration for target 18 in test-series 1999. Front face.

Figure D.89. Post test configuration for target 18 in test-series 1999. Back face.

Figure D.90. Post test configuration for target 18 in test-series 1999. Projectile.

Target 19

Figure D.91. Post test configuration for target 19 in test-series 1999. Front face.

Figure D.92. Post test configuration for target 19 in test-series 1999. Back face.

Figure D.93. Post test configuration for target 19 in test-series 1999. Projectile.

Target 20

Figure D.94. Post test configuration for target 10 in test-series 1999. Front face.

Figure D.95. Post test configuration for target 10 in test-series 1999. Hole in the steel rail reinforcement made by the projectile .

Target 21

Figure D.96. Post test configuration for target 21 in test-series 1999. Front face.

Figure D.97. Post test configuration for target 21 in test-series 1999. Back face.

Target 22

Figure D.98. Post test configuration for target 22 in test-series 1999. Front face.

Figure D.99. Post test configuration for target 22 in test-series 1999. Back face.

Target 23

Figure D.100. Post test configuration for target 23 in test-series 1999. Front face.

Figure D.101. Post test configuration for target 23 in test-series 1999. Back face.

Figure D.102. Post test configuration for target 23 in test-series 1999. Projectile.

Target 24

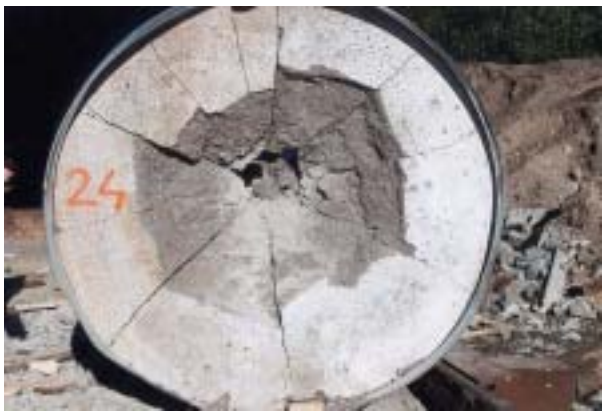

Figure D.103. Post test configuration for target 24 in test-series 1999. Front face.

Figure D.104. Post test configuration for target 24 in test-series 1999. Back face.

Target 25

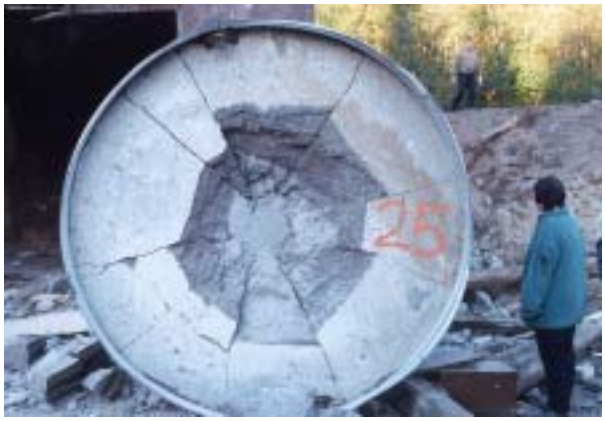

Figure D.105. Post test configuration for target 25 in test-series 1999. Front face.

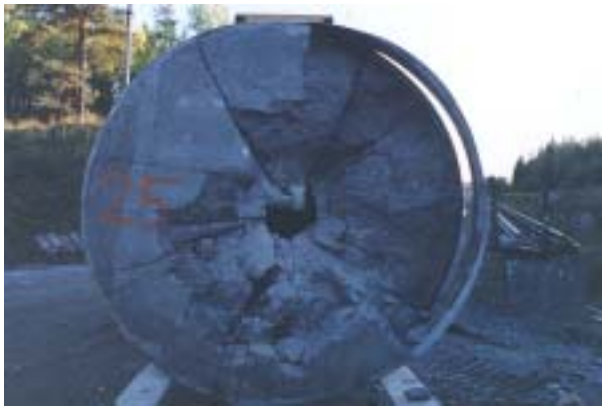

Figure D.106. Post test configuration for target 25 in test-series 1999. Back face.

Figure D.107. Post test configuration for target 25 in test-series 1999. Projectile.

E DOPPLER RADAR REGISTRATIONS

Test series 1997

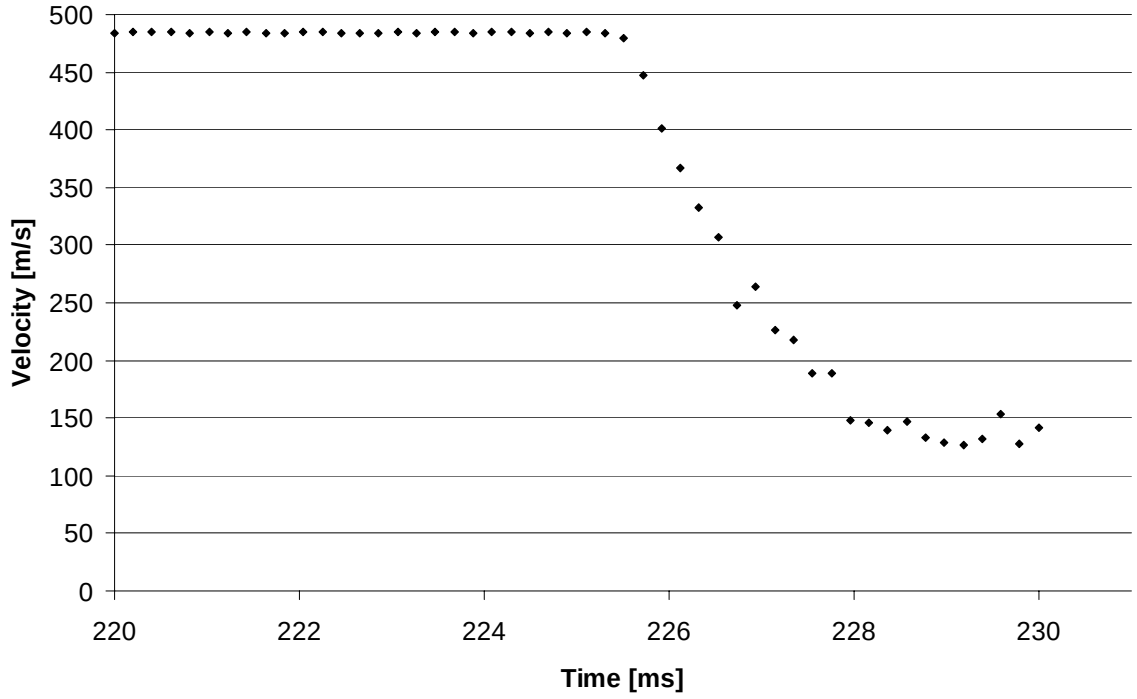

Figure E.1. Doppler radar registrations for target 1 in test-series 1997.

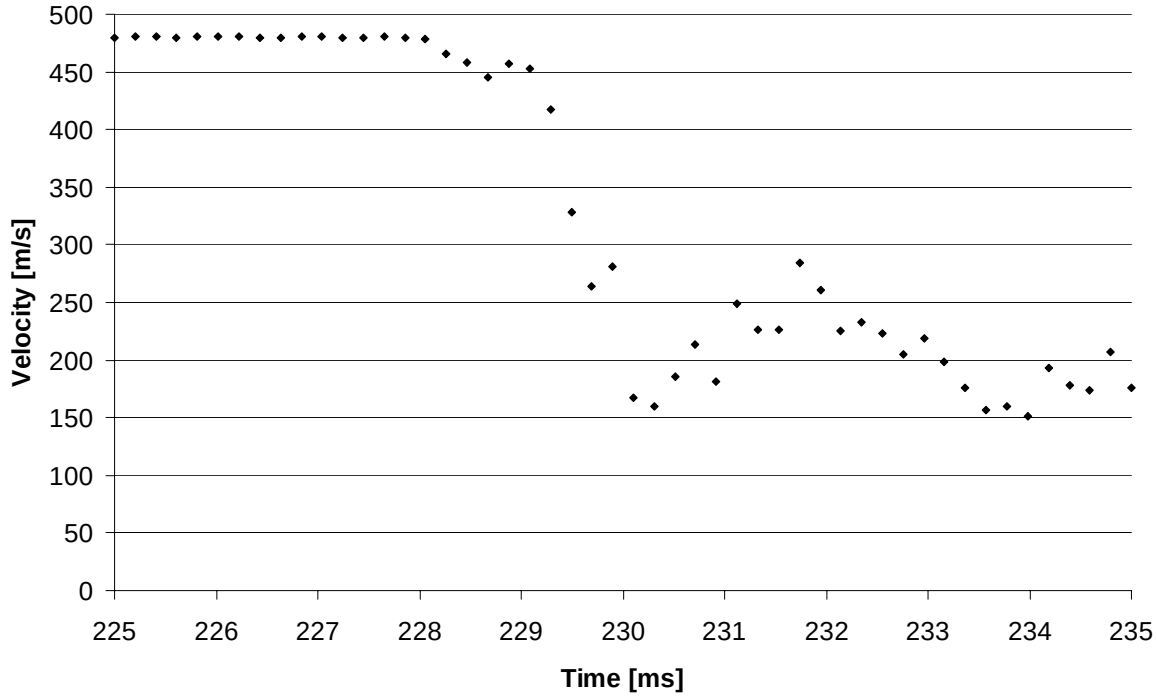

Figure E.2. Doppler radar registrations for target 2 in test-series 1997.

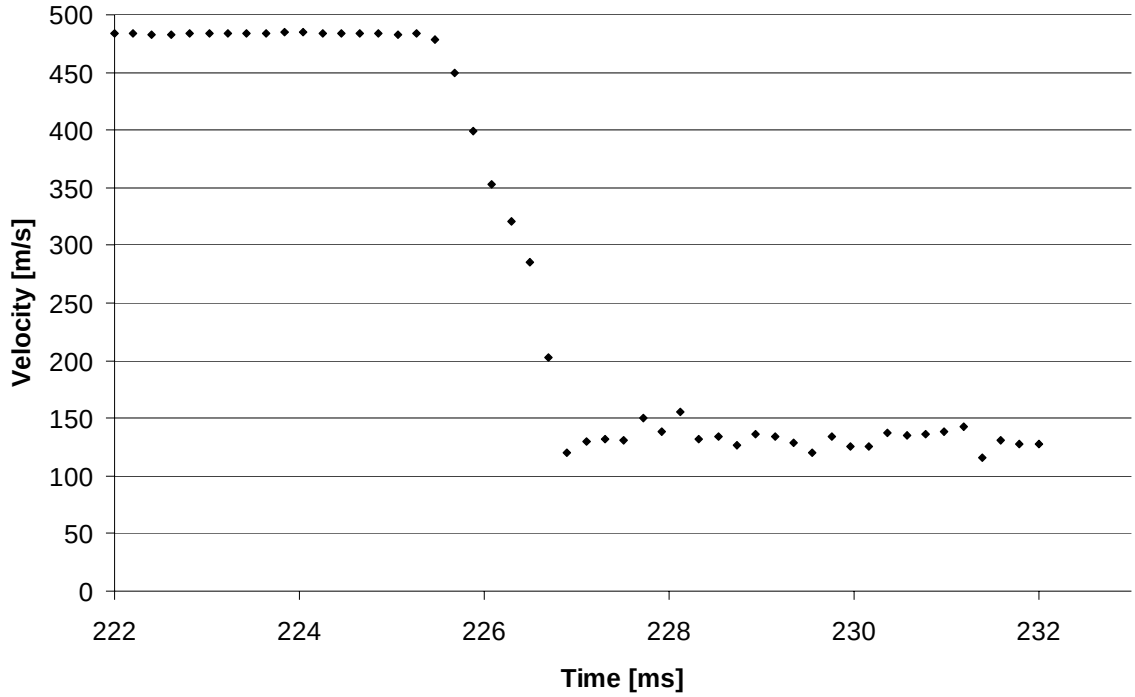

Figure E.3. Doppler radar registrations for target 3 in test-series 1997.

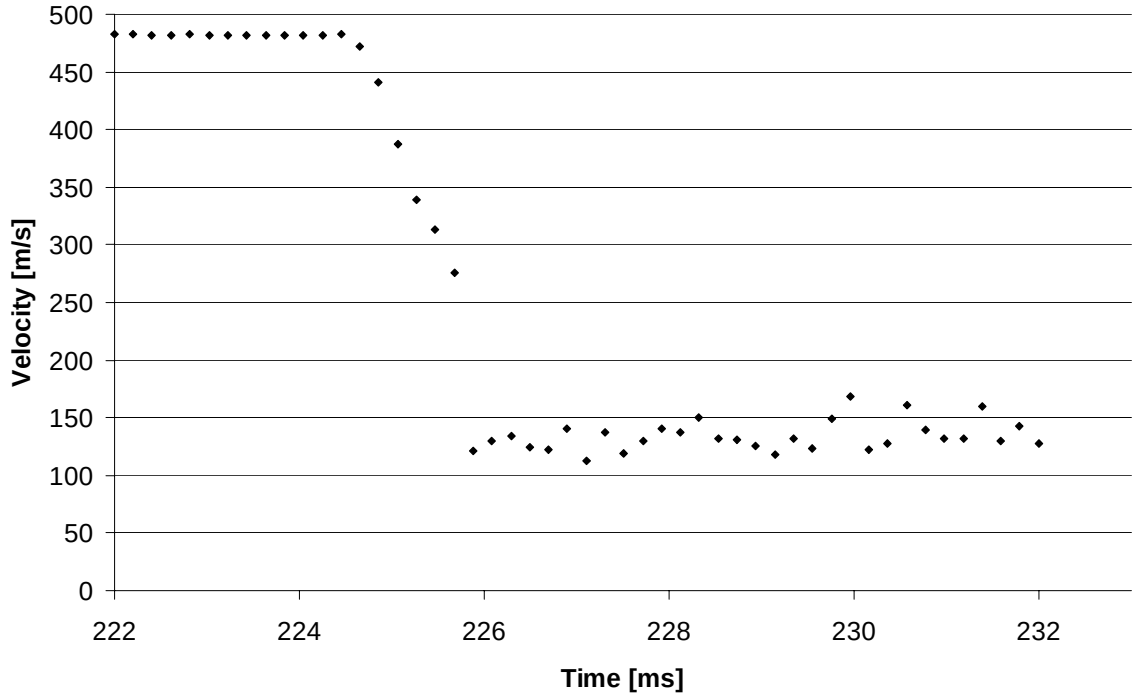

Figure E.4. Doppler radar registrations for target 4 in test-series 1997.

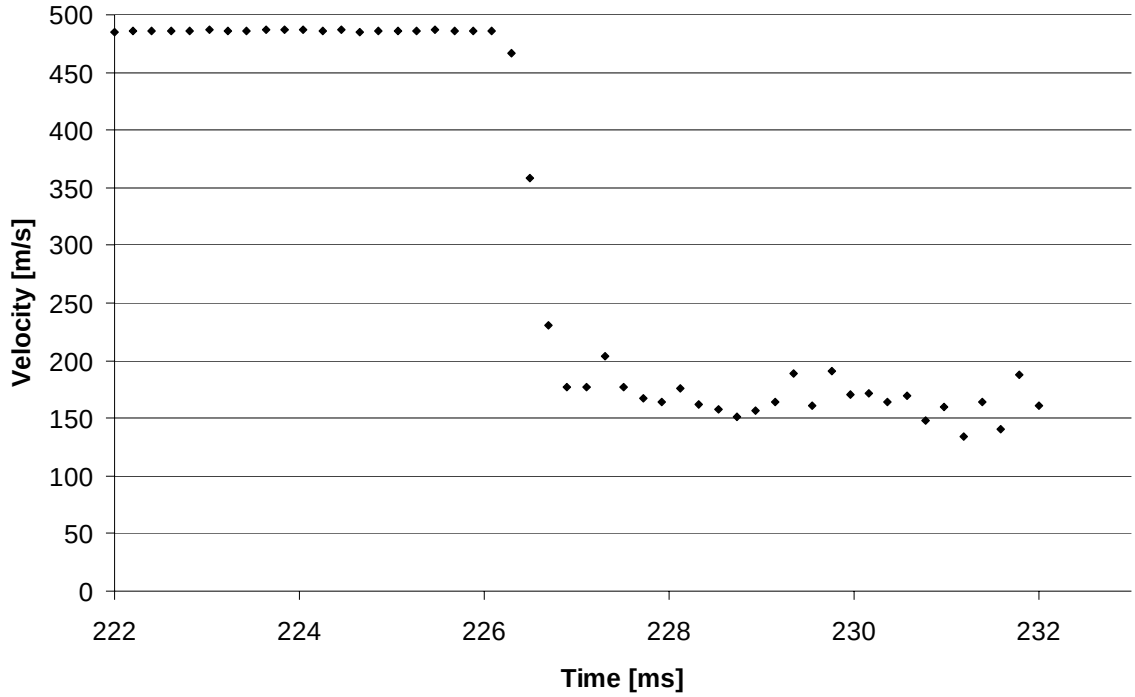

Figure E.5. Doppler radar registrations for target 5 in test-series 1997.

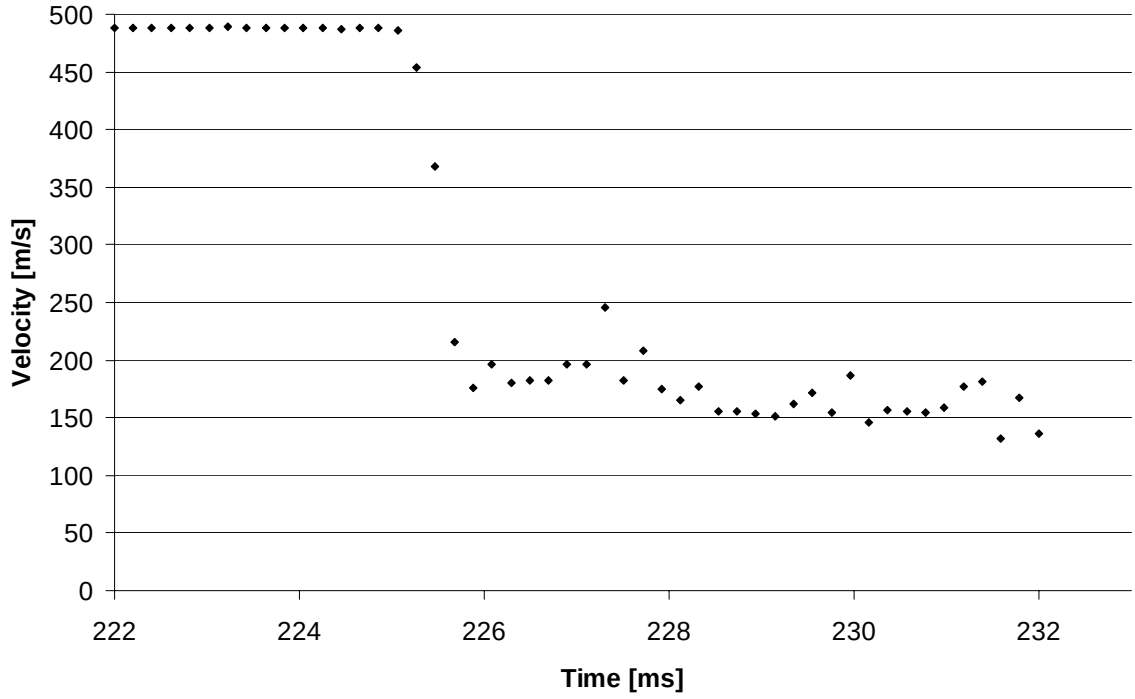

Figure E.6. Doppler radar registrations for target 6 in test-series 1997.

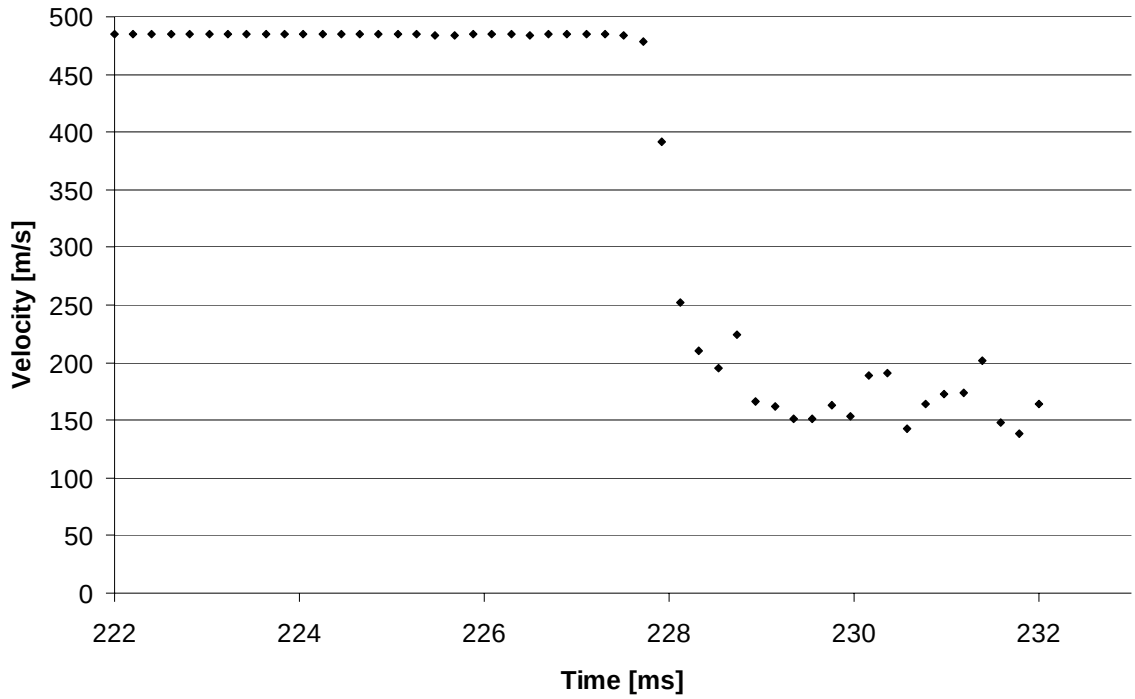

Figure E.7. Doppler radar registrations for target 7 in test-series 1997.

Test series 1998:1

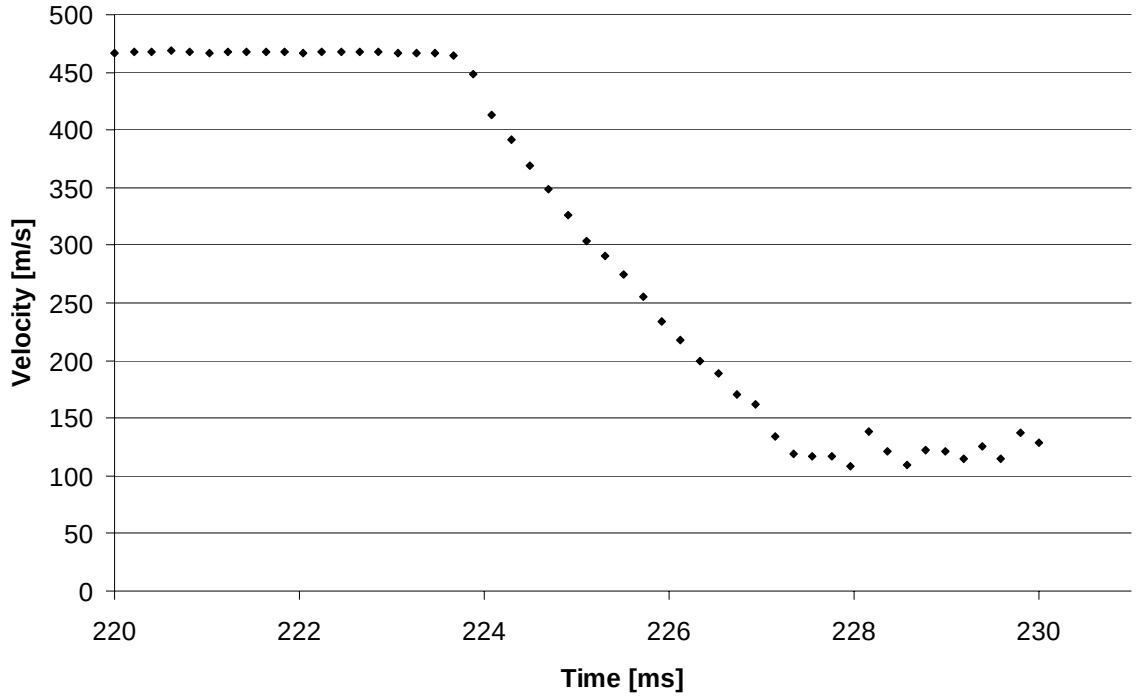

Figure E.8. Doppler radar registrations for target 1 in test-series 1998:1.

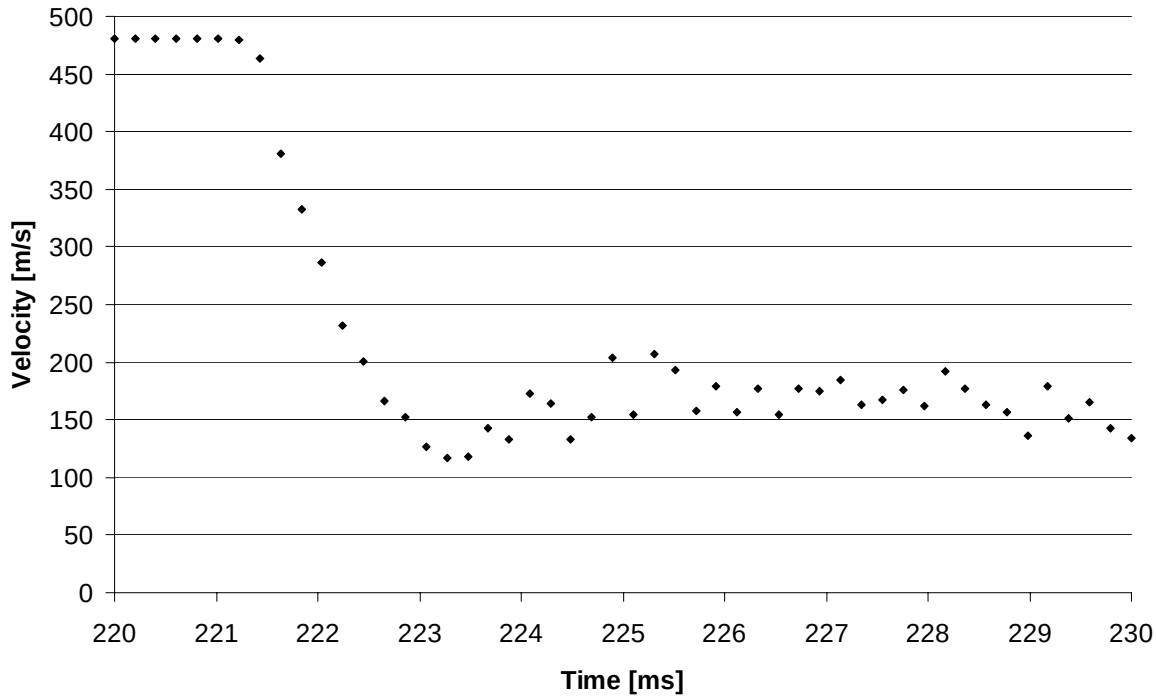

Figure E.9. Doppler radar registrations for target 2 in test-series 1998:1.

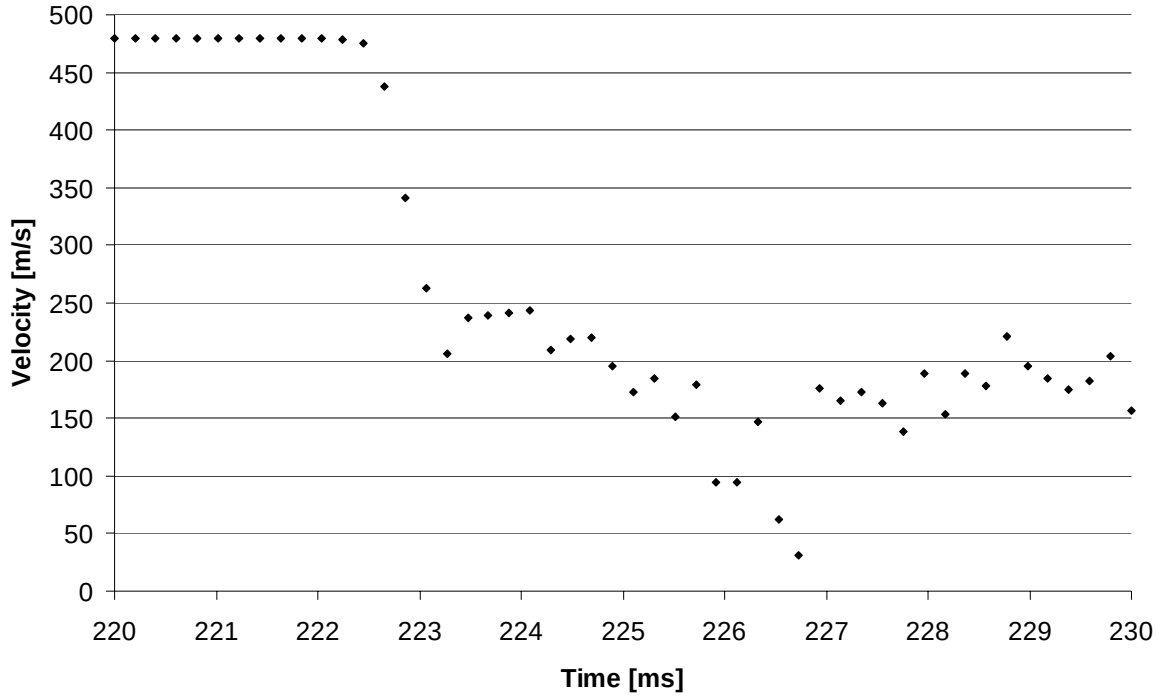

Figure E.10. Doppler radar registrations for target 3 in test-series 1998:1.

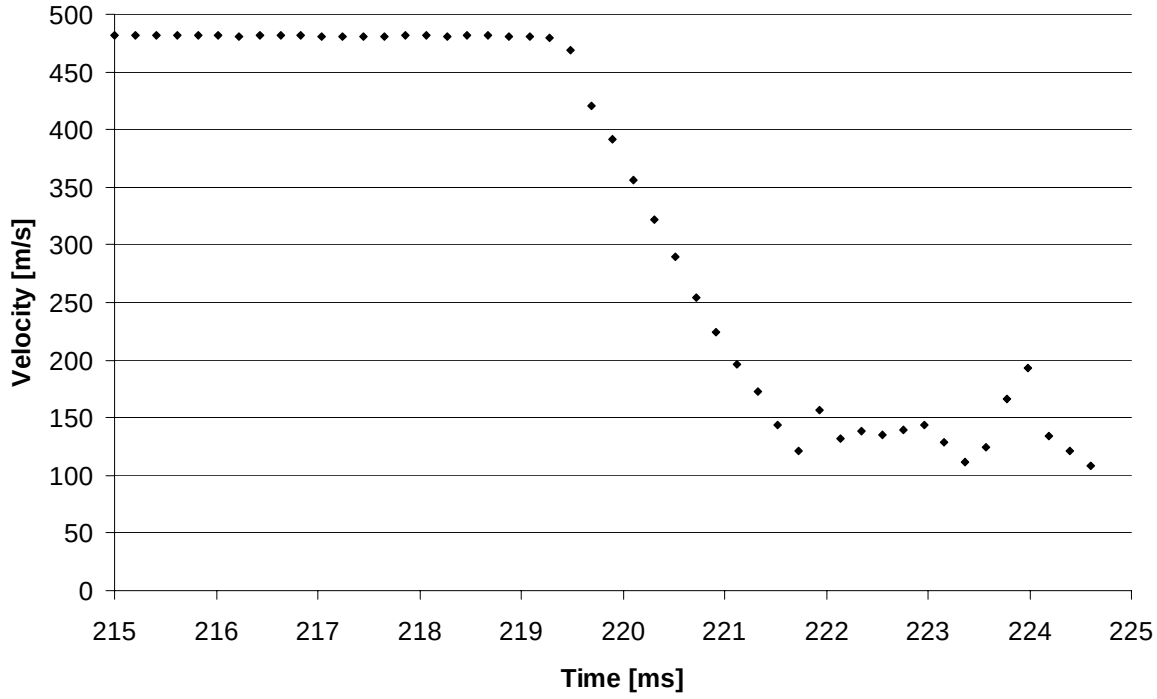

Figure E.11. Doppler radar registrations for target 4 in test-series 1998:1.

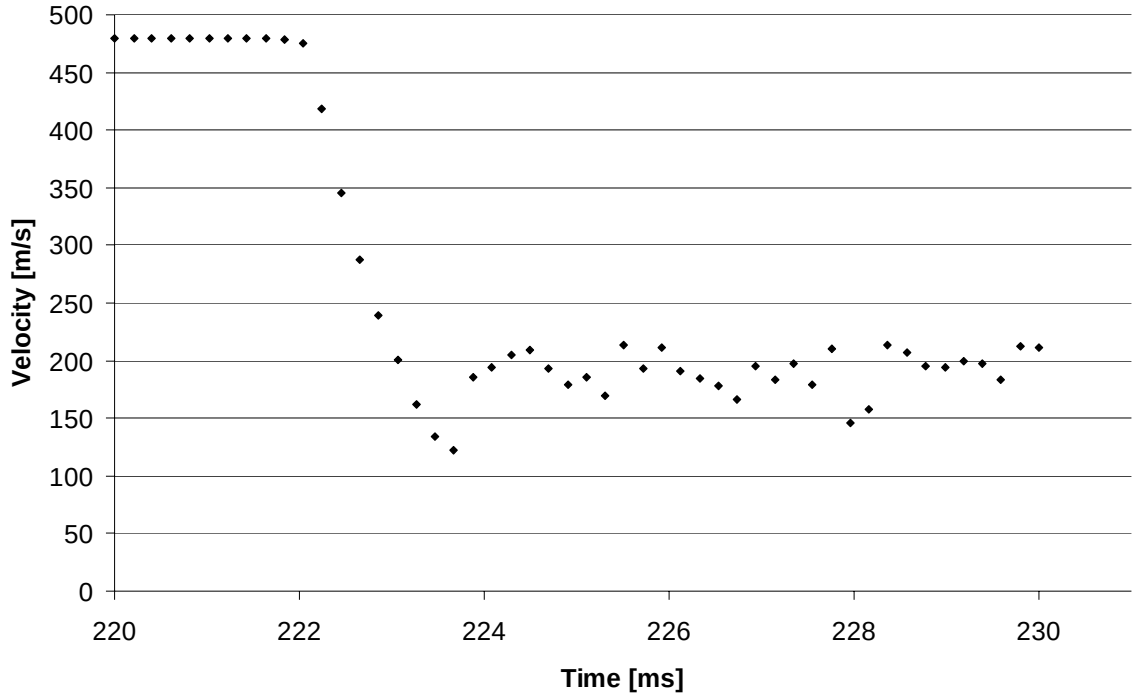

Figure E.12. Doppler radar registrations for target 5 in test-series 1998:1.

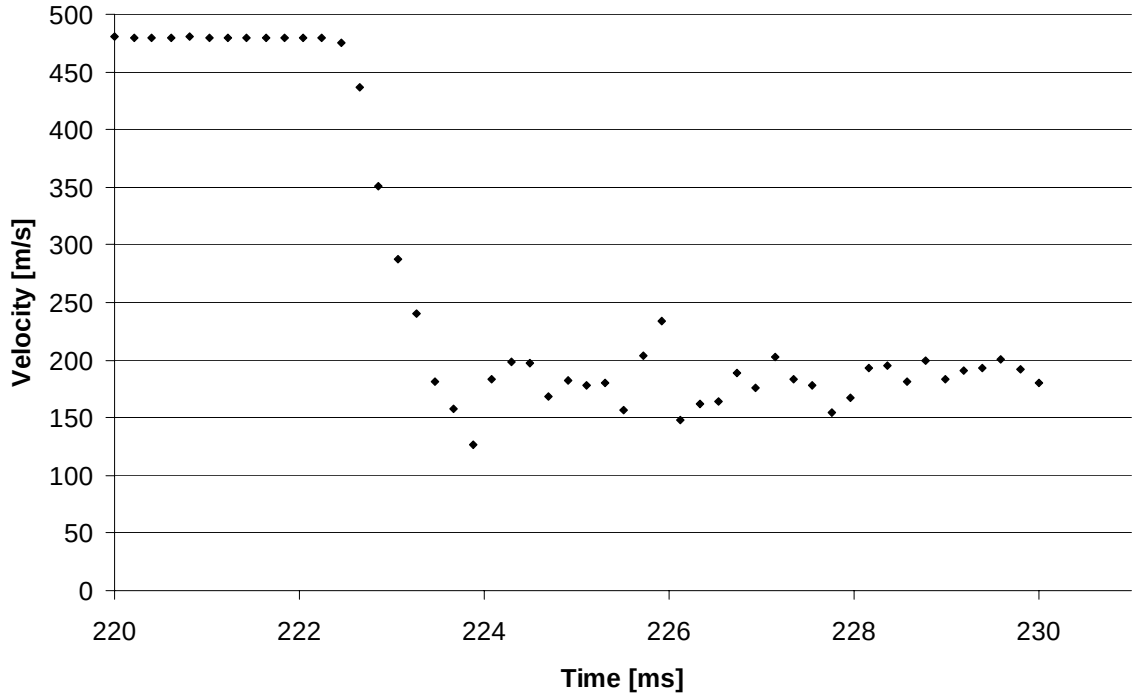

Figure E.13. Doppler radar registrations for target 6 in test-series 1998:1.

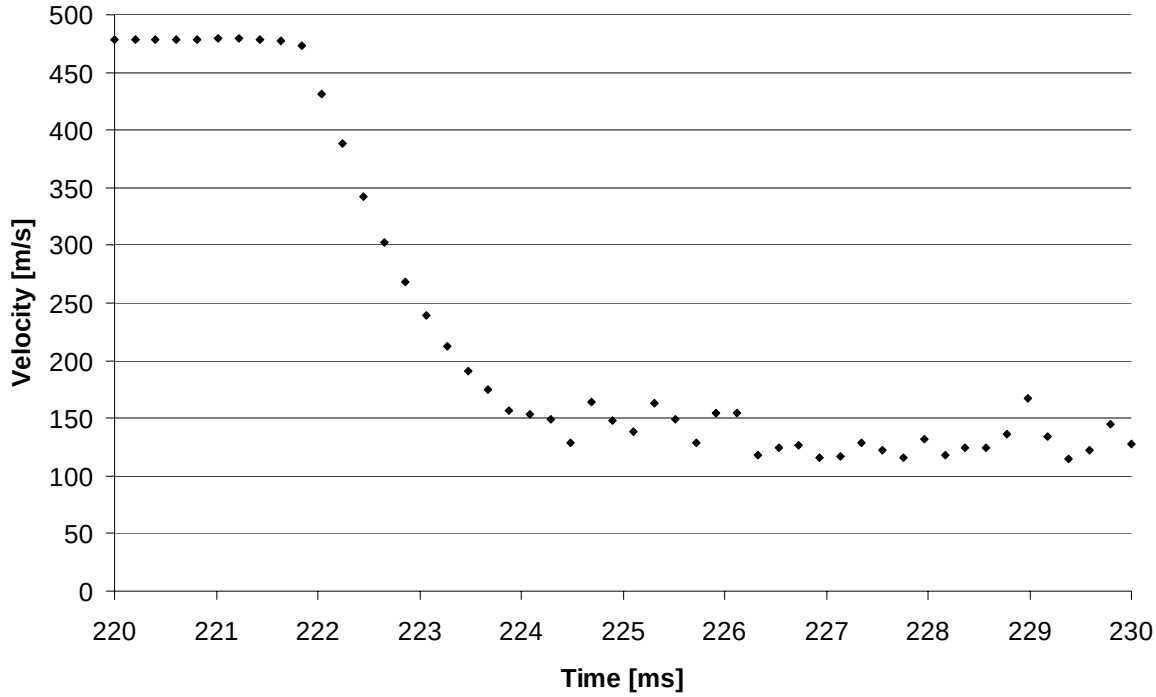

Figure E.14. Doppler radar registrations for target 7 in test-series 1998:1.

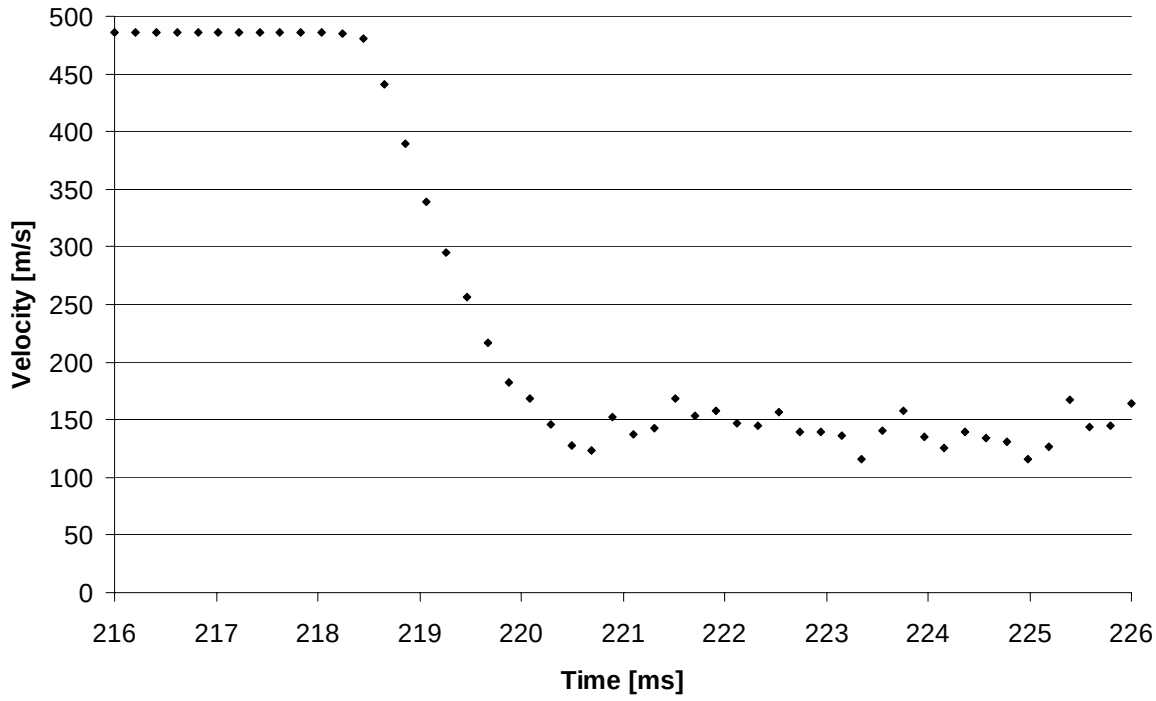

Figure E.15. Doppler radar registrations for target 9 in test-series 1998:1.

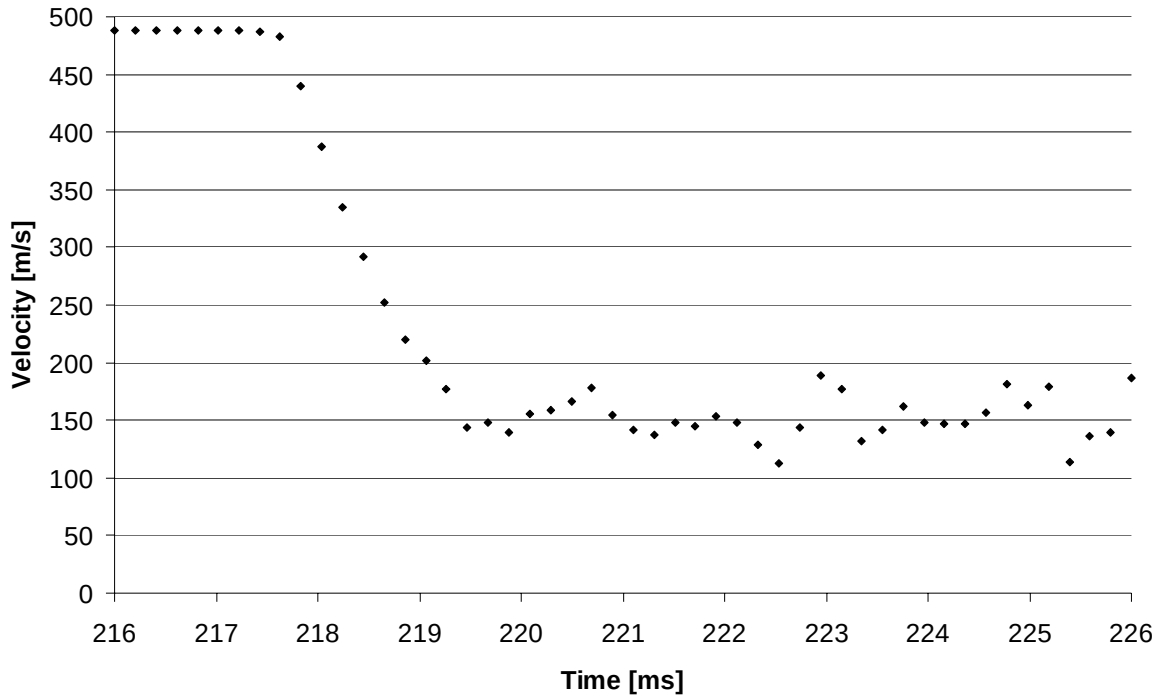

Figure E.16. Doppler radar registrations for target 10 in test-series 1998:1.

Test series 1998:2

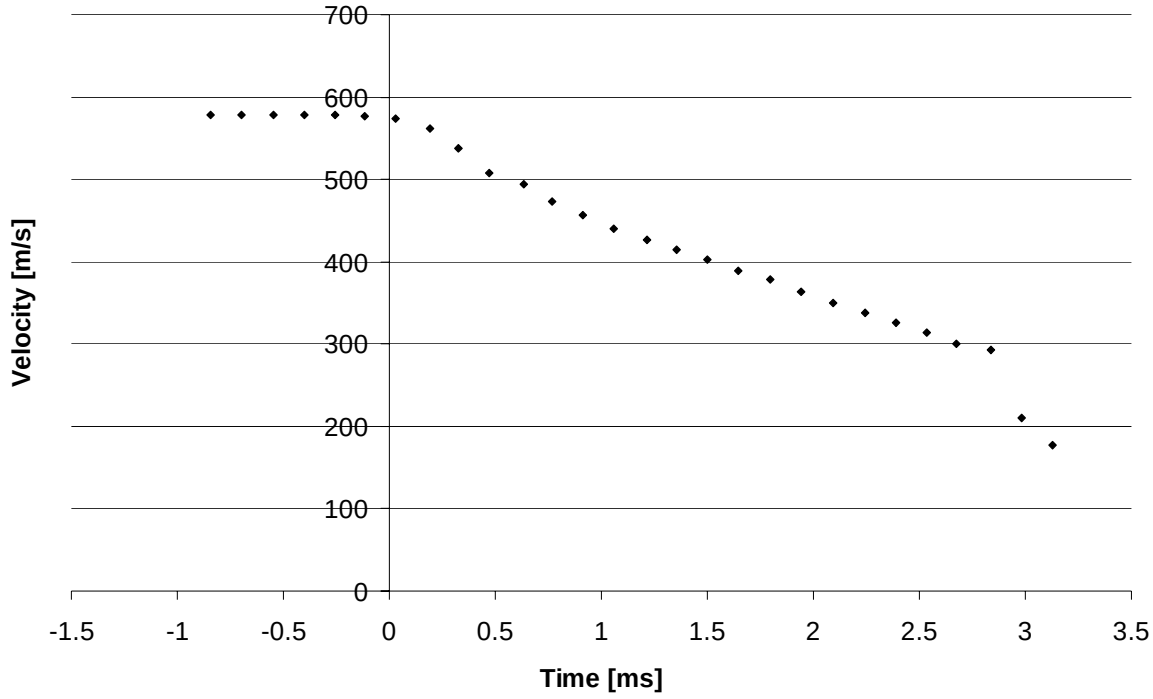

Figure E.17. Doppler radar registrations for target 1 in test-series 1998:2.

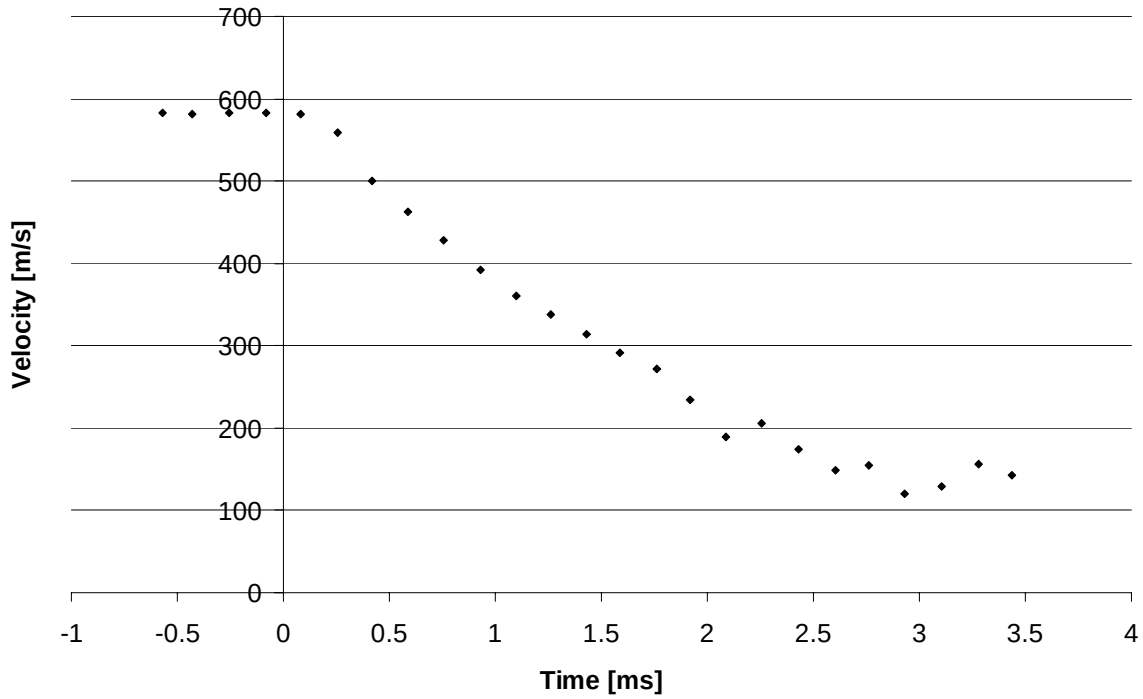

Figure E.18. Doppler radar registrations for target 2 in test-series 1998:2.

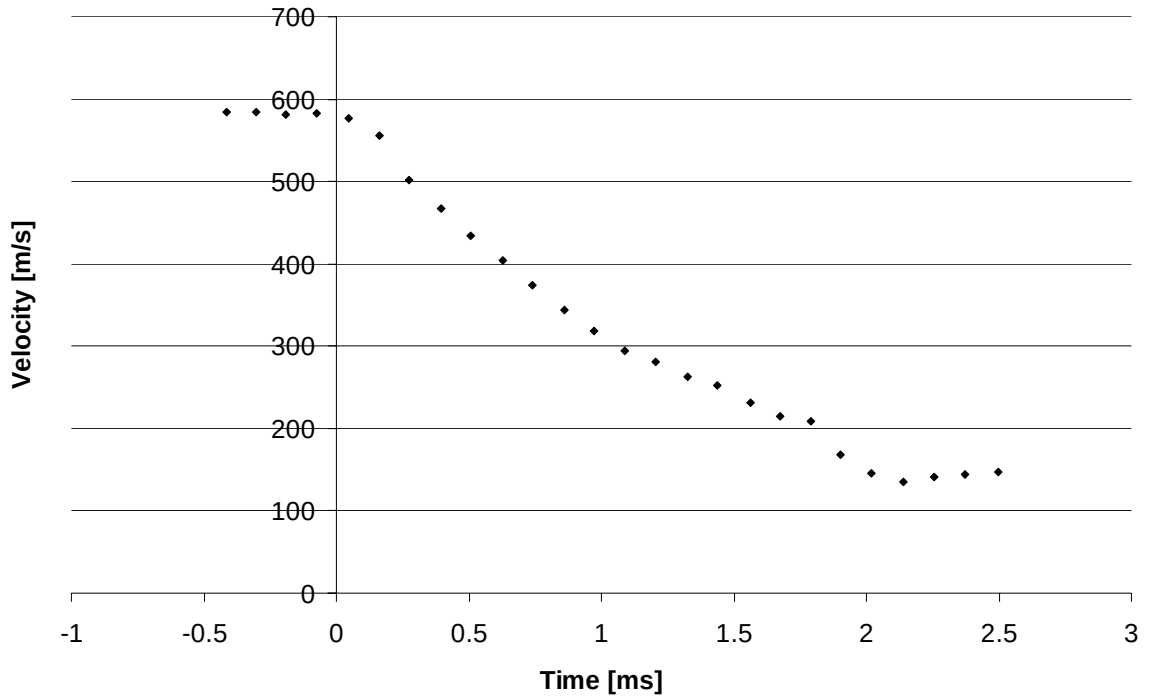

Figure E.19. Doppler radar registrations for target 3 in test-series 1998:2.

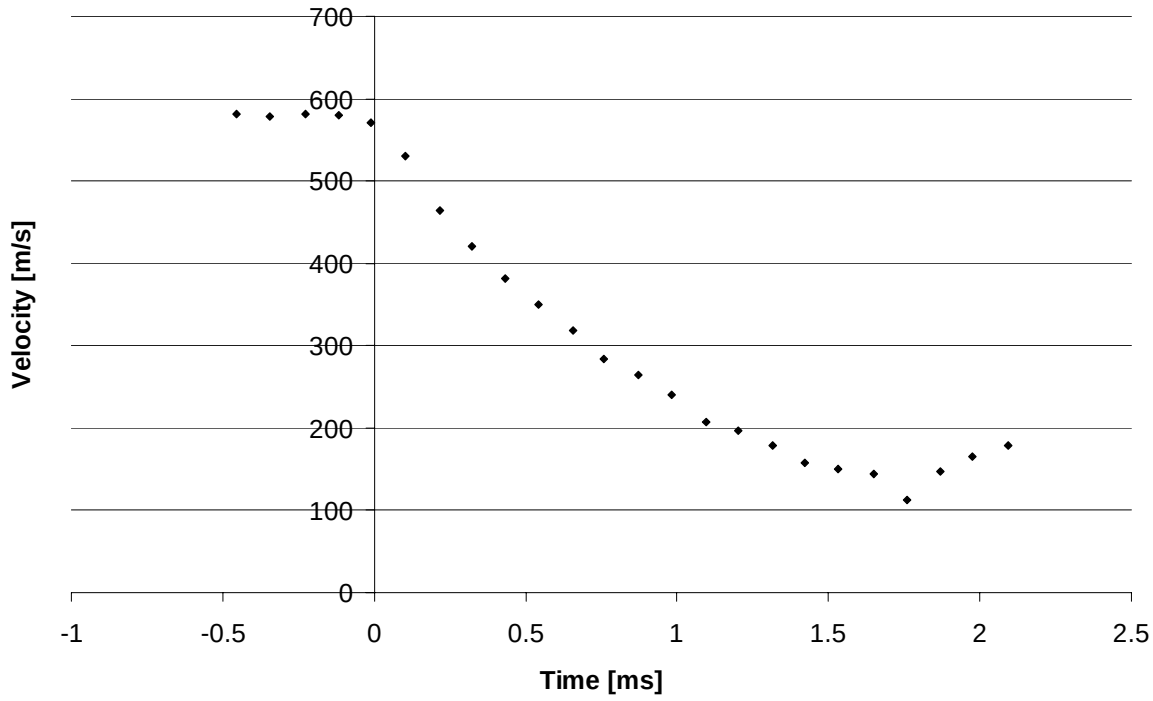

Figure E.20. Doppler radar registrations for target 4 in test-series 1998:2.

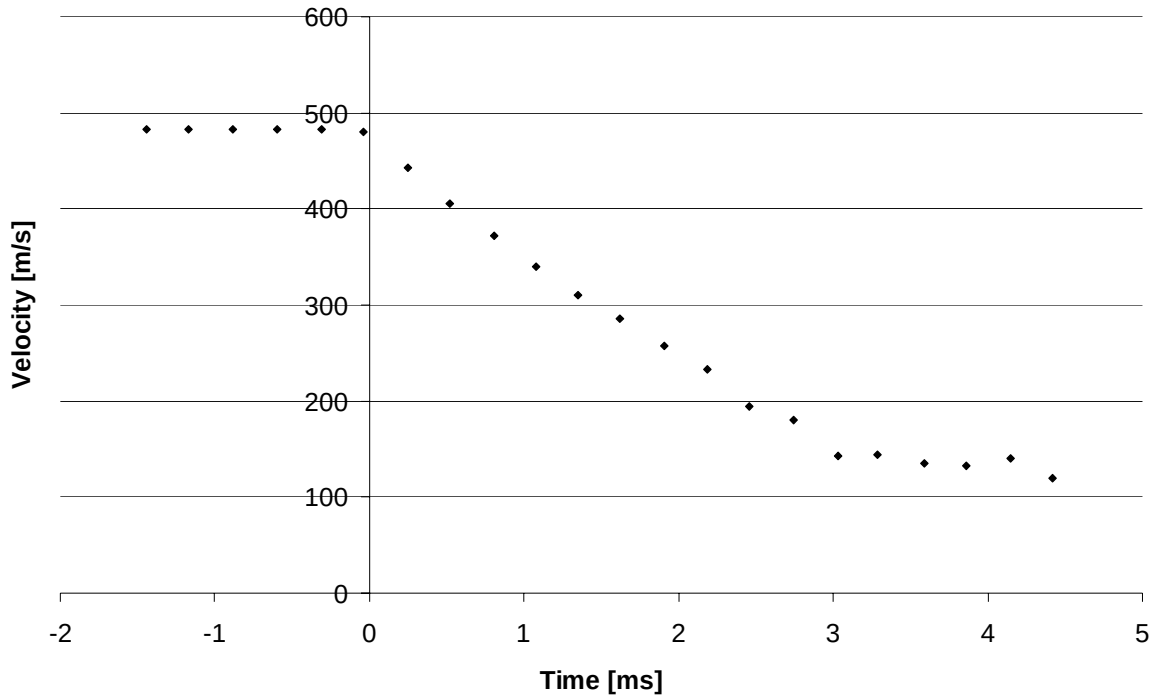

Figure E.21. Doppler radar registrations for target 5 in test-series 1998:2.

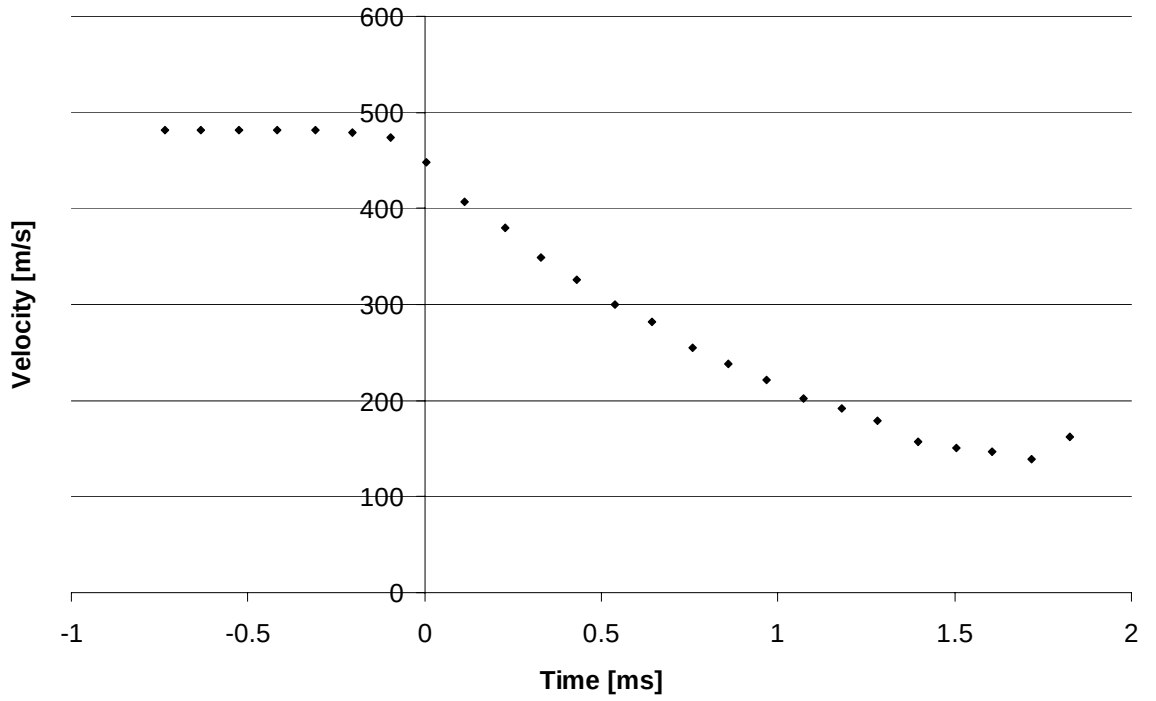

Figure E.22. Doppler radar registrations for target 6 in test-series 1998:2.

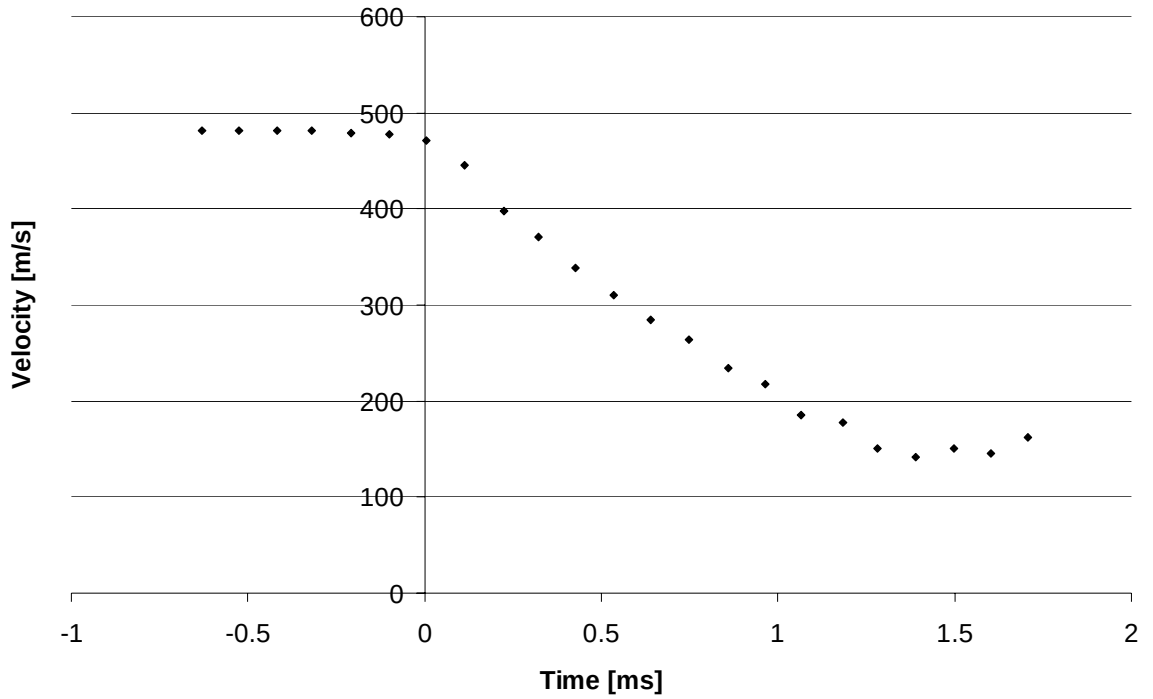

Figure E.23. Doppler radar registrations for target 7 in test-series 1998:2.

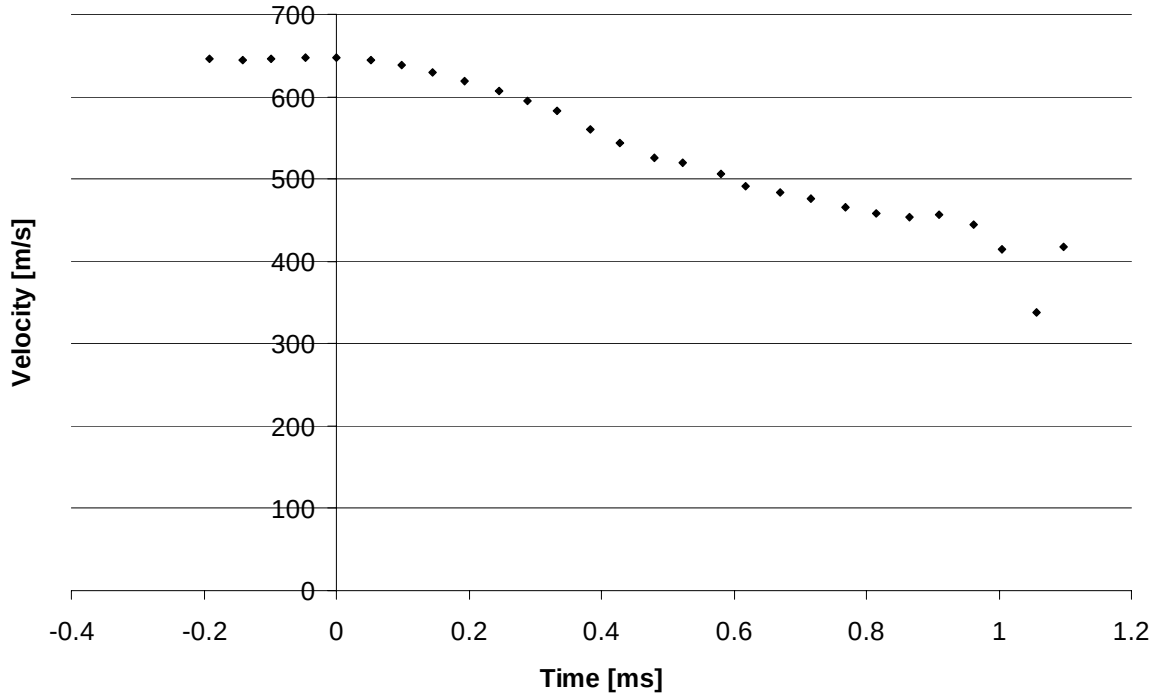

Figure E.24. Doppler radar registrations for target 8 in test-series 1998:2.

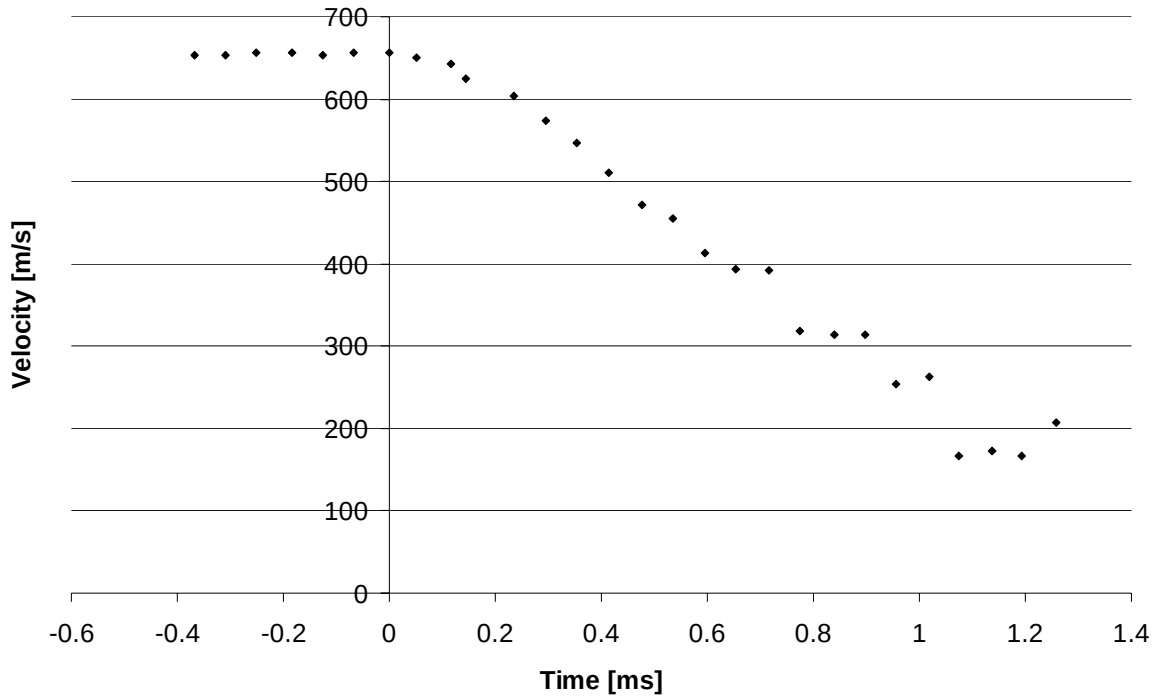

Figure E.25. Doppler radar registrations for target 9 in test-series 1998:2.

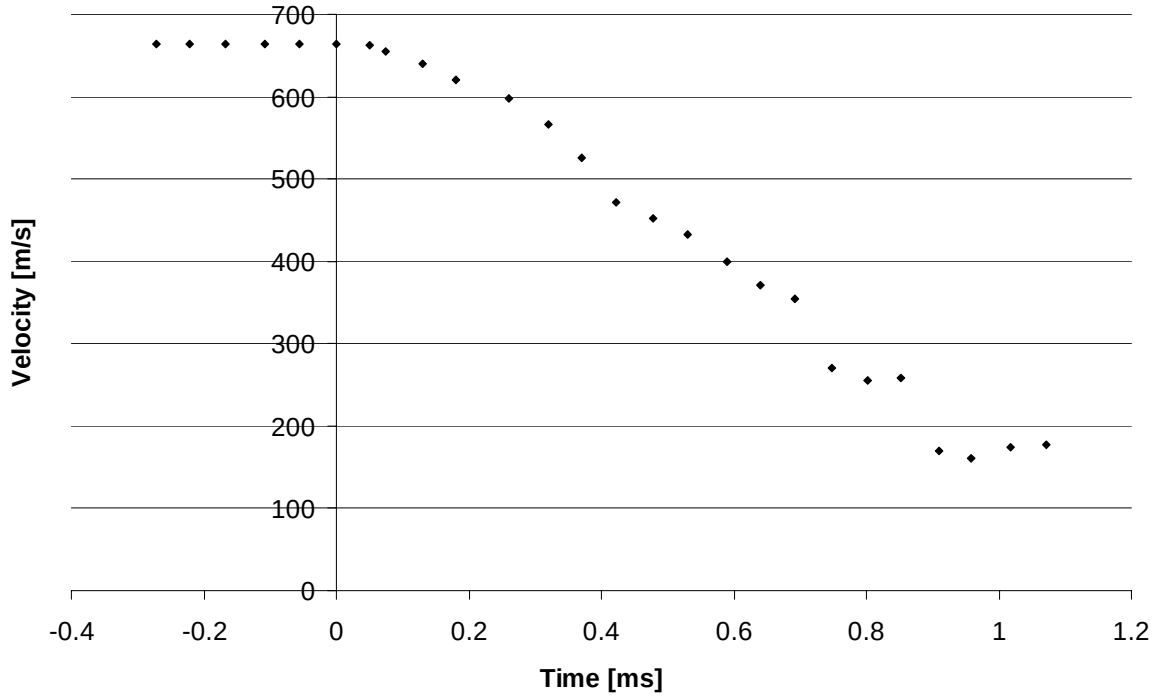

Figure E.26. Doppler radar registrations for target 10 in test-series 1998:2.

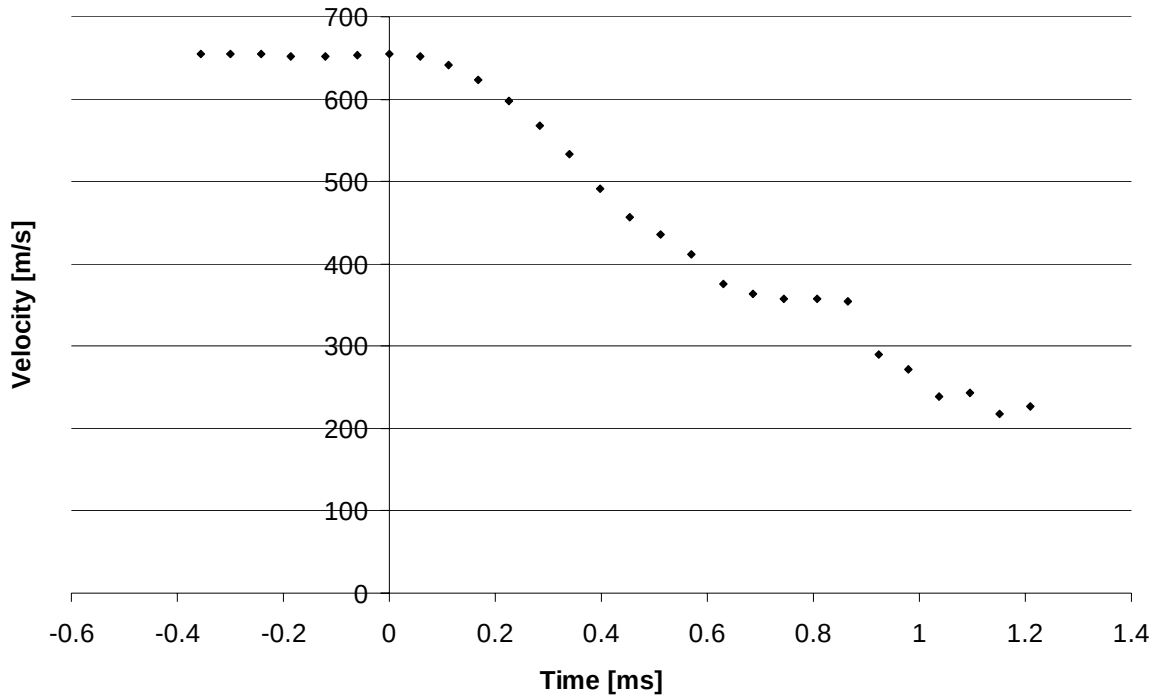

Figure E.27. Doppler radar registrations for target 11 in test-series 1998:2.

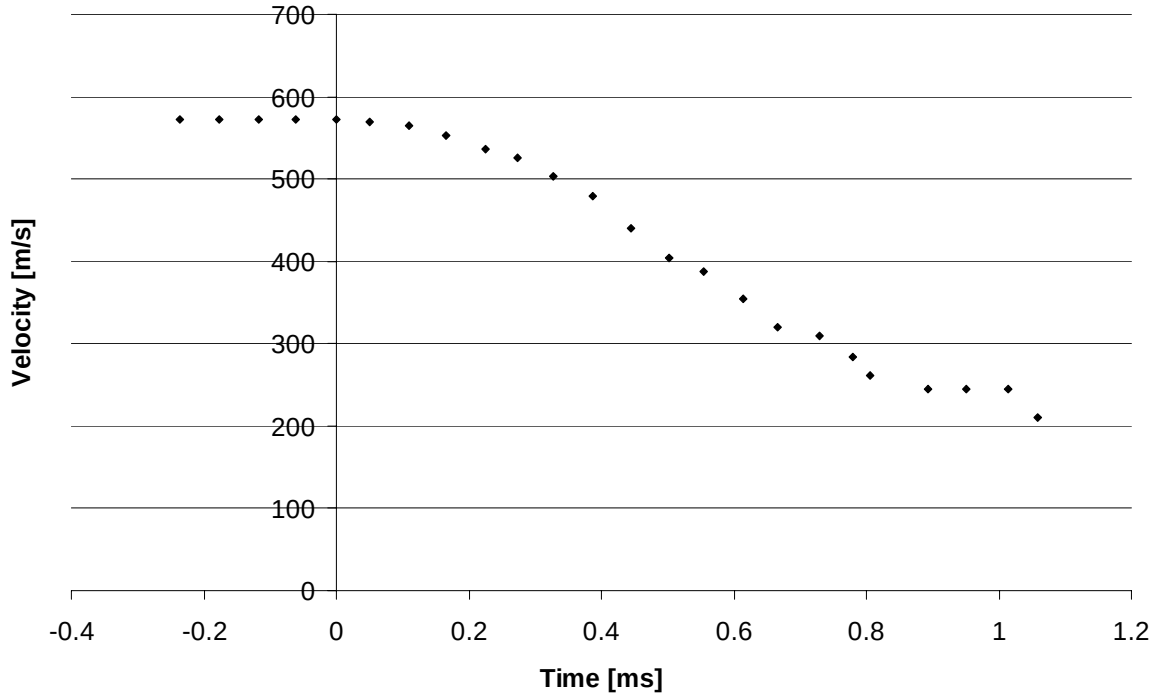

Figure E.28. Doppler radar registrations for target 12 in test-series 1998:2.

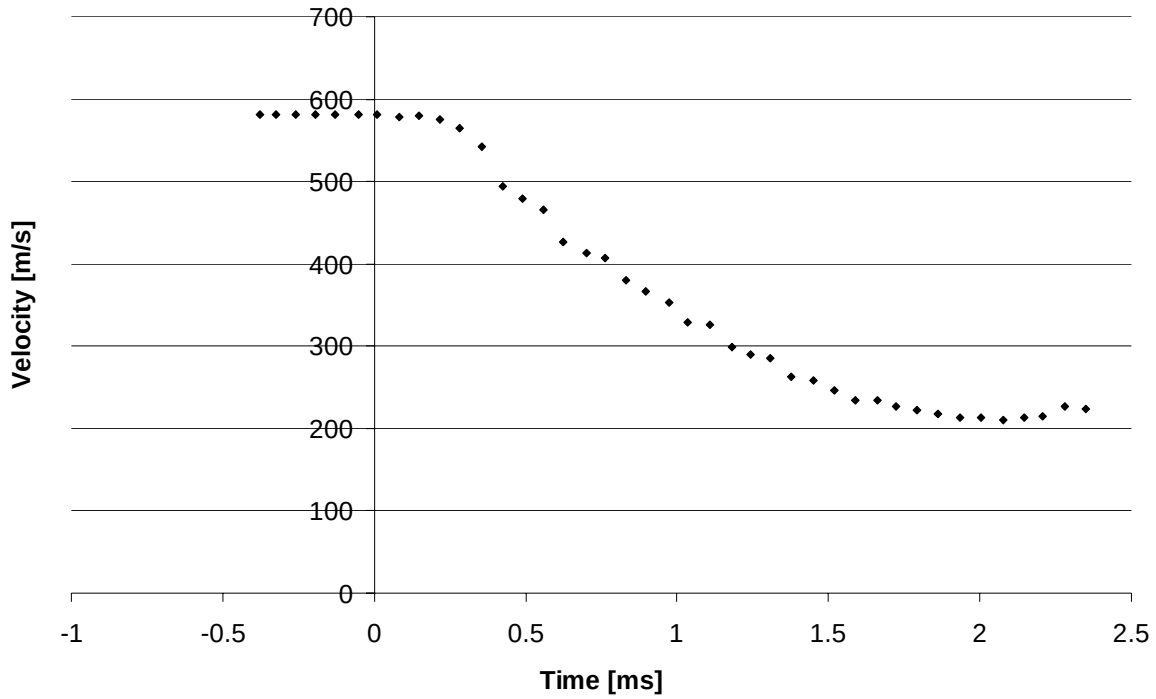

Figure E.29. Doppler radar registrations for target 13 in test-series 1998:2.

Test series 1999

The figures showing Doppler radar registrations for targets 1-9 and 24-25 were processed in Matlab. For the other targets plots supplied by Bofors Testing Center were scanned and for some of them there is no zooming of the penetration phase data.

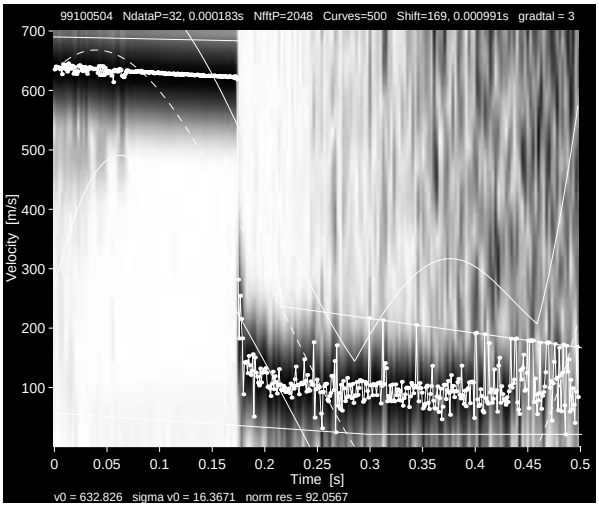

Figure E.30. Doppler radar registrations for target 1 in test-series 1999. All data.

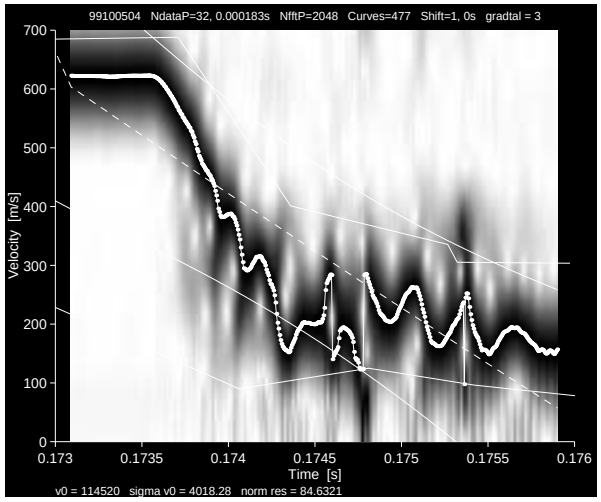

Figure E.31. Doppler radar registrations for target 1 in test-series 1999. Penetration phase data.

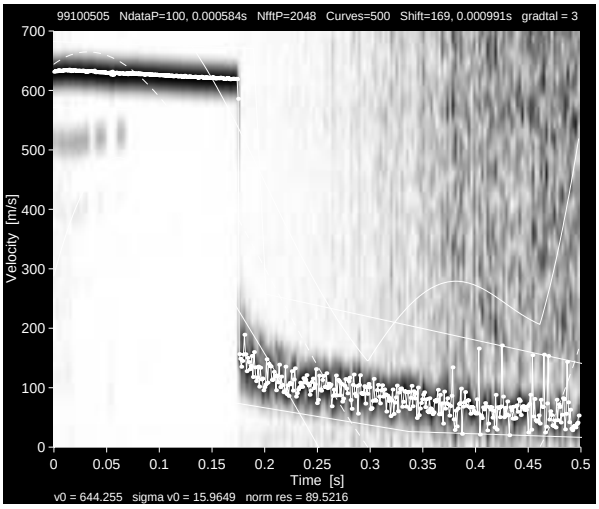

Figure E.32. Doppler radar registrations for target 2 in test-series 1999. All data.

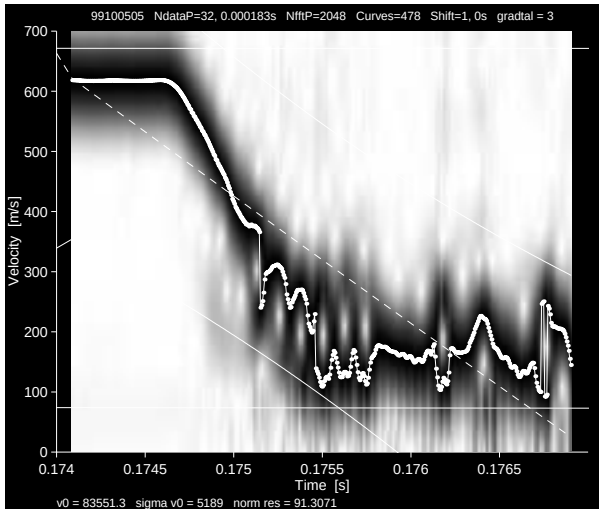

Figure E.33. Doppler radar registrations for target 2 in test-series 1999. Penetration phase data.

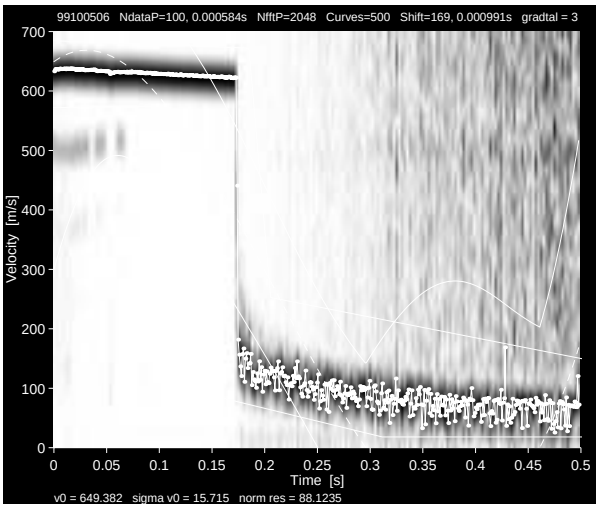

Figure E.34. Doppler radar registrations for target 3 in test-series 1999. All data.

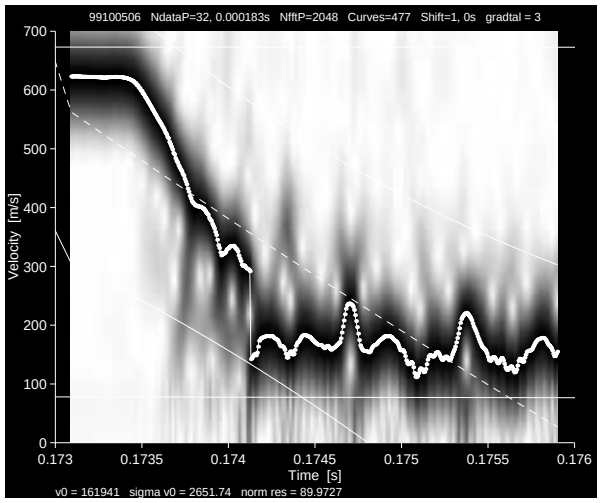

Figure E.35. Doppler radar registrations for target 3 in test-series 1999. Penetration data.

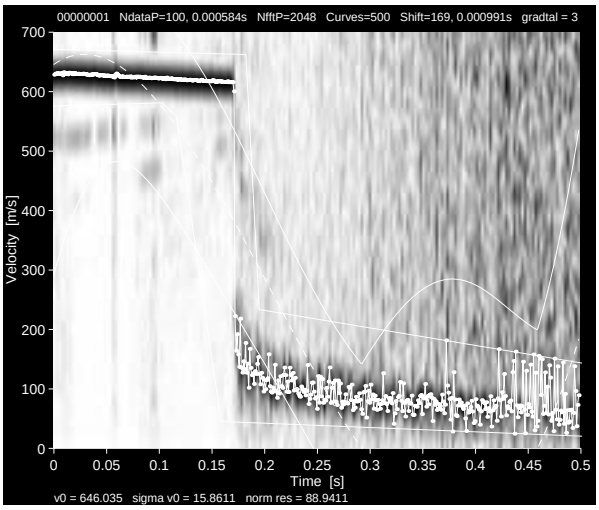

Figure E.36. Doppler radar registrations for target 4 in test-series 1999. All data.

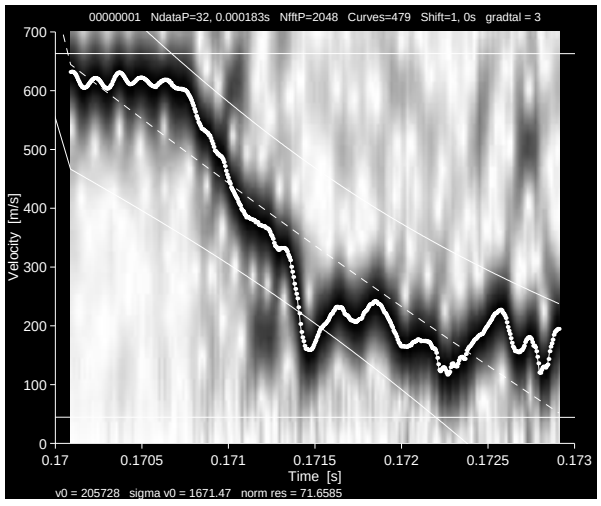

Figure E.37. Doppler radar registrations for target 4 in test-series 1999. Penetration data.

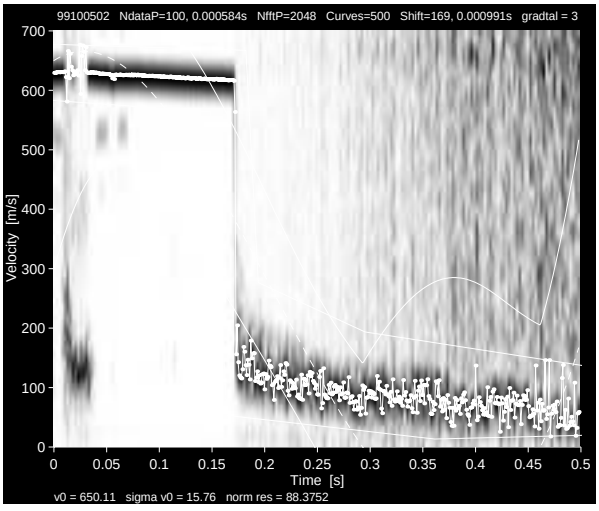

Figure E.38. Doppler radar registrations for target 5 in test-series 1999. All data.

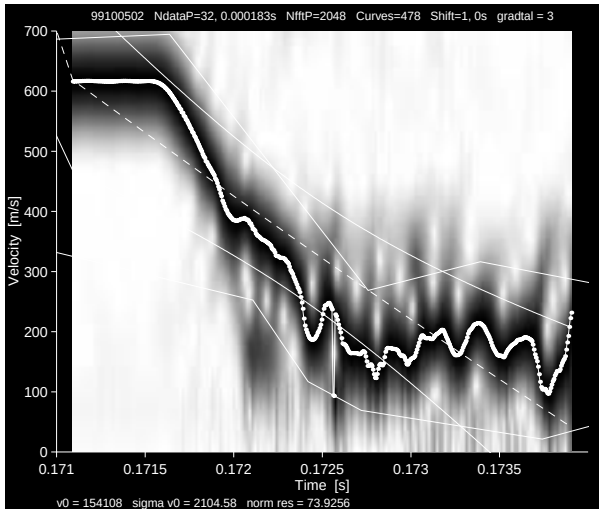

Figure E.39. Doppler radar registrations for target 5 in test-series 1999. Penetration data.

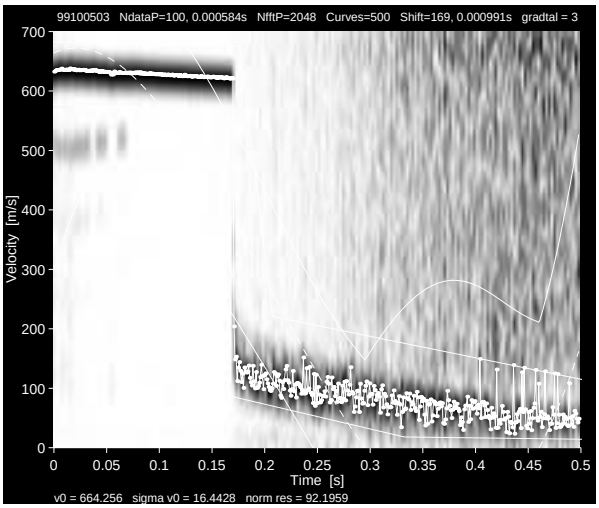

Figure E.40. Doppler radar registrations for target 6 in test-series 1999. All data.

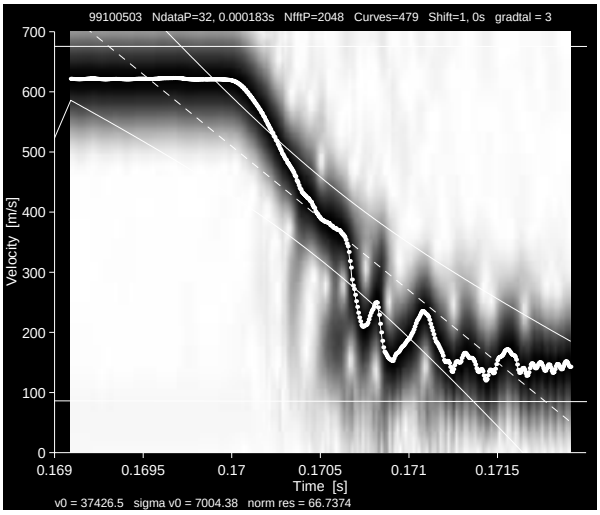

Figure E.41. Doppler radar registrations for target 6 in test-series 1999. Penetration data.

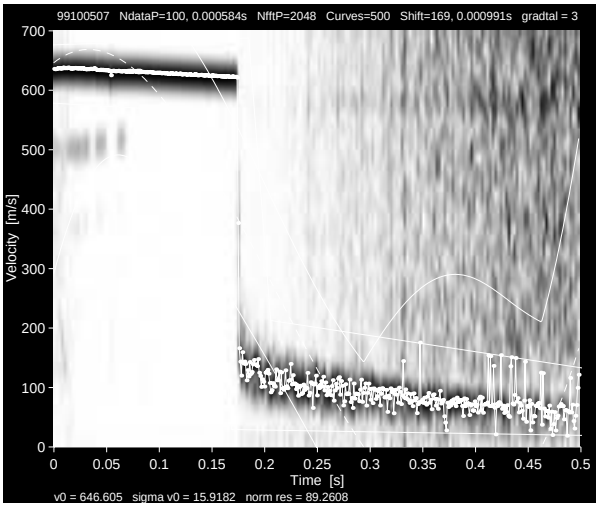

Figure E.42. Doppler radar registrations for target 7 in test-series 1999. All data.

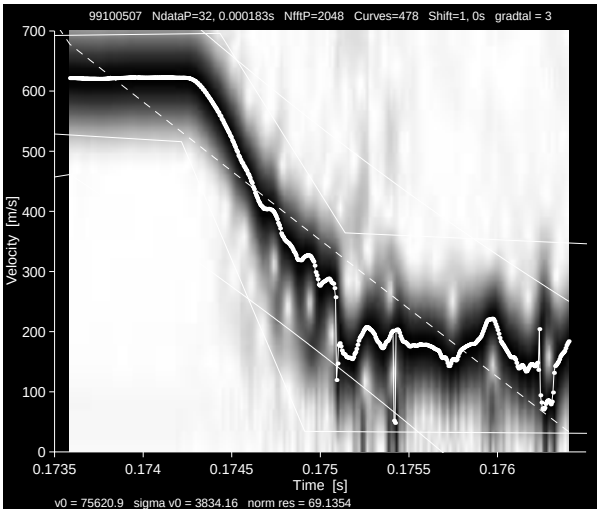

Figure E.43. Doppler radar registrations for target 7 in test-series 1999. Penetration data.

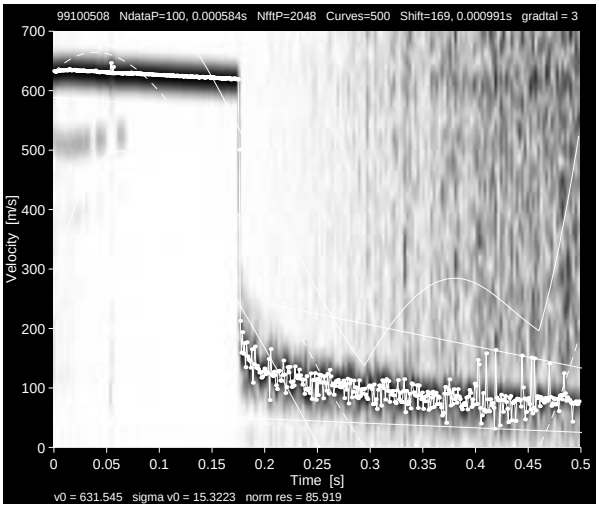

Figure E.44. Doppler radar registrations for target 8 in test-series 1999. All data.

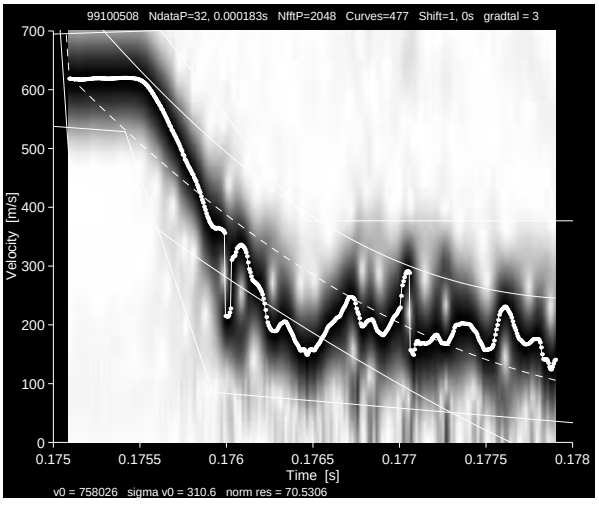

Figure E.45. Doppler radar registrations for target 8 in test-series 1999. Penetration data.

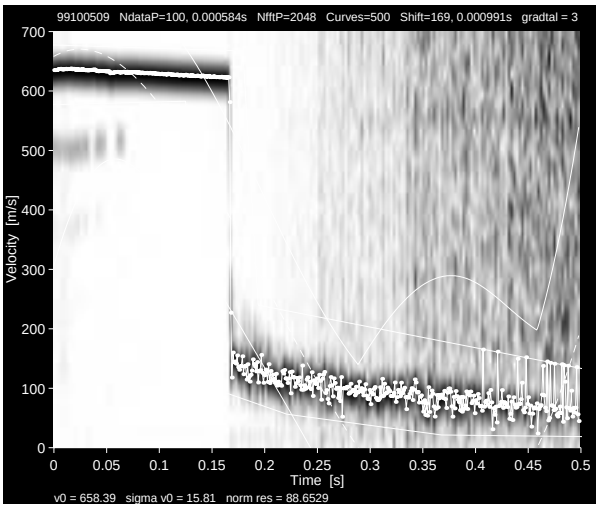

Figure E.46. Doppler radar registrations for target 9 in test-series 1999. All data.

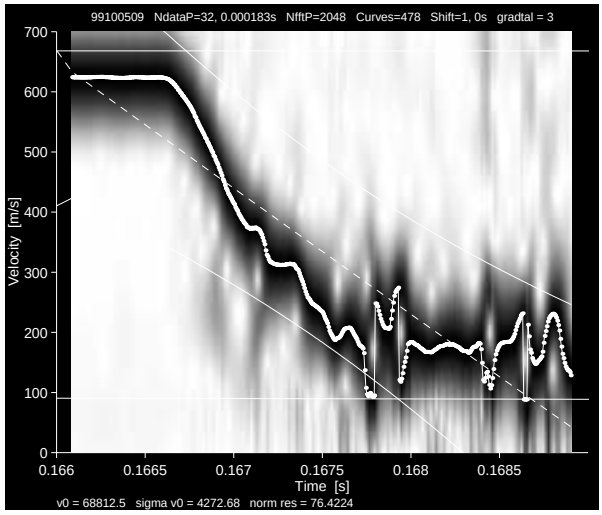

Figure E.47. Doppler radar registrations for target 9 in test-series 1999. Penetration phase data.

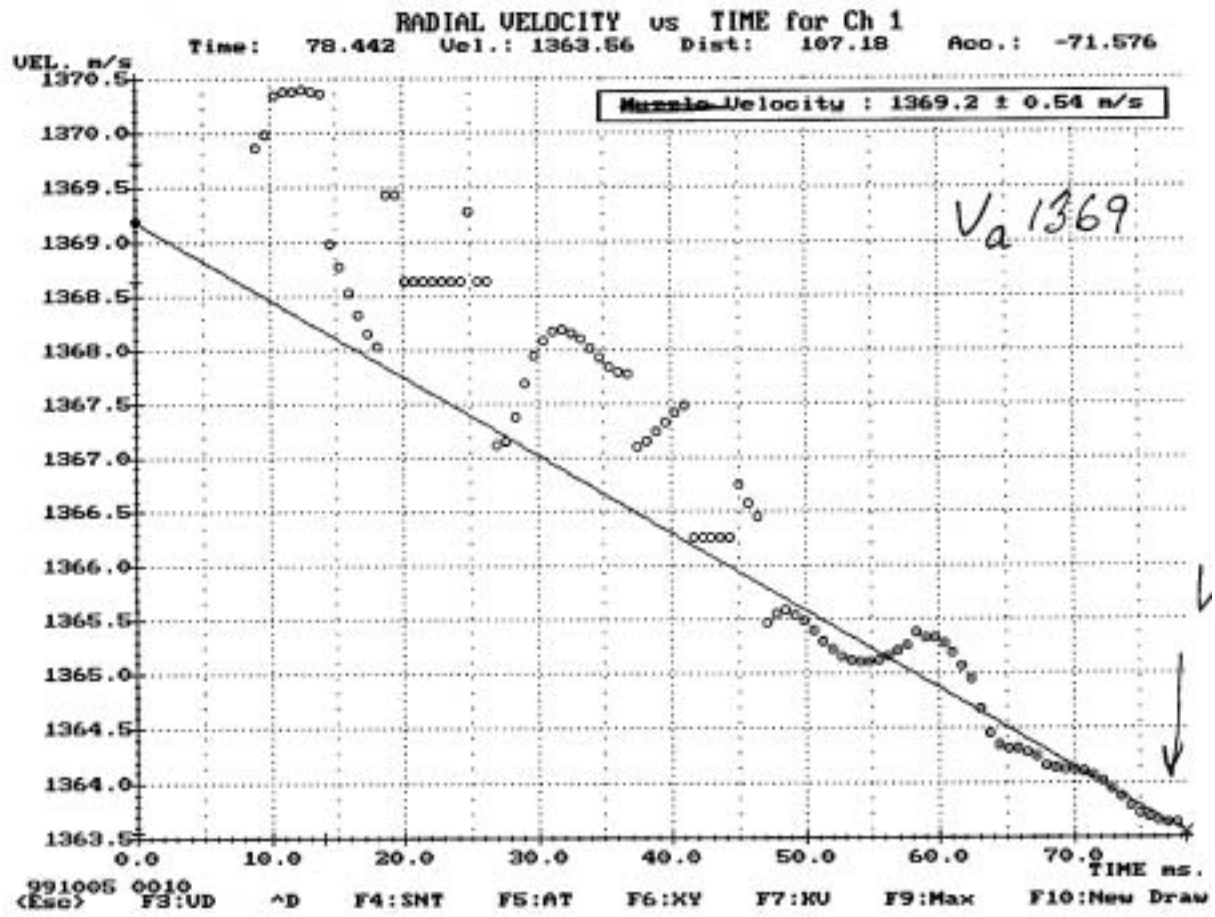

Figure E.48. Doppler radar registrations for target 10 in test-series 1999.

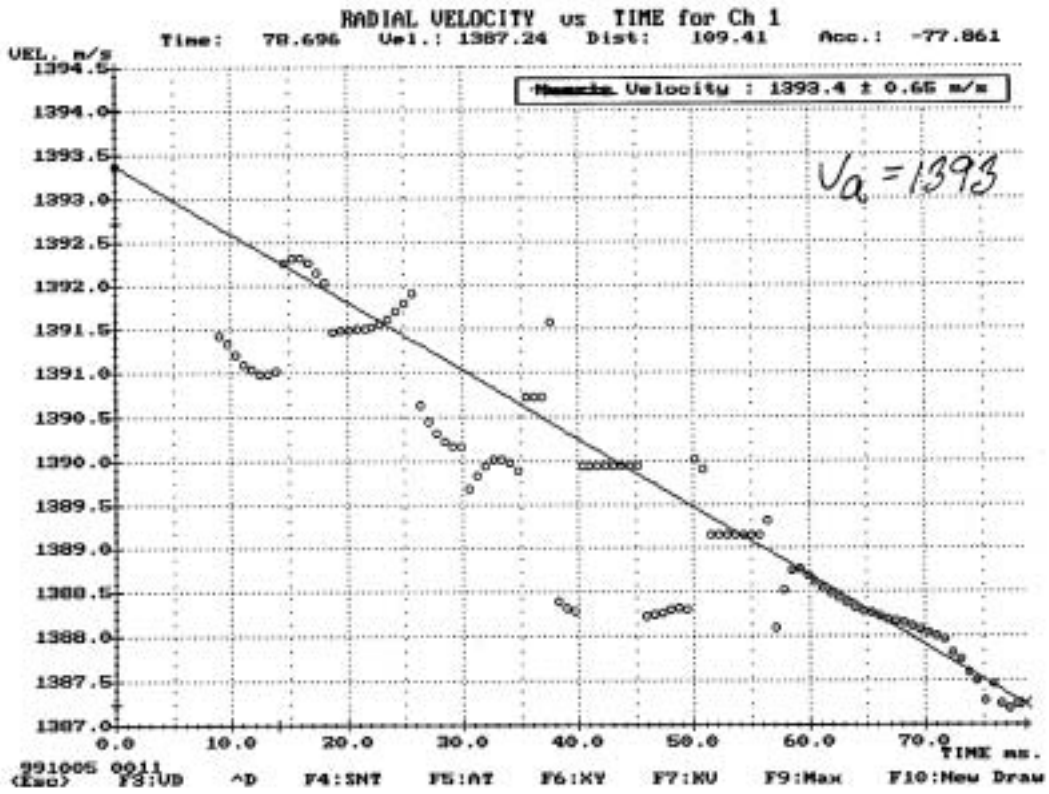

Figure E.49. Doppler radar registrations for target 11 in test-series 1999.

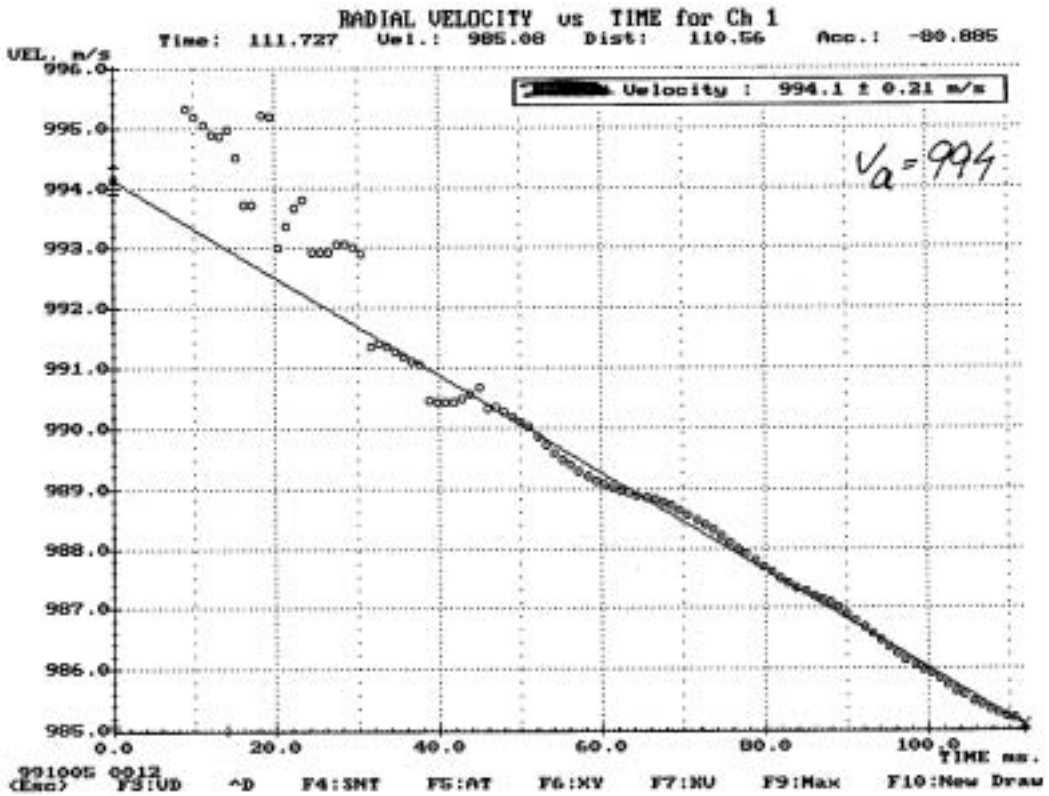

Figure E.50. Doppler radar registrations for target 12 in test-series 1999.

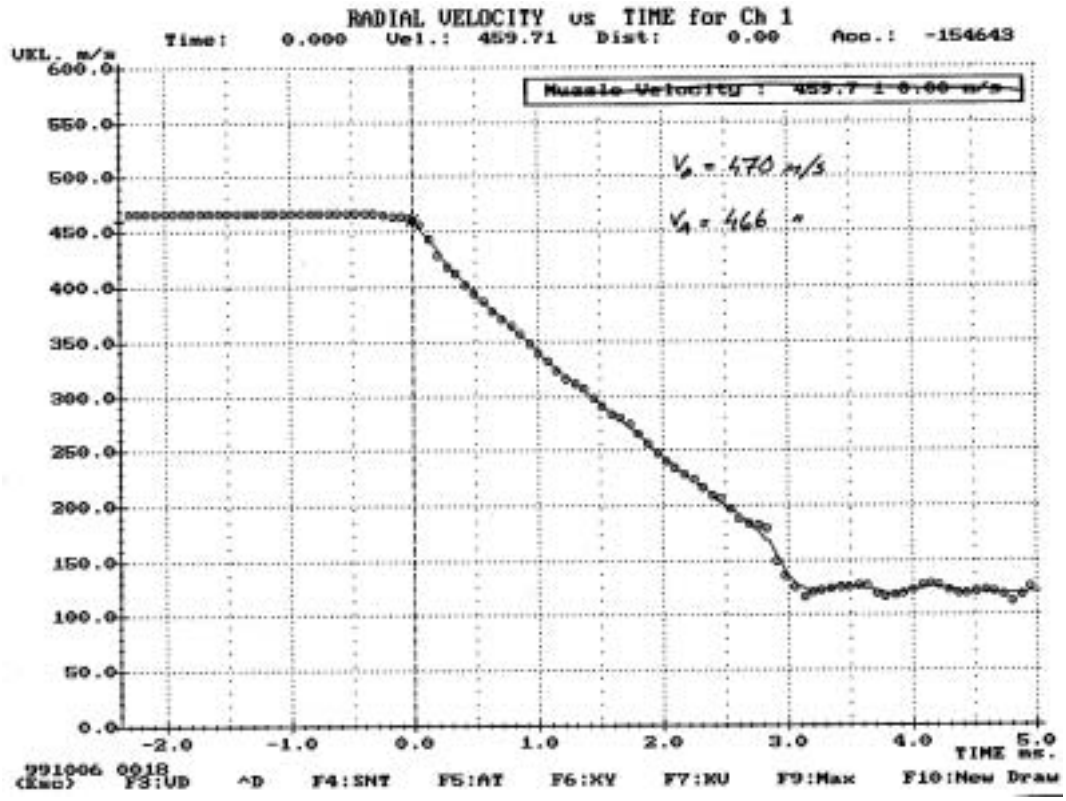

Figure E.51. Doppler radar registrations for target 13 in test-series 1999.

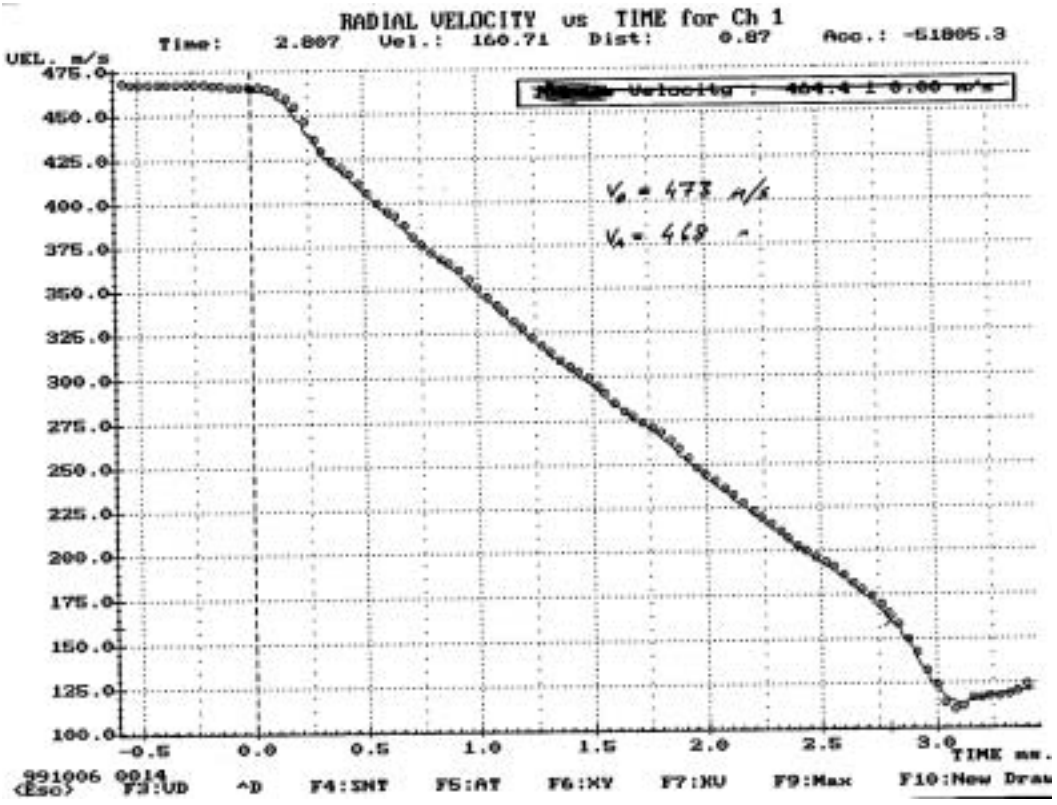

Figure E.52. Doppler radar registrations for target 14 in test-series 1999.

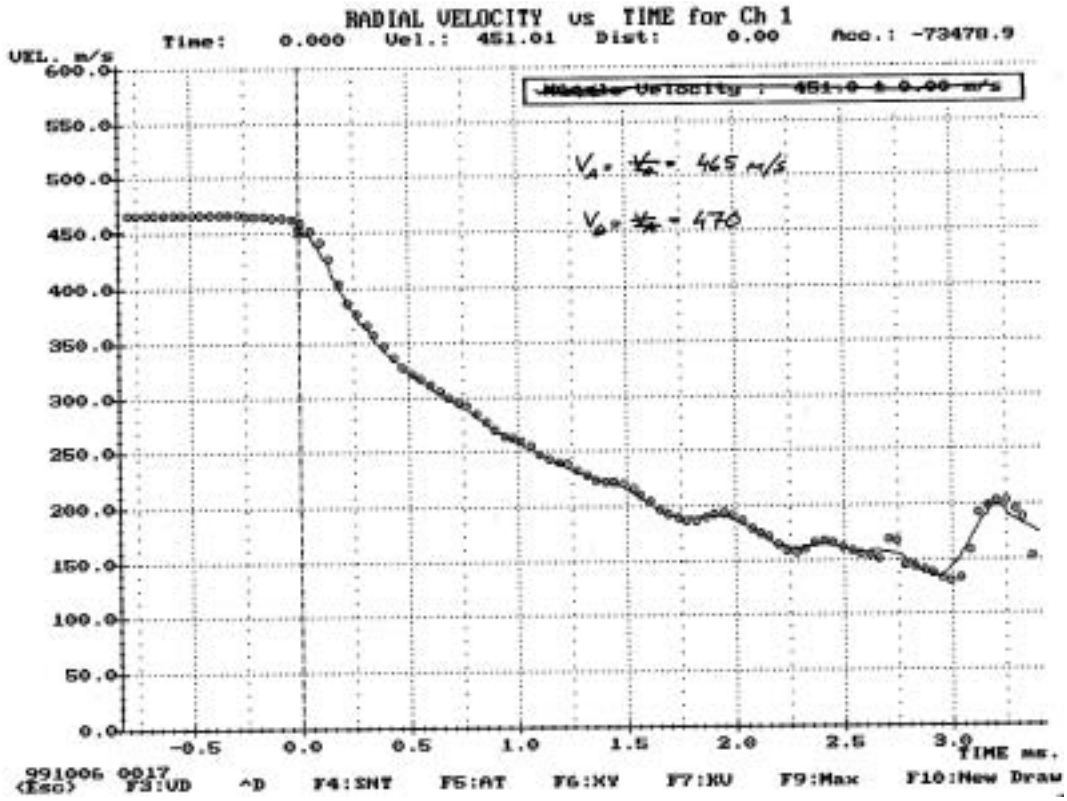

Figure E.53. Doppler radar registrations for target 15 in test-series 1999.

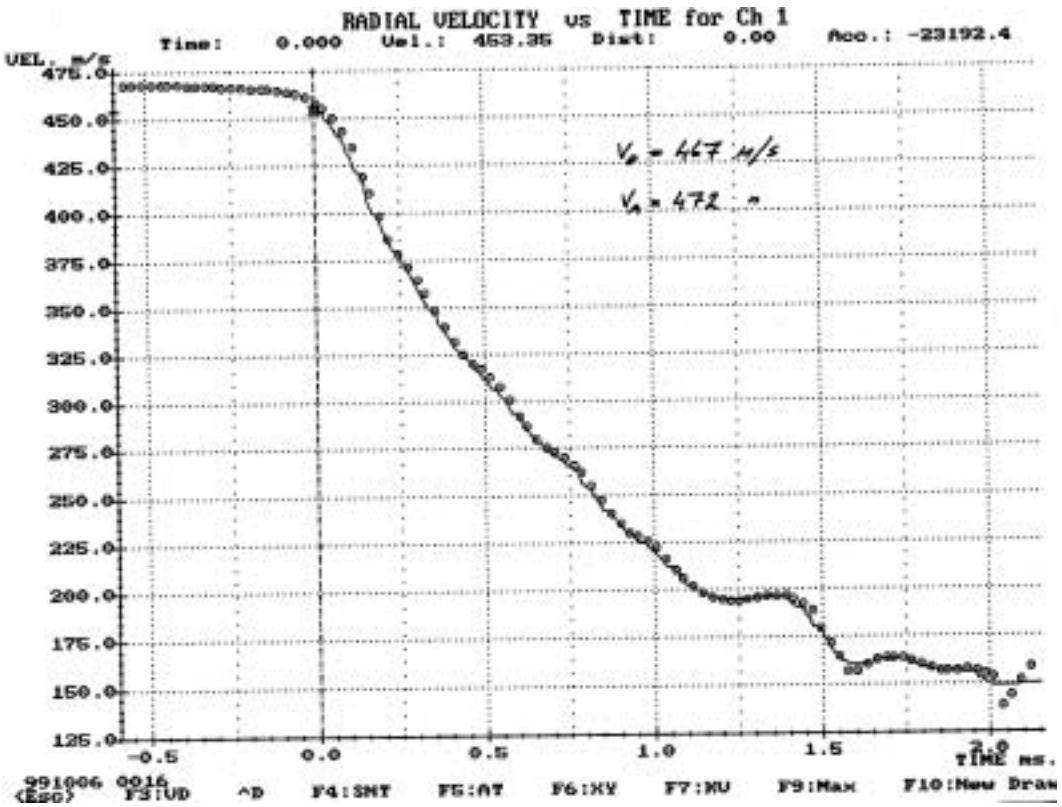

Figure E.54. Doppler radar registrations for target 16 in test-series 1999.

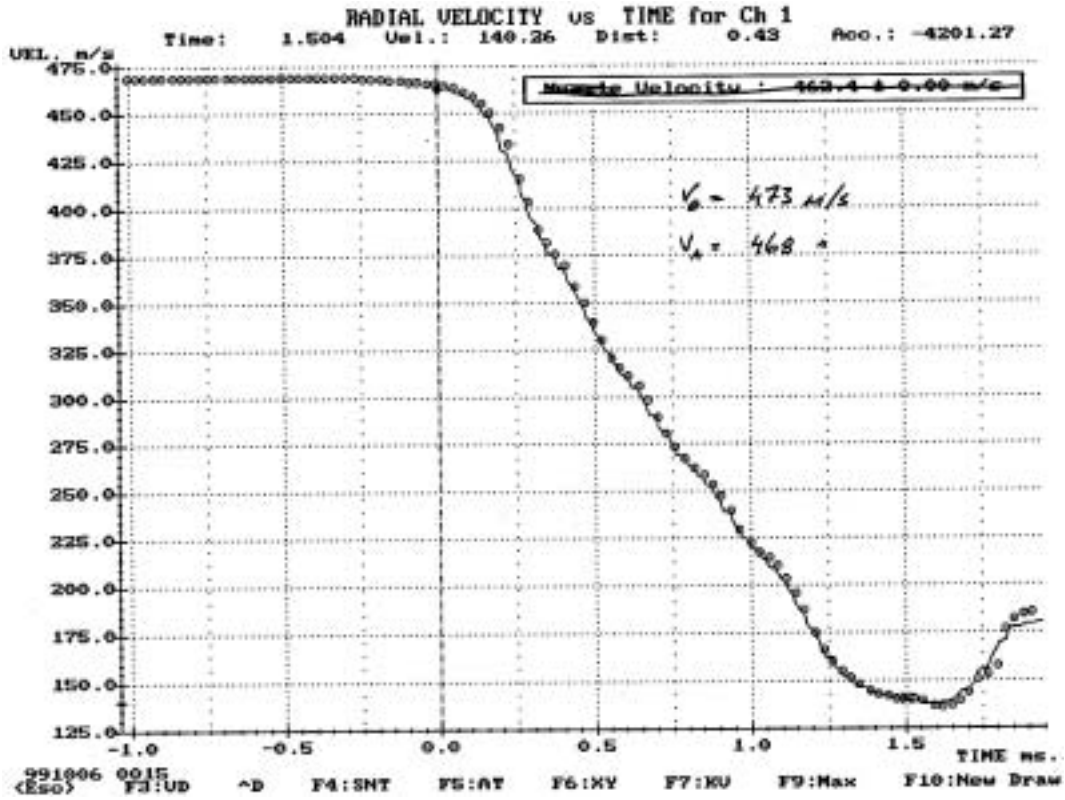

Figure E.55. Doppler radar registrations for target 17 in test-series 1999.

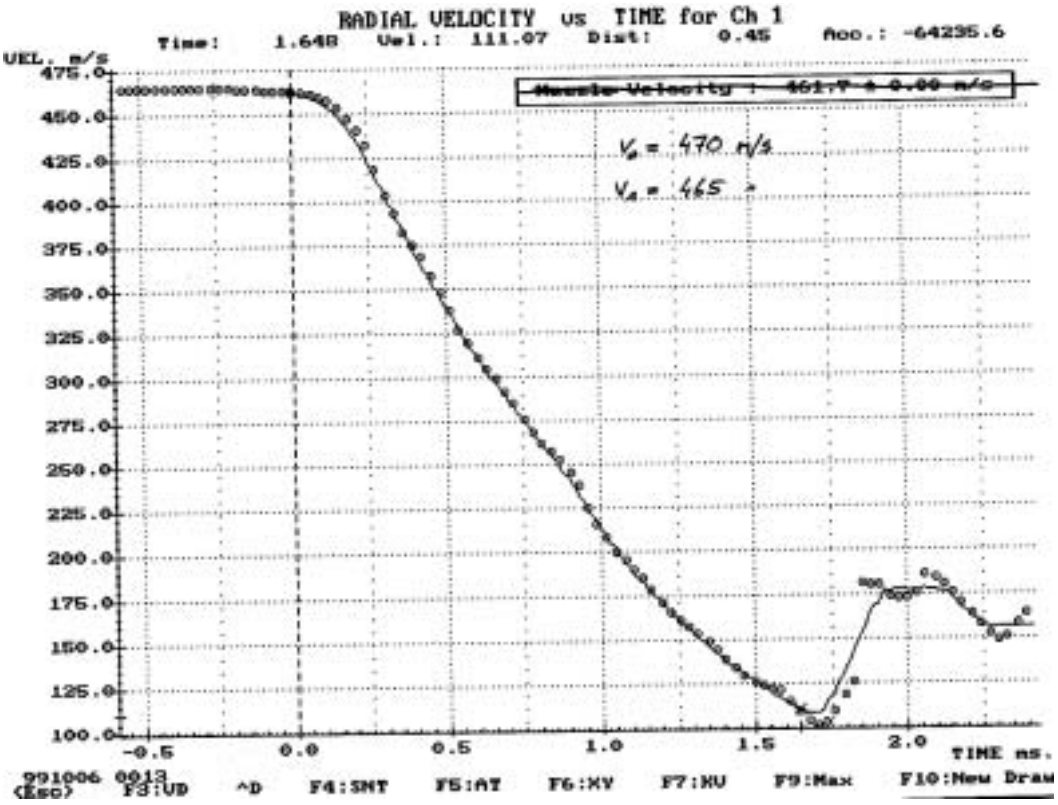

Figure E.56. Doppler radar registrations for target 18 in test-series 1999.

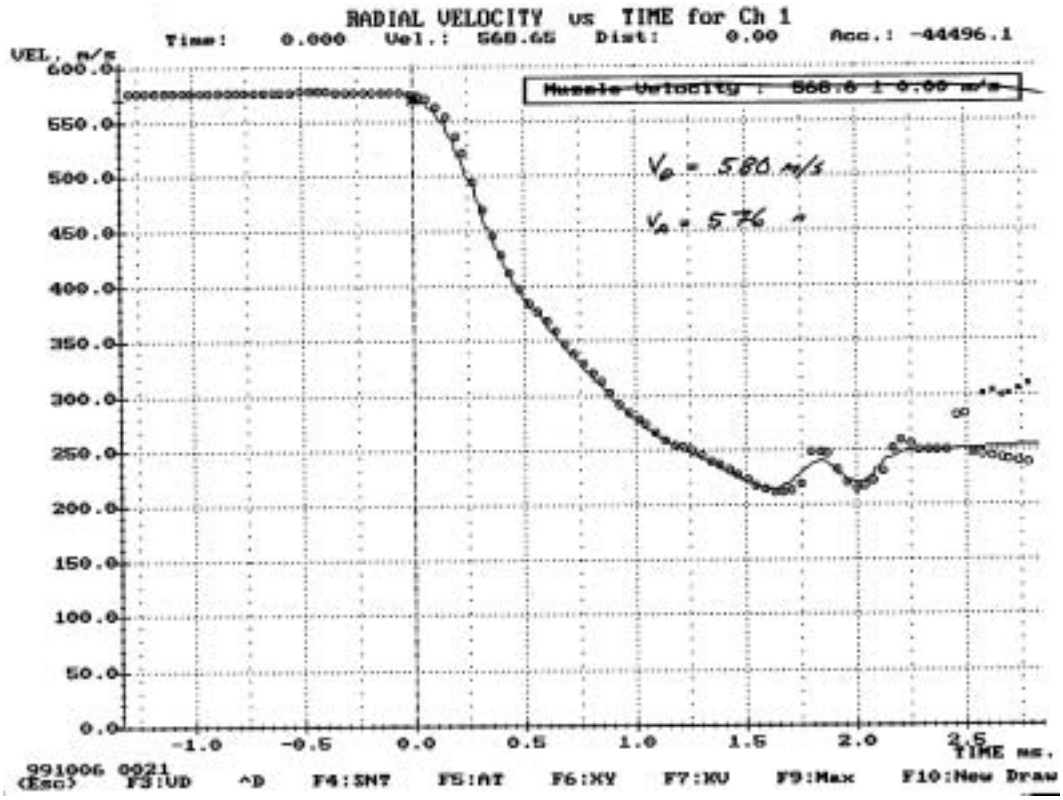

Figure E.57. Doppler radar registrations for target 19 in test-series 1999.

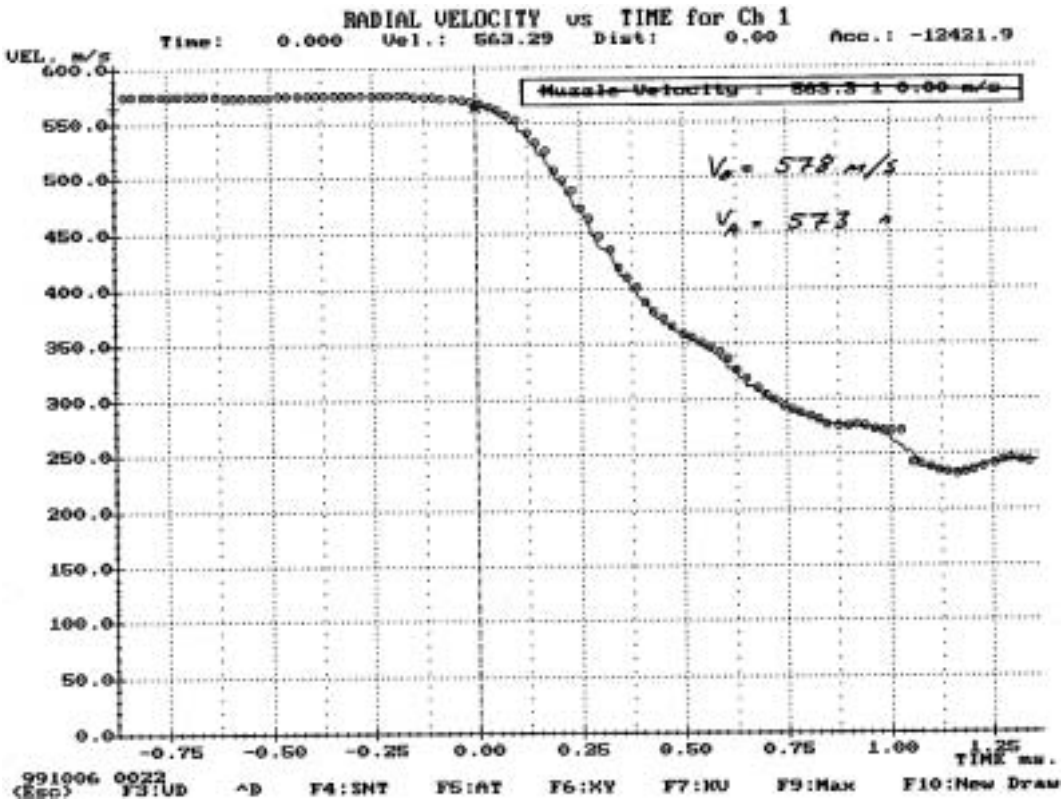

Figure E.58. Doppler radar registrations for target 20 in test-series 1999.

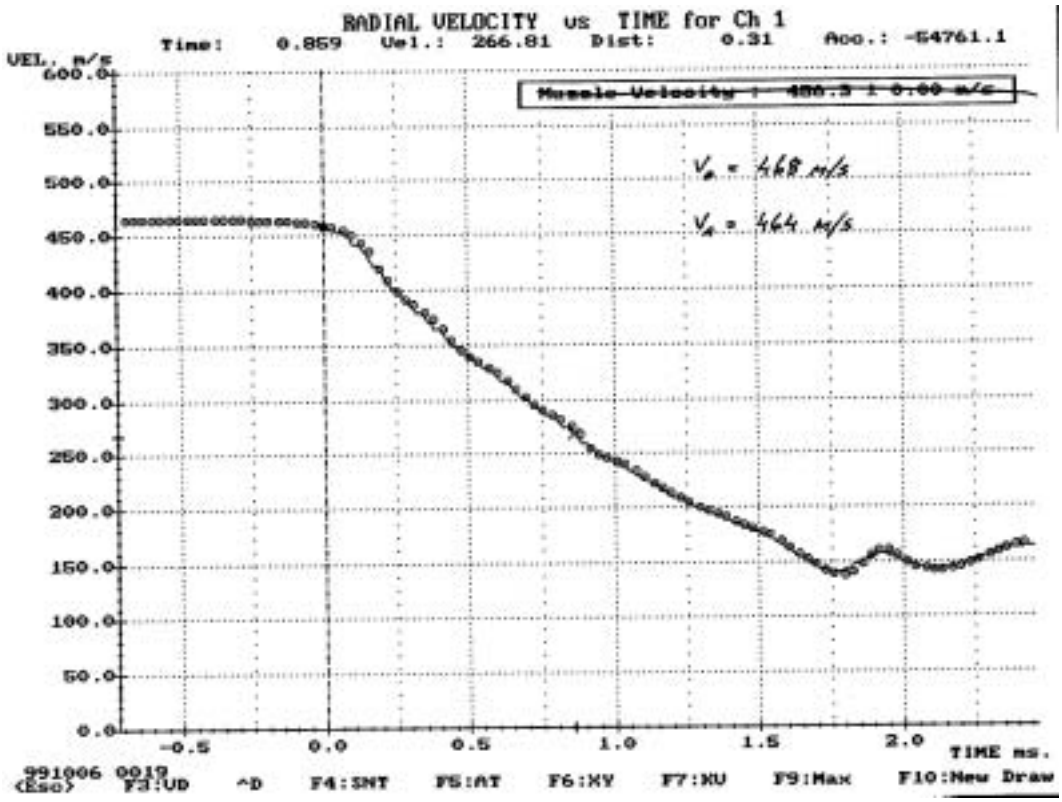

Figure E.59. Doppler radar registrations for target 21 in test-series 1999.

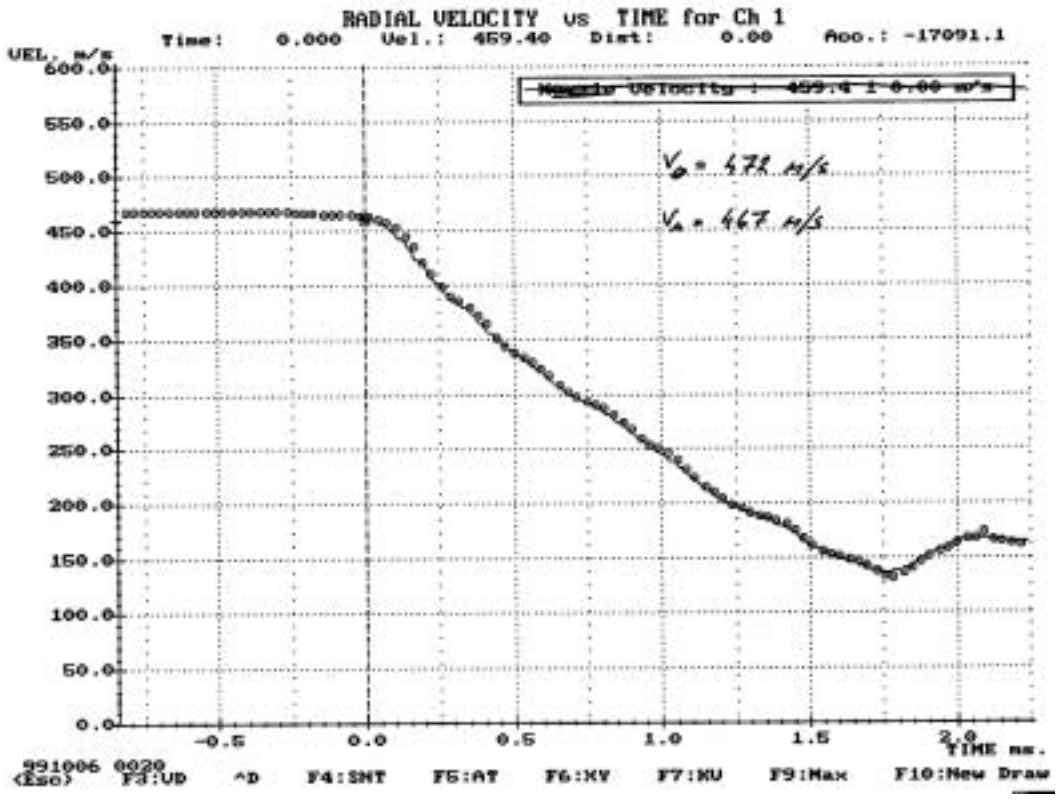

Figure E.60. Doppler radar registrations for target 22 in test-series 1999.

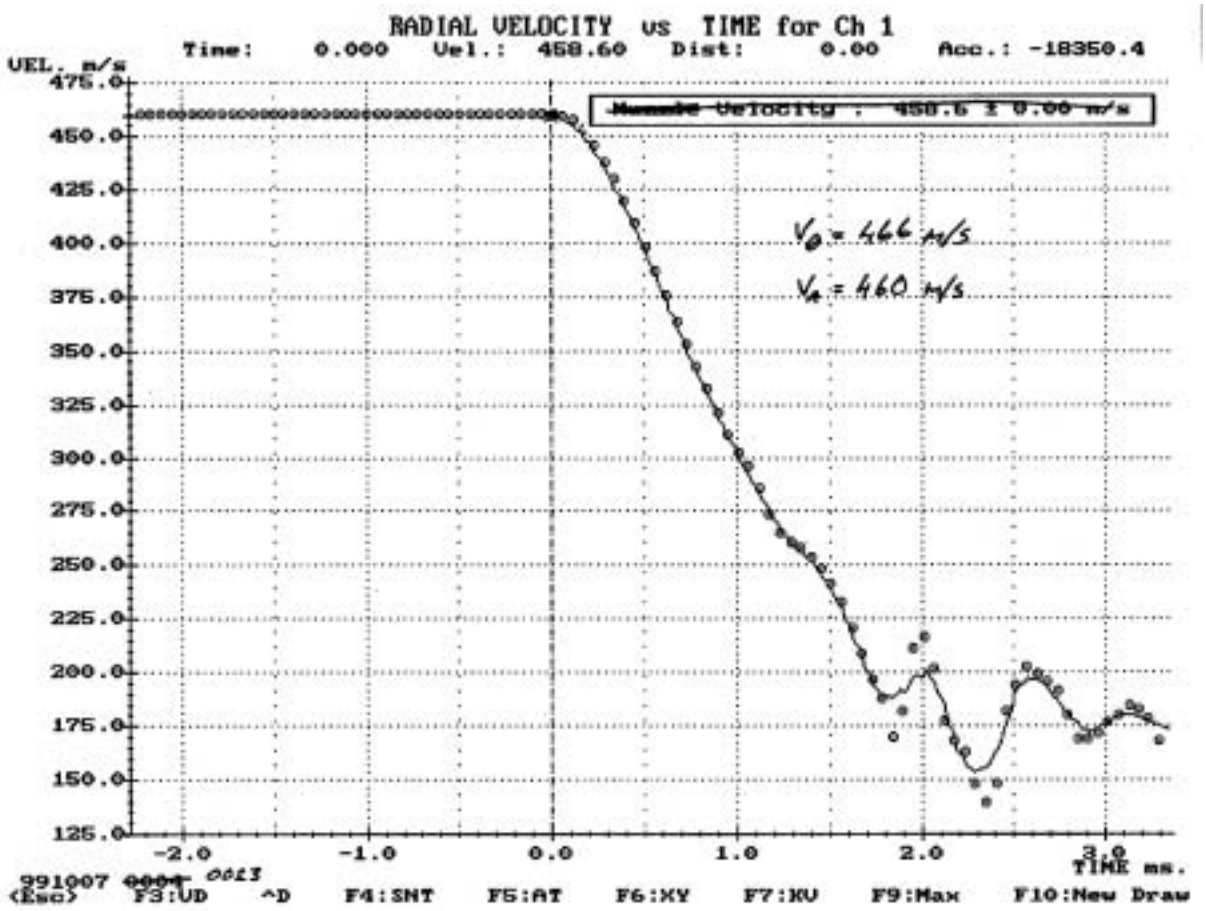

Figure E.61. Doppler radar registrations for target 23 in test-series 1999.

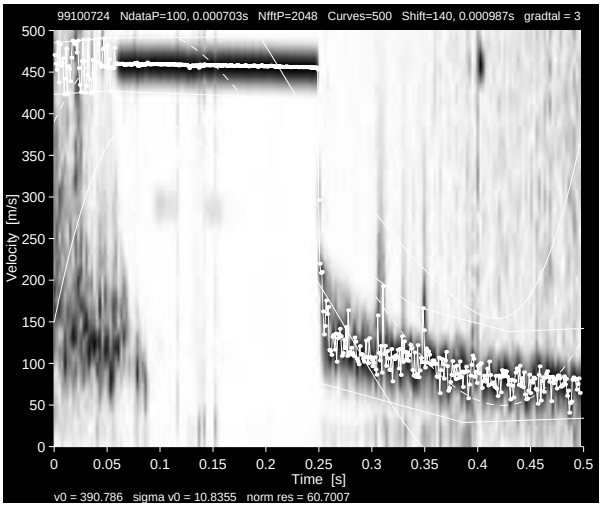

Figure E.62. Doppler radar registrations for target 24 in test-series 1999. All data.

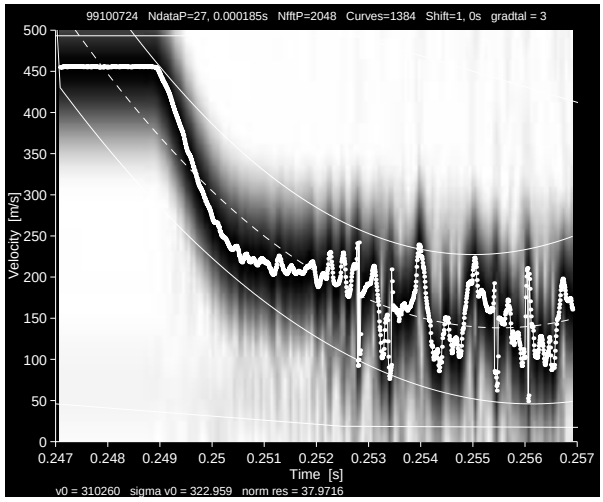

Figure E.63. Doppler radar registrations for target 24 in test-series 1999. Penetration phase data.

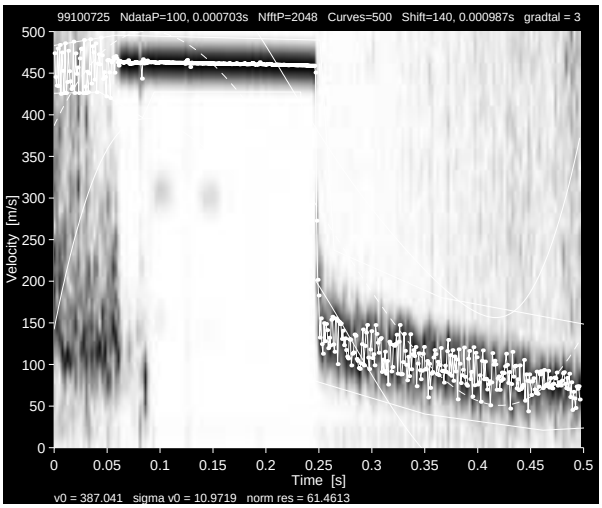

Figure E.64. Doppler radar registrations for target 25 in test-series 1999. All data.

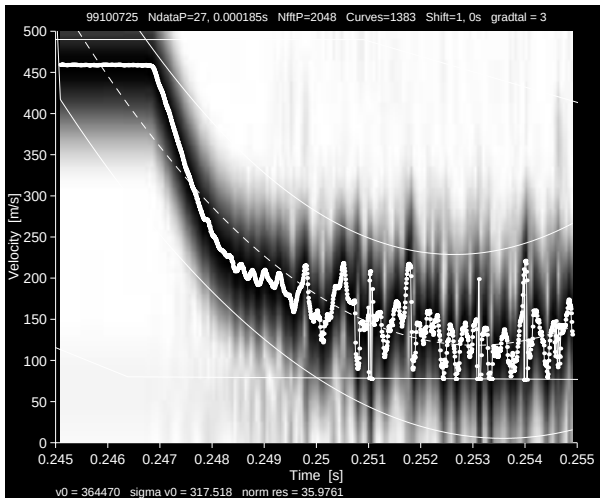

Figure E.65. Doppler radar registrations for target 25 in test-series 1999. Penetration phase data.

F PRESSURE GAUGE REGISTRATIONS

For the plots a moving average filter of five values were used. For target 24 and 25, 250 and 100 MS/s were used respectively.

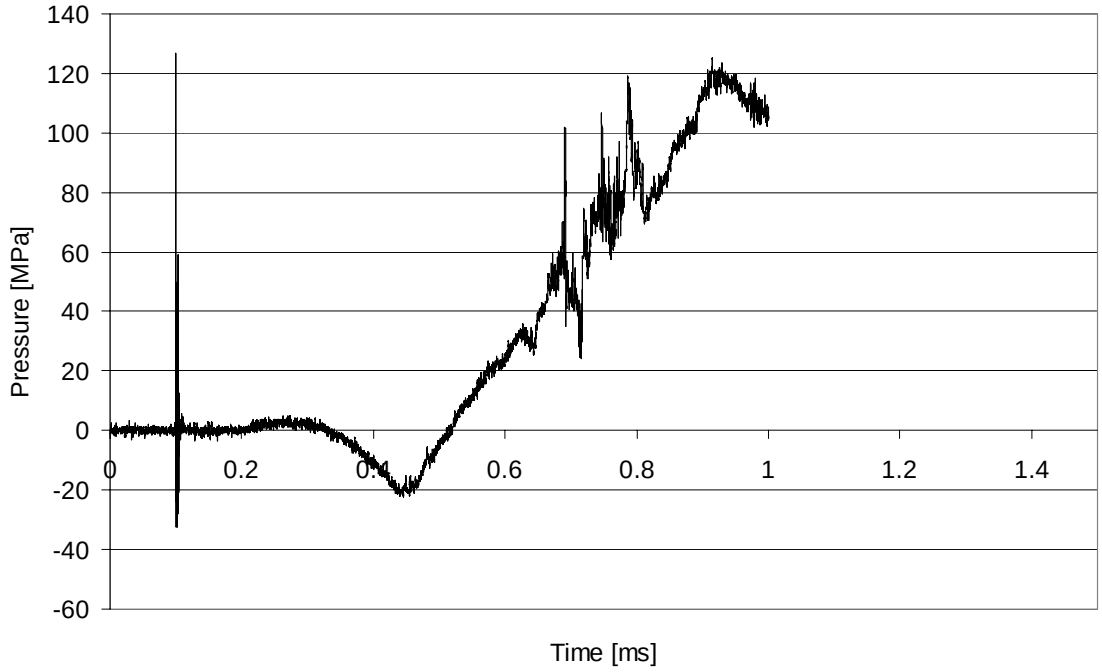

Figure F.1 Pressure gauge registration for target 24 in test-series 1999.

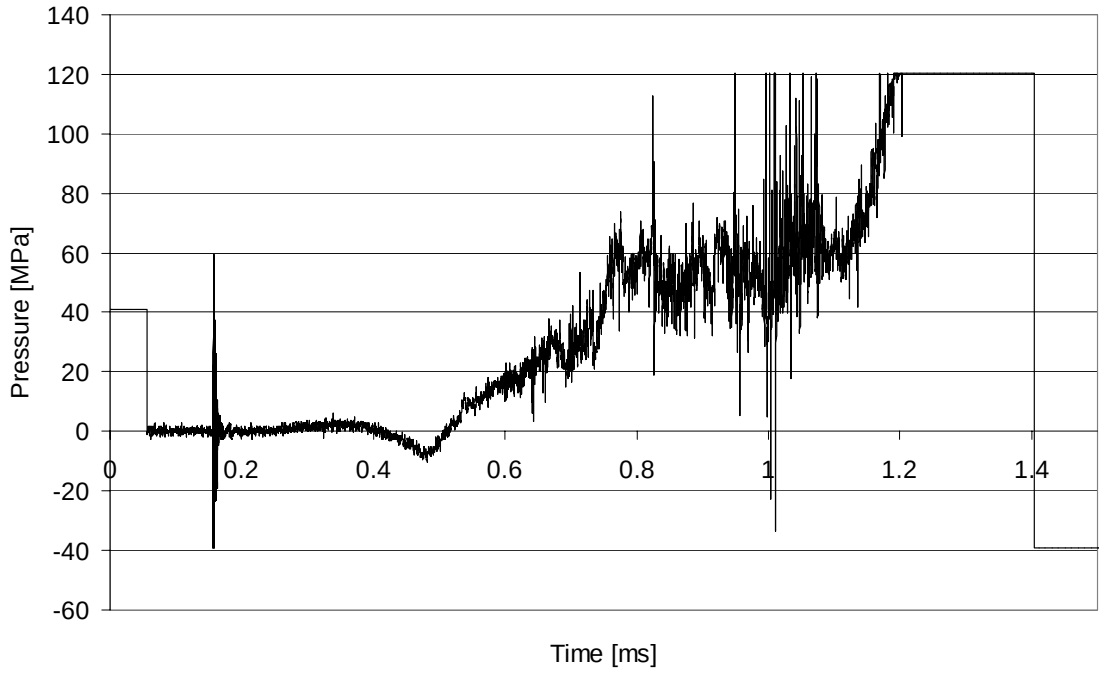

Figure F.2 Pressure gauge registration for target 25 in test-series 1999.

G PROJECTILE ACCELERATION REGISTRATIONS

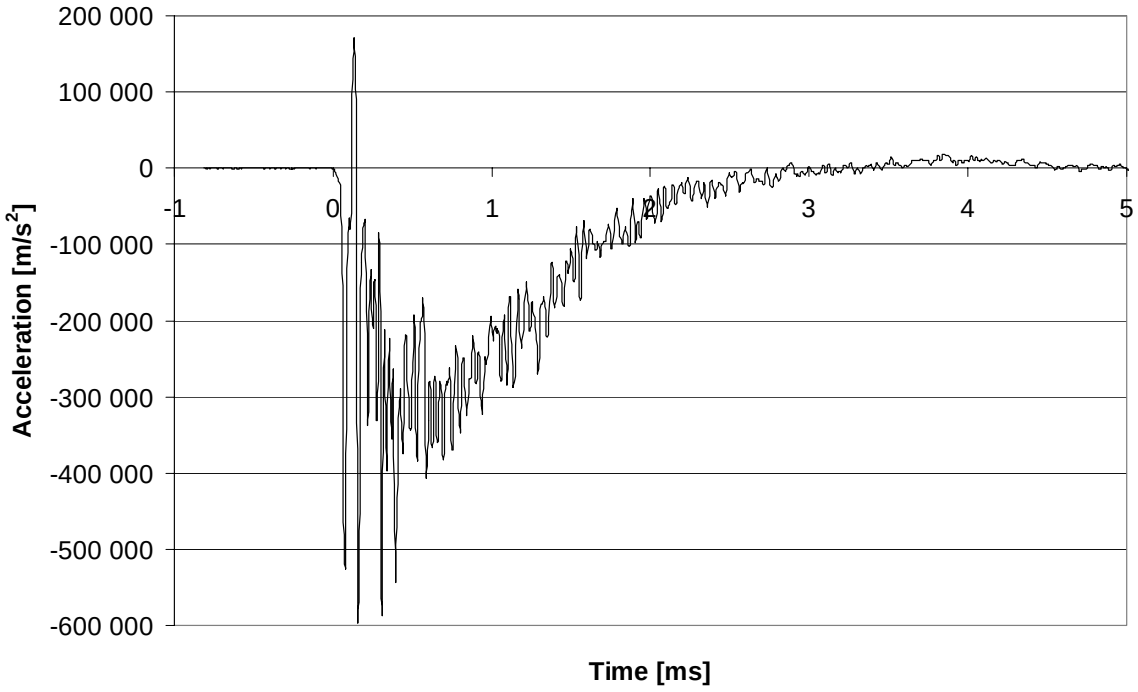

Figure G.1 Projectile acceleration history according to instrument package registration for target 25 in test-series 1999. Target impact at time=0.

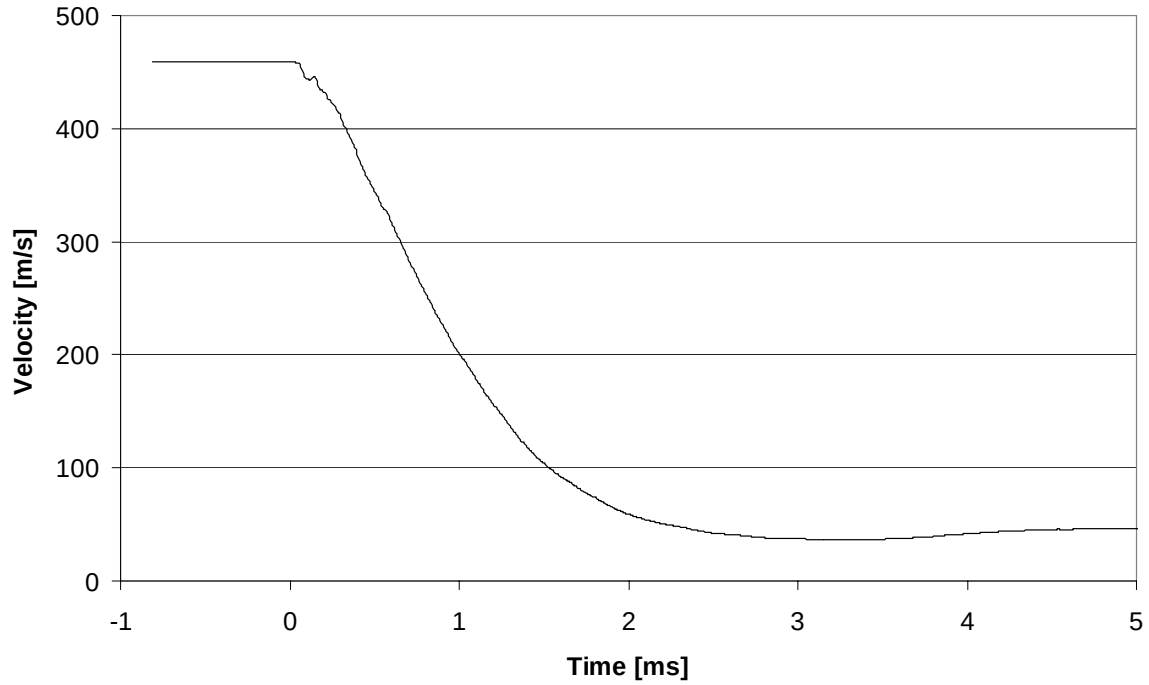

Figure G.2 Projectile velocity history according to instrument package registration for target 25 in test-series 1999. Target impact at time=0.